CRANFIELD UNIVERSITY

JANINE SARAH CAYGILL

MICROARRAY SENSORS FOR DETECTING AIRBORNE EXPLOSIVES

CRANFIELD HEALTH

ENGD THESIS
Academic Year: 2007 - 2011

Supervisor: PROFESSOR SÉAMUS P. J. HIGSON
OCTOBER 2011

CRANFIELD UNIVERSITY

CRANFIELD HEALTH

ENGD THESIS

Academic Year 2007 - 2011

JANINE SARAH CAYGILL

MICROARRAY SENSORS FOR DETECTING AIRBORNE EXPLOSIVES

Supervisor: PROFESSOR SÉAMUS P. J. HIGSON

OCTOBER 2011

This thesis is submitted in partial fulfilment of the requirements for the degree of EngD

IN MEMORANDUM:
ALAN CAYGILL
1949-2006

Declaration

This is a declaration to certify that no portion of the work referred to in this thesis has been submitted in support of an application for another degree or qualification of this or any other university, or institute of learning.

Janine Sarah Caygill

October 2011

ABSTRACT

Due to the enhanced level of national security currently required due to the possibility of terrorist attack, monitoring devices for trace levels of explosive materials are now of the upmost importance. One such method that offers a possible route towards the development of a system for the detection of such analytes is via an electrochemical regime, coupled to the use of disposable sensor technology.

Within this study, the use of modified carbon screen-printed sensors for the detection and analysis of such analytes of importance has been investigated. The modification of the base carbon substrate has been undertaken in a two-fold manner; firstly the incorporation of an enhanced electroactive mediator (Cobalt Phthalocyanine) has been investigated as an aid to facilitate the signal response and secondly the use of a novel surface modification technique to produce microelectrode arrays upon the carbon has also been employed. Microelectrodes hold intrinsic advantages over planar electrodes, such as stir independence, low detection limits and increased sensitivity due to their hemispherical diffusional profile. An array of microelectrodes can retain these properties whilst including the added advantage of enhancing the current response. The integration of these two approaches, the microelectrode array coupled with the mediated electrodes, has been developed with the ultimate objective to develop an accurate and sensitive detection system for trace quantities of explosives, namely 2,4,6-trinitrotoluene (TNT).

This thesis describes work focussed towards the optimisation of each of the individual components involved in the formation of a sensing device for the detection and measurement of trace levels of explosive materials. In particular, factors and techniques that may facilitate the enhanced sensitivity of the measurement device are described. At every stage, each modification step was also undertaken with a suitable redox probe, ferrocenemonocarboxylic acid to allow for a quantitative assessment to be made.

The use of unmediated and mediated carbon ink has been assessed in terms of suitability as a host material for the detection of TNT, with concentrations of 400 nM being measured on these base substrates. Further to this, microelectrode arrays were then formed upon these planar carbon surfaces via insulation with poly(phenylenediamine) coating and subsequent ultrasonic ablation. These thin film microelectrode arrays (~40 nm, pore population ~7.0×10^4 cm^{-2}) were also investigated in terms of response to TNT and were seen to offer an enhanced response in terms of signal differentiation. A final stage was then applied where the microelectrode array was further modified to incorporate a conductively grown polymer from the pore areas. Within this conductive growth, an enzyme/co-factor matrix specific to TNT was deposited which was seen to further increase signal responses, although displaying a lack of sensitivity at lower concentrations.

As a final step the developed sensor methodologies were then used in conjunction with an air-sampling system, the Coriolis®μ cyclone, to mimic the use of the sensors in realistic environments for practical employment. The sensors were used to successfully measure TNT samples from a concentrated stock sample of 4.4 mM collected via the cyclone technique.

ACKNOWLEDGEMENTS

I would like to thank those that have provided the most invaluable help and support during my time at Cranfield – firstly my supervisor, Professor Séamus Higson, for his enthusiasm and unwavering encouragement no matter how dire the situation seemed to me; thank you to Dr Stuart Collyer for his enduring patience, for always having time for emergency discussions and his advice that has gone beyond what should be expected of him; thank you to Dr Jo Holmes for tracking down my TNT when I thought all was lost and for her advice and support – especially in the final stretch; and thank you to Dr Frank Davis for his help getting my review paper submitted on time.

I would like to thank the Engineering and Physical Sciences Research Council for providing the funding for this project and Leeds University for the kind loan of the Coriolis®μ air sampling system.

I would like to add a thank you to all those characters I have spent my leisure time with at Cranfield, specially Phil and Matt with whom I have spent many lunch hours debating, discussing and laughing. And a big shout out to all those, past and present, in Séamus' research group – Will, Stuart, Duncan, Tim and Laura.

Finally, I would like to attempt to express my thanks and gratitude to my darling Martin for his help, support, pep talks, patience and love throughout the past four years. Without you I wouldn't be where I am today, so thank you.

Table of contents

Table of figures

List of tables

Table of equations

Abbreviations

A	Ampere
AD	Aggregate demand
Ag/AgCl	Silver/silver chloride
AN	Ammonium nitrate
Aq	Aqueous
Au	Gold
AS	Aggregate supply
CE	Counter electrode
CE’	Capillary electrophoresis
CoPc	Cobalt phthalocyanine
CP	Conjuagted polymer
CRDS	Cavity ringdown spectroscopy
DAN	Diaminonaphthalene
DMAB	Dimercaptoazobenzene
DNT	2,4-dinitrotoluene
e^-	Electron
E	Potential
E. coli	Escherichia coli
ERC	Explosive related compound
ET	Electron transfer
FeCA	Ferrocenemonocarboxylic acid
FMN	Flavin mononucleotide
g	Gram

G	Gibbs free energy
GC	Gas chromatography
GCE	Glassy carbon electrode
GDP	Gross domestic product
GOD	Glucose oxidase
H_2O_2	Hydrogen peroxide
HMTA	Hexamethylene tetramine
HMTD	Hexamethylene triperoxide diamine
HMX	Cyclotetramethylenetetranitramine
HPLC	High-performance liquid chromatography
HRP	Horseradish peroxidase
i	Current
IATA	International Air transport Association
iCVD	Initiated chemical vapour deposition
IMS	Ion mobility spectroscopy
IHP	Inner Helmholtz plane
IR	Infra-red
k_m	Michaelis constant
LED	Light emitting diode
LIBS	Laser induced breakdown spectroscopy
LOD	Limit of detection
LRAS	Long-run aggregate supply
M	Molar
m	Milli (10^{-3})
m	Metal

MA	Microelectrode array
MEKC	Micellular electrokinetic chromatography
MS	Mass spectrometry
MS/MS	Tandem mass spectrometry
MS-TOF	Mass spectrometry
n	Nano (10^{-9})
NAD(P)H	β-Nicotinamide adenine dinucleotide 2'-phosphate (reduced)
nm	Nanometre
NTR	Nitroreductase
O	Oxidation / oxidative
OHP	Outer Helmholtz plane
PAMAM	Poly(amidoamine)
PANI	Polyaniline
PBS	Phosphate buffer solution
PETN	Pentaerythritol tetranitrate
PoPDA	Poly(phenylenediamine)
ppb	Parts per billion
ppm	Parts per million
ppt	Parts per trillion
Pt	Platinum
q	Charge
QCM	Quartz crystal microbalance
R	Reduction / reductive
R	Resistance
RDX	Hexahydro-1,3,5-trinitro-1,3,5-triazine

RFID	Radio-frequency indentification
s	Seconds
SAM	Self-assembled monolayer
SAW	Surface acoustic wave
SCE	Saturated calomel electrode
SERS	Surface enhanced Raman scattering
SHE	Standard hydrogen electrode
SPCE	Screen-printed carbon electrode
SPR	Surface plasmon resonance
SRAS	Short-run aggregate supply
SWV	Square wave voltammetry
TATP	Triacetone triperoxide
TEA	Thermal energy analyser
THz	Terahertz
TNB	Trinitrobenzene
TNT	2,4,6-trintrotoluene
UV	Ultra-violet
V	Volt
µ	Micro (10^{-6})

1. Research rationale

Since the terrorist attacks on the World Trade Centre in 2001 and the London bombings in 2005 there has been a recognised need for heightened security around the world. In the immediate aftermath security in airports, for example, was increased such that liquids and foodstuff were not allowed to be carried onto planes, hand luggage was restricted and passengers were subject to far more stringent search procedures. This caused severe delays at the time and required passengers to arrive at airports significantly earlier due to the extra security procedures implemented.

Traditional security measures at airports have included the use of metal detectors to identify any weapons that may be concealed and x-ray machines for viewing the contents of baggage. One remaining problem is that explosive substances are not detectable using these precautions. Apparatus to detect volatile substances, such as gas chromatography coupled with mass spectrometry in conjunction with swabbing, are in use but are largely only suitable to use for items of hand baggage.

A need has, therefore, been identified for a more flexible yet robust system for screening for explosive vapours with high sensitivity. Any technique must also be capable of producing a real-time result with a low possibility of producing false positive or negative readings. Although there are electronic noses available, and of course trained sniffer dogs, these are not without their flaws. High sensitivity techniques quite often require a pre-concentration stage, which is not possible if a near instantaneous response is required. Dogs can become fatigued; there is frequently little correlation between the sensitivity of different dogs and indeed the performance of the same dog can vary on different days.

The device to be developed within this research programme needs to be inexpensive and easy to manufacture, so as to allow it to be mass produced and widely used. The technology must be simple to use and automated so as to allow it to be used by security staff as opposed to requiring a staff of scientists to be available on site. It is also essential that the response time is minimal. This project is focussed towards the development of a technology that will deliver this aim.

This project was initially undertaken through collaboration between Analytical Nanotechnologies Plc. (ANTnano), Microarray Ltd. and Cranfield University. ANTnano are specialists in airborne detection techniques and have already utilised this technology within the chemical manufacturing market to analyse workplace exposure to certain materials. This has been carried out within industries that produce products such as washing powder, where the enzymes can cause serious health problems to those employed if inhaled at sufficiently high levels over extended periods of time (Saum et al., 1998). This technology has also been used within the pharmaceutical industry (Armstrong et al., 2001), within factories manufacturing contraceptives that can cause health issues to workers if exposed to a significantly high dosage.

Leeds University also made available a commercial cyclone collection system, the Coriolis®μ air sampler from Bertin Technologies, which is a condensing system that draws in large quantities of air at speeds of up to 300 litres per minute enabling the collection of airborne pollutants, present in low levels, to be concentrated within a small drop of liquid. Air is aspirated into the collection cone, which has been primed with an aliquot of collection fluid, in a whirling motion that forms a vortex. This pulls the airborne particles against the walls due to the centrifugal force exerted which enables collection in the form of a concentrated fluid. This liquid can then be analysed for any airborne contaminants present.

Microarray Ltd. specialise in producing tunable ultrasensitive biosensor technologies that enable detection of specified substances in real-time situations. This involves embedding or immobilising a suitable enzyme or other biological reagent onto the surface of an electrode and analysing the change in response when the sensor is exposed to the analyte in question. This project will exploit the Coriolis®μ air transitory technology in conjunction with Microarray Ltd.'s ultra-sensitive monitoring apparatus.

By exploiting these two technologies in conjunction with each other, the aim is to produce an ultra-sensitive, real-time and relatively inexpensive approach to detecting the volatile vapours associated with an explosive substance.

1.1. Research objectives

The overall objective of this research is the development of a detection technique for explosives and explosive related compounds. Characteristics of the final analytical tool will be to:

1. **Achieve a rapid response time**

   Due to the sensitive nature of detection of substances of this kind, it is necessary to obtain real-time results so that preventative action may be taken.

2. **Provide a highly sensitive test and be capable of low limits of detection**

   This device needs to be capable of detecting trace amounts of explosive related substances in various mediums as bulk substances may not be present. Trace amounts may include residues and particles found on clothing due to previous handling of explosives.

3. **Achieve a unit cost that is inexpensive to produce and maintain**

   For this technology to be widely available and widely utilized it needs to be inexpensive to purchase and use. In this manner, the technology can effectively be located in all public places.

4. **Develop a test that is simple to use and interpret**

   This technology must be open to all to use, not requiring a resident scientist to interpret results or maintain the system. This also helps to keep costs low.

5. **Have a low chance of false positive or negative readings**

   Both a false positive and negative reading can have devastating effects and so this technology needs to as accurate as possible.

This will be achieved by meeting all of the following intermediate objectives:

- The use of screen-printed carbon electrodes to keep unit cost and complexity low;
- Utilisation of commercially available substrates where possible such as, for example, appropriate enzymes for the analysis of various explosive substances;
- Minimising the size of the design for increased future portability and miniaturisation;
- The immobilisation of enzymes upon the surface of an electrode;
- Developing microelectrode arrays with the intention of increasing the sensitivity of the design;
- Incorporation of the microarray biosensor platform into the cyclonic collection system.

2. Introduction and literature review

2.1. Introduction to explosives

An explosion can be described as "*a sudden and violent release of physical or chemical energy, often accompanied by the emission of light heat and sound*" (White, 2004). There are two types of explosive substance (see Figure 2.1): deflagrating, or low explosives, have a subsonic rate of reaction; whilst detonating, high explosives, have a supersonic reaction velocity. High explosives may be subdivided into primary and secondary classes of explosives. Primary explosives tend to be extremely sensitive and prone to detonation through shock, friction and burning. Secondary explosives are less sensitive and often more powerful than primary explosives. Detonation of a secondary explosive is usually achieved via the use of a small amount of primary explosive as an initiator.

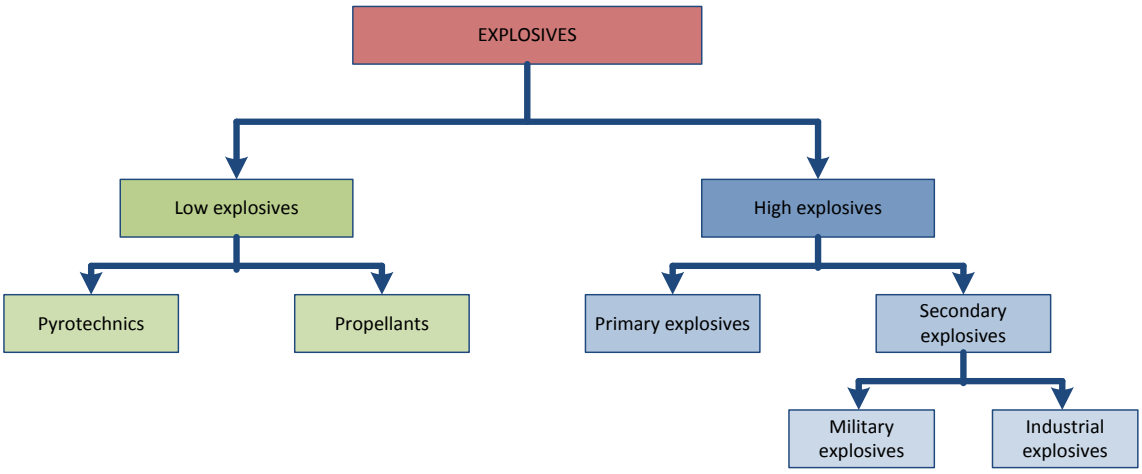

Figure 2.1 - Classification of explosives

An explosive compound requires a mixture of fuel with an oxidising agent; as the reaction propagates at high speeds, the oxidising agent becomes the limiting factor as further oxygen cannot be drawn from the air. Nitrogen atoms within the explosive enables a highly exothermic decomposition - this being the reason that explosive compounds often contain nitrogen although structures with a strained ring or with a

high enthalpy of formation can also react explosively (Moore, 2004). There are a number of peroxide based explosives that are extremely sensitive to shock and friction and produce a lower detonation velocity; consequently these are not used for mainstream activities. These are of particular forensic interest as they may be produced with ease and are, therefore, often used by terrorists.

2.2. Explosive detection technology

Section 2.2 forms the basis of the review paper, the published version can be found in appendix 1

Concerns relating to homeland security have given rise to increased research into explosive detection as well as further developments for existing analytical techniques to enable faster, more sensitive, less expensive and simpler determinations to aid in the early identification of explosives.

Traditional security measures at airports have included the use of metal detectors to identify weapons that may be concealed in conjunction with x-ray machines for viewing the contents of baggage. One major problem is that explosive substances are often not easily detectable using conventional approaches and in this context many terrorist groups have adapted to avoid the use of metallic objects. Approaches to detect volatile substances, such as ion mobility spectrometry in conjunction with swabbing, while in routine use - are largely only suitable for the screening of items of hand baggage.

For detection of explosive substances in the air, issues related to the low vapour pressures of many explosives are only exacerbated further when these explosives are wrapped or packaged to avoid detection. The increasing use of peroxide based explosives has led to much research into detection of this group of explosive substances, the issue being that many current chemical identification techniques are based on the nitrogen and carbon content of a substance to identify it as being of interest and this practice is not suitable for peroxide explosives.

This review primarily focuses on the detection of concealed explosives and their precursors / degradation products. Areas that are covered include trace, bulk and vapour detection techniques and those described for the stand-off detection of explosive substances. Peer reviewed papers from the last 5 years are presented as well as referring to other review papers of particular interest.

2.2.1. State of the art and widely used approaches for the detection of explosives

2.2.1.1. Ion mobility spectroscopy

Ion mobility spectrometry (IMS) is one of the most widely used detection techniques in routine use due to its ability to characterise the sample both qualitatively and quantitatively - as well as the very low detection limits that are often attainable. The reader is referred to a 2001 critical review of ion mobility spectrometry for the detection of explosives and explosive related compounds (Ewing et al., 2001).

IMS characterises a sample through the mobility of ions within the gas-phase of the instrument whilst an electric field is applied (see Figure 2.2). The sample vapours are ionised at atmospheric pressure before introduction into the drift tube. The drift times are related to the mass of the ions and by determining the mass/charge ratio, it is possible to identify components within the sample through comparison with known standards.

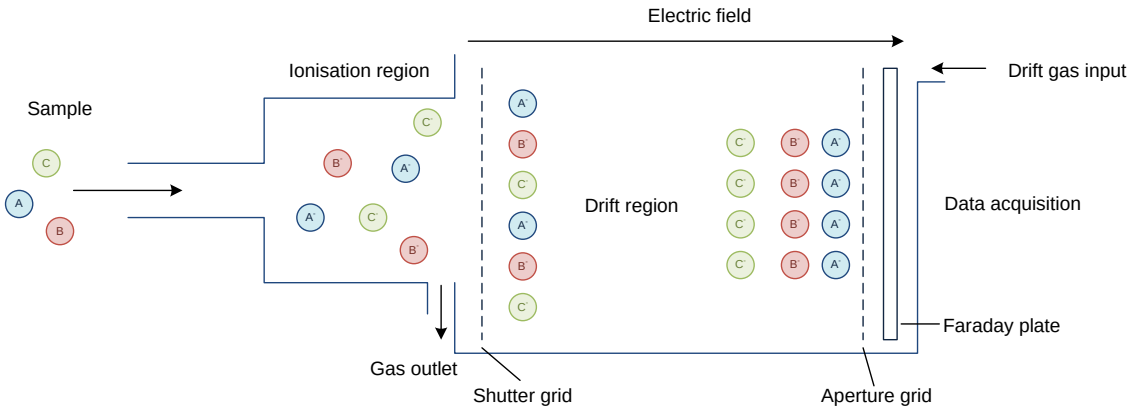

Figure 2.2 - A schematic representation of a simplified ion mobility spectrometer

Most commercially available apparatus use ^{63}Ni or ^{241}Am (Ewing and Waltman, 2009) as the ionisation source. The radioactive nature of these ionisation sources, however, can cause concerns relating to safety and environmental impact. As such, there has been investigation into alternative sources for ionisation with a focus towards negative corona discharge approaches (Ewing and Waltman, 2009; Khayamian et al., 2003).

Corona discharge as an ionisation source does have some associated complications, namely the variation of reactant ions produced, as compared to those gained with a ^{63}Ni source – as well as susceptibility to degradation and failure at the discharge point. Waltman et al., 2008, described a distributed plasma atmospheric pressure ionisation source that involved the application of a high-voltage alternating current across a dielectric to produce plasma within which the sample was ionised (Waltman et al., 2008). This technique was reported to be unaffected by tip erosion (of which corona discharge approaches can be prone) – and moreover requires less power than corona discharge sources.

Investigation into enabling the miniaturisation and portability of IMS apparatus for field deployment has increased over recent years. Tabrizchi and Ilbeigi, 2010, investigated a positive corona discharge technique that, with the addition of a curtain plate that prevents the diffusion of NO_x into the ionisation region, allowed analysis in air as opposed to nitrogen, thus decreasing the complexity of the device (Tabrizchi and ILbeigi, 2010). A shortening of the length of the drift tube and minimising the ionisation source would usually be associated with a corresponding decline in sensitivity, however, the use of a capacitive-transimpedance amplifier has been illustrated to offer resolution comparable with, and sensitivity exceeding, commercial bench top instruments (Babis et al., 2009). An ion focussing aspiration condenser has been described where two parallel gas flows travel through a transverse electric field; the upper flow contains the ion stream which is then geometrically focussed until the ions are forced into the lower gas stream and onto the base electrode. The different ion species are separated by their mobility into separate beams and then detected. This apparatus typically uses less power, is less costly to manufacture as well as being smaller than many commercial instruments – and for these reasons may be incorporated into a hand-held system (Zimmermann et al., 2007).

Martin et al., 2007, describe a micro-fabricated hotplate coated with a sorbent polymer as a technique to trap analytes of interest prior to analysis with IMS; this technique reportedly enhanced sensitivity by at least one order of magnitude (Martin et al., 2007). A technique to decrease false positive results without any significant

increase in analysis time has been described, using a short column packed with adsorbent packing material; this method enables pre-separation after ionisation of the sample and furthermore offers the capacity to retain interferences for longer, thus minimising their influence on the resulting spectra (Kanu et al., 2008).

2.2.1.2. Mass spectrometry

Mass spectrometry (MS) in various forms has been used successfully to detect explosives due to its specificity in identifying substances and the speed at which analyses are completed. Due to the size and expense of previous MS devices, this technique has not been widely used within some security led areas. Mass spectrometry separates and analyses the chemical composition of a substance according to its' mass-to-charge (*m/e*) ratio. Two methods by which this may be achieved include time separation and geometric separation based approaches. There are many forms of mass spectrometry including, for example: quadrupole, ion trap, time-of-flight (TOF) and tandem based techniques (Yinon, 2007).

The use of a mass spectrometer for security or forensic analyses would often involve the substance of interest either being within a complex sample matrix or absorbed upon a surface. Work has been undertaken towards improving the techniques for the introduction of samples into the mass spectrometer. The aim is not only the improvement of selectivity towards material of interest, but also to remove the necessity for pre-concentration of samples before analysis. In addition to these factors, miniaturisation and reduction of unit cost have also been key research areas.

Ambient ionisation techniques have been investigated to address some of the issues mentioned above. Atmospheric pressure chemical ionisation (APCI) involves the ionisation of a sample and carrier gas within the gas phase using corona discharge. Song and Cooks, 2006, further developed this technique by using carrier gases acetonitrile and air to enable selective detection of nitroaromatic explosives through the formation of adducts that subsequently fragment in a predictable manner (Song and Cooks, 2006). APCI has also been investigated using a reversed gas flow

introduction into the source which improves the ionisation of nitro-compounds before introduction into the tandem mass spectrometer (Takada et al., 2002). Samples were collected both using a swab and directly from the skin of a hand that had handled explosive material. Using this approach 2,4,6-trinitrotoluene (TNT) was detected at a concentration of 3 pg L^{-1}. A single proton laser ionisation technique has been described as a rapid laser-based technique and enables explosive detection with little fragmentation, thus allowing easier identification of the parent ion (Mullen et al., 2006). Limits of detection for nitrobenzene and 2,4-dinitrotoluene (DNT) were reported to be 90-130 ng L^{-1} and 320 ng L^{-1}, respectively. This technique was, however, only suitable for molecules with an ionisation energy above 10.49 eV.

Desorption electrospray ionisation (DESI) enables analysis of the substance of interest in its ambient environment by bombarding it with a mist of electrically charged droplets so creating ions which are drawn into the mass spectrometer with a vacuum (Cooks et al., 2006). This technique has been employed in the swift and specific detection of explosives on skin (Justes et al., 2007) and within complex matrices such as diesel fuel and lubricants (Cotte-Rodríguez et al., 2008). Direct analysis in real time (DART) is a technique similar to DESI in that a sample may be analysed in its ambient location without preparation; however, in DART an electrical potential is applied to a carrier gas and the resulting excited-state species desorb molecules from the sample which are introduced into the mass spectrometer (Cooks et al., 2006; Takáts et al., 2004). This technique has been comprehensively tested on various surfaces including clothing, currency and concrete – as well as a wide variety of chemicals of interest (Cody et al., 2005; Nilles et al., 2010). A desorption corona beam ionisation source (DCBI) is also able to work under ambient conditions without preparation of the sample. This technique is similar to DART, however in this case a visible thin corona beam is generated which may be used to analyse a specific area of the sample surface or even to visualise the surface of the sample on a molecular level (Wang et al., 2010). The reader is referred to several recent reviews that consider the advancements in ambient mass spectrometry in greater depth (Alberici et al., 2010; Green et al., 2010).

The size of mass spectrometers have previously presented a drawback to their use, however, much work has been undertaken into the miniaturisation of components and addressing safety considerations to enable the development of field deployable instruments. A simulation was undertaken in 2004 to establish the worth of a miniaturised system involving an array of micrometre sized cylindrical ion traps that decreased the voltage necessary for operation and the resulting size of the device in its entirety (Blain et al., 2004). The use of DESI with a portable mass spectrometer has demonstrated rapid detection of explosive compounds in situ from a variety of surfaces; for example with RDX (1,3,5-Trinitro-1,3,5-triazacyclohexane) on paper, a LOD of less than 1 ng was observed (Mulligan et al., 2006). Sanders et al, 2010, demonstrated the detection of explosives on surfaces with a miniaturised system capable of detecting negatively charges ions. Samples of explosives were randomly applied to a large surface in 1μg cm^{-2} quantities and a DESI mass spectrum corresponding to each of the explosive signals was observed (Sanders et al., 2010). Further investigation into the use of atmospheric pressure ionisation techniques with a cylindrical ion trap field-deployable mass spectrometer setup has demonstrated LOD of 1 ng and 250 pg for RDX and PETN (pentaerythritol tetranitrate) respectively (Wells et al., 2008). A system integrating three methods has recently been described, employing thermal desorption, single photon ionisation and ion trap mass approached. This system was tested using pure samples and those within a matrix. While significant fragmentation with those complex samples was found, the system was found to be free from false readings (Schramm et al., 2009).

2.2.1.3. Terahertz spectroscopy

The field of terahertz (THz) spectroscopy has been investigated many times over previous years as a technique for the detection of explosive vapour signatures (Leahy-Hoppa et al., 2009; Woolard et al., 2005; Liu et al., 2007). There have been, however, drawbacks associated with this technology that had prevented development into a feasible system, and these include: the frame rate speed, a loss of attenuation as distance from sample increases, and, power requirements for the system (Federici et

al., 2005). Recently some of these issues have been addressed and the technology is further being considered as not only an explosive detection method, but also a way to detect weapons and other concealed objects within luggage and beneath clothing. Terahertz radiation lies in the far infra-red region – from 0.1 to 10 THz. In this range waves can penetrate through many non-polar dielectric materials, such as wood or leather, and the low photon energies are at a level one million times less than that of X-ray photons. Most explosives and explosive related compounds have spectral fingerprints within this range as many apparatus operate within the range 0.1-2.0 THz; this highlights THz radiation as a prospective sensor and imaging agent for the detection of concealed explosive substances.

Liu et al., 2006, described the detection and identification of both exposed and covered samples of RDX using diffusely reflected THz waves (Liu et al., 2006). When the THz waves strike a smooth sample surface, the reflected beam has the same angle as the incident angle; this is known as specular Fresnel reflection. In reality, the sample surface is not usually smooth or aligned precisely in the THz beam and consequently the direction of detection is difficult to determine. As such, studying the diffuse Fresnel reflection (the reflection angle gained when a THz wave hits an uneven section of the surface) is more applicable to field-based analyses. Using this technique, Liu et al demonstrated the detection of RDX, exposed and covered by various materials, with a consistent fingerprint present at 0.82 THz.

Chen et al., 2007, investigated the absorption spectra of seventeen explosives and explosive related compounds (ERC) using THz spectroscopy (Chen et al., 2007). Most of the substances examined exhibited characteristic absorption features in the 0.1-2.8 THz range. These results may be used to form a fingerprint database of explosives and ERCs. Through improvements in emitters and sensors, new spectral features have also been established for explosives within the frequency region of 3 – 6 THz (Woolard et al., 2005; Liu et al., 2007; Leahy-Hoppa et al., 2007).

Work has been undertaken into the influence of confusion materials such as, for example, food or toiletries, on the resulting spectra of any explosive compound also present (Lo et al., 2006). It was established that while most of the confusion materials

do not exhibit sharp spectral features in the terahertz region substances containing sugar did have a spectral signature – although this does differ from the explosive substances within the test and so did not cause interference to identification.

2.2.1.4. Olfactory type sensors

Dogs have long been known to have a highly developed sense of smell and this has been exploited for the detection of explosives since World War II (Furton and Myers, 2001). The use of sniffer dogs for the detection of volatile explosive vapours is still widespread due to their fast, directional and real-time capabilities. Some studies have been undertaken into the reliability of canines for detection of explosives as the inconsistency between different dogs and the same dogs at different times (Gazit and Terkel, 2003). Other animals have also been studied to establish any suitability for vapour detection. Rats have a sensitive and discriminating olfactory sense and have been shown to correctly discriminate between odours and alert when explosives are present using a remote monitoring technique (Otto et al., 2002). Insects, such as *Drosophila melanogaster*, have also been investigated due to the capability they have to detect a large range of odours and the simple olfactory system they possess. Incorporation of insect olfactory receptor neurons into a biosensor array has been reported by Marshall et al, 2010, with some success towards detecting illicit substances (Marshall et al., 2010).

There has been work attempting to establish the method by which an animal is able to detect an explosive target, whether it is through establishing an olfactory search image (Gazit et al., 2005) or if the olfactory ability is predetermined by the polymorphisms in olfactory receptor genes - in this case, of the canine (Lesniak et al., 2008). Detection of TNT and RDX has been demonstrated with olfactory sensory neurons obtained from rats and pigs (Corcelli et al., 2010), suggesting that explosive compounds do indeed interact with and activate olfactory receptors.

A comprehensive review describing fluid dynamic sampling and its potential relationship to artificial olfactory devices has been published (Settles, 2005) which

includes a broad discussion of contemporary artificial sampling techniques as well as suggestions for future research areas.

A table documenting those state of the art explosive detection systems that are currently available for commercial use is presented in Table 2.1 including information with relation to sensitivity, price and weight – all aspects this PhD project seeks to address.

Table 2.1 - Comparison of commercial explosive detection devices (from Caygill et al., 2012)

Comparison of commercial explosive detection devices

Company	Cost ($K)	Detection method	Advertised sensitivity	Weight
Barringer Instruments, Inc. IONSCAN 350	0.25	IMS	50-200 pg	105 lb
Barringer Instruments, Inc. IONSCAN 400	50	IMS	50-200 pg	60 lb
Electronic Sensor Tech, Inc. EST Model 4100	60	GC/SAW	100 ppb	35 lb
EXSPRAY Field Test Kit Model M1553	25	Colormetry	20 ng of most nitrated high explosives	3 aerosols, 1 lb
GE EntryScan3 "Puffer"	160	IMS	16 common explosives	Custom
Intelligent Detection Systems ORION	70	GC/IMS	pg-ng	240 lb
Intelligent Detection Systems ORION Mail Scanner	75	GC/IMS	pg-ng	240 lb
Intelligent Detection Systems ORION Plus	155	GC/IMS	pg-ng	240 lb
Intelligent Detection Systems ORION Walk-Through	300	GC/IMS	pg-ng	Custom
Intelligent Detection Systems SIRIUS	75	GC/IMS	pg-ng	240 lb
Intelligent Detection Systems V-bEDS	Custom	GC/IMS	pg-ng	Custom
Ion Track Instuments Exfinder 152	5	GC/ECD	20 ng of most nitrated high explosives	1.5 lb
Ion Track Instuments ITEMISER	44	IMS	100-300 pg	43 lb
Ion Track Instuments ITMS Vapor Tracer	38	IMS	100-300 pg	7 lb
Ion Track Instuments Model 85 Dual Scan	52	GC/ECD	1 part EGDN vapor in 10^{11} parts air	600 lb
Ion Track Instuments Model 85 Entry Scan	52	GC/ECD	1 part EGDN vapor in 10^{11} parts air	600 lb
Ion Track Instuments Model 97	20	GC/ECD	Most nitrated high explosives	40 lb
JGW International, Ltd. Graseby GVD4	5	GC/ECD	Explosive vapor exceeding 1 in 10^{9}	1.6 lb
JGW International, Ltd. Graseby GVD6	16	IMS	Explosive vapor exceeding 1 in 10^{9}	21 lb
JGW International, Ltd. Graseby PLASTEC	35	IMS	1 ng of TNT, NG, RDX, PETN	38 lb
MSA Instrument Division FIS	29	FIS	10-1000 ppt	20 lb
Scintrex/IDS EVD-3000	23	TR	< 1 ppb or < 100 ng for particulate	7 lb
Scintrex/IDS EVD-8000	43	GC/ECD	< 50 ppt or < 5 ng for particulate	48 lb
Smiths, IONSCAN 500DT	49	IMS	> 40 substances	43 lb
Thermedics Detection, Inc. EGIS Model 3000	150	GC/CL	All nitrogen based explosives	400 lb
Thermedics Detection, Inc. SecurScan Portal	300	GC/CL	All nitrogen based explosives	Custom
VIKING Instruments Spectra Trak	70	GC/MS	Low ppb by volume	150 lb
XID Corporation XID Model T-54	13	GC/ECD	0.01 ppb	18 lb

Adapted from: "Guide for the Selection of Commercial Explosives Detection Systems for Law Enforcement Applications", NIJ Guide 100-99. C.L. Rhykerd, D.W. Hannum, D.W. Murray, J.E. Parmeter, National Institute of Justice

CL = chemiluminescence; ECD = electron capture detector; SAW = surface acoustic wave; TR = thermal redox.

2.2.2. Spectroscopic techniques

2.2.2.1. Infra-red spectroscopy

Fourier transform infra-red (FTIR) spectroscopy is a technique largely used in to replace the more traditional dispersive instruments; this enables a considerable decrease in the time taken for sample analysis since it is capable of scanning all IR frequencies simultaneously rather than individually. An FTIR spectrum obtained was shown to allow identification of substances through its absorption at different wavelengths of light.

Primera-Pedrozo et al, 2009, reported a technique for the detection and quantification of high explosive residues on metallic surfaces using fibre optic coupled reflection/absorption infrared spectroscopy (RAIRS). When an infrared beam is directed at a smooth surface it passes through the sample and is reflected back through this coating again; this is known as specular reflectance and is the basis for the RAIRS technique. Coupling this technique with a Fourier transform probe, containing fibre optic cables that transmit in the mid-infrared range, enables analysis of samples in-situ rather than within the spectrometer sample chamber. Micro-RAIRS may also be used for topographical analysis of the substrate surface before sample examination. Low detection limits were reported of 160 ng cm^{-2} for TNT and Tetryl; 220 ng cm^{-2} for PETN and DNT; and 400 ng cm^{-2} for HMX (Octahydro-1,3,5,7-tetranitro-1,3,5,7-tetrazocine) (Primera-Pedrozo et al., 2009).

The detection and identification of explosive particles in fingerprints has been described by Mou and Rabalais, 2009, using attenuated total reflection-Fourier transform infrared (ATR-FTIR) spectromicroscopy. Particles are first located within the ridges of the fingerprint using the ATR probe and then analysed with infrared radiation. The ATR-FTIR technique is classed as non-destructive as the ridge patterns of the fingerprints remain the same and are therefore suitable for subsequent identification. The explosives particles present are able to be identified using a spectral library; however, in this work the library was not specific and did not contain

the spectra of TNT and DNT - the analogue dinitrobenzene (DNB) was identified as closely matching those explosive compounds (Mou and Rabalais, 2009).

2.2.2.2. Laser-induced breakdown spectroscopy

Laser-induced breakdown spectroscopy (LIBS) uses a high intensity laser to vaporise the sample under investigation creating a plasma plume, the light subsequently emitted from this plasma enables characterisation of the sample. LIBS, as a detection technique, holds many advantages especially in the field of explosives detection some of which include: no need for sample preparation; the ability for real time results; apparatus that may be ruggedized and miniaturised for field work; a sensitive technique requiring only a small sample; and, the capacity for stand-off detection approach. For a more in-depth look at LIBS for explosive detection the reader is referred to Gottfried et al, 2009 (Gottfried et al., 2009).

Despite the obvious advantages of LIBS as a detection method, there are drawbacks associated with this technique. To enable use as a stand-off detection method, detection will usually need to be performed in the open air. The main constituents of many explosives are carbon, hydrogen, nitrogen and oxygen and it is the ratios of oxygen and nitrogen relative to carbon and hydrogen that form a distinguishing characteristic of many high explosive compounds. Inferences from oxygen and nitrogen in the atmosphere affect these ratios and, therefore, the characterisation of explosive compounds. This was illustrated by Lucena et al, 2010, in a comparison detection study of explosives in air and in helium (Lucena et al, 2010). De Lucia et al, 2007, proposed the use of a double pulse LIBS technique to diminish the effects of atmospheric interference. The double pulse increased the amount of excited atoms in the sample due to an increased plasma plume and it is believed that this also decreased the atmospheric gas density around the sample. This technique removed most of the atmospheric interference and aided discrimination between the explosive RDX and an organic material, diesel fuel (De Lucia Jr. et al., 2007).

To enable the detection of explosive materials at stand-off distances and in difficult to access areas Bohling et al, 2007, reported a LIBS system coupled to a probe like device which consisted of optical fibres, a focussing lens and a mechanical shutter system to protect the optics from any debris during use. The active fibre acts as an amplifier for the microchip laser and the passive optical fibre directs the laser pulses to the tip of the sensor. This system has the potential to be attached to an automated device and with principle component analysis (PCA) and neural networking, also reported in this paper, an identification of hidden objects was demonstrated with accuracy above 80% and false identifications below 5% (Bohling et al., 2007).

Dikmelik et al, 2008, proposed the use of femtosecond laser pulses to decrease the amount of fragmentation during the LIBS process. Nanosecond laser pulses are generally utilised although this tends to fragment a sample into its elemental constituents. When ultrafast excitation is employed, the fragmentation is less severe and emission is observed from CN and C_2 molecules which may be used as a marker for, in this case, TNT (Dikmelik et al., 2008).

2.2.2.3. Raman spectroscopy

Raman spectroscopy measures the vibrational transitions in a sample through the collection and analysis of scattered photons once the sample has undergone laser excitation. Resulting spectra can offer a fingerprint of the item under analysis that can identify individual components of the sample. Due to this, the near instantaneous results and possible stand-off capacity (Izake, 2010), the offer of this technique for possibly being used as an explosives detection method has met with considerable work within this area. A review that described advances in the capacity of portable Raman instrumentation has also highlighted some of the issues relating to producing instrumentation for field deployable apparatus (Moore and Scharff, 2009).

Pacheco-Londoño et al, 2009, reported the use of a continuous wave laser technique to increase the resulting SNR and thus improve stand-off distances for explosive detection. Detection at distances of up to 7m was described for the explosives TNT,

DNT, RDX, TATP (triacetone triperoxide) and C4. Semtex could not, however, be distinguished from the background interference due to the fluorescent nature of the explosive mixture. Limits of detection were achieved at 2 mg for DNT and TNT; 3 mg for RDX and C4 and 10 mg for TATP at a distance of 7 m (Pacheco-Londoño et al., 2009). This study was not, however, conducted in a manner that transfers readily into a field-operable device since determinations were undertaken indoors and in the dark to minimise interferences.

A study into stand-off explosive detection in realistic field environments was undertaken by the Swedish Defence Research Agency. Measurements of various improvised explosive devices (IEDs) at stand-off distances of 20, 30 and 55 m were performed in varying weather conditions – from snow to sun and temperatures ranging from +22 ºC to -8 ºC. The instrumentation, including a 532 nm pulsed laser source, was kept inside throughout the study that proved to be insensitive to weather variations. Bulk quantities of samples were satisfactorily identified through both regular glass bottles (green and brown) and PET (polyethylene terephthalate) containers (Pettersson et al., 2009). Issues that may arise include possible interfering fluorescence in the visible spectral region due to the container as well as how this system may cope with detection of trace amounts of the explosive substance.

The issue of interfering fluorescence may be addressed using a narrow gate width to exclude the majority of the interfering agents whilst still collecting the Raman signal relating to the sample. Fleger et al, 2009, propose such a technique – the interaction time for Raman scattering is less than 1 ps but luminescence takes much longer between excitation and decay. As such, when a sample is interrogated with a short laser pulse, all Raman photons are generated almost instantaneously but the luminescence photons are generated slower. When the detection system has a narrow gate, all Raman photons will be collected with the minimum amount of luminescence. This allows a greater signal to noise ratio and enables detection of explosive substances with strong luminescent properties, such as Semtex (Fleger et al., 2009).

The detection of explosive particles with backward coherent anti-Stokes Raman scattering (B-CARS) was studied by Portnov et al, 2010. Coherent anti-Stokes Raman scattering (CARS) involves three laser beams which interact with the sample and generate a new coherent optical signal at the anti-Stokes frequency. A spectrum with the same information as a spontaneous Raman spectrum is obtained though, with much higher sensitivity. B-CARS utilises the signal obtained from the diffuse reflections gained when a sample is interrogated using CARS. Using this technique the spectral fingerprint remains fundamentally the same as when processed with Raman, but the intensity is much greater and signal to noise ratio more favourable. Stand-off distances were extrapolated to be as great as 180, 21 and 13 m for potassium nitrate, PETN and RDX respectively (Portnov et al., 2010).

Confocal Raman microscopy enables the detection and identification of explosive substances and can also provide information on physical properties such as the crystal structure, molecular orientation and possible interactions. Raman microscopy uses a focused laser beam within a microscope and operates in a confocal mode through the use of an aperture within the microscope - this enables depth recognition alongside the spectral profile usually gained with Raman spectroscopy.

Confocal Raman microscopy has been utilised for the detection and identification of explosive substances on the surface of human nail and from beneath a coating of nail varnish. It was discovered that although the nail itself produced spectral bands they did not inhibit identification of the explosives under examination, in this case PETN, TNT, AN (ammonium nitrate) and hexamethylenetetramine (HMTA), since interference could be excluded with careful focussing of the confocal beam. Coating the explosive and nail with nail varnish presented no problem for detection, with a two-dimensional Raman map gained for PETN and with no significant interference in the Raman spectra (Ali et al., 2009a). The same technique has been investigated for the detection of single particles of the explosives: PETN, AN and TNT (Ali et al., 2009b); and HMTA and pentaerythritol (Ali et al., 2009c), on clothing. These studies looked at both natural and synthetic fibres, dyed and undyed, to imitate the in-situ detection of a person who may have handled explosive substances. Confocal Raman microscopy produced

identifiable Raman fingerprints for each of the explosive compounds where each explosive particle was within the maximum dimensions of 5-10 µm. Interference from the fibres, although present, did not fall within the Raman spectral profile of explosives tested. The main issue with this technique would appear to be visual identification of the explosive particles prior to testing.

2.2.2.4. Cavity ring down spectroscopy

In cavity ringdown spectroscopy (CRDS) a short pulse of light is injected into a resonant cavity which is surrounded by highly reflective mirrors. When sufficient radiation has built up within the cavity, the laser is turned off and the exponential decay of the intensity of the light is measured over time. The decay time for an empty cavity is then compared with one containing a substance of interest and a spectrum is obtained. The molecular absorbance, and therefore the concentration, may also be derived from the rate of decay. For a more in-depth overview of CRDS as a technique see Paldus and Kachanov, 2005, and Berden et al, 2000 (Paldus and Kachanov, 2005; Berden et al., 2000).

Ramos and Dagdigian, 2007, described a study into the use of ultra-violet CRDS as a means to improve on the low sensitivities related to infra-red CDRS. It was the case that IR-CRDS was able to detect the explosive related compounds 2,4-DNT and 2,6-DNT at concentrations 100 times less than their room temperature vapour pressures. The issue, however, was that this technique was unable to decisively identify specific samples due to its poor selectivity in the 240-260 nm spectral range (Ramos and Dagdigian, 2007a). This seems to be in opposition to IR-CRDS which has distinct spectral features but much lower sensitivity. There was also an issue with atmospheric interferences, especially ozone. It was suggested, however, that coupling this device with a less sensitive but more selective technique could overcome these problems. An increase in laser pulse energies may also lower the noise related to the photon decay; however, applying this technique to improve sensitivity also has the capacity to distort the decay profile through pre-dissociation of the compound leading to issues of identification (Ramos and Dagdigian, 2007b).

Snels et al, 2010, reported a feasibility study involving the use of flash heater in a CRD cell to evaporate solid explosive samples prior to detection in the near infrared (see Figure 2.3).

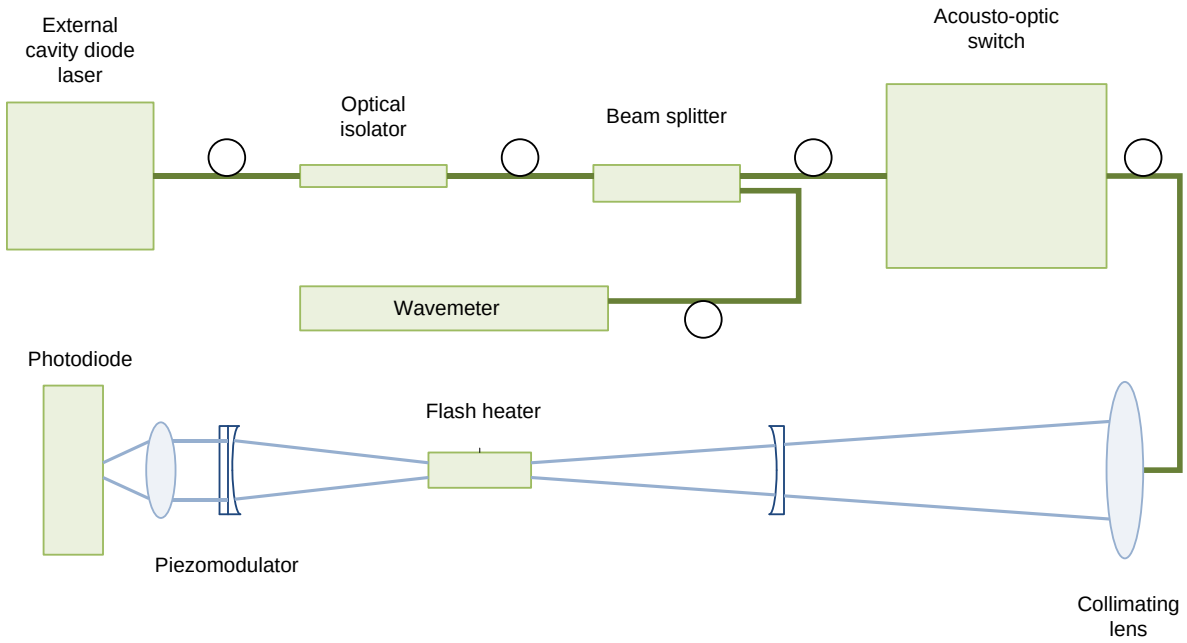

Figure 2.3 - A schematic representation of the cavity ringdown spectroscopic set-up as described by Snels et al, 2010.

This technique aimed to address issues previously described in the literature such as poor selectivity in the UV region and the inability to record a full CRD spectrum in short time periods when recorded in the mid-infrared range. The discrimination between three similar compounds, 2,4-DNT, 2,6-DNT and TNT, was possible with the use of PCA and detection limits being reported at around 75 ng. Suggestions to improve this technique include the use of higher reflectivity mirrors and alternative heating geometry (Snels et al., 2010). This technique was performed in ambient atmosphere with little interference, however, measurements at room temperatures were not possible and neither were investigations into explosive vapours in air possible.

2.2.3. Sensor techniques

2.2.3.1. Electrochemical sensors

Electrochemical sensors can be categorised into potentiometric (measurement of voltage); amperometric (measurement of current) and conductimetric (measurement of conductivity) based devices according to the transduction approach adopted (Singh, 2007). These types of sensor are fast, inexpensive with high sensitivity and a viable option for miniaturisation (Rabenecker and Pinkwart, 2009). Electrochemical detection techniques can respond to redox substances; the electrical output results from a flow in electrons or ions caused by the chemical reaction that takes place at the surface of the electrode. Due to this, the redox properties of nitroaromatic explosive substances ideally lend themselves to electrochemical detection. The detection of peroxide based explosives is more complex due to the fact they do not fluoresce, have minimal UV absorption and a lack of nitro groups – all necessary parameters upon which traditional detection techniques are based (Wang, 2007a). Electrochemical sensors in this context offer an opportunity to detect peroxide based explosives that would otherwise prove problematic.

Square-wave voltammetry (SWV) is an often described technique for field-based operations due to the speed of scan rates, the sensitivity and the compact, low power instrumentation available (Wang, 2006). Agüí et al, 2005, described a technique that coupled carbon-fibre microelectrodes with SWV to increase the surface area of the working electrode and also provide fissures within its surface into which nitroaromatic compounds adsorb. Resulting detection limits obtained were reported to be as low as 0.03 µg mL^{-1} (Agüí et al., 2005).

Cizek et al, 2010, reported a preliminary study into the integration of a preconcentration device to thermally desorb the TNT from the gaseous phase before electrochemical reduction with a screen-printed hydrogel-coated electrode using SWV. This preconcentration step allowed detection of TNT vapours from a solid sample upstream of the apparatus (Cizek et al., 2010).

A technique involving a layer by layer assembly of alternate layers of mesoporous SiO_2 (MSU) and polydiallyldimethylammonium chloride (PDDA) upon the surface of a glassy carbon electrode was found to increase pore volume, diameter and, therefore, surface area of the working electrode; this increased sensitivity to nitroaromatic compounds especially when at lower detection limits. This approach suffers, however, from an intrinsic issue with silica of poor conductivity which can have an effect on the performance of the sensor platform. The limit of detection for TNT was found to be 340 ng L^{-1} (Shi et al., 2007). Fu et al, 2010, reported the synthesis of a SiO_2 microsphere comprised of a mesoporous silica shell modified with 3-aminopropyltriethoxysilane (APTS) to attach amino functional groups. This system was applied to glassy carbon electrodes as a sensing layer for nitroaromatics, especially TNT. Using square wave voltammetry, a detection limit of 114 ng L^{-1} was achieved and 81% of this signal was still obtained with the same sensor after 30 days, demonstrating its shelf-life (Fu et al., 2010). Ordered mesoporous carbon (OMC) has, more recently, been investigated to improve sensitivity towards nitro-explosives and the performance of the electrochemical sensor. The OMC provided a much improved surface area, as with the silica based system, and an enhanced conductivity which produced a sensor with lower limits of detection (Zang et al., 2011).

The detection of peroxide-based explosives has become increasingly important due to the ease which some may be synthesised from commercially available substances and hence their link to terrorist activities. Lu et al, 2006, described a technique for rapidly monitoring liquid peroxide-based explosives using an electrode modified with Prussian-blue as an artificial peroxidase and amperometric detection of the resulting hydrogen peroxide generated (Lu et al., 2006). Detection limits were reported as 7.4 µg L^{-1} for TATP after a 15 s irradiation time. Parajuli and Miao, 2009, reported an electrogenerated chemiluminescence (ECL) technique that was enhanced (by up to 20 times) by the inclusion of silver nitrate at the platinum electrode. This system involved the oxidation of HMTD by the electrogenerated species allowing a detection limit of 1 mg L^{-1} to be achieved (Parajuli and Miao, 2009).

Wang and Pumera, 2006, produced a microchip flow-injection analysis for trace amounts of TNT. The authors described the need for 'lab-on-a-chip' technology to achieve a fast, simple and cheap alternative to laboratory-based techniques (Wang and Pumera, 2006). This approach used electro-osmotic flow to move samples through the microchip manifolds and measures response to TNT amperometrically. Amalgam mercury/gold disc electrodes were used due to their favourable signal-to-noise ratio and detection limits of 7 μg L^{-1} were described, with the added advantages of a high-throughput system and minimal sample consumption.

Chuang et al., 2010 reported a textile based electrochemical sensing system as a means to provide a wearable chemical sensor. Here, various textiles were analysed to assess performance as a screen-printed electrode and the breathable and waterproof fabric Gore-Tex (TM) was found to exhibit promising properties for use in this field. Properties such as, for example: hydrophobicity; consistent printing quality on the fabric and the subsequent electrochemical activity of the sensors. Detection of nitroaromatic compounds was demonstrated and an initial assessment into the resilience of the fabric as a sensor platform was conducted successfully.

The development of single use processes to enable disposable electrochemical sensing has become more desirable to facilitate a portable explosive sensor. Chen et al, 2006, described the use of a Nafion (TM) coated, preanodised screen-printed carbon electrode that increased the sharpness of peaks and, therefore, the ease of identification of substituent groups upon the nitroaromatic compound. Detection of TNT from spiked lake water was 95.7%, with this complex matrix only affecting the sample slightly (Chen et al., 2006).

Yu et al, 2009, reported the combination of electrochemical and piezoelectric transduction mechanisms as a detection technique, using the ionic liquid $BMIBF_4$ (1-methyl-3-butylimidazolium tetrafluoroborate) as both the electrolyte and the sorption solvent to enable this multi-faceted system. The accuracy of a system such as this was increased due to the validation that one system may have over the other (Yu et al., 2009).

2.2.3.2. Immunochemical

Immunochemical sensors exploit characteristics of the antibody-antigen reaction in such a manner that produces a device that can be highly specific to its target molecule. This feature and the fact that it is possible to produce antibodies for a specific purpose make this an expanding field of research into explosives detection.

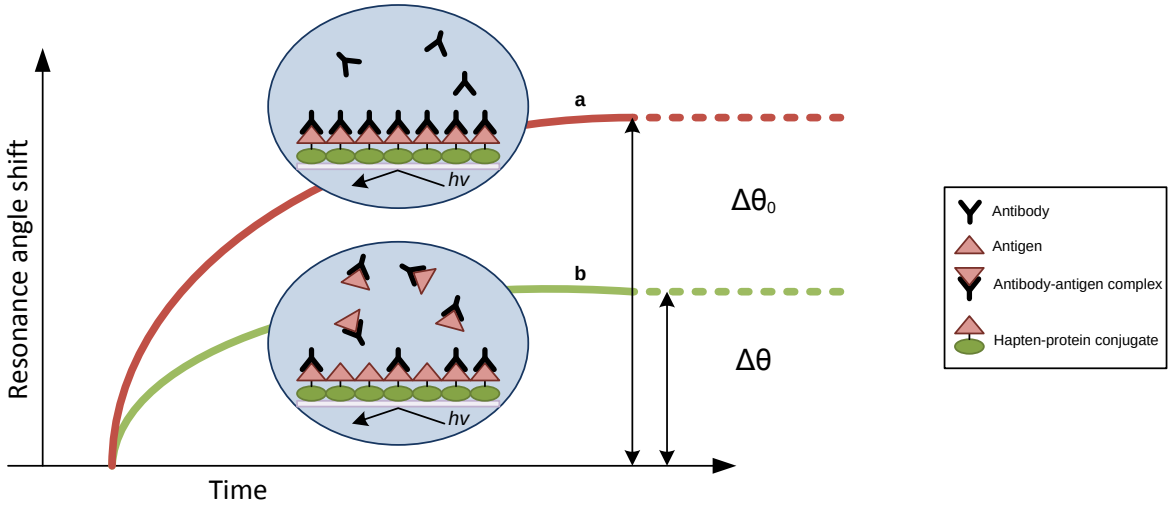

Figure 2.4 - A schematic representation of the principle of competitive inhibition assay on the surface plasmon resonance immunosensor where a). represents the SPR system and b). represents the decrease in resonance shift angle when the competitive analyte is introduced into the system.

A recent review by Smith et al, 2008, provides a more comprehensive report on not only immunochemical sensors, but also biosensors and biologically-inspired systems for explosive detection in general (Smith et al., 2008).

Anderson et al, 2006, reported a multiplexed immunoassay approach using a flow cytometer, the Luminex^{100}, which contains 100 different sets of fluorescent latex microspheres, each of which is encoded by two fluorescent dyes. The ratio of the emission recorded at two different wavelengths enables identification of each set. The limit of detection for TNT was found to be 1.0 µg L^{-1} (Anderson et al., 2006). Detection of peroxide based explosives using immunoassays have been less reported. Anderson et al, 2010, described the comparison of two monoclonal and one polyclonal

commercial antibodies as well as the development of llama polyclonal antibodies for use in the detection of PETN. As before, evaluation was performed with the Luminex^{100} flow cytometer. Binding was found to occur between bioconjugates of PETN and the antibodies but binding with the free PETN was limited (Anderson et al., 2010). This can often be the case when the target molecule is small and so further development within this area is necessary before detection of PETN in this manner becomes a possibility.

Surface Plasmon resonance (SPR) immunosensors act by detecting a change in the refractive index at the surface of the sensor due to an alteration in the binding of molecules immobilised on this surface. Where a large molecule binds with the immobilised antibody, a large signal is gained. Explosive molecules tend to only give rise to a small signal due to their relatively small size and this causes an issue with sensitivity, this is especially apparent in miniaturised systems. As such, amplification techniques have been investigated to improve detection of small analytes and competitive inhibition is often employed. Nagatomo et al, 2009, reported a novel oligo (ethylene glycol) (OEG)-based self-assembled monolayer upon a bare gold chip using an anti-DNT antibody for an indirect competitive binding effect. In the presence of DNT, there was an inhibition of surface binding, decreasing the SPR angle. This system exhibited high sensitivity for DNT, with a limit of detection of 20 ng L^{-1} (Nagatomo et al., 2009). A nano-scale biosensor chip surface modified with a polyamidoamine dendrimer was reported to enhance the anti-body surface loading capacity and increased the selectivity towards TNT molecules in a stable, easily regenerated system (Singh et al., 2009).

2.2.3.3. Luminescence sensors

Luminescence based sensors for detecting explosive compounds may be described as either direct or indirect detection methods. Direct detection techniques utilise any fluorescence which the sample may emit itself or through inducement with a chemical reaction. Indirect detection involves the implication of explosives being present through their effect on a fluorescent material such as, for example, via quenching.

While recent developments within this area are examined here, the reader is referred to a more comprehensive review of luminescence-based explosive detection methods available (Meaney and McGuffin, 2008).

Toal et al, 2006, reported a technique to visually detect the quenching of photoluminescence in the presence of nitroaromatic explosives using a metallole-containing polymer. Under illumination with UV light, quenching was observed and detection limits were as low as 5 ng for TNT. One issue with a technique such as this is that observation of a colour change can be a subjective when performed by eye and so combining this with another, more qualitative system or an automated approach may be necessary (Toal et al., 2007). This group's work was continued to make the sensor more selective by incorporating a tandem process that first quenches the metallole in the presence of nitroaromatics as described above; then a thin film of 2,3-diaminonaphthalene (DAN) is applied which cancels the polymetallole luminescence and then in the presence of nitroamine and/or nitrate-ester explosives a reaction with the DAN forms a blue luminescent complex (Sanchez et al., 2007b). An investigation into synthesising polymers and copolymers and their relevance to explosive detection was also undertaken by this group which reported some polymers able to detect nitroaromatic, nitro-amine and nitro-ester explosive compounds (Sanchez et al., 2007a). Further work was reported that coupled the tandem process mentioned previously with an efficient blue-emitting silafluorene-fluorene copolymer system that was able to detect trace particulates of samples of all of the nitro-based explosives, allowing detection limits as low as 1 pg cm^{-1} (Sanchez and Trogler, 2008).

Shi et al, 2008, described the quenching effect that nitroaromatic compounds have on oleic acid covered CdSe quantum dots. This work reported detection limits around 10^{-6} to 10^{-7} M for a range of compounds making this a viable screening technique. Further technique optimisation is necessary before it may be seen as a workable alternative to fluorescent polymers (Shi et al., 2008). The combination of quantum dots with a dendrimer, such as PAMAM (poly(amido amine)) generation 4 (Algarra et al., 2011), has been reported to increase biocompatibility and biostability and increase reactivity. Such improvements increased water solubility and as a consequence signal output.

Photo-fragmentation of nitro-based explosives at 193 nm has been demonstrated by Monterola et al, 2008. At this wavelength the NO_2 moieties are released from the compound and may be detected through their chemiluminescent interaction with a solution of luminol. Trace amounts of PETN were detected at 3 ppb (40 ng L^{-1}) and analysis of PETN in a soil matrix yielded a LOD range of 0.5-4.3 µg g^{-1}. This technique is fast and simple but does not identify the specific molecule, giving only a general identification of a nitro-based sample being present (Monterola et al., 2008).

Ponnu and Anslyn, 2010, produced a cyclodextrin (CD) sensor by combining the CD with a fluorophore, bis(phenylethynyl)anthracene (BPEA), to produce a cyclodextrin inclusion complex. The cavities of this complex are less polar than water and so are able to extract hydrophobic molecules from aqueous environments. When applied to solutions containing explosives, quenching occurred in the presence of nitroaromatic compounds – but not other nitro-based explosives. Quenching effects were found to be greater with the complex as opposed to the fluorophore alone (Ponnu and Anslyn, 2010).

Caron et al, 2010, reported a portable fluorescent detector capable of ultra-trace detection of the nitroaromatic compounds TNT and DNT, which was unaffected by environmental humidity or interfering substances (Caron et al., 2010b; Caron et al., 2010a). Although at present this device only detects nitroaromatics, a multi-faceted design may be possible using several fluorescent material platforms. A sensor array of commercially available fluorescent polymers was evaluated by Woodka et al, 2010, to attempt to limit the possibility of false positives due to a high concentration of non-explosive electron withdrawing compounds (EWC). The responses gained from a variety of explosives, explosive related compounds and non-explosive EWCs were analysed using principal component and linear discriminant analyses. The array was found to discriminate between the explosive, non-explosive and explosive related electron withdrawing compounds and in this way was demonstrated as a platform approach for minimising the likelihood of false positives (Woodka et al., 2010).

2.2.4. Nanotechnology

Nanotechnology has become a rapidly expanding area of research over recent years as techniques and knowledge have developed. Materials often possess unique characteristics when in a nanoscale form as compared to bulk materials and as such, the incorporation into existing techniques to enhance sensitivity and selectivity is an active area of research.

2.2.4.1. Molecularly imprinted polymers

Molecularly imprinted polymers (MIPs) are generated through both covalent and non-covalent interactions of functional monomers with the molecule of interest or its analogues, which acts as a template. MIPs allow the formation of molecules with recognition sites specific for a target analyte producing a substance specific coating which may then be incorporated onto a sensing platform. MIPs are stable and robust which accounts for the interest in researching possible uses for them as sensing materials. A more extensive review into the use and synthesis of these polymers can be found in the literature (McCluskey et al., 2007).

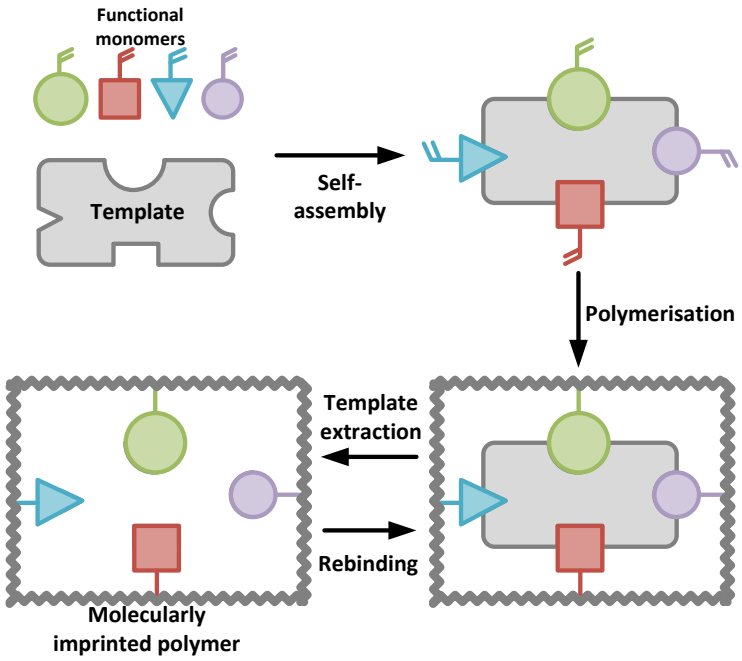

Figure 2.5 - A simplified schematic representation of the development of a molecularly imprinted polymer

The proposal of MIPs for the detection of explosive compounds was first described by Chianella et al, 2004 (Chianella et al., 2004), where MIPs were designed for PETN, RDX, Tetryl and TNT. A patent filed by Schwartz et al, 2005, described an array of MIP coated fibre-optic cables which, when coupled to a suitable algorithm program, is capable of identifying either single or multiple explosive target molecules (P. D. Schwartz, G. M. Murray, O. M. Uy, et al.).

More recently, research has been undertaken into the optimisation of polymerisation techniques and assessing the merit of various monomers for the synthesis and subsequent specificity towards explosives compounds. Bunte et al, 2007, described the comparison of various monomer/solvent complexes and the use of a spray gun, alongside conventional techniques, to apply the thin film to a quartz crystal microbalance (QCM). Response times for TNT were found to be in the pg per µg MIP per minute range (Bunte et al., 2007). The same group, based at the Fraunhofer Institute for Chemical Technology, described further work into MIP application using a nanoplotter and a spin coating device to assess the resulting quality of the layers (Bunte et al., 2009) as well as the use of a continuous segmented flow microreaction process to allow uniform sized pre-polymer droplets to be generated. This enabled the size required to be defined, so minimising the need to sieve before use in columns (Roeseling et al., 2009).

Stringer et al, 2010, described the use of quantum dots as the fluorescent species in a fluorescent-labelled MIP system. The quantum dots, rather than incorporation into the polymer matrix, were inserted post-processing to extend the shelf-life of the system. Lower limits of detection were found to be 30.1 and 40.7 µmol L^{-1} for DNT and TNT, respectively (Stringer et al., 2010). Whilst this system was unable to match detection limits of other MIP based detection techniques (Thomas III et al., 2007), response times were found to be as low as 1 minute.

2.2.4.2. Nanotubes

The unique properties of nanotubes have generated great interest towards the study and development of this field of research. These include, for example, their electrical properties as conductors, insulators or semiconductors, depending on the structure and their high thermal conductivity, but only in the axial direction – thermal conductivity is low in the lateral direction. There are many more examples of their unique kinetic, optical and mechanical properties that ensure this area of study is continually expanding (Saito, 1998).

Wang et al, 2004, reported the surface modification of glassy carbon electrodes with multi-walled carbon nanotubes (MWCNT) for the detection of TNT with adsorptive stripping voltammetry (ASV). Modification of the electrode in this manner aided the accumulation of TNT at the electrode surface due to the increased surface area. This resulted in quantification of TNT down to the sub-µg L^{-1} level and a LOD of 0.6 µg L^{-1} (Wang et al., 2004). It was also discovered that this system performed better in a seawater matrix, with increased sensitivity when compared to a synthetic NaCl solution. A number of issues with selectivity were reported, however, since other nitroaromatic compounds were found capable of interference.

Chen et al, 2010, reported the use of semiconducting single walled carbon nanotubes (SWCNT) as wearable chemical sensors, firstly positioning the SWCNT in an aligned array on quartz using chemical vapour deposition and then transferring the array onto textile. This coated textile section was then incorporated onto a chip carrier with an electrical and gas feed, essentially becoming a wearable transistor. In air, the LOD for TNT was found to be 8 ppb (80 ng L^{-1}). The same group also reported the production of metal oxide nanowires with a LOD for TNT of 600 ng L^{-1} (Chen et al., 2010a).

A SWCNT based chemiresistive immunosensor was described by Park et al, 2010, which provided a label-free, sensitive and selective technique for detection of nitroaromatic explosives. The SWCNT was first modified with trinitrophenyl (TNP), an analogue of TNT, which was then functionalised with an anti-TNP single chain

antibody. This antibody has a greater affinity for TNT and thus the introduction of TNT caused a large change in the resistance of the system with the detection range of 5 ng L^{-1} to 50 µg L^{-1} TNT being reported (Park et al.,).

As previously mentioned, detection of peroxide based explosives can be complex due to these compounds containing neither the nitro groups nor aromatic behaviours traditionally used for analysis (Schulte-Ladbeck et al., 2006). Banerjee et al, 2009, suggested the use of a one-dimensional titania (TiO_2) nanotube array where metal ions, in this case zinc Zn^{2+}, are coated upon the surface. When present the TATP bonded to the metal ions and the signal current output, as detected by a potentiostat, increased by between 3 to 5 orders of magnitude although this was found to be prone to saturation under ambient conditions (Banerjee et al., 2009).

The use of both carbon nanotubes and metallic nanoparticles were described by Hrapovic et al, 2006, for the electrochemical detection of nitroaromatic compounds. The nanocomposite was composed of a SWCNT with copper nanoparticles within a Nafion matrix, selected for their stability, reproducibility, low background current and prominent peak display with cyclic voltammetry and anodic stripping voltammetry, ASV. A detection limit of 1 µg L^{-1} was reported in tap water, river water and washed contaminated soil samples (Hrapovic et al., 2006).

2.2.4.3. Nanoparticles

Jiang et al, 2008, described a simple colorimetric visualisation of TNT at picomolar levels based on the donor-acceptor (D-A) interaction between TNT and primary amines, in this case cysteamine. The cysteamine acts as both primary amine and stabilizer to the gold nanoparticles (Au NP); introduction of TNT into the solution caused aggregation of these amine covered Au NPs which resulted in a colour change from red to violet which can be observed without further analysis. An addition of 114 pg L^{-1} of TNT changed the solution colour such that it could be visualised by the naked eye (Jiang et al., 2008).

Surface-enhanced Raman scattering (SERS) is a technique that enhances the intensity of Raman scattering spectra through the proximity of a molecule to a roughened metal surface or, in the case of nanomolecules, between gaps in nanostructures. Dasary et al, 2009, described a SERS probe coated with gold nanoparticle-cysteine conjugates; this system was able to form aggregating Meisenheimer complexes in the presence of TNT. A result of this was hot spot formation and an enhancement of the Raman signal intensity, allowing TNT to be detected at a concentration of 0.45 ng L^{-1} (Dasary et al., 2009). A similar technique was described by Yang et al, 2010, using functionalised silver nanoparticles coated on silver molybdate nanowires with crosslinking provided by p,p'-dimercaptoazobenzene (DMAB). TNT was detected in this case at concentrations of 0.23 ng L^{-1} (Yang et al., 2010). The detection of peroxide based explosives has also been described using a similar approach. Chang et al, 2009, reported a SERS-active nanoporous substrate based on porous alumina membranes combined with mixed nanoclusters comprising gold nanorods and gold nanoparticles. The plasmon resonance from hot spots produced by the above system photo-decompose molecules of HMTD enabling analysis of the fragments. The LOD for HMTD has been interpolated as 2 pg or ~ 3 ppm (Chang et al., 2009). A self-assembled gold octahedral array has been described that used a droplet evaporation process. This process produced a nanoparticle array with nanoscale interparticle gaps which provide an enhancement to the SERS detection of TNT through improved sensitivity and reproducibility (Liu et al., 2011). There has been significant work within this area to establish optimal working conditions of the system including, for example, the effect of exposure time and temperature on the resulting signal (Fang and Ahmad, 2009; Wackerbarth et al., 2010b) as well as addressing false positives due to musk based perfumes of similar structure to TNT (Wackerbarth et al., 2010a), in this case it was found that the compounds musk ketone and musk xylene can be distinguished from TNT using the SERS technique.

An imprinted composite coating of bisanline-gold nanoparticles was developed using Kemp's acid as an imprinting molecule upon a gold surface for the detection of RDX. This technique used surface plasmon resonance (SPR) which reveals changes in the

refractive index occurring due to adsorption or desorption at the surface. Detection of RDX was possible at 2.6 pg L^{-1} due to the formation of π-donor-acceptor complexes between RDX and the bisaniline bridging units (Riskin et al., 2010). Kawaguchi et al, 2008, describe the use of gold nanoparticles on the immunosurface within a miniaturised SPR system that amplified the signal for TNT by four times that which is seen when the gold nanoparticle was absent (Kawaguchi et al., 2008).

Wang et al, 2008, reported electrochemical competitive displacement immunoassays for the detection of TNT. Poly(guanine)-functionalised silica nanoparticles were complexed with anti-TNT coated magnetic beads using an analogue of TNT, trinitrobenzene. When exposed to TNT the analogue was displaced and there was an increase of guanine in the solution. The magnetic beads were removed and the solution electrochemically interrogated upon a screen-printed electrode in a solution of PBS with mediator. The limit of detection for this system was found to be ~0.1 ng mL^{-1} (Wang et al., 2008).

Chen et al, 2010, described a chemosensor based on pyrene-functionalised Ru (ruthenium) nanoparticles, using 1-vinylpyrene (Ru=VPy) and 1-allylpyrene (Ru=APy). Both of these particles exhibited enhanced detection of nitroaromatic compounds as compared to monomeric pyrene; and of the two particles under examination Ru=VPy nanoparticles displayed higher sensitivity. Increased nitration on the aromatic ring increased the response, and for this reason TNT exhibited the greatest fluorescence quenching of the nitroaromatics under consideration (Chen et al., 2010b).

2.2.4.4. Quartz crystal microbalance

The quartz crystal microbalance utilises the resonance frequency change due to changes in mass upon the crystal surface as a means to detect the presence of a substance of interest. This technique is further enhanced through coating the surface with various compounds which help provide specificity to this system. Although this paper will relate the use of a QCM in relation to the field of nanotechnology, the reader is referred to a comprehensive review of the many uses of QCM (Marx, 2003).

Larsson et al, 2006, reported a potential selective detector chip for TNT using thiol self-assembly with a TNT analogue upon a gold biochip and a subsequent competitive label-free immunoassay. Several combinations of TNT analogue/organosulphur compounds were evaluated as a possible self-assembled monolayer (SAM) for this system and the analogue dissociation was monitored with both a QCM and via surface plasmon resonance (SPR). The detection limit for TNT was within the 1-10 pg μL^{-1} range depending on the TNT-analogue used (Larsson et al., 2006b), with one analogue, ANA1, presenting shorter recovery times after exposure and a higher relative response to TNT.

Cerruti et al, 2009, further investigated the selective detection of TNT and DNT using QCM with a polymer-oligopeptide coating upon a gold chip capable of providing a stable and high density set of receptors with selective binding capabilities. This system was capable of providing real-time detection, in water, of TNT whilst the presence of DNT exhibited no resonance frequency change (Cerruti et al., 2009). A different approach by Lubczyk et al, 2010, was to combine several differently coated microbalances to distinguish the peroxide based explosive TATP from chemically related compounds. Analytical detection methods for TATP often rely on the detection of hydrogen peroxide (H_2O_2) as an indicator of the presence of peroxide based explosives; however, as H_2O_2 can be found in other substances there can be an increased risk of false positives if merely detecting this substance. This work attempted to address this issue using a combination of a modified phenylene dendrimer, a cyclodextrin and a cholic acid derivative as the separate coatings on an array of QCMs. Response times were found to be in the range of a few seconds and rapid system recovery was also possible. Combining this approach with high frequency QCM a lower limit of detection for TATP was reported at 1 ppm (6.6 $\mu g\ L^{-1}$) (Lubczyk et al., 2011).

Yu et al, 2009, described a combination of electrochemical and piezoelectrical transduction techniques for the sensitive and selective detection of nitroaromatic compounds. This system used an ionic liquid, $BMIBF_4$, as both the electrolyte for the amperometric sensing and the sorption solvent to coat the QCM. The amperometric

and QCM sensing systems were integrated onto a single quartz chip permitting miniaturisation. Sensing was performed in the 0-70 µg L^{-1} region for ethylnitrobenzene, validating the combination of these two systems and the use of ionic liquids as both solvent and electrolyte in a miniaturised system such as this (Yu et al., 2009).

2.2.4.5. Thin film sensors

The design of selective polymers for the detection of explosive compounds has been described earlier. Tenhaeff et al, 2010, employed initiated Chemical Vapour Deposition (iCVD) to deposit a nitro-aromatic selective polymer, poly(4-vinylpyridine), inside microfabricated trenches. This coating was subsequently coated with a gold/palladium electrically conductive layer. When the polymer coating absorbed the analyte of interest it swelled producing an interaction between the conductive layers on either side of the trough and this contact can subsequently be measured electrically. Although this system demonstrated the transduction of a chemical interaction into an observable measurement there were several issues that would need to be addressed before translation into a viable detection device, such as the switch presently being irreversible and the length of response times – the shortest for nitrobenzene being 10.2 minutes. The authors do, however, claim concentration and mass limits of detection for TNT as low as 9.5 ng L^{-1} and 3 fg, respectively, through modelling based on optimal conditions (Tenhaeff et al., 2010).

Long et al, 2009, reported an electrospun nanofibrous film doped with a fluorescent conjugated polymer (CP) for the detection of DNT. CPs have greater fluorescent quantum yields and amplified sensory responses as compared to small fluorescent molecules, although they experience self-aggregation and thus self-fluorescent quenching. The authors employed electrospinning to construct a nanofibrous film that decreased opportunities for self-aggregation. The polymer was further doped with a supporting matrix and a porogen to increase the surface area and porosity of the surface; this enabled target analytes to diffuse close to the sensing elements so increasing the quenching capabilities (Long et al., 2009).

Lock et al, 2009, described the use of a self-assembled monolayer upon the surface of a microcantilever, which undergoes chain polymerisation in the presence of peroxide radicals which are produced when the sample vapours are passed through a heating filament. This sensor was capable of detecting hydrogen peroxide and tertbutyl peroxide, leading to the hope that it may be suitable for use within a peroxide explosive sensor. This system also displayed reversibility, returning to baseline without need for thermal regeneration (Lock et al., 2009) and was reported as being selective to peroxide vapours, although this may not be sufficiently discriminating to prevent some false positives.

2.2.5. Conclusions and future outlook

It can be observed that almost all analytical techniques addressed in this review have undergone significant changes to improve one or more aspects of their working practises over the last five years; including, for example: sensitivity, specificity, cost, ease of use and miniaturisation. Further advancement will be necessary to provide a system that incorporates all aspects of an ideal explosive identification technique due to the inherent issues that are associated with this – low volatility of explosive vapours, concealment, interferrents and the actual damage caused by a false response. Significant improvements have been made in the portability of apparatus; spectroscopic techniques, such as IMS and mass spectrometry, which were largely stationary are now become field deployable. Terahertz spectroscopy, once beleaguered with issues, has been realised as a technique that can identify explosives and other concealed objects beneath clothing and within luggage. Nanotechnology over the last decade has become increasingly important, with research to incorporate new nano-based aspects into existing technologies to improve sensitivity, selectivity and portability.

It seems likely that, looking to the future, work will progress in the same direction. Miniaturisation and portability should remain important aspects and, as such, nanotechnology is likely to play an important role – not only in and of itself, but in enabling other technologies to develop further. Improving the sensitivity and

specificity of explosive detection technology are principles that continue to be important; lower detection limits of devices have improved considerably and work in this area is certain to remain on-going.

2.3. Introduction to biosensors

A biosensor may be defined as "*a device incorporating a biological sensing element connected to a transducer*" (Eggins, 2002); this can be illustrated pictorially as below in Figure 2.6.

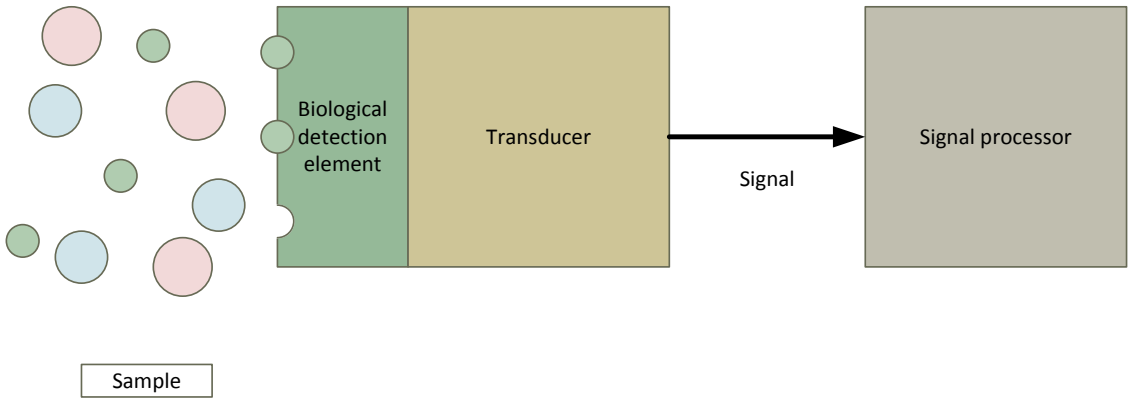

Figure 2.6 - Schematic of a biological sensing system

The substrate interacts with the biological detection entity of the biosensor which causes a response. This response is converted into a form that can be observed using a transducer; this may, for example, be electrochemical, thermal or optical in nature. The signal can then be passed to a signal processor which can convert it into an appropriate format for subsequent analysis via, for example, a computer programme.

The selective detection sensor component of a biosensor will be of biological origin such as, for example; an enzyme, nucleic acids, an antibody or an antigen. Biosensors frequently however have the capacity to detect and measure analytes of both chemical and biochemical origin. The biological recognition entity is crucial to the operation of a biosensor as the molecule either selectively catalyses a reaction or bonds to the analyte within the substance that is undergoing investigation. The biological species is normally immobilised adjacent to or in direct contact with the transducer.

2.3.1. Enzyme biosensors

A number of definitions of enzyme biosensors have been reported within the literature such as, for example: *"An enzyme biosensor is an analytical device that combines an enzyme with a transducer to produce a signal proportional to target analyte concentration"* (Mulchandani and Rogers, 1998). The immobilisation of enzymes upon the sensor can be achieved by both physical and chemical means. Physical methods can minimise the possibility of causing damage to the structure of the enzyme and thus the disruption of its function. Physical techniques include entrapment within a polymer gel matrix and adsorption upon the surface. Chemical techniques available include cross linking and covalent binding either to the surface of the electrode or to a hydrophilic membrane on its surface. It is also possible to incorporate the enzyme onto a polymer film already coating the sensor, such as polyaniline, via methods such as biotinylation.

Enzyme biosensors may be coupled to a variety of different transducers including, for example, potentiometric, amperometric and conductimetric based devices.

2.4. Electrochemistry

Electrochemical methods can be used to study the properties of a solution. Monitoring the changes in an electrochemical cell may be used to determine concentration of an analyte or the presence of a species in the electrolyte solution. The examination of electron transfer reactions between the electrode and the reactant is known as dynamic electrochemistry. The electrode is known as the solid phase and is often metallic but can take other forms, such as carbon, and the reactant molecules are generally in the solution phase. The transfer of charge, or electrons, between the electrode and the reactant solution takes place across the electrode/solution interface and may be better illustrated by Equation 2.1.

$$Fe^{3+}_{(aq)} + e^{-}_{(m)} \Leftrightarrow Fe^{2+}_{(aq)}$$

Equation 2.1

The above equation represents the transfer of electrons between two phases, the metallic electrode (m) and an aqueous solution (aq).

It is possible to operate an electrochemical cell by introducing a current flow through the application of another potential to the system that differs from the equilibrium potential. This current stimulates the movement of electrons between the electrode and the solution and so changes the oxidation state of the molecules in that solution, promoting electrolysis. This system can take place in either direction – a molecule in solution may donate an electron to the electrode, where it may be said it has been oxidised, as shown in the example of Equation 2.2, or it may accept an electron from the electrode, in which case it has been reduced, such as in the example of Equation 2.3.

$$Fe^{2+}_{(aq)} \rightarrow Fe^{3+}_{(aq)} + e^{-}_{(m)}$$

Equation 2.2

$$Fe^{3+}_{(aq)} + e^{-}_{(m)} \rightarrow Fe^{2+}_{(aq)}$$

Equation 2.3

The reductive pathway introduced above (Equation 2.3) describes the conversion of Fe^{3+} into Fe^{2+} at the electrode/solution interface. When a current is passed through the cell to enable this reaction the rate of depletion of Fe^{3+} through electrolysis at the interfacial region is significantly increased. The lesser speed at which the Fe^{3+} is replenished from the bulk solution through diffusion creates a disparity between the concentration of the species in the interfacial region and the bulk solution.

The electrolytic current can be observed to be dependent upon two factors: the movement of reactants to and products from the electrode surface, known as rate-determining mass transport, or the rate of heterogeneous electron transfer, which are rate-determining electrode kinetics.

2.4.1. Electron transfer rate

As illustrated in the previous section, potential can control the electrode kinetics for any electrolytic reaction. It is, therefore, beneficial to examine the rate of electron transfer – this can be undertaken using a simplified charge transfer process (Equation 2.4) where the oxidised species, O, and the reduced species, R, are both soluble and in solution.

$$O_{(aq)} + ne^{-}{}_{(m)} \underset{k_{ox}}{\overset{k_{red}}{\rightleftharpoons}} R_{(aq)}$$

Equation 2.4

The oxidative species is transformed into the reductive species through the receipt of n electrons. It is assumed in Equation 2.4 that the solution contains a finite amount of both O and R; and K_{red} and K_{ox} represent the first order rate constants for the reductive and oxidative electron transfer processes. The electrons in the electrode have a maximum energy distributed around that of the highest occupied atomic orbital, known as the Fermi level E_F. Electrons can only be donated or received at this level of energy unless an external potential is applied. In these circumstances the Fermi level may be altered through the influence of this external voltage enabling the acquisition or removal of electrons at different energy levels. For a successful reduction of a molecule in solution the electrons must possess a minimum amount of energy to be transferred to the receptor molecule, O; for an oxidation reaction the electrons in the donor molecule of R must possess energy that is equal or higher to that of the electrode's Fermi level.

To facilitate the examination of the relationship between the energy levels of a species and the tendency for that species to donate or receive electrons, it is necessary to observe the potential dependence of the heterogeneous rate constant for that electron transfer reaction. The reductive and oxidative processes illustrated in Equation 2.4 can be represented using the equations Equation 2.5 and Equation 2.6, respectively;

$$i_c = -FAk_{red}[O]_o$$

Equation 2.5

$$i_a = FAk_{ox}[R]_o$$

Equation 2.6

where $k_{red}[O]_o$ and $k_{ox}[R]_o$ signify the respective flow of the electroactive species to the electrode, F is Faraday's constant (9.6 x 10^4 $Cmol^{-1}$), A is the area of the electrode (cm^2) and i_c and i_a are the reductive (cathodic) and oxidative (anodic) currents (A) respectively. The net flowing current (i) may, therefore, be demonstrated with Equation 2.7:

$$i = i_a + i_c$$

Equation 2.7

It follows that through the substitution of Equation 2.5 and Equation 2.6 into Equation 2.7, we acquire:

$$i = FA(k_{ox}[R]_o - k_{red}[O]_o)$$

Equation 2.8

When the fluxes $k_{red}[O]_o$ and $k_{ox}[R]_o$ are balanced the reaction represented by Equation 2.4 is at equilibrium where the current flow will be zero. Equilibrium is the only instance in which the fluxes are balanced:

$$k_{red}[O]_o = k_{ox}[R]_o$$

Equation 2.9

The transition state model may be used to describe electron transfer (ET) reactions (see Figure 2.7). The reaction involves the reactants ($O_{(aq)}$ + e^-) overcoming an energy barrier, the peak of which is known as the transition state region, on the conversion pathway to become reaction products ($R_{(aq)}$). The rate of the reduction reaction is predicted, using transition state theory, to be:

$$k_{red} = Af \exp\left(\frac{-\Delta G_{red}^{\Phi}}{RT}\right)$$

Equation 2.10

where ΔG^{Φ}_{red} is the free energy of activation, R is the molar gas constant, T is the absolute temperature in Kelvin and Af is a frequency factor representing the rate of collisions between the electroactive molecule and the electrode surface.

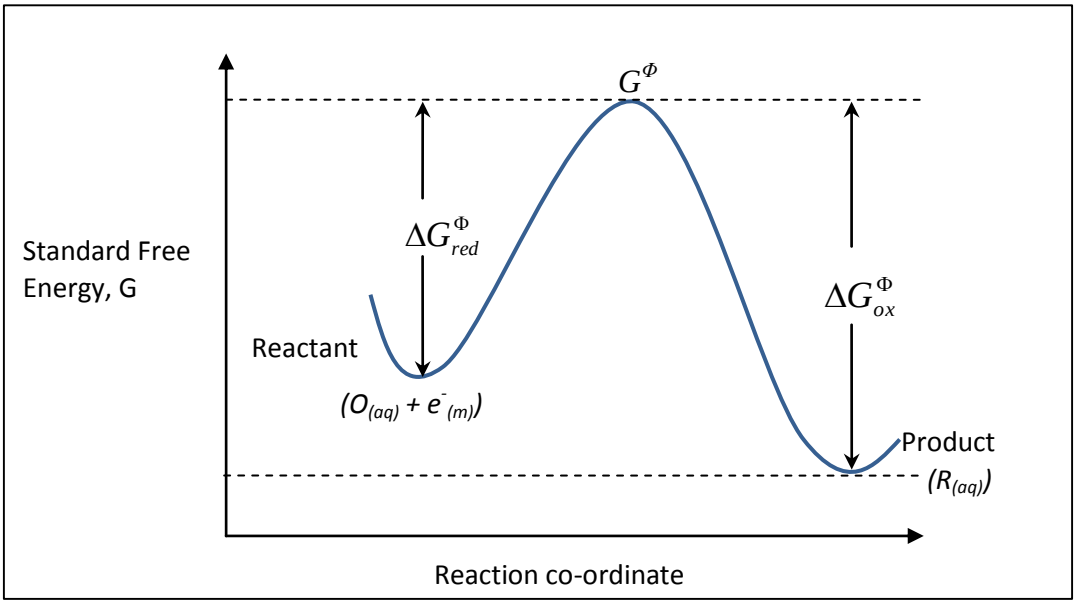

Figure 2.7 - Free energy plot for the simple one electron reduction of species $O_{(aq)}$

The activation free energies for the reductive and oxidative processes can be observed in Equation 2.11 and Equation 2.12, where G_{red} and G_{ox} signify the free energy changes of the product and reactant (at a fixed temperature and pressure).

$$\Delta G^{\Phi}_{red} = G^{\Phi} - G_{ox}$$

Equation 2.11

$$\Delta G^{\Phi}_{ox} = G^{\Phi} - G_{red}$$

Equation 2.12

Electrochemical reactions are, as has been discussed previously, influenced by altering the energy levels of the electrode – what can be described as the interfacial potential. This causes the theory relating to electrochemical reactions to break away from that associated with the kinetic model when applied to homogeneous chemistry; the concept being that when the applied potential (E) and the equilibrium potential (E_e) are equal no current will flow through the system (see Equation 2.9). If E is of another

value then this equation no longer holds; i.e. there is no longer an equilibrium and, therefore, electrolysis is thermodynamically viable once more. The kinetics of the electrode reaction in the system will dictate whether a current flow subsequently ensues. It can be seen that in order to initiate a reaction with an applied potential, the potential must differ from that at equilibrium, E_e. When a more negative potential is attained, the electron energy at the electrode is raised which may affect the transfer of electrons to the species in solution – a reductive current. The opposite, an oxidative current, occurs when electrons in solution flow towards a more positive electrode surface. The deviation of potential from that at equilibrium is known as overpotential (η) and is given in Equation 2.13:

$$\eta = E - E_e$$

Equation 2.13

All discussion thus far has assumed a one electrode in solution system; however, in most experimental systems there is a two or three electrode electrochemical cell where the current variation is assessed against the application of an overpotential. This relationship can be predicted using an equation developed through the combination of work into electrode kinetics by Butler and Volmer – the Butler-Volmer equation:

$$i = i_o\left(\exp\left\{\frac{(1-\alpha)F\eta}{RT}\right\} - \exp\left\{\frac{-\alpha F\eta}{RT}\right\}\right)$$

Equation 2.14

Where the observed current, i, can be shown to vary as a function of the overpotential, η, and the transfer coefficient, α. The concentrations of the reactants at the surface and in the bulk are assumed to be equal in a well stirred solution, or $[R]_o = [R]_\infty$ and $[O]_o = [O]_\infty$. When the standard exchange current, i_o, is large, little or no applied overpotential is required to induce the movement of current in either the cathodic or anodic direction, this is known as a reversible process. Conversely, when i_o is small a high overpotential is required to stimulate current flow and the system is said to be irreversible. The terms large and small are related concerned with the time in which

materials transport to and from the electrode/solution interface which relates to the kinetics of the electrode.

2.4.2. The electrode/solution interface and the electrical double layer

In solution, the electrode is surrounded by a layer of water molecules, ions and other molecular or atomic species. It is due to this that there is an accumulation of charge around the electrode surface. This region, known as the interfacial region, is where the charge transfer reactions between the electrode and the electrolytes in solution occur and where the greatest potential difference within the electrical circuit exists. The manner in which this area is structured can dictate the rate at which the charge transfer takes place.

In 1853 Helmholtz proposed a theory to describe the interfacial region between the electrode surface and the solution. An assumption was made that no faradaic processes occur at the electrode and that the electrode possesses a charge density (q^m); the value of which depends on either an excess (q^m negative) or deficiency (q^m positive) of electrons at the surface. The charge that has accumulated at the surface attracts the charged species in the solution (q^s) as the interface must maintain electrical neutrality (see Equation 2.15).

$$q^m = -q^s$$

Equation 2.15

The excess or deficient charge on the electrode surface was believed to be matched by electrostatic redistribution of ions; this produces a monolayer of counter-ions of opposite charge at a distance, d, from the electrode surface, thus creating the electrical double layer. The distance, d, will depend on the size of the counter-ions and a line drawn through the radius of those ions represents the minimum distance from the electrode surface, known as the Outer Helmholtz Plane (OHP). A potential difference results from this migration producing an electrical field gradient which repels or attracts ions towards the electrode surface, thus producing a build-up of anions or cations depending on the charge there (see Figure 2.8).

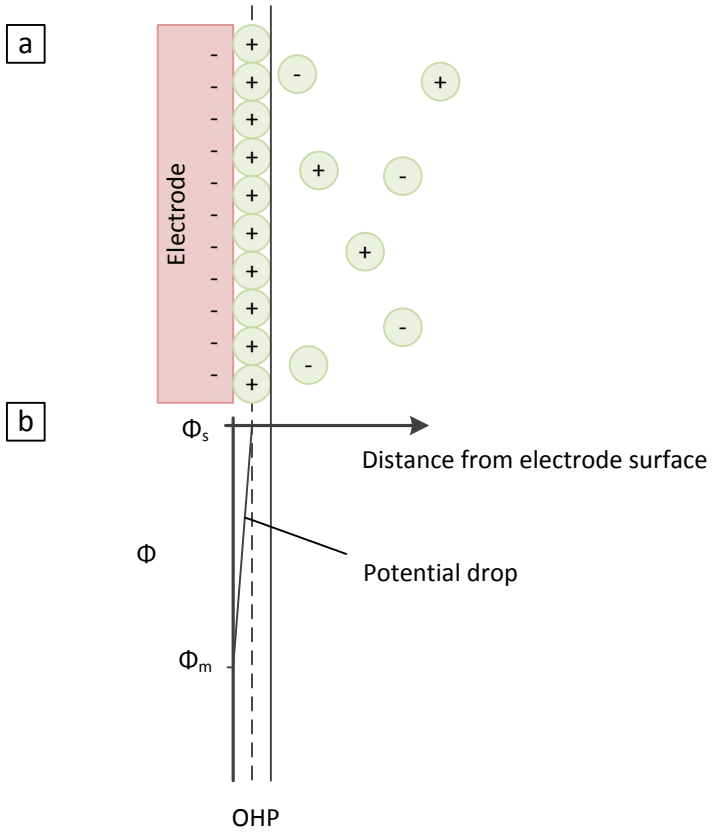

Figure 2.8 - Schematic of a) the Helmholtz electrical double layer model and b) the potential drop across the interfacial region

This system as described by Helmholtz is the equivalent to an electrical capacitor, where the layers of charge have a fixed distance from one another and the potential drop between the two layers is linear.

Gouy and Chapman improved this model by proposing that the excess charge density in the solution was not solely found at the OHP but that this charge is also dispersed throughout a diffuse layer in close proximity to the electrode surface where the net charge density decreases with increasing distance from the electrode surface (Figure 2.9 a). This proposal was based on the principle that the electrostatic forces mentioned earlier are offset somewhat by the effects of Brownian motion dispersal of the excess ions. The potential drop is concentrated in the region closest to the electrode surface but decreases gradually across the diffuse layer, see Figure 2.9 part b.

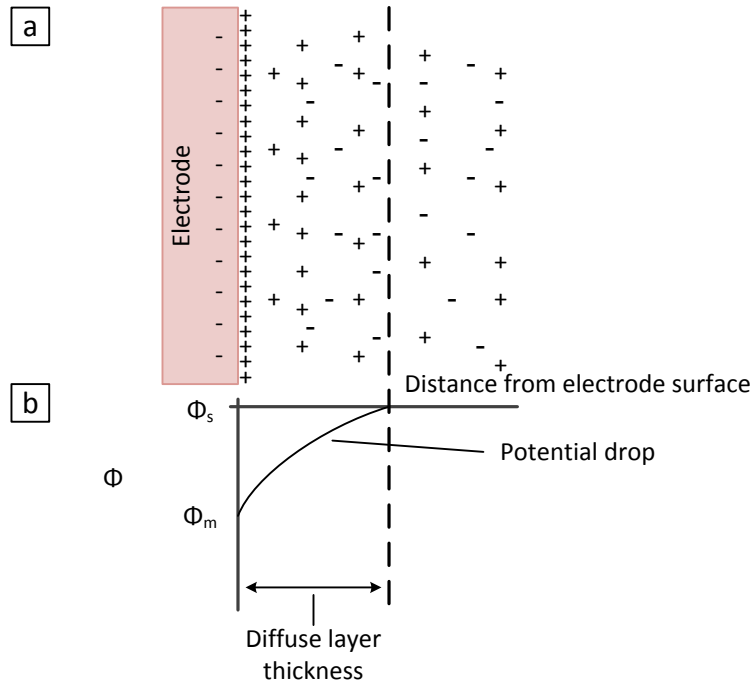

Figure 2.9 - Schematic illustrating a) the Gouy-Chapman model of the electrical double layer and b) the potential drop across the interfacial region

These two models were subsequently combined by Stern in 1924, where it was accepted that the ions have a plane of minimum distance from the electrode as described by Helmholtz (the Outer Helmholtz Plane) but also are affected by Brownian motion and, therefore, a diffuse layer is generated in the solution proximal to the electrode. The result of this combination is a sharp initial potential drop, between the electrode surface and the OHP, which gradually falls back to the value found in the bulk solution.

In 1947, Grahame proposed that the area in close proximity to the electrode surface was mainly occupied by solvent molecules; however, he suggested that ionic or uncharged species could also infiltrate this zone – where the solvation shell was absent or lost as the ion approached. These ions are understood to be specifically absorbed on the surface of the electrode and the charge of the ions involved can be irrelevant to this absorption.

The form of the interfacial region was modified to include the specifically absorbed species and a closer minimum distance of approach, the inner Helmholtz plane (IHP), was proposed which passes through the centre of these absorbed molecules (see

Figure 2.10). The specific absorption upon the electrode surface serves to diminish the charge density required to counterbalance the charge on the electrode.

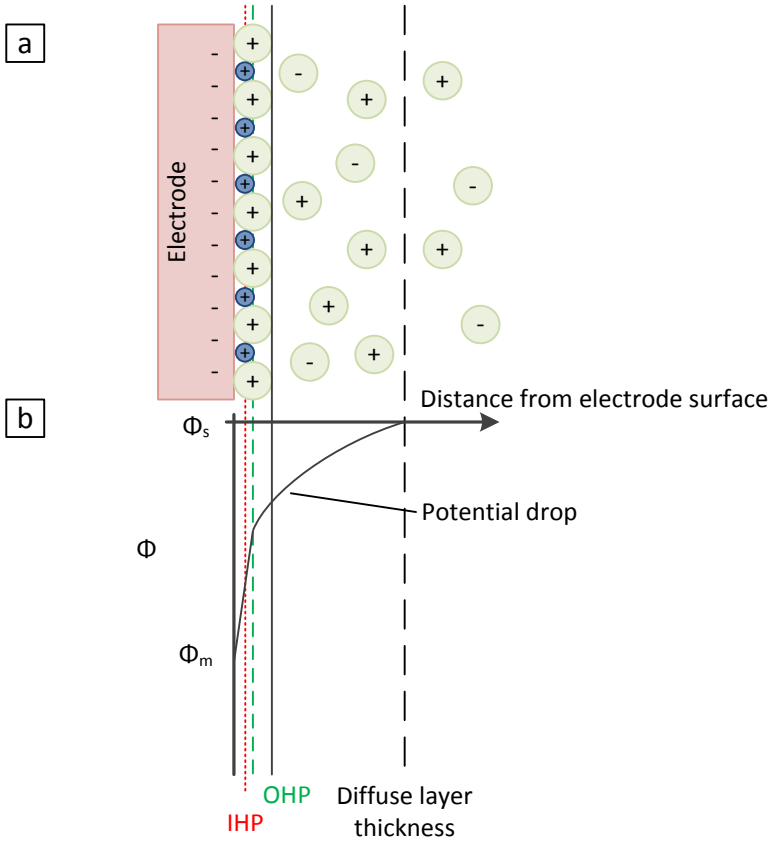

Figure 2.10 - The Grahame model of the electrical double layer

Modern theories relating to the electrical double layer involve statistical mechanics which are not within the scope of this thesis.

2.4.3. Voltammetry

Voltammetric techniques involve observation of the current variation within an electrochemical cell as a function of the applied potential to that cell. It is a method that provides a vast amount of information relating to the mechanism of the reaction under investigation. Voltammetry may be transient or steady-state – transient voltammetry is more complex than steady-state approaches, where the current and potential are inter-related, and this allows a more detailed investigation into the properties of an analyte. There are two main types of transient voltammetry: controlled-potential voltammetry and controlled-current voltammetry. Controlled-potential apparatus involve the measurement and subsequent analysis of the current in a cell against time and as such is also known as chronoamperometry. Controlled-current voltammetry (chronopotentiometry) measures the potential change, also as a function of time. Aside from potential sweep methods there are step and pulse techniques where a succession of potential steps of varying heights are analysed through the resulting pulse of current which can be related to the analyte within the system. There are several such techniques including normal pulse voltammetry, differential pulse voltammetry and square wave voltammetry (SWV). SWV involves the superimposition of a square wave form onto a staircase potential sweep (Bard, 2001). Current samples are taken twice during one cycle, the first pulse in the forward direction and the second in the reverse direction. Due to the speed of this technique in comparison to other voltammetric methods, analyses can be carried out at higher scan rates and detection limits of 10-8 M are achievable (Brett and Brett, 1998).

The sensor platform described in this work uses cyclic voltammetry as a means of analysis and, as such, this will be described further in section 2.4.5. A brief overview of the apparatus required to perform voltammetric interrogations will also be discussed (section 2.4.4).

2.4.4. The electrodes of an electrochemical cell

The typical requirements for an electrochemical experiment are a vessel containing the solution of interest, generally an electrolyte, into which at least two independent electrodes are submerged. These electrodes are linked with external connectors and an electrical circuit is complete – the solution forming a conducting phase to enable this. One of the two electrodes is the working electrode (WE) and is where the reaction under investigation occurs. The second electrode is known as the counter electrode (CE) and enables the potential drop between the solution and the WE to accurately defined through the provision of a fixed potential to contrast against

$$Potential\ Drop\ (\Delta\Phi) = \Phi_m - \Phi_s$$

Equation 2.16

In a two electrode system, a complementary or opposite redox reaction takes place at each electrode to ensure that a net consumption of electrons does not occur (see Figure 2.11). This two electrode system works well for the measurement of the current or voltage where a tiny current is passed. The obvious example of this would be with a microelectrode system where the potential drop can be described as a fixed term due to the relatively small currents passing through the system and the voltage drop, *iR*, is also negligible. Changes in the applied potential in this two electrode case are directly indicated in the driving force and so it may be said that:

$$E = (\Phi_m - \Phi_s) + constant$$

Equation 2.17

For larger electrodes the potential drop can cause problems. Where the assumption allows a finite current flow between the working and reference electrodes, the voltage applied will be:

$$E = (\Phi_m - \Phi_s) + iR + (\Phi_s - \Phi_{REF})$$

Equation 2.18

Where $(\Phi_m - \Phi_s)$ describes the driving force for electrolysis in the interfacial region, *iR* depicts the voltage drop caused by the transit of current between the electrodes, and

$(\Phi_s - \Phi_{REF})$ is the potential drop at the electrode/solution interface of the reference electrode – this is predetermined by the composition of the reference electrode. The movement of larger currents across the reference electrode can alter the composition and so this term may not be considered a constant as it was with a microelectrode system. The solution resistance (*R*) can also have an effect on the potential measured at the WE. As can be seen, the changes in applied potential with a large electrode cannot be directly related to a change in the driving force of the system as described previously (Equation 2.17) as such, it is necessary to use a third electrode, the counter or auxiliary electrode (CE), demonstrated in Figure 2.11.

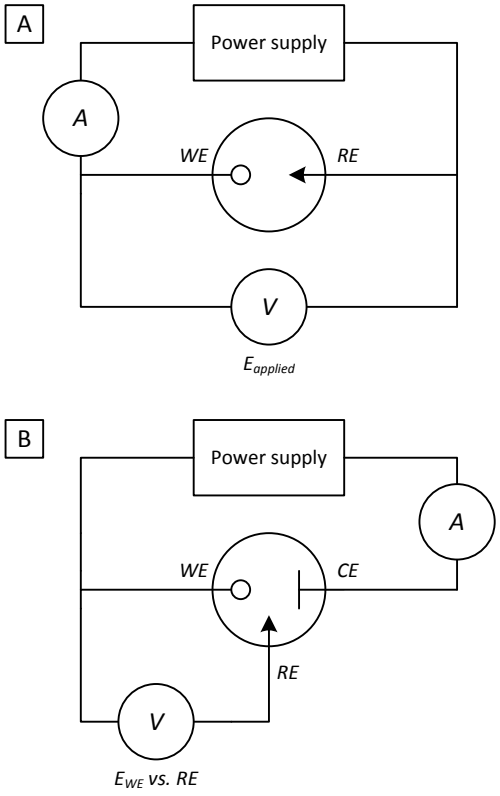

Figure 2.11 - The electrical circuit of an A). two electrode and B). three electrode cell

The three electrode arrangement has a current flowing between the WE and the CE with the potential at the WE monitored with respect to the reference electrode. A potentiostat maintains the potential across the electrodes irrespective of the current measured within the system and ensures that the current flow is between the WE and CE only. Although this system mitigates some of the concern relating to the electrical

resistance within the solution (*R*), this cannot be removed completely unless the RE is in direct proximity with the WE. As the RE is moved further from the surface of the working electrode there is an increase in the *iR* which will be included in any potential measurements.

The good performance of the working electrode is vital to ensure a favourable electrochemical analysis. The response should be reproducible with a high signal to noise ratio. The working electrode is required to be a good electron conductor to enable the necessary charge transfer reactions to take place unrestrictedly. Materials that form the WE are, consequentially: mercury, noble metals such as gold (Au) or platinum (Pt) and, more recently, less expensive substances such as carbon. Consideration of factors such as the redox behaviour of the analyte and the potential range required for the analysis, or indeed, the cost and availability of the WE should be taken into account when selecting a WE.

Reference electrodes should, ideally, be non-polarisable – no current should flow across the interfacial region at the RE surface so that it may provide a stable potential difference against which the rest of the system may be compared. Standard electrode potentials are calculated using the standard hydrogen electrode (SHE). This type of RE is generally not used in electrochemical analyses due to its size there are, however, a number of other reference electrodes available such as the silver/silver chloride (Ag/AgCl) or the saturated calomel electrode (SCE).

The counter electrode should be significantly larger than the working electrode so as to ensure that it does not form the rate limiting aspect in the charge transfer reactions under examination at the surface of the WE. It may be necessary to position the counter electrode away from the working electrode if the CE produces products via electrolysis that may reach the WE surface.

2.4.5. Linear sweep and cyclic voltammetry

The electrode potential in a chronoamperometric analysis may be varied either in a stepped manner or ramped so as to allow for a more gradual change. Stepped potential approaches may employ a single step, many equally spaced steps or steps in both the forward and backward direction. Ramped potentials may include a single scan, as within linear sweep voltammetry, or a forward and reverse scan, termed cyclic voltammetry. When a potential is applied and swept to another potential (see Figure 2.12) whilst monitoring the resulting change in current, this is known as linear sweep voltammetry and provides a basis for electrochemical analysis of a substance.

These techniques allow a quick investigation into the properties of the solution and can give an indication of the concentration as this is directly proportional to the resulting current output.

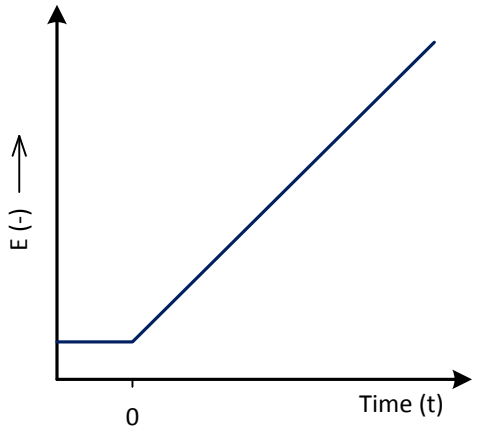

Figure 2.12 - Potential sweep in linear sweep voltammetry

A potential is applied to an electrode and initially no current flows as the potential is insufficient to promote electron transfer.

$$O_{(aq)} + ne^{-}{}_{(m)} \underset{k_{ox}}{\overset{k_{red}}{\rightleftharpoons}} R_{(aq)}$$

Equation 2.19

Let us consider a reduction of O to R as within Equation 2.19. If the scan is commenced at a potential significantly more positive than that at equilibrium then

initially then only non-faradaic currents flow until a position near the equilibrium potential, E_e, is reached. As the potential becomes more cathodic and reaches the proximity of E_e, the reduction of the analyte is induced and a current starts to flow. The current will increase consistently with the potential due to the increased electron transfer taking place – the flux of the analyte to the surface of the electrode increases as the surface concentration drops. At increasing cathodic potentials this current finally slows due to the consumption of O at the electrode surface, reaching a peak current. The current then falls as the diffusion of the reducible species from the bulk solution is a slower process. As the reaction continues, the distance by which the analyte needs to travel to the electrode surface also increases, diminishing the current rate further until equilibrium is once more achieved. The current response can be described as a peaked potential-curve.

Cyclic voltammetry is effectively a continuation of linear sweep voltammetry in which a reverse potential sweep is applied (see Figure 2.13). The reverse potential sweep is applied in the opposite direction to the initial potential sweep. This cycle may be repeated if required.

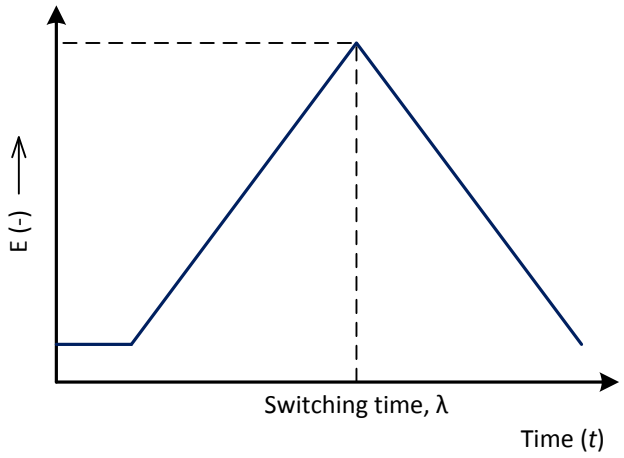

Figure 2.13 - Potential sweep in cyclic voltammetry

Let us consider once more Equation 2.19, in this case the re-oxidation of R to O. The solution-electrode interface has a large concentration of oxidisable analyte present that enables the current to continue to slowly drop. At the point where the peak cathodic current was observed, oxidation becomes favourable and the rate of reaction

increases at a higher rate but as an oxidative current. The current increases once more until the surface concentration of R is significantly diminished and a second, opposite peak can be observed. The current decreases further as the sweep tends towards the original potential applied. The observed current profile is much the same as the forward peak.

2.5. Mass transport

The rate at which an electron transfer reaction occurs at the electrode/solution interface may be affected by a variety of factors, including:

- Electron transfer at the electrode interfacial region
- Chemical or surface processes that precede or follow the actual electron transfer
- Mass transport

In order for electrolysis to take place, there must be a supply of the required reactant from the bulk solution at the interfacial region of the electrode; the reactant product should also diffuse away from the electrode surface. The overall rate of the reaction can, therefore, be limited by either the mass transport of the reactant or the rate of the actual charge transfer at the electrode surface. In a simple example, where fast electron transfer reactions take place and the mass transfer from bulk solution is the rate determining step, the current is mass-transport limited. This is known as reversible or Nernstian as the reactions obey thermodynamic relationships at the surface of the electrode.

Mass transport can be defined as the movement of material from one location to another in solution; this can be due to chemical or electrical differences between the two locations or through the movement of a volume constituent of solution (Bard, 2001). Mass transport occurs by three different modes: migration, diffusion and convection.

2.5.1. Migration

Migration is the movement of a charged species under the influence of an electric field such as, for example, an applied potential gradient. This mode of mass transport can be used to describe the mechanism by which charge flows between two electrodes in solution as a result maintaining the charge balance between them. Migration effects have perhaps the least influence to the overall rate of the mass transfer of

electroactive species as there is generally an inert supporting electrolyte which facilitates the charge flow and regulates potential gradients within the system.

The addition or removal of electrolytic ions to the supporting inert electrolyte aids in the understanding of how the supporting electrolyte works as this prompts a redistribution of its anions and cations to maintain the neutral electrical state near the interfacial region (with the exception of the area in close proximity to the electrode). This surplus of accessible background ions minimises the possibility of an electrical field building up in the solution as the reaction takes place.

2.5.2. Diffusion

Diffusion is the natural movement of a species down a concentration gradient, from a region of high to a region of low concentration until the solution equilibrates. Diffusion may be thought of as the flow or flux of *J* (number of moles diffusing through a unit area per second) into and out of a zone with boundaries, *x* and *x + dx,* separated by the distance *dx* (Figure 2.14).

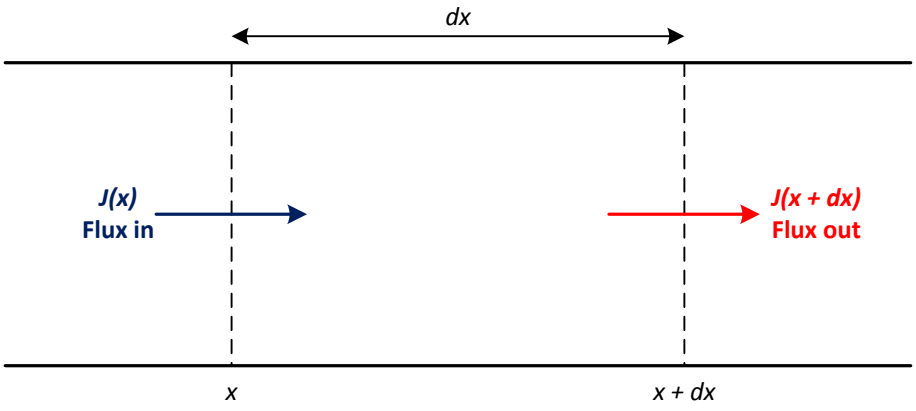

Figure 2.14 - Schematic representation of the diffusion of species from left to right down a concentration gradient

Diffusion may be described with the mathematical formula established by Fick (1855) known as Fick's first law of diffusion:

$$J = -D\frac{\partial[C]}{\partial x}$$

Equation 2.20

Where *J* is the diffusional flux, ∂[C]/ ∂x the concentration gradient in direction *x* and *D* the diffusion coefficient of the species within an aqueous solution. The value of D will depend upon the solution but this tends to be between 10^{-5} to 10^{-6} cm^2 s^{-1}. For more practical purposes Fick extended this first law to represent the concentration change at a specific point as a function of time rather than distance, this is known as Fick's second law of diffusion:

$$\frac{\partial[C]}{\partial t} = D\left(\frac{\partial^2[C]}{\partial x^2}\right)$$

Equation 2.21

In this case, the concentration is given as a function of position and time ($\partial[C]/\partial t$) and the concentration gradient is represented as $\partial^2[C]/\partial x^2$.

The Cottrell equation (Equation 2.22) may be derived from Fick's second law of diffusion and can be used to calculate the current variation, *i*, with time, *t*, for a planar electrode:

$$i = nFAJ = \frac{nFAD^{1/2}[C]_\infty}{(\pi t)^{1/2}}$$

Equation 2.22

Here, *n* is the amount of electrons transferred in the reduction or oxidation of the species (per mole), *F* is Faraday's constant, *A* is the area of the electrode (cm^2) and $[C]_\infty$ is the bulk concentration of the electroactive species.

With respect to a simplified redox reaction mentioned earlier (Equation 2.19) the effect of diffusional transport may be examined. Initially the concentration of the electroactive species is uniform throughout the solution; with the commencement of electrolysis at the surface of a planar electrode the reduction of *O* will produce a zone where the surface concentration of *O* is less than the concentration in the bulk solution. A gradient is therefore created along which a flux of unreacted *O* from the bulk solution will flow towards the electrode surface. Gradually a diffusion layer is constructed close to the electrode surface which increases progressively as the electrolysis process proceeds.

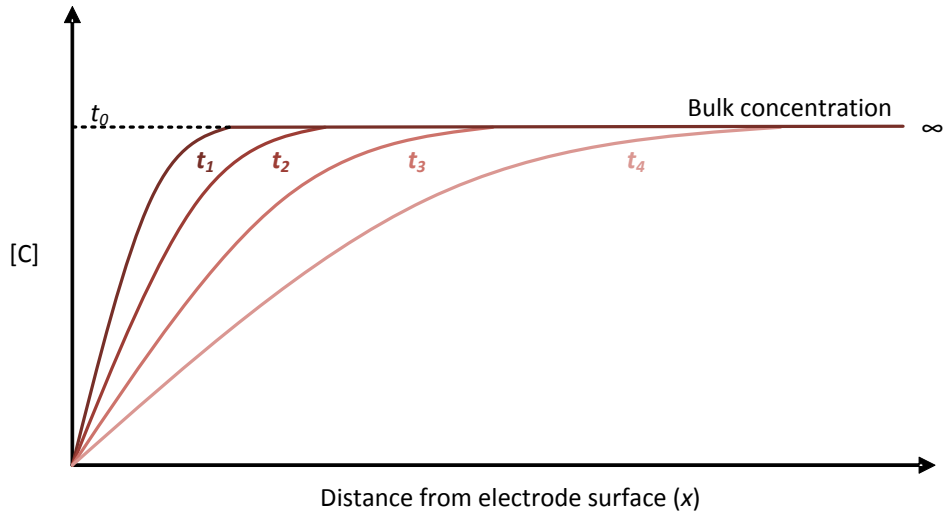

Figure 2.15 - Schematic representing the increasing thickness of the diffusion layer into the bulk solution as a function of time, t.

This process will, theoretically, continue until all of the available *O* species has been consumed. To enable the comparison between different electrodes and electroactive species it is advantageous to identify the thickness of the diffusion layer, *δ*. Where the reaction is classified as Nernstian the following equation may be applied:

$$\frac{i}{nFA} = D\left(\frac{\partial[C]}{\partial x}\right)_0 = D\frac{\left([C]_\infty - [C]_0\right)}{\delta}$$

Equation 2.23

Where all terms have been identified previously with the exception of $[C]_0$ which represents the surface concentration at the electrode surface. When $[C]_0 = 0$:

$$\frac{i}{nFA} = D\left(\frac{\partial[C]}{\partial x}\right)_0 = D\frac{[C]_\infty}{\delta} = k_d[C]_\infty$$

Equation 2.24

Where k_d is the mass transfer coefficient which corresponds to the diffusion coefficient, D, divided by the diffusion layer thickness, *δ*. When applied to the Cottrell equation (Equation 2.22) the mass transfer coefficient and the diffusion layer thickness may be given by Equation 2.25 and Equation 2.26 respectively:

$$k_d = \left(D/\pi t\right)^{1/2}$$

Equation 2.25

$$\delta = (\pi Dt)^{1/2}$$

Equation 2.26

It has been illustrated that the flux of material to the electrode surface can be estimated (Equation 2.24). Where the concentration of the electroactive species at the surface of the electrode, $[C]_0$, is significantly less than that within the bulk solution, $[C]_\infty$, the rate by which the mass transfer occurs is swift and the resulting current is large. The maximum observable current is limited by the rate by which O reaches the interfacial region from the bulk solution. Equation 2.24 establishes that if the electrode potential is increased until $[C]_0$ becomes zero, at this stage the limiting current (i_L) has been achieved and the process is transpiring at its maximum rate (Equation 2.27).

$$i_L = \frac{DFA[C]_\infty}{\delta}$$

Equation 2.27

2.5.3. Convection

Convection may be defined as the movement of species towards the electrode via a physical movement, the driving force of which can be an external application of mechanical energy such as, for example, stirring or bubbling gas through the solution or vibrating or rotating the electrode. These are examples of forced convection; convection may also occur naturally due to thermal gradients or density differences within the solution (Wang, 2006).

Within an electrochemical system natural convection can take place due to the reactions taking place at the electrode interfacial region increasing the density products present in this area. The species within the system are driven via these convective forces. This event limits the distance by which the diffusion layer may extend into the bulk solution – the greater the convective forces the more restricted the diffusion layer becomes and the greater the concentration gradient.

2.6. Microelectrodes

2.6.1. Definition

Historically known as ultramicroelectrodes, microelectrodes (as they will be referred to throughout this work) are electrodes that possess at least one dimension within the tens of micrometres or less (Štulík et al., 2000). As a basic definition this is adequate; it is not, however, quite as simple as this. The generally agreed essential aspect of a microelectrode is that the electrode is smaller than the thickness of the diffusion layer created under normal experimental timescales. This miniaturization of the electrode and the resulting properties can only be described as a microelectrode until the size reaches a certain point – beyond this and as the critical dimension decreases to a point comparable to the thickness of the double layer or the molecules under investigation, or typically around 10 nm, the electrode system has been defined in some literature as a nanode and the behaviour of such an electrode is expected to be different (Bard, 2001).

2.6.2. Microelectrode behaviour

Due to the small currents that are passed through a microelectrode only small amounts of electrolysis are induced in the solution and therefore a decrease in the diffusion layer is seen near the electrode surface and for this region a greater concentration gradient occurs because of this. These factors lend themselves to an increase in the rate of mass transport possible in the electrochemical cell and this limits the influence of the electrode in the study of fast electron transfers and chemical reactions. Microelectrodes are for this reason often used in the study of fast kinetic electrode processes.

A microelectrode naturally possesses a smaller electrode surface area which enables a smaller charging current to accumulate near the surface. This charging current affects the dispersal of ionic species near the surface and this movement of charge can sometimes mask the reaction under investigation. Due to the smaller surface area of

the microelectrodes this effect is not as significant as it might be with a macroelectrode and, as such, the potential sweep rate in voltammetric studies may often be increased.

Ohmic drop, the drop of voltage in solution due to the flow of current between electrodes, is to some extent avoided with microelectrodes as the currents passed are small (Bond, 1994). This means that where electrochemical studies with macroelectrodes require background electrolyte solutions to diminish the resistance of the bulk solution, the use of microelectrodes may enable interrogations in non-polar solvents and highly resistive solutions as microelectrodes pass only very small currents. It has also been shown that microelectrodes have the ability to be used in hostile environments such as frozen solvents and supercritical fluids (Wang, 2006; Bond, 1994).

Another point that should not be overlooked when considering the advantages microelectrodes offer over electrodes with larger dimensions is simply that the small critical diameter enables the analysis of small samples and localised measurements. This factor can allow in vivo monitoring in the cells of living organisms such as, for example, the simultaneous monitoring of ascorbic acid and dopamine (Štulík et al., 2000).

2.6.3. Microelectrode arrays

Despite the many advantages microelectrodes offer, as presented above, the small size does yield some drawbacks – the most obvious of which are the small currents generated with a single microelectrode, sometimes in the pico or even femto amp region (Bard, 2001). The signal size can be shown to be dependent on the electrode area and so the decreased area of the microelectrode will inevitably generate a much smaller current. This can lead to excessive noise when undertaking electrochemical interrogations since the small signal size may become swamped with electrical noise associated with the instrumentation. To avoid this issue, and the necessity for current amplifying instrumentation (Bard, 2001), a system of many microelectrodes connected in parallel can be produced (Ross et al., 1992), where a large number of very small conductive regions are separated from one another by insulating regions of comparative dimensions (Wang and Zadeii, 1988), which improves the current flow whilst retaining the microelectrode attributes discussed earlier (see section 2.6.2), this system is termed a microelectrode array (Figure 2.16).

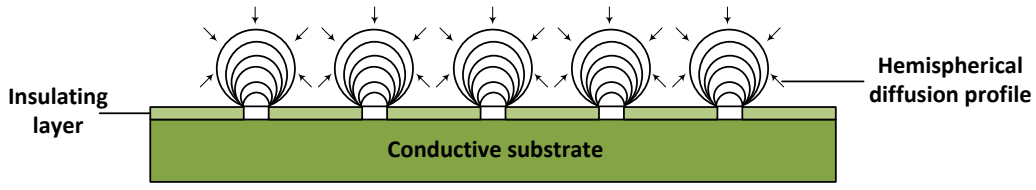

Figure 2.16 - Schematic representation of a microelectrodes array

2.6.4. Microelectrode fabrication methods

Brief reviews of some of the most common microelectrode fabrication techniques are now described; this is by no means an exhaustive discussion.

Glass encapsulated microelectrodes involve sealing fine metal (platinum or gold) or carbon wires within glass. A glass capillary is sealed at one end with heat before insertion of the wire. This is held in place under a vacuum and inserted into a larger glass tube which is subsequently sealed around the wire with the gradual application of heat. The surface of the electrode should then be examined under an optical microscope for imperfections about the wire and then polished with successively finer grades of sandpaper followed by alumina until a scratch free surface is obtained. Electrical connection is created through the injection of silver epoxy into the open end and inserting a connecting wire (Zoski, 2002). This approach is often used in scanning electrochemical microscopy where a microelectrode with a radius of 10 µm is required for close proximity analyses.

For the fabrication of similar disk-shaped microelectrodes on a smaller scale a pipette puller can be utilised. This involves inserting the fine wire into a glass capillary and pulling; this decreases the diameter of the wire and creates a tight seal between the two. The wire will be coated entirely with the glass of which some must be subsequently removed to expose the metal core. This can be achieved through etching with hydrofluoric acid or micro-polishing. Use of a pipette puller in this manner allows control of the rate of pulling and the temperature at which the pulling is performed and enables reproducible fabrications (Zoski, 2002).

Gold microbead microelectrode fabrication has been reported using microbeads with a diameter in the range of 1.5 to 3.0 µm. This lowered the cost in comparison to using a wire for the microelectrode fabrication as less gold is required. The microbeads are injected in a suspension into a glass capillary and the water is evaporated off in an oven. The heat is then increased and the gold beads are sintered into a solid mass which is then sealed within the capillary. The electrical contact in this system is made using an electrolyte solution.

Carbon fibre and metal disk microelectrodes may also be fabricated using chemical vapour deposition enabling an insulating silica coating to be deposited along the length of the heated carbon fibre or metal wire. A diamond fibre optics cleaver is used to truncate the end at a point along the length with an appropriate thickness of silica film, producing a clean tip surface. Metal disk microelectrode fabrication by this technique involves coating a 25 μm diameter tungsten wire with silica before removing some tungsten through electrochemical etching. This creates a cavity at the electrode tip which enables an element of selectivity when electrodepositing materials with selectivity towards the analyte of interest upon the microcavity.

Spherical microelectrodes can be fabricated through the self-assembly of gold nanoparticles and 1,9-nonanedithiol at the top of a pulled glass capillary. The inside of a pulled glass capillary is coated with a conductive carbon layer to which the 1,9-nonanedithiol is applied; this is then immersed in a solution containing the suspended gold particles and linkages occur at the tip. The result of this technique is a smooth spherical tip that is reproducible and which exhibits electrochemical properties of gold and microelectrode behaviour.

Carbon ring-disk microelectrodes are fabricated initially in much the same manner as carbon disk electrodes – where the carbon fibre is insulated using chemical vapour deposition of silica. At this stage the insulated fibre is purged with argon and a layer of pyrolytic carbon is the deposited. The silica deposition process is then repeated until the microelectrode is insulated. Once more the fibre is truncated and the tip polished. A ring disk microelectrode with platinum and gold has been described where a platinum wire is encapsulated in a glass capillary and the tip sharpened. A thin gold sputter coated film is then applied and then insulated with commercial nail polish. The ring-disk microelectrode is then exposed through polishing with aluminium oxide paper.

Electrochemical etching of metal wires can produce finite conical microelectrodes with dimensions in the tens of nanometres. This technique involves the application of an alternating voltage between the microwire and a platinum coil surrounding the wire whilst submerged in an etching solution bath. Once etching is complete, the wire is

coated with an insulating material leaving a small area exposed as the microelectrode. Carbon fibres have been etched by passing the fibre through an oxygen/methane flame before insulating with the electrochemical deposition of a poly(oxyphenylene) film or sealing in glass.

Microfabrication techniques have been used to produce reproducible microelectrodes with exact geometrical parameters. This technique has produced finite conical microelectrodes through first etching the silicon and then deposition of thin layers of silicon dioxide, platinum and silicon nitride. A photoresist layer was applied to all but the tips of these thin-films before removal of the silicon nitride tip with plasma etching resulting in a Pt finite cone microelectrode (Thiébaud et al., 2000). A microfabricated electrode that performs as an inlaid microdisk microelectrode was produced using a silicon wafer as the substrate. A silicon oxide layer was thermally grown on this surface and a photoresist layer was spin-coated onto both sides of this wafer and treated with UV light to develop the geometric design for the electrode assembly. Chemical etching then defined this pattern and one side was coated CR and then a thin layer of Pt. This metallic layer adheres to the Cr and so when the photoresist template is removed a layer of metal remains in the geometrical pattern of the microelectrode (Zhou et al., 1994). A similar technique was used to produce an integrated needle type solid state microelectrode system with a gold working and counter electrode – and an Ag/AgCl reference electrode for use in situ (Chen et al., 2010c).

2.7. Chemically modified electrodes

2.7.1. The dissolved oxygen electrode

In 1956, Professor Leyland C. Clark first described the oxygen electrode. This device combined a platinum working cathode, a silver reference electrode and a semi-permeable polyethylene membrane designed to screen all solutes other than oxygen. This oxygen electrode was designed for the determination of oxygen within biological fluids for cardiac core applications (Turner et al., 1986). Oxygen is electrochemically reduced at the working electrode and so the current measured is related to the concentration of oxygen present.

$$\beta\text{-D-glucose} + O_2 \xrightarrow{\text{GOD}} \text{gluconic acid} + H_2O_2$$

Equation 2.28

2.7.2. First generation biosensors

A first generation biosensor describes a sensor where the either the depletion of a substance or the production of a product is tracked at the transducer. The above device was subsequently modified by Clark and Lyons who were the first to demonstrate the principle that an enzyme could be incorporated into an electrochemical cell to produce a biosensor - specific for a particular substrate. First described in 1962, Clark and Lyons suggested incorporating an enzyme layer into the electrode system, *"the specificity of response is regulated by the placement and nature of the enzyme, the nature of the detector electrode, and the nature of the membranes"* (Clark and Lyons, 1962). This sensor was proposed to provide continuous monitoring of blood glucose for biomedical applications. Glucose oxidase would cause the reduction of glucose near the surface of the electrode. This reaction required oxygen and, therefore, the decline in oxygen levels can be shown to be inversely proportional to the glucose concentration present in the solution, see Equation 2.29.

$$^1/_2\,O_2 + 2H^+ + 2e^- \xrightarrow{\text{-600mV (vs. Ag/AgCl)}} H_2O$$

Equation 2.29

Although the initial use for this sensor was for the determination of glucose concentration, the possibilities that an enzyme sensor such as this could provide were quickly recognised. By 1969, Clark had industrial backing from Yellow Spring Instrument Company for a prototype of a dedicated glucose analyser, although there were at this time some unresolved issues surrounding the apparatus. The initial principles of an enzyme sensor were expanded upon further with the use of a dual cathode oxygen electrode and the incorporation of the enzyme into a polyacrylamide matrix upon the electrode surface (Updike and Hicks, 1967). This helped to eliminate some of the problems associated with fluctuations in oxygen tension. This two electrode format (where one electrode is covered with the active enzyme), allowed for the subtraction of the current of the enzyme-free electrode from that of the enzyme electrode to effectively remove these fluctuations.

In 1973, an enzyme electrode was proposed that, instead of detecting oxygen, operated via the detection of hydrogen peroxide liberated in a glucose-glucose oxidase reaction at an anodic potential (Guilbault and Lubrano, 1973).

$$H_2O_2 \xrightarrow{\text{-600mV (vs. Ag/AgCl)}} O_2 + 2H^+ + 2e^-$$

Equation 2.30

This determination of hydrogen peroxide was found to provide a more reliable and therefore accurate approach for following the glucose oxidase reaction, due to hydrogen peroxide being a direct product of the reaction between the enzyme and substrate (see Equation 2.28). There were, however, issues relating to other electroactive molecules in the blood that could also be oxidised at the anodic potential employed; the oxidation of other substances could act as interferrents which could cause erroneous readings.

The Yellow Spring Instrument Company now had the technology available for a viable hand-held device and a dedicated glucose analyser, and by 1974 this led to the launch of the Model 23 YSI analyser, Figure 2.17. This device included a selective barrier to

combat the interferences from other electroactive molecules in the blood, such as uric acid and ascorbate (Turner et al., 1986).

Figure 2.17- The YSI 23A blood-glucose analyser

2.7.3. Second generation biosensors

Second generation biosensors involve a mediator in the reaction mechanism between the reaction of interest and the transducer. Glucose oxidase may not directly transfer electrons to the electrode surface due to its' thick protein layer that surrounds the flavin redox centre (Wang, 2001). This spatial separation can impede the performance of a sensor and so a number of studies into circumventing this issue through replacing the oxygen with a different electron acceptor have been undertaken. The use of artificial mediators is one such approach that can circumvent this problem and this comprises what is known as a second generation biosensor approach.

An artificial mediator, such as ferrocene or one of its derivatives, can enable a measurement to become largely oxygen independent through transporting electrons between the redox centre of the enzyme and the electrode surface – the mediator acting as an artificial electron acceptor. This may be illustrated by the following reaction sequence (Cass et al., 1984), where Fe is ferrocene:

$$\text{glucose} + \text{GOD}_{(\text{ox})} \longrightarrow \text{gluconic acid} + \text{GOD}_{(\text{red})}$$

Equation 2.31

$$\text{GOD}_{(\text{red})} + 2\text{Fe}^{+} \longrightarrow \text{GOD}_{(\text{ox})} + 2\text{Fe} + 2\text{H}^{+}$$

Equation 2.32

$$2Fe \longrightarrow 2Fe^{+} + 2e^{-}$$

Equation 2.33

Ferrocene undergoes a reversible reaction, moving the electrons whilst not becoming consumed itself.

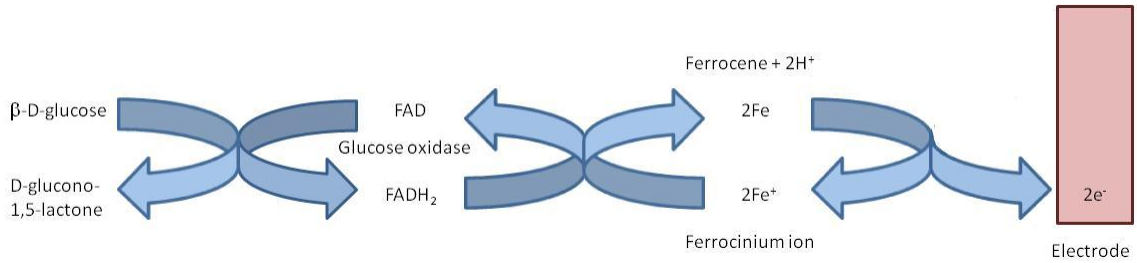

Figure 2.18 - Ferrocene mediated glucose oxidase electron transfer

Using a mediator in this manner allows for a rapid, reproducible analysis and importantly due to the ability to perform measurements at a lower working over-potential, there is less interference from other electroactive species which may erroneously contribute to the response of the sensor (Wang, 2001). The use of a mediator in this way facilitated the development of a low cost, portable, self-diagnosis system – the MediSense® blood glucose sensor. This system uses a small sample of the user's blood on a disposable screen-printed electrode; the current flow is measured with a potentiostat and the glucose concentration displayed on an LCD screen.

2.7.4. Third generation biosensors

The third generation biosensors apply to reactions where any products or mediators are not directly measured as the reaction itself causes the response that is appraised. Another development to improve the communication between the enzyme and the electrode surface has been through the covalent bonding of electron-transfer relays to the enzyme (Degani and Heller, 1987). This allows the electrons to be transferred from the redox centre to the relays, which are closer than the periphery of the enzyme.

These will in turn be transferred from the relays to the electrode. This technique allows for the rate of electron transfer from the enzyme to the electrode to be greatly increased.

These improvements have allowed increased development and subsequent marketing of enzyme sensors since they were first introduced. There have also been developments in other types of biosensors, including those that exploit the properties of other biological recognition agents such as antibodies and nucleic acids.

2.7.5. Future developments

There has been continual research towards the development of other types of sensors, for example, photometric sensors which may be used to measure pH, oxygen, carbon dioxide, ammonia and ions (Eggins, 2002). Such sensors can include techniques such as optical analysis - bioluminescence and chemiluminescence or fluorescence emission. Electronic noses represent another class of sensor which attempt to mimic the mammal olfactory receptors, detecting specific chemical fingerprints which can reveal, for example, information regarding food freshness or quality (Zhang et al., 2008).

2.8. Polymers

The term polymer is reported in modern literature as deriving from the Greek '*poly*' meaning 'many' and '*meros*' meaning 'units' thereby inferring that a polymer refers to a large molecule created from many repeating monomer units. This is not, however, the original use of the term which was, in fact, a description of polymerism – where molecules have identical empirical formulae but vastly different characteristics (Nicholson, 2006).

Polymers may be synthesised from their monomer units either chemically or electrochemically in various ways. Chemical syntheses can generally be divided into two distinct categories: step-growth polymerisation and chain-growth polymerisation. Electropolymerisation involves a three-electrode cell where the electrochemical bath comprises a solution of the monomer in solvent and the appropriate electrolyte. This technique is discussed further in the next section.

2.8.1. Electropolymerisation

Electrochemical thin-film deposition provides a simple technique for the controlled application of polymer coatings to a variety of surfaces and for a variety of uses such as, for example, electrode materials for rechargeable batteries (Sivakumar and Saraswathi, 2002), polymer solar cells (Krebs, 2009) and electrochemical biosensors (Ramanavičius et al., 2005; Ates and Sarac, 2009).

Electropolymerisation of a polymer onto the surface of an electrode has advantages over historical polymer coating techniques, such as casting (Sittampalam and Wilson, 1983), as it enables automation (Beck, 1988), is reproducible, provides total control over film thickness (Bartlett et al., 1990) even on non-flat surfaces (Osaka, 1997).

Polymer films are deposited electrochemically through the oxidation or reduction of a monomer solution to form either insulating or conducting polymer films on the surface of the working electrode. Insulating polymer films are said to be self-limiting in nature as increasing the number of potential cycles naturally lowers the electrical conductivity

of the sensor until it is completely insulated. At this point the electrodeposition cannot proceed further as the electrode has essentially been isolated from the monomer solution. Conducting polymers are less affected by this phenomenon as they display properties such as electrical conductivity, low energy optical transitions and high electron affinity (Gerard et al., 2002).

The electrochemically induced deposition of a polymer is generally performed with a standard three-electrode configuration as described in section 2.4.4 in an electrochemical bath containing the monomer dissolved in an appropriate solvent within an electrolyte solution. The deposition is initiated and propelled by the application of a power supply to the electrochemical cell this may be carried out either potentiostatically, where the voltage is held at a constant, or galvanostatically – at a constant current (Deshpande and Amalnerkar, 1993).

Variations in the electrochemical deposition procedure can have an influence on the resulting polymer film; deposition time and temperature, solvent system, electrolyte, deposition charge, the number of cycles and the electrodes used can all have an effect on the surface morphology and conductivity of the polymer film (Guimard et al., 2007).

2.8.2. Conducting polymers

Conducting polymers contain a conjugated backbone – a system of alternating single and double bonds where each bond possesses a chemically strong localised *sigma* bond and each double bond also contains a less localised, weak *pi* bond. This conjugated nature leads to, in part, the unusual properties associated with conducting polymers, such as the electrical conductivity and high electron affinity (Gerard et al., 2002). The electrical conductivities of these polymers can be seen to approach that of metal and for this reason they are often referred to as synthetic metals (Nicholson, 2006).

The electrically conducting nature of conducting polymers can be related to the transference of charge along this conjugated chain, between chains or between particles. The transfer of charge can occur where there is an unoccupied electron position, or vacancy, which leads to this position being filled by a neighbouring electron. The movement of this neighbouring electron creates another vacancy which, again, is filled by a neighbouring electron – in this manner; a positive charge can migrate along the polymer. The addition of a charge carrier that may add or remove an electron from the polymer, and thus alter the polymer into its conducting form, is referred to as *doping* in the literature and the conducting form is known as a doped material. These charge carrying materials are, naturally, known as *dopants* and may take the form of an acid or inorganic molecule that serves to initiate the charge transfer in conducting polymers through the addition or removal of electrons (Nicholson, 2006) although the precise mode of action is not clear (Nicholson, 2006).

3. Economic theory, terrorism and the management of a new product development for security applications

3.1. Introduction

Macroeconomics is related to the study of the total, known as the aggregate, measure of economic activity. This involves national income, output and expenditure and the consequences for employment and prices (Nellis, 2004). Macroeconomics is also associated with the international economy as a whole and the flow of trade and capital between countries. Microeconomics, on the other hand, relates to individual aspects of the economy or the immediate environment to a firm or sector such as, for example, the revenues and costs of production of a single firm, or individual market prices.

The study of economic theory can be applied to many areas, such as security, defence and ecology as well as the household and human needs. This is because all of these areas are involved in and have influence on the state of the economy. It is common to assume that the economy relates simply to the market and the state – it will be shown, however, that the non-monetary economy is fundamental to both human life and to the operation of the formal economy – the reverse of which is not correct (Anonymous1992).

This section will first explain some macro-economic and behavioural economic theory, as pertinent to this work, before relating these theories to terrorism and security as well as the cost this can have on both the national and international economy. Once the significance of the cost of terrorism on both capital market and the world economy has been established, a review will be attempted to evaluate the parameters effecting new product entry into the market, with reference to the defence and security sector.

3.2. Macroeconomic theory

3.2.1. The economy

As mentioned earlier, macroeconomics is related to the economy as a whole – the national output, income and expenditure and how this impacts on employment and prices (Nellis, 2004). The measurement of economic activity is necessary to enable reliable and rational decisions to be made. Changes in the level of production of goods and services are usually the manner in which economic activity is assessed; this is known as the national income. The flow of national income can be measures in three ways: the output (or production method), the income method or the expenditure method. Theoretically, the same monetary value should be obtained when calculating the national income from any of the three above methods since they each measure the same flow of income around the economy, just at different stages (Nellis, 2004).

3.2.2. The circular flow of income

The circular flow of income model refers to the flow of income between the households and firms within the economy – both forward and back (Nellis, 2004). Economies are comprised of five broad sectors into which all economic agents may be placed. These are:

- The household sector,
- The firm sector,
- The government sector,
- The financial services sector, and
- The foreign sector

These sectors are all interrelated and the flow of income between sectors can have an influence on the balance of the economy and economic growth. Macroeconomic involves assessing these relationships between sectors and relating this to the activity of the economy as a whole.

3.2.3. Aggregate supply and demand

Aggregate demand

Aggregate demand equates to the actual output of the economy and therefore the aggregate planned expenditure – the consumer spending, government spending, investment spending and export (minus import) spending. Where there is an increased level of aggregate demand in the economy there will also be an increase in the output of the economy (GDP). This may be illustrated with an aggregate demand curve which demonstrates that a change in price level is dependent on a change in aggregate demand, see **Error! Reference source not found.**. The downward slope of his demand curve is due to the real money balance effect and the substitution effect which will be discussed further below.

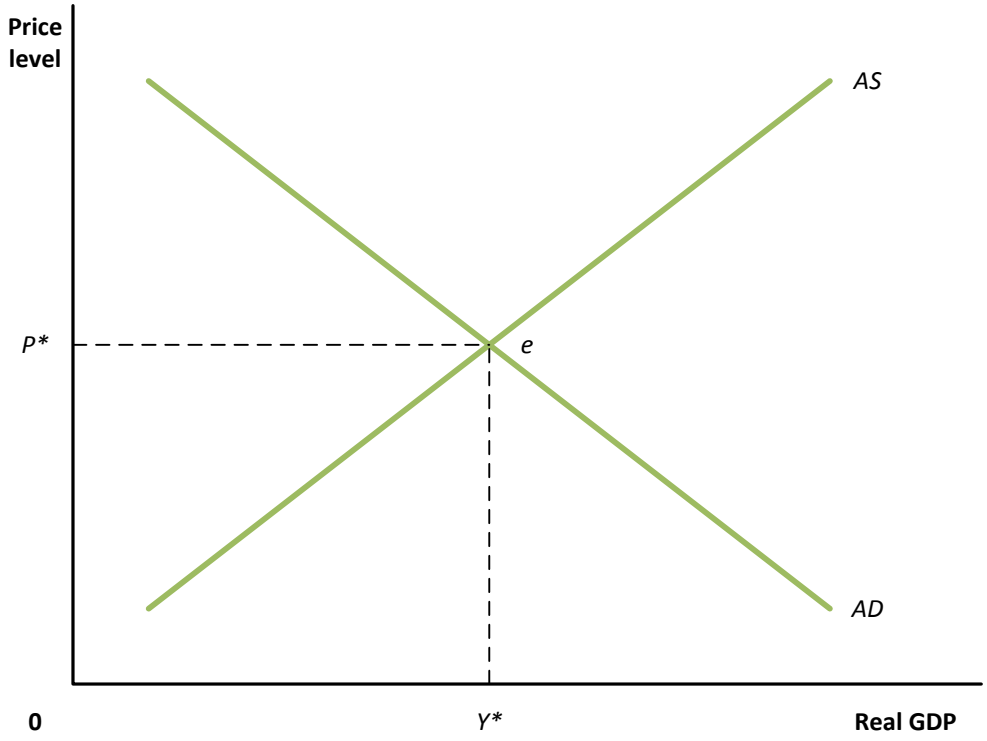

Figure 3.1 - The macroeconomic equilibrium between the aggregate demand and the aggregate supply

Changes in aggregate demand

There are many factors that influence the aggregate demand, the most significant of which are government macroeconomic policy, expectations of firms and households and global trends. These will be reviewed briefly here, but will be discussed in greater detail in section 3.5.2.

Changes in the fiscal policy, the expenditure and taxation policies, of the government will have a direct impact on the aggregate demand of household and firms. An increase in taxation and reduction of government spending will have a contractionary effect, lowering the GDP of the economy; an increase in government spending and decrease in taxation will stimulate growth in the economy – an expansionary effect, see **Error! Reference source not found.**. These trends only hold when all other aspects emain constant.

Global trends can have a substantial effect on the economy of individual national economies, not only as it can affect the expectations of firms and households for the future, but because the amount of exports and imports of an economy can be heavily related to changes in currency exchange rates. More imports and fewer exports will shift an aggregate demand curve to the left, effectively reducing the real GDP of the economy. The reverse of this is also true – an increase in exports and decrease in imports will expand the economy (illustrated by a shift in the aggregate demand curve to the right). Due to the reliance between countries on trade it can be observed that when one large economy is labouring this will have a direct effect on many other economies in the world – this was highlighted in the late-2000s with the financial crisis initiating in the USA but quickly spreading to many of the world's major economies.

Aggregate supply

Aggregate supply in an economy is, as described earlier, the total amount of goods and services available at a particular time. This depends upon the labour, capital, land and the technology (including technical knowledge) available within that economy. Essentially it would seem that the more of these factors available, the larger the economy will be; but it should be noted that simply having these factors available may

not indicate their effective utilisation, for example, skilled labour is more productive than unskilled labour.

Short-run aggregate supply

Short-run aggregate supply relates the price level in the economy with the real GDP. A higher price level may induce a raise in the level of production of goods and services when not at the maximum production level; lower price levels will tend to decrease the levels of real production in the economy. The upward slope of the curve represents an increase in real GDP rather than price as the aggregate demand increases **Error! Reference source not found.**.

The macroeconomic equilibrium

The aggregate demand and short-run supply curves can be placed together on a chart to demonstrate the macroeconomic equilibrium. This equilibrium is reached where the two curves intersect and at this point the aggregate demand for goods and services is equal to the aggregate supply of goods and services, see **Error! Reference source not ound.**. The equilibrium can be seen to be when there is a real GDP of *Y** and a price level of *p*.*

3.3. The economics of human needs

The continuous failure to satisfy human needs can result in progressive, and sometimes irreversible, human malfunctions. The most obvious needs are those of sustenance and survival – food, water, light and air. Although, other many needs are suggested in the model below, see Figure 3.2.

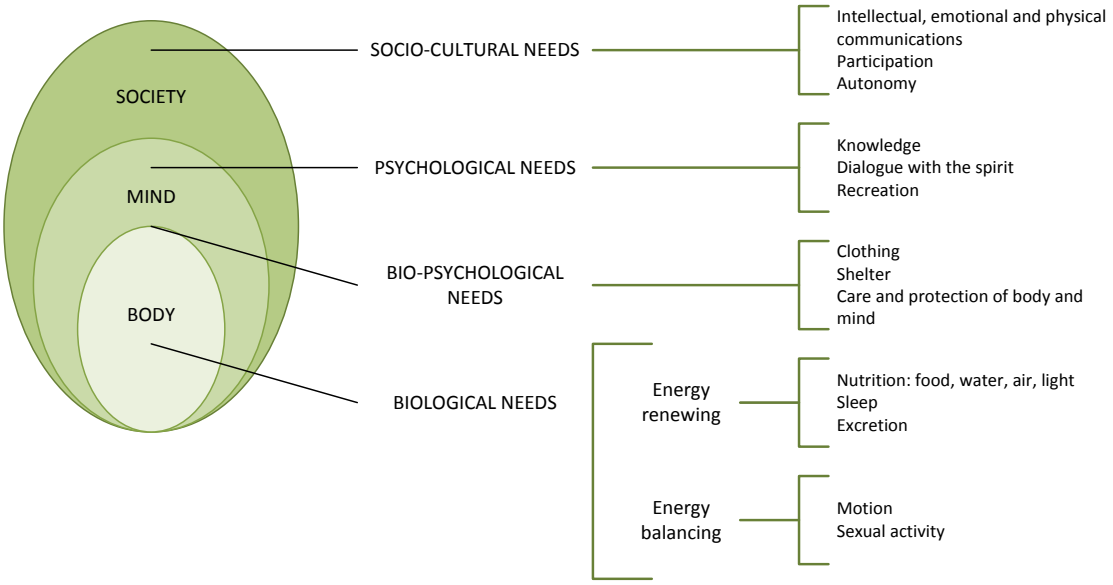

Figure 3.2 - A model representing a minimum set of needs for a human being (from (Anonymous1992)**)**

Needs cannot be influenced by society or by the will of the conscious mind since they stem from the unconscious – unlike desires or wants which are very individual in character and can be modified or resisted through will-power and rational decision making.

This model suggests that the satisfaction of needs at any level above the biological needs level, as seen in Figure 3.2, must first have the satisfaction of those needs in the levels below.

When one or more needs are left unsatisfied, human beings will find techniques to attempt to reduce the deprivation effects. This theory has been used to describe the amount of consumption observed in those who are rich but feel emotionally isolated. Human beings have developed a societal structure than enables an increased possibility of attaining these vital needs with a reduced risk to the individual.

Improvements in economic systems can work towards improving the satisfaction of the needs of the human – improved production, technology and education facilitates this, as does the role of communities – not only for basic socio-cultural requirements but also for the protection against brutality and violence that can be a real threat in situations where basic needs are not met (Anonymous1992).

3.4. Human rationality and decision making

The neo-classical theories of economics were based upon a simple assumption – that humans are essentially working to maximise their satisfaction levels, also known as utility, in all aspects of economic life. The behaviour of humans in this context was described as rational and all decision making would be based on this rational approach.

Work beginning in the 1950s performed by both economists and psychologists attempted to relate the neoclassical economic theories to actual human behaviour – this entailed considering the emotional behaviour of the human being. It was discovered that instead of this rational behaviour, humans were often influenced by changes in context and in uncertainty to the market; and that they partook in *mental accounting*, whereby different values of utility were placed upon short or long term goals and outcomes (Dowling and Chin-Fang, 2007).

There are many circumstances when individuals do not make decisions in a fashion that may maximise their utility; a brief review will now be made of some of the reasons for this. The first reason is simply due to the inherent *short-sightedness* of some human beings. This has been postulated to be due to three emotional factors: impulsivity, compulsivity and inhibition, where those who are more compulsive, for example, will be more likely to save for retirement while those who are impulsive will be unable to postpone their consumption, leading to higher probabilities of debt.

Another example of irrationality in decision making is that consumers often do not have the time or are unwilling to carry out a full survey of the price of equivalent standard products within a market before they make the decision to purchase. Due to this, the variation in price of some products can be considerable – this would not be the case if all consumers completed this research as prices would generally gravitate to a lower price across the board.

It can be the case that people in general underestimate the probability of a future unwanted or unpleasant event which can lead to greater risk taking activities and

under-insuring. There is, however, also an argument that attitudes towards risk can depend upon the likely risk or gain expected from that behaviour – with most people there is a greater tendency to act in a risk adverse manner since the fear of loss is greater than the possible gain attached to the risky behaviour.

Probabilities of likely and highly unlikely situations and events can be given different weight by people – examples could include unlikely events such as a plane crash which has a statistically very low probability of occurring but is often given a higher psychological weight than a more likely event, such as a car crash. This may be due, in part to the amount of press coverage such an event will command which stays in the human consciousness when making decisions (Dowling and Chin-Fang, 2007). In such cases, the role of memory has been suggested to increase the probability of an irrational decision. Those events that are easily remembered are believed to be more probable. These beliefs persist even after it has been demonstrated that this increase in probability is false. The greater the vividness and evocativeness of these events, the greater the degree of recall and consequently, the greater the belief in that event reoccurring. This phenomenon is called *hysteresis*.

3.5. The effect terrorism has on the economy

3.5.1. Introduction

There are many descriptions and definitions of what terrorism is but they are mainly focussed in the same area; terrorism is broadly the use of any type of violence that endangers the public, or a section of the public, for political gain. It is a criminal act that affects the public significantly beyond just those directly involved in the violent attack. It is this factor that the terrorist uses as a specific strategy to draw attention to their cause – terrorists plan their acts to achieve as much publicity as they can and choose targets which symbolise all that they oppose.

3.5.2. Human behaviour, perceptions and terrorism

It has been suggested that not only do acts of terrorism have an effect on the economy, but that the economic climate can influence the incidence of terrorism within that climate. Blomberg et al, 2004, examine this premise with an examination of 127 countries over the period between 1968 and 1991. Using economic variables such as the growth in GDP per capita and levels of investment they were able to assess the influence economic conditions have on the likelihood of terrorist attacks.

Due to the large and varied data set it was possible to surmise that during periods of adverse economic conditions there is in general two possible ways that those who oppose the regime may act – either with a rebellion or a terrorist attack. It was also reported that this choice is based on the type of economy under examination; for example, a democratic, high income country would be more likely to suffer a terrorist attack whereas a country with low growth rates, high government taxation and higher political unrest have an increased likelihood of a rebellion since the payoff to such an attack would be considerable and the cost to initiate may be considerably less than in the example of a democratic country (Blomberg et al., 2004b).

Human perception and attitudes towards terrorism were discussed in section 3.4 where it was highlighted that although the level of occurrence of terrorist attacks

remains fairly low in many countries that actual perception of risk remains quite high. Turvey et al, 2010, examined this phenomenon with regards to bird flu and terrorism and the affect the perception of risk in these areas has on the economy. It was noted that after such an incident there is a decrease in consumer demand which will modify the aggregate demand curve, Figure 3.3 (Turvey et al., 2010).

The effect of consumers' perception of risk has is that they become more resistant to price decreases, a traditional strategy that suppliers would use to increase consumer demand for goods and service; this can be observed with the shift in the aggregate demand curve.

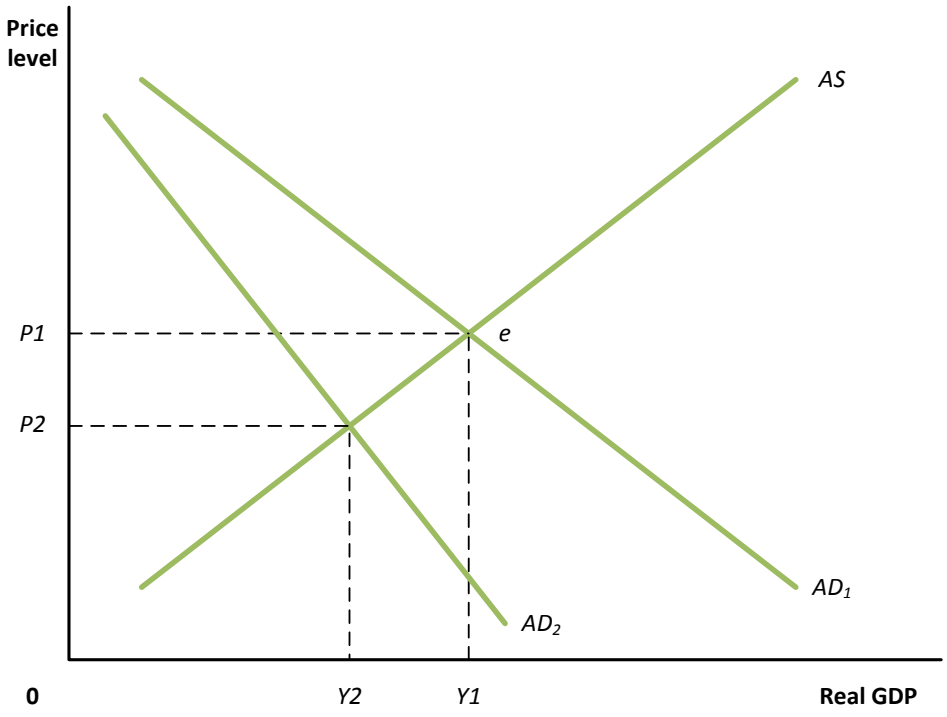

Figure 3.3 - Effects of an economic shock on consumer demand, GDP and price

Much of economic theory relies on the consumer being assumed to be rational, when there is a perception of fear this irrationality opposes those economic analyses – hence the price reduction does not provide the desired effect.

It is necessary to calm the markets through convincing the public that the risk is actually fairly low; it has, however, been highlighted that despite the threat being

removed it can take considerably more time for consumers to reverse their negative consumption habits, the phenomenon known as hysteresis. (Turvey et al., 2010).

Drakos and Müller investigated the risk perception differences in various countries across Europe and attempted to explain the variations between these perceptions of risk of terrorism. Using the question *"what do you think are the two most important issues facing (OUR COUNTRY) at the moment?"* allowed the respondents freedom to choose from a list that they themselves hold rather than introducing possible issues that may influence their reply. The terrorism risk concern was then calculated from the number of respondents that mentioned terrorism in response. Further data was aggregated and analysed relating to the amount of terrorist attacks each country had suffered, the death rate and the rate of injury in these attacks. It was concluded that risk perception variation can only be explained by the long-term terrorism risk faced by each country; so the risk perception observed in the respondents is related to the long-term trend of terrorism and not by the arrival of new terrorist threats. If this is the case, then the resolution of the perception of terrorism would be difficult to address as it would take significant time to reduce the perception of long-term risk (Drakos and Müller, 2011).

The effect of terrorism on human behaviour has been examined in another context by Gould and Stecklov, 2009, as they research and argue that terrorism raises the *cost of crime* to criminals. The hypothesis behind this research was that through two channels the opportunity cost of committing a crime on the day of the attack and for up to five days afterwards is such that rates of crime diminish in this time period. There are two postulated reasons for this reduction: firstly, the increased presence and activity of the police force and secondly, the terrorist act causes more people to stay at home rather than partake in leisure activities. As such, property crimes, such as burglary, auto-theft and thefts from cars see a reduction in occurrences both in the private home, where the owners are present, and in public places, where the police are present. Conversely criminal acts such as trespassing and disrupting police see an increase – probably due to the increased police presence allowing officers to catch criminals in the act (Gould and Stecklov, 2009).

3.5.3. Terrorism and capital markets

"Prices of individual stocks reflect investors' hopes and fears about the future, and taken in aggregate, stock price movements can generate a tidal wave of activity" (Chen and Siems, 2004). Due to the ease at which stocks and bonds may be bought and sold, unforeseen circumstances can have disastrous consequences within the financial market. Chen and Siems, 2004, undertook an event study of 14 terrorist / military attacks within and the effects these incidents had on the both the US and global financial markets. As the markets today are truly global due to the speed at which information is disseminated, a terrorist attack in one country can quickly and adversely influence the financial markets throughout the world – this is known as the contagion effect.

Where some markets, such as the United States, may have the ability to quickly rebound, other financial markets do not. Reasons postulated for this relate to the stability of the financial and banking sector prior to any incident. For example, the US market has become increasingly resilient to shocks over time, with the amount of trading days before the Dow Jones Industrial Average index returns to the pre-shock level decreasing from 795 after Hitler's invasion into France to 40 days after the September 11, 2001 attacks. While most countries in the study rebounded within 2 – 60 days after this event, some took much longer, for example, Saudi Arabia took 100 and Austria took 98 days to reach the pre-shock trading level. This has been attributed to several factors: an improvement in technology had led to improved communication leading to information acquisition and transmission allowing the markets to be more efficient; also, flexible monetary and fiscal policies assure markets and promote stability (Chen and Siems, 2004).

Arin et al, 2008, reported research in the same theme, also investigating the effects of terrorism on financial markets and the magnitude of the effects on emerging versus established markets. While it can be argued that stockholders may hedge against expected events, unexpected changes cause uncertainty (risk) and therefore volatility in the market. The behaviour of stock market volatility in relation to shocks produced

by terror events was examined to assess the influence they may have on the markets of six countries selected for examination. It was found that the response to terror varies between countries although there was evidence of significant causality effects in all six countries. It was also highlighted that of the six, the two European countries faired best as they were generally less affected by terror shocks indicating that financial investors are more resilient (Arin et al., 2008).

This theory was supported by the event study conducted by Kollias et al, 2011, into the effects of terrorist attacks on a small and a large capitalisation market. Using the London stock exchange as the large market and the Athens stock exchange as the example of the small market for this study, the authors examined the market activity in relation to terror events between 1984-2005 and 1958-2000, for London and Athens respectively. The aim was to discover whether the reaction to terrorist events has changed over time, whether market size and maturity determine the reaction and whether the reaction of the market depends on the target or the perpetrators of the attack. It was concluded that there was not a definitive pattern in the reactions of the market, although in the small market there was an increased adverse reaction where businessmen had been targeted; and while the effects in general are transitory, attacks weighted by the number of casualties and fatalities significantly affect the volatility of the market. As surmised earlier, the small market fared worse than the larger one; the reason postulated for this is that the more mature, larger market has more effective internal checks and balances that can absorb shocks caused by external events (Kollias et al.,).

The same authors (Kollias et al, 2011) carried out research to analyse the effects of the bomb attacks on Madrid and London in 2004 and 2005, respectively. In this paper, it was reported that although the reaction to the bombing in both Madrid and London was similar on the day of the event, with both markets adversely effected, London began to rebound on the same day while Madrid, although displayed an initial drop that was calculated to be statistically insignificant, continued to see these negative falls for 11 days afterwards before beginning to rebound consistently. Explanations for this were along the lines of those postulated in the previous paper: including the size,

structure and liquidity of the market. It has also been noted that although effects on the markets can be relatively short-term, the feeling of insecurity among the general public can last much longer (Kollias et al., 2011).

3.5.4. Terrorism and the world economy – macroeconomic effects

"It has been argued that terrorism should not have a great effect on economic activity because terrorist attacks only destroy a small section of the stock of capital of a country" (Abadie and Gardeazabal, 2008). In reality, it is generally observed that a terrorist event can have a large effect on the economy of the country that experienced the event. Abadie and Gardeazabal, 2008, illustrate this point and establish that the mobility of productive capital is such that the transfer of it to safer markets is a simple and swift reaction to such events.

From an economic perspective, terrorism has four main effects on a country: capital stock (human and physical) is reduced, terrorist threat increases levels of uncertainty, terrorism increases expenditure in anti-terrorism R & D thus removing from other areas of research, and terrorism negatively affects certain industries, such as tourism. As the world functions as a global economy due to the ease by which foreign investments may be made, it can be observed that a reallocation of capital away from a volatile market often accompanies a terrorist incident. This can be seen, for example, in the case of the USA just after the September 11th terrorist attacks in 2001. In the year 2000, the foreign direct investment, the FDI, represented 15.8% of the gross fixed capital formation of the country; this figure had decreased to 1.5% in 2003 and the outflows had increased marginally during this same period.

Beyond increasing uncertainty, terrorism also reduces the expected return on investment which encourages investors to diversify their stocks across a range of countries to minimise the risk, causing large movements of capital across countries in reaction to terrorist incidents (Abadie and Gardeazabal, 2008).

Research along the same theme was conducted by Blomberg et al, 2004, who conducted a study of 177 countries over the period between 1968 and 2000 into the effects of terrorism on the macroeconomy and found that the incidence of terrorism does have a significant negative effect on growth. Once more it is observed that there is a redirection of economic resources away from investment spending and towards government spending – in particular spending on anti-terrorism research. It is also

highlighted that while it is the developed nations that suffer the greatest proportion of terrorist attacks, it is those attacks on the developing world that have the greatest effect on negative economic growth. It is thought that the cause of the terrorist incidents in developed countries can be related, in part, to the isolation of certain groups as a consequence of modernisation; this modernisation also provides the means of equipping these groups in a cost effective manner (Blomberg et al., 2004a).

Eckstein and Tsiddon, 2004, looked at the consequences of terrorism on the macroeconomy of Israel. They highlight many of the same concepts as those reported before. Fear and bewilderment can negatively influence the economic activity of the individual and this paper focuses on this increased uncertainty about life and the reaction that governments and the individual have to this uncertainty. The total cost of terror can be related to the changes in consumption and investment of the individual in reaction to this perceived reduction in life-span; as well as the increased expenditure on defence by the government (Eckstein and Tsiddon, 2004).

"Terrorism may range from ethnically motivated to state sponsored, from religious to ideologically motivated; it can directly target the government, the military or the civilian population, assassinate individuals or threaten the use of weapons of mass destruction" (Llussá and Tavares, 2011). The cost of these terrorist attacks can be substantial, and when a country is targeted continuously this cost may increase further as the uncertainty in the economy increases. Llussá and Tavares, 2011, undertook a study into the economic cost of different types of terror attacks on different economic aggregates using the economic variables: rate of growth of output, private consumption, investment and public consumption. It was discovered that private consumption and investment are negatively affected by all indicators of terrorist attacks (target of attack, how many killed, how many injured, who performed the attack). Growth output and public consumption are less effect, leading the authors to propose that output might not be the ideal indicator to use when assessing the impact of a terrorist event on the economy. The most important determinants of expected falls in consumption and investment are the number of victims (killed or injured) and the number of attacks (Llussá and Tavares, 2011).

The adverse impact of terrorism on economic growth and the stability of various industries has been well documented; perhaps one of the industries that is most effected in this manner is the airline industry. Apart from the obvious impact of terrorist hijackings, such as those occurring on September 11th 2001, causing a reduction in demand for air travel, there are other factors that induce further stress on this industry. The price of airline stocks suffered a significant decline in the immediate aftermath – American airlines had an average price devaluation of 53% and the average for non-American airlines was 31%. Aside from this, volatility has also increased due to the escalation of uncertainty in the market. This has an effect on the likelihood of investors investing within this industry and increases the probability of these investors spreading their portfolio between this and more stable industries. This in turn has an effect on the ability of the airlines to raise capital which is necessary for them to address some of the issues highlighted by the 9/11 attacks, such as increasing security techniques and staff training (Drakos, 2004).

As mentioned earlier, the airline industry is not the only one that is directly affected by the impact of terrorism. The example provided previously is the significant movements of government funds into security and military projects as preventative measures against terrorist attacks. This can detract spending from other research and development projects and economically productive investments as the immediate priority is presented as the prevention of future attacks and to reassure the population. This can be detrimental – as was especially seen in the economic climate surrounding the 9/11 attacks where the economy was already struggling.

Furthermore, it was observed in the aftermath of 9/11 that there was a significant decrease in the amount of foreign students admitted into the USA to study due to the stringent security checks that were put in place by the government to restrict access to scientific and technical information. This tactic will decrease the talent pool from which further technological innovations may be generated.

This depletion of government spending is not the only cost to the economy, trade flows were also observed to be adversely effected. Those industries that had instilled a ‘just in time’ approach to keep their supply chain lean now found that it was

necessary to increase buffer periods to offset an increase in processing times and unpredictability related to customs when exporting and importing goods. Companies with large quantities of vulnerable assets found themselves needing to spend significantly greater amounts on the security and protection of these assets; especially as insurance companies began to either raise their premiums or retract their coverage for terrorism-related risk altogether (Koh, 2006).

Despite these highlighted issues, there are opportunities that arise from terrorist incidents such as these, this has been the case over many years and has influenced the development of many technological improvements. The most influential improvements are likely to be observed in information technology – one Wall Street trading firm, Cantor Fitzgerald, lost nearly 700 employees in the September 11th terrorist attacks and with this vast quantities of facts, names, phone numbers, wisdom and tacit knowledge. There was also a huge amount of non-computerised paperwork that was lost in this attack, such as contacts, wills and mortgages that had not been transferred to a database. This has led to an increase in cloud computing, where data is saved off-premises to ensure its safety should something happen to a company headquarters.

Biometrics, where humans are recognised automatically based on unique physiological or behavioural characteristics, has seen an increase in investment as a direct consequence of the 9/11 terror attack. Systems to examine cargo shipments have been developed primarily to identify explosives but also illegal drugs entering the United States. Radio-frequency identification (RFID) tags are another industry that has the capacity to help improve the security around ports. This technology enables the real-time tracking of individual containers throughout the supply chain.

There has also been an increase in funding towards treatments and vaccines, for example Anacor Pharmaceuticals was launched in 2001 with $21.6 million from Pentagon and venture-capital funding and are performing animal testing of antibiotics to treat anthrax, whilst Dynport has developed a faster acting anthrax vaccine.

From this it can be observed that the increased government spending and the reallocation of research priorities can improve technology in areas other than the immediate defence and security of an economy (Lin et al., 2007).

Frey, 2009, has conducted research into the best approaches for businesses to cope with terrorism. The first proposition is to reduce the incentives for a terrorist to attack a business. Once more assuming that terrorists are rational, and that they intend to produce the maximum effect with each attack, it is expected that highly visible targets will attack more attention from the media and the public in general. As such, Frey suggested having decentralised headquarters and main administrative offices. In this manner, the company itself will be able to continue trading despite a terrorist incident giving the impression that the attack was less efficient. It was also suggested that all decision makers should not be employed in the same building for the same logistical reason. Another suggestion, perhaps most relevant to companies operating in a hostile country, is to endeavour to employ the friends and relative of the terrorist group; this increases the cost to the terrorist of carrying out attacks on the company but obviously holds possible disadvantages too. It was also proposed that a strategic plan should be in place for the swift reconstruction of physical capital should an attack occur, enabling the company to continue trading within a short period of time (Frey, 2009).

Sandler and Enders, 2004, look at the policies that have been made to deal with terrorism and their relative effectiveness. Once again highlighting the over response that the general population are prone to when considering terrorist incidents where the actual risk to oneself may be minimal, the authors investigate how governments respond to quench this perceived risk and the effectiveness of these policies, such as using deterrents, game theory and non-negotiation strategies. It was also noted that, despite the public and media reaction, international terrorism is not on the rise; in fact the opposite is true. High and low levels of terrorism come in waves or cycles; this has been attributed to a number of factors: the heightened public sensitivity following an attack encourages other terrorists to strike in this climate for maximum media attention, these cycles may also be a result of attacks and counterattacks between the

terrorists and authorities – when a government crackdown takes place after an attack a temporary lull can often occur. During this time terrorists can regroup and spend time recruiting to prepare for further offensive strikes when these government defensive measures are relaxed (Sandler and Enders, 2004).

3.6. Defining the market

The market, with reference to management and marketing, can be defined as the group of consumers that have the means, motive and are permitted to acquire a product (herein a product may describe either a goods or service). Starting from the total population, the potential market may be described as all those within the total population who are interested in the acquisition of a certain product and this is then subsequently narrowed as sections of the market are excluded: the available market can be defined as those who have the money to buy the product, the qualified available market describes those who are permitted by law or regulations to purchase the product, the target market relates to those groups who have satisfied the above parameters and who the firm has elected to serve and the penetrated market are those groups that have purchased the product. The market, as described above, may be considered to be either a local market, where local can mean simply the potential market population within a general locality or the entire domestic market depending on the size and type of the firm, or a global market.

The market into which the sensor described in this work would most likely be situated is the defence and security sector. This is a fast growing sector both in the UK and globally – the UK export market in defence sector rose from £20bn in 2001 to £29bn in 2007 and was the top global defence exporter in 2007 with a 33% market share. The global security market is worth £120bn and estimated to reach £200bn within 10 years, within this are counter-terrorism, border control, transport security and forensic sectors into which a fully developed system based on the sensor system described in this work could function ((Government,).

One sector that might be viewed as having suffered in a monetary sense with relation to the threat of terrorism and the subsequent security requirements would be the aviation sector. Spending on aviation security has increased significantly since the terrorist attacks on the Twin Towers, NY, in 2001. A report conducted by the International Air Transport Association (IATA) published in 2011 states that airline spending on security has reached €4.9bn ($7.4bn / £4.6bn) per year, an increase of

25% since the 2001 terrorist attacks (McNeilly, 2011; Driscoll, 2011; Milmo, 2011). The security costs to airports has also been significantly affected with the costs related to security rising from 5-8% (on average for a European airport) to 29% of the operating costs of an average airport (Driscoll, 2011). London Gatwick, the UK's second largest airport, has, for example, invested £45m on security in 2011 (Driscoll, 2011) and Belfast International Airport has reported a spending of £10m annually, three times the amount spent on security in 2001 (McNeilly, 2011). The requirement to ensure that the aviation industry is as safe as possible for the passengers and staff has clearly come at a great cost to the industry. It is because of this that manufacturers of security scanning equipment have seen a corresponding increase in annual revenues since the same terrorist attack. The Smith Group, for example, manufacture airport scanning devices and have seen their revenue increase from £130m in 2001 to £574m in 2011 (McNeilly, 2011; Milmo, 2011). As such, as insensitive as it may seem, the security sector would apparently present a lucrative opportunity for competitive new products to be launched.

There are, as might be expected, many large scale players within this area due to the substantial returns that can be expected when a successful contract has been won. Some of the technologies available for explosive detection, whilst performing the task well, are costly. Even the training of explosives sniffer dogs, one of the most established explosive detection methods, is substantial – the cost to purchase a trained explosives dog is $10000 and a subsequent $2000 is required each year for care and feeding (Haupt et al., 2004). This can pose an exclusion factor on smaller businesses without the vast purchasing power of, for example, the aviation industry. The cost of some of the devices currently available can be observed in Table 2.1 this table also provides information relating to the size of the instrument (in weight) (Caygill et al., 2012). Factors relating to the adoption of new products into an established industry are discussed in section 3.7.4.

3.7. The management of new product entry

The development of a strategy that can best manage the entry of a new product into the marketplace is necessary to identify the likely growth options associated with entry into different types of market. The market may already be established, as in the case of ion scan instrumentation at airports, and new products entering into that market will be in direct competition with those established products. Conversely, a new product can be such that it creates a new market. The position of the product and the type of market into which it is entering will necessitate a different management strategy.

The definition of a new product can be a difficult task to undertake, is a product new or simply an extension to, or adaption of, an already existing technology? A product has many dimensions such as, for example, price, packaging, technology, quality specifications, brand name and level of service, to highlight a few. The change of any one of these might constitute a product change and, therefore, create a new product. It has been stated that as long as a product is perceived to be new it *is* new (Trott, 2005) insinuating that the concept of newness is a relative term. The majority of purported new products can often be seen to be developments or variations on existing formats, with as little as 10% of new products released being new to both the market and the firm (Trott, 2005). The classification of new product developments has often been attempted and, whilst there will inevitably be cross-overs between groups, below is a list of the broadly accepted categories of new product developments:

- New to the world products
- New product lines
- Additions to existing lines
- Improvements and revisions to existing products
- Cost reductions
- Repositionings

It can be observed (see figure 3.8) that improvements on existing products and lines account for the majority of new products within a portfolio.

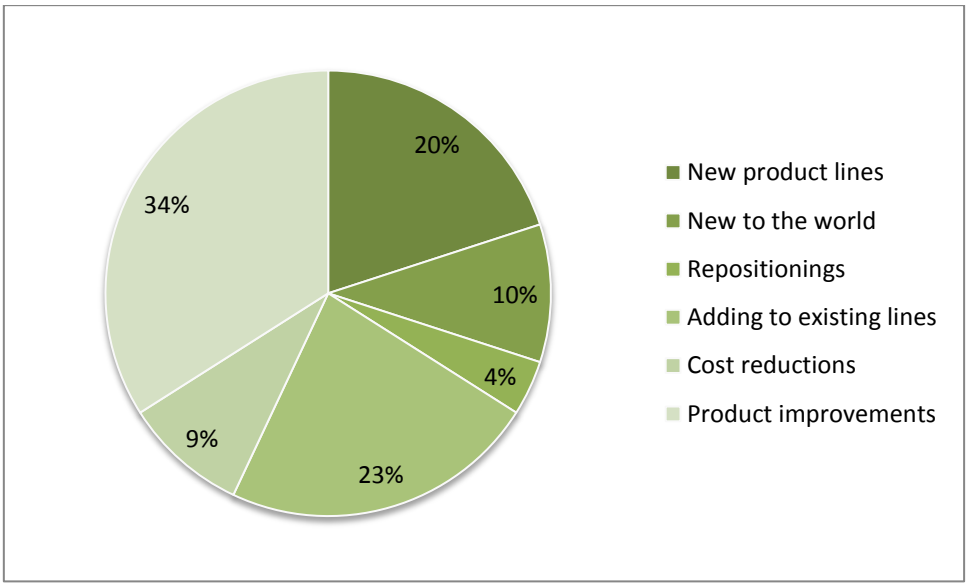

Figure 3.4 - Chart demonstrating the percentage allocation of new product types (adapted from Trott, 2005)

This can be allied with the degree of risk that is associated to each product type – improvements to products and existing lines possess a low risk factor whilst the entry of entirely new products hold a considerably greater risk aspect. The failure rate of new products can be high – as high as 20-25% for industrial and 30-35% for consumer products (Urban et al. 1987). Due to this factor, the development of entirely new to the world products can be a costly undertaking with those products that are successfully received in the market being expected to recoup somewhat the funds spent on the many products and ideas that did not reach the market and those that failed once released.

Within industry, the research and development of new products has been focussed more towards financial gain than the advancement of knowledge, this is where universities and research institutes can fill the gap. It can often be observed that industries tend to focus primarily on the development side, leaving the fundamental research to universities and other such institutions see figure 3.9 (Trott, 2005).

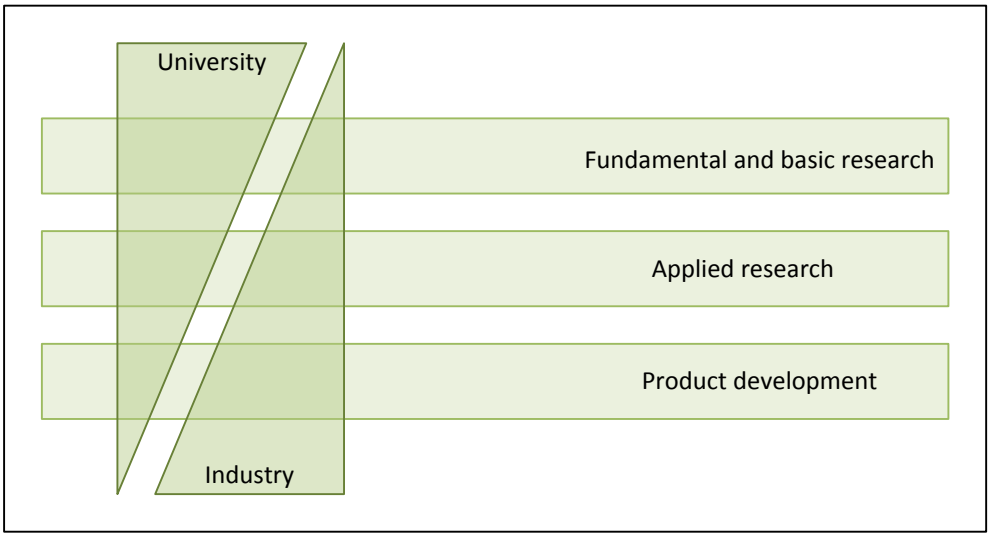

Figure 3.5 - Schematic demonstrating the relationship between university and industry and the majority allocation of research and development

The operations that encompass research and development (R&D) are presented here, the first of which is *basic research*. This can involve general work within an area that can subsequently be applied to a broad range of applications – this is the fundamental science that is most often associated with universities. The results of these investigations are often presented in peer reviewed journals, with some outcomes being advanced further to produce new technologies. *Applied research* involves employing existing principles to develop a product that enables the resolution of an issue, this can lead to the development of patents and new products. *Development* also uses existing scientific principles but for the solution of an issue pertaining to a new product. This can be, for example, the development of several prototypes before a final product is established. *Technical service* is the final aspect, which involves improvements to existing products in areas such as performance and cost which can improve a company's market share and/or profit margins.

The management of R&D can be heavily influenced by external factors, be they political, social, environmental or economic. This was, for example, demonstrated in section 3.5, where a terrorist attack can have profound effects on capital markets and on the psychology of human decision makers. As such, R&D managers need to have a planning process that takes into account, as much as one can, likely future events using environmental forecasts, capability analyses and risk spreading. The strategic

management of R&D and new product development is essential to keep a firm competitive and reduce risk.

3.7.1. Opportunity identification

It is necessary for a firm with the intention of entering a new product to market to assess the current market place and devise an entry strategy within a specific area. The identification and detailed analysis of markets that offer the most promising opportunities for the products under development is essential before subsequently assessing how these new products can be introduced. General market criteria and ways in which these can be measured are presented in table 3.2 (Urban et al., 1987).

Table 3.1 - General market criteria and their relative measures

General characteristics	Measure
Potential	Size of market
	Growth rate
Penetration	Vulnerability of competitors
Scale	Share of market
	Cumulative sales volume
Input	Investment in money and technology
Reward	Profits
Risk	Stability
	Probability of losses

The six criteria in table 3.2, when applied to a particular market, may be seen to have conflicting aspects. To attempt to evaluate the market an analysis can be undertaken where each criterion is afforded a rating which establishes the importance of that aspect to the firm. Once this is completed the markets under investigation can be analysed and each aspect awarded a score. The tally of each market analysed in this manner can then aid in the identification of the best opportunities for a given product.

The identification of the primary target group of consumers is also advisable prior to market entry. This can help to determine the likely size of the potential market, influence pricing structure and identify possible distribution channels. Market segmentation, identifying a group of similar consumers that have needs or responses

dissimilar to other consumers, can help to connect relevant marketing strategies to the product. The most common method for segmentation is by demographic or socioeconomic variable (Urban et al., 1987) but it is also viable to use attitudes, usage rate and preference/choice. The latter criterion can be useful in the management of new product entry to market and can be thought of as benefit segmentation, for example whether performance or safety is a more important aspect of automobiles to a particular group.

It can be observed that it is possible to enter most markets with a major innovation, however, not all markets will provide the same degree of return or harbour the same extent of risk. It can also be possible to create a new market for your product – this can enhance profits simply as the product dominates the market, conversely a greater degree of risk can be associated with this as opposed to entry into an established market.

The generation of ideas for innovative products can come from a variety of sources. A large percentage of successful technology based products have been developed due to the recognition of market needs and demands (Urban et al., 1987). This technique would also provide a decent financial return due to the satisfaction of an obvious gap within the market. Awareness of technological changes within the wider market can also enable opportunities for the generation of ideas for innovation within a specific area. As improvements to technology are progressive they can open new opportunities for exploitation in a variety of areas. It can also be valuable to research new patents and keep informed of modifications in technology as presented in scientific journals as a source of ideas for new product development. It should be noted that keeping abreast of product modification and innovation in competing firms can enable a better understanding of their products and this might be used to better challenge them within the market.

3.7.2. Product planning and positioning

It is necessary to undertake the process of product planning substantially before resources are allocated to a project, in this way the introduction of a new product can be managed to fit within an existing company portfolio and utilise existing product platforms. Managing new product entry in this manner can enable cost savings and reduce the risk somewhat associated with an entirely 'new to the world' product entry through reducing the initial outlay costs and associating a product with one already established.

It can also be important to assess the timing of the introduction of a new product, both for the benefit of existing products and to maximise a company's competitive strategy. It can depend on the strategy of an organisation as to which type of new product is released (see figure 3.8), for example it may be important for a particular company to release new to the world products ahead of its competitors – the organisational strategy being the imperative on being 'first to market' or the key innovator. This can enable a considerable initial market share and at times initiate a barrier to entry for some other organisations. There are many companies, however, that adopt the strategy of follower which enables them to quickly follow the market leader into the field and thereby reduce their market share. This strategy can often enable some reduction in unit cost and therefore place the new entrant (the follower) in a position to sell a similar product to the key innovator but at a reduced price.

Analysis of the competitive environment is essential prior to resource allocation and new product release. This can involve an assessment of the current technology as well as estimates on how technology is expected to change in the future. It can also be important to attempt estimates in how the actual industry is going to change in the future – new entrants, strategic shifts of competitors or the introduction of global players with significant funding can all shift an industry from an attractive prospect to one that should be entered with caution. The regulatory framework relating to a product or market place may change over time thus presenting more or less opportunities for both existing and new entrants to that market. Perhaps the most

influential aspect of the competitive environment that requires careful analysis is that of customer requirements – if these reduce or change in some manner that can have tremendous consequences for organisations. It is important for all of these aspects to be assessed both in the present environment and an attempt at an analysis of the future environment to limit any potential issues and exploit opportunities as they present themselves (Trott, 2005).

The positioning of a product within a specific market is another essential strategy that needs to be considered in the management of products. This often is a case of differentiation, attempting to set one product apart from that of competitors and so increasing the perceived benefit to the consumer. It is vital to ensure that this differentiation is apparent and valued by the prospective buyer; if not successful then any differentiation is essentially irrelevant. Differentiation may be sort on many aspects such as, for example, price, quality or uncommon features. Levitt, 1986, proposes four levels that may describe a product type:

1. The core product – which encompasses the essential aspects required to compete within a product market
2. The expected product – describes what customers have come to consider normal within the product range
3. The augmented product – provides features and services that exceed normal expectations for a product
4. The potential product – includes all of the features and services that could be predicted to add a benefit to consumers

It should be noted that customer requirements and expectations change, therefore the position of products and features within these categories would not be static. A feature that may have been considered augmented can quickly change to become an expected aspect of a product and competition between organisations has a tendency to elevate customer expectation in this manner.

It should be noted that evaluation of the positioning of a product within the market, according to the perception of the customer, is a useful factor to assess and understand customer decision making. Positioning studies first evaluate a similar,

relevant set of products that may be assessed as viable alternatives to the product being managed. A list of relevant attributes that insinuate differentiation and preferred features, as assumed by the customers, can then be assembled and weighted. This type of evaluation can identify whether those products are viewed to be similar, whether the desired attributes are satisfied and any obvious gap exists. Positioning strategy can enable the selection and exploitation of an appropriate base that holds benefit to customers and is not already overpopulated by the competitors. These six bases, as described by Wind, 1982 (from Trott, 2005) are:

- Product feature
- Benefits
- Use occasion
- User category
- Against another products
- Dissociation from all other products

These bases were extended to include parentage (where it comes from), manufacture (how it is made) and endorsement (people you respect say it is good) by Crawford in 1997 (Trott, 2005). Most products possess several features that describe the positioning of their product, it can also be necessary to re-evaluate these features as the product life-cycle progresses and consumer requirements change.

To enable a high degree of competition with rival firms there are several product strategies that a firm may undertake to differentiate themselves from their competitors. These include emphasis on: product proliferation, value, design (outward appearance), innovation or service. As products within the same market are inevitably compared to one another a product strategy that highlights a particular factor may help to persuade a consumer to choose that product over a similar one. This is especially the case in industrial markets (Trott, 2005) where product performance criteria are often forwarded to a selection of suppliers in the form of a call to tender and the quotes received compared against the required factors and price. Common product performance criteria can be seen in table 3.3.

Table 3.2 – Product performance aspects

Product performance factors			
1	Performance in operation	9	Safety in use
2	Reliability	10	Ease of maintenance
3	Sale price	11	Parts availability and cost
4	Efficient delivery	12	Attractive appearance/shape
5	Technical sophistication	13	Flexibility and adaptability in use
6	Quality of after-sales service	14	Advertising and promotion
7	Durability	15	Operator comfort
8	Ease of use	16	Design

(From Trott, 2005)

It can be seen from these details that differentiation between products can significantly increase the competitive advantage one firm may have over another and that the influence of customer perception of benefits and differences can be even more significant.

3.7.3. Testing and improving

The purpose of product testing is to estimate the market's reaction to a new product under consideration – this generally takes place prior to any costly production and promotional expense (Trott, 2005). Attempting assessment at a later stage is less tempting to managers of new products as the costs of a reportedly undesirable product has already begun to increase. Assessments are made of various factors, such as the market itself (buying patterns, segmentation and the customer view of current products) the intention to purchase (trial or repeat purchasing, barriers to changing brands and the cost for switching) and improvements to the new product (overall concept or alterations to specific proposed features).

Testing can take various forms; some products can undergo all variations of testing techniques but most require some form of adaption of one or more techniques. It may also be important to test individual aspects of a product, known as component testing, prior to testing of the product as a whole. This can be seen in figure 3.10.

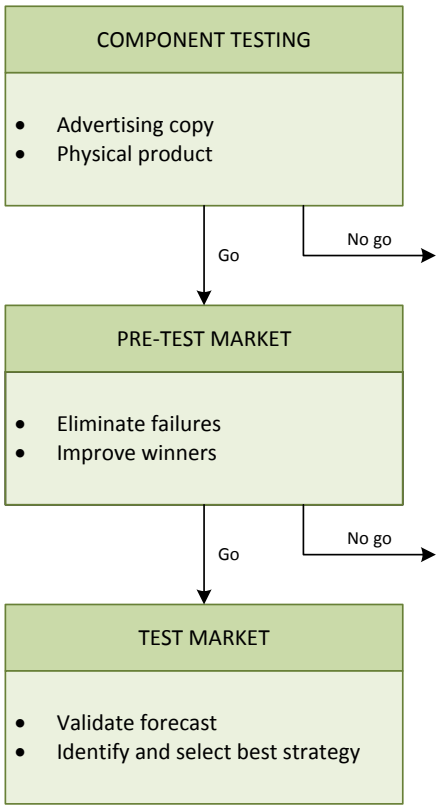

Figure 3.6 - Schematic representing planned product testing

Testing techniques that may be applied are: concept tests, test centres, hall tests/mobile shops, product-use tests, trade shows, monadic tests, paired comparisons, test panels and placement tests.

Testing the acceptance or otherwise of a new product prior to release can be viewed as an essential stage in its release. The testing of a completely new to the world product is difficult due to the lack of standards or comparative products of which to judge the product against (Wills et al., 1973). Testing in these circumstances, therefore, generally involve a single placement test, such tests are often associated with favourable bias and so their value for market testing is diminished somewhat. It has also been highlighted that market testing of an unknown product that produced negative opinions of its use and purpose does not necessarily equate to that product being unsuccessful upon release. There are examples of products that were initially rejected by manufacturers, retailers and consumers at the testing stage but went on to become highly successful – such as the Dyson cyclone cleaner (Trott, 2005). It is necessary to balance the risk of failure in the market against the risk of rejecting a good product before it reaches launch phase (Urban et al., 1987).

Testing can help to reduce the risks associated with the introduction of a new product but there are also drawbacks to this strategy; mainly, that it can increase the delay in introduction to market. This can have serious adverse effects, especially if a competitor can release a similar product to market first thus gaining a time advantage.

Testing of the explosive sensor presented in this work might best be undertaken with a modified placement test – where a small group of potential consumers are selected to use the product for an amount of time. They are then invited to evaluate the potential of the product and any issues that were apparent. It can also be assessed whether they are likely to purchase the product when it reaches the market. This can be an important option for a new product and as aspects of this product are considered new within the defined market, this type of testing is a good option.

3.7.4. Entry strategy

The decision regarding the best time in which to enter the market and through what means can make a considerable difference in the success or otherwise of a new product. There are three primary factors that can help the product introduction and stimulate the market's evolution (Trott, 2005). The first of which is *entry timing*. It may be the case that early entry has been considered optimal to gain the benefits from 'first mover advantage' – gaining a position of quality and thereby influencing the future opinions of consumers as to what should be expected in a product. In many cases the first movers are considered to be the market leaders at a later stage. It can be observed, however, that unless a pioneering entrant has a product that was fully ready for market and the financial backing to continue to innovate where necessary, an early entrance into the market can actually result in financial losses before being surpassed by a 'fast follower'. The second aspect for consideration prior to market entry is *positioning*. The positioning of a firm within a market place can highlight what the consumer expects from its products. Positioning oneself as the innovator – consistently producing technological modifications can provide a firm with status, however, if not well managed competitors can quickly react demanding a substantial portion of the market. The third factor is the *scale of entry* which can be seen to affect how the market evolves subsequent to the entry of a product. The greater the market presence of the new product, through advertising, press exposure and distribution channels, for example, the better the chance for good product performance. This can require considerable effort and resources.

Once the product has been launched it is necessary to continue to manage it, most importantly until the product is well established within its market. The manner in which this should be undertaken depends on the type of product and its initial reception into the market. Close monitoring of the reactions of both competitors and customers needs to be engaged in so that opportunities that arise can be exploited and issues resolved swiftly.

Entry strategy for a new, innovative product can be undertaken in a variety of ways. For an accomplished and well financed firm, development of a product and its entry to market are practises that can often be dealt with in-house. For smaller firms, start-ups, R&D groups and university spin-offs the levels of financing, manufacturing, marketing and distribution may provide a barrier to entry. As such, strategic alliances can be sort between groups, even competitors, where two or more partners share knowledge or resources in a manner beneficial to all. In recent years, this 'octopus' strategy has even been exploited by larger firms more traditionally associated with a 'go it alone' strategy. Strategic alliances can occur intra-industry or inter-industry and can involve one of seven generic types (Trott, 2005):

1. Licensing
2. Supplier relations
3. Joint venture
4. Collaboration (non-joint venture)
5. R&D consortia
6. Industry clusters
7. Innovation networks

For the development of an innovative, new product researched within a university, as in the case of this work, might best be suited in a collaboration type of strategic alliance. This form of alliance enables flexibility and can offer the option for further cooperation if mutually acceptable. For example, this work utilises screen-printed carbon sensors from Microarray Ltd. (Manchester, UK) and as such a collaboration might be possible between this company and either the university itself or another manufacturer, perhaps one that can produce a hand-held electrochemical sensor format with an output display into which the modified disposable sensor can be placed.

Entry into the explosives detection market, an already well-populated market, requires new product entry to offer an aspect that is different from the main competitors. It would seem that the best opportunity for a new product based on the technology described within this work would be to provide a system capable of

competing on cost. As mentioned previously, the core analytical technique with relation to this work involve the utilisation of disposable screen-printed carbon sensors; the analysis is undertaken with a hand-held potentiostat (Uniscan PG-580) and a cyclone detection system (Berkin, Coriolis μ air sampler). These items are all available for purchase 'off the shelf', minimising costs through the utilisation of available technologies. With the purchase of increasing quantities of these items, the price of each component will inevitably drop. At the present time, the cost of the next generation of the handheld potentiostat (PG-581) base unit is £2775.00 and the Coriolis μ air sampler £4285 (see appendix 3 for company price lists). The price of each disposable sensor when buying 175 (the minimum order quantity) is £1.78 – the prices of these sensors are directly related to the quantity ordered and so this is the maximum unit cost. It is clear to see that the total cost of the necessary instrumentation (without factoring in R&D expenditure, operating costs and profits) is substantially lower than the current technology presented in table 3.1.

As previously mentioned, those firms already present within a market attempt to guard their business against the entry of new products. This can be done through a variety of means such as, for example, expensive initial outlay for the purchaser then subsequent periodic updates to the product to keep the customer satisfied. The large initial outlay decreases the desire to change from one form of technology to another; as the initial cost is sunk the decision to abandon this technology requires giving up the benefit without regaining the cost. As such, companies can view it as necessary to gain back the value for money for an expensive purchase (Hall and Khan, 2003). As the security market is already well-populated this might lead to a conservative uptake of new product entries.

The standard Rogers Adoption Curve, seen below in figure 3.11, is the underlying model of technology adoption. This bell shaped curve identifies the five types of adopters of technology with exponential growth demonstrated in the beginning and a slowdown of adoption during the more conservative late maturity period.

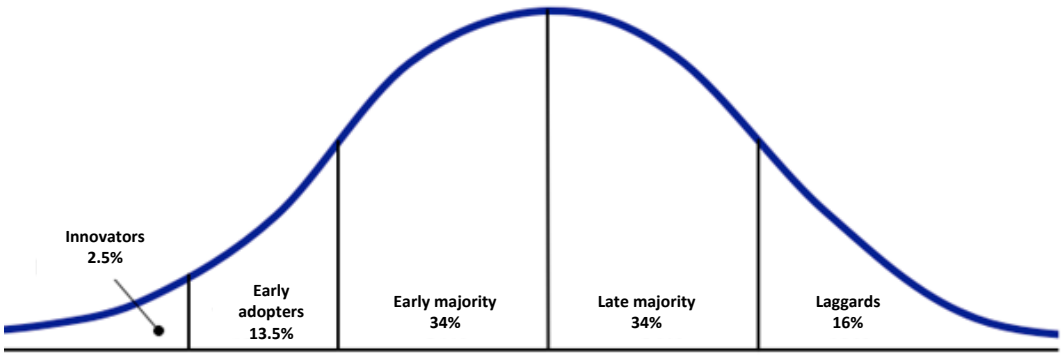

Figure 3.7 - The standard Rogers Adoption Curve

The innovators can be considered as the technically-oriented who are willing to take the risk of extra costs and the possibly imperfect products of new and unfamiliar technology for the kudos of being first in the market. Early adopters enter the market to attempt to gain a competitive advantage. The early majority are considered pragmatic – waiting long enough to assess the value of the technology but unwilling to risk an earlier adoption. Late majority adopt the new technology once its value has been well demonstrated, preferring the incremental product improvements to innovation jumps. Laggards are traditional and conservative, pointing out the issues related to the new technology, which can drive improvements, before reluctant acceptance (Vowles et al., 2011).

It is important to assess and understand the market so that new product entry can be carefully managed. It seems likely that, despite the significantly reduced theoretical price of the instrumentation discussed in this work, the security market may show characteristics of late adoption and slow diffusion throughout the industry. This can be expected for a number of factors such as, for example, the funds already sunk in security equipment in many industries and the real cost of a new technology within this market not working properly. False positive and negative results can have significant detrimental effects ranging from increased waiting times and queuing to injury and loss of life and property. It may be necessary to attempt to enter the market without targeting the larger, well known customers so that the technology can be demonstrated as a success by customers normally priced out of obtaining such products. This would enable the acquisition of market share whilst

demonstrating the value of the product to the larger firms to neutralise any associated apprehension they may hold.

3.7.5. Managing the life-cycle

Although the introduction of a new, innovative product into a market can provide a significant initial financial return the extent of the profit cannot be expected to remain static. Products have a life-cycle and if this is not adequately managed then the resulting profit potential associated with the entire life-cycle may not be realised. In general, a product follows a specific path – introduction, growth, maturity and decline. During the introduction phase sales grow slowly until the growth stage where the sales increase more rapidly. These sales then plateau in the maturity phase before diminishing in the decline stage.

In reality, the life-cycle of a real product often only slightly resembles that of an ideal life-cycle. A more cyclical cycle can often be found – especially in areas that are significantly affected by technological changes and marketing activities or even external factors such as the political and economic state. This variety in the product life-cycle implies that the life-cycle can be managed through careful strategic planning – the final stage of the implementation of a new product to market, see figure 3.11.

Competitive defence of the product against new entrants to the market is important to improve the profitability of the product over time. As is the management of the product at its maturity stage, the release of additional features and upgrades can help to extend the life of a product, thus prolonging the stage before decline. A well-managed product portfolio within a firm can ensure that new products are being introduced while mature products are being phased out.

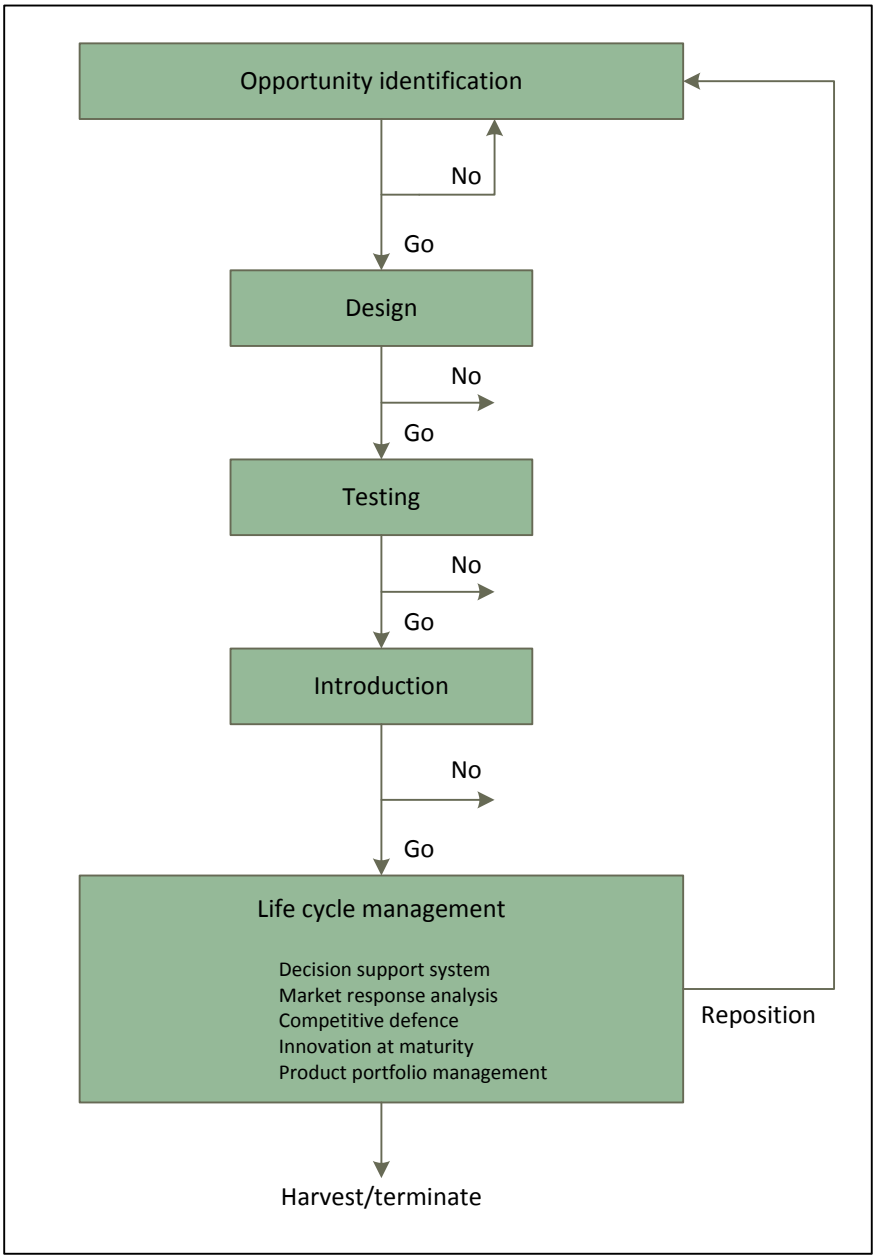

Figure 3.8 - Schematic representing the management of a product life-cycle

3.8. Conclusion

The macroeconomic theory and the economics of human needs and rationality was discussed at the beginning of this chapter to provide focus to the work looking at the economics of terrorism and how this can affect the economy of the world and individual nations.

Terrorism has a significant cost, not only in the human and physical capital that can be lost through a terrorist incident but also through the effect this has on those people close to the event, the population in general and how this subsequently has consequences to the economy at large.

Aside from the initial cost to infrastructure, there often comes a direct government response that diverts spending from other investments into improvements in security and military spending. It has also been observed that as a consequence of a terror attack, namely those that occurred in the USA on September 11th 2001, wars have been initiated costing those economies involved billions of dollars. This diversion of spending can result in a limitation of economic growth due to the lack of spending in other areas that promote this.

As the cost to the economy has been demonstrated and the relocation of government investments into defence and security has been highlighted, work to develop counter-terrorism measures which are of relatively low cost and are capable of distribution and use in a wide variety of locations represents a viable area of research.

A review of the necessary stages related to the research and development of a new product and the issues surrounding taking this product to market has also been discussed, including product planning and positioning, market entry strategies and the management of the entire life-cycle of a new product. This has been related, where appropriate, to the sensor system that has been developed within this work.

4. Materials and methods

4.1. Introduction

This chapter catalogues the materials and methods used in the preparation for and carrying out of experimental work for the electrochemical detection of explosives. The various experimental techniques are also described.

4.2. Reagents

Acetic acid, Sodium dihydrogen phosphate, disodium hydrogen phosphate and sodium chloride (all AnalaR grade) were obtained from BDH Laboratory Supplies (Poole, Dorset, UK).

2,4,6-Trinitrotoluene (1000 μg/ml in acetonitrile) and 2,4-Dinitrotoluene (1000 μg/ml in acetonitrile) were obtained from Supelco (Bellefonte, Pennsylvania, USA).

Acetonitrile (AnalaR), ferrocene carboxylic acid, *o*-phenylenediamine dihydrochloride (1,2-diaminobenzenedihydrochloride), aniline, aniline hydrochloride, β-nicotinamide adenine dinucleotide 2-phosphate (reduced tetrasodium salt) and nitroreductase (type nfsA from Escherichia coli) were obtained from Sigma (Poole, Dorset, UK).

Potassium chloride, sulphuric acid and hydrogen peroxide (30%), were purchased from Fisher Scientific (Loughborough, Leicester, UK).

4.3. Buffers and solutions

All solutions were prepared with deionised water (≥18 MΩcm^{-1} resistivity) from an Elga Purelab UHQ-II Water System (Vivendi Water Systems, High Wycombe, Buckinghamshire, UK).

A pH 7.0 phosphate buffer solution was prepared, comprising: 4.3 x 10^{-3} M sodium dihydrogen orthophosphate 1-hydrate, 5.6 x 10^{-3} M disodium hydrogen orthophosphate 12-hydrate and 7.87 x 10^{-2} M sodium chloride. This buffer solution was used within interrogations for the analysis of 2,4,6-trinitrotoluene and 2,4-dinitrotoluene.

A pH 7.4 phosphate buffer solution was prepared, comprising: 1.3x10^{-2} M sodium dihydrogen orthophosphate 1-hydrate, 5.28 x 10^{-2} M disodium hydrogen orthophosphate 12-hydrate and 5.1 x 10^{-3} M sodium chloride.

A pH 4.5 acetic acid buffer was prepared, comprising: 8.1 x 10^{-3} M acetic acid, 1.8 x 10^{-3} M sodium acetate and 0.1 M sodium chloride.

A solution of >3 M potassium chloride was prepared in for the production of a silver / silver chloride wire pseudo reference electrode.

Solutions of 5 mM and 10 mM *o*-phenylenediamine were prepared in pH 7.4 phosphate buffer solution for the electropolymerisation of *o*-phenylenediamine and subsequent insulation of both plain carbon and cobalt phthalocyanine-doped planar screen-printed electrodes.

A 0.2 M solution of aniline hydrochloride was prepared in either a pH 4.5 acetic acid buffer or a pH 7 0 phosphate buffer for the electrogeneration of polyaniline and also the immobilisation of 20 units of nitroreductase and a concentration of 0.1 mM NADPH within the conducting polymer upon the surface of the plain carbon and cobalt phthalocyanine-doped screen-printed electrodes.

1 mM and 5 mM solution of ferrocenemonocarboxylic acid were prepared in pH 7.0 phosphate buffer solution for electrochemical characterisation studies on both plain

carbon and cobalt phthalocyanine-doped screen-printed electrodes when uncoated, insulated and with a conductive polymer coating.

All other solutions were prepared in pH 7.0 phosphate buffer solution.

A Piranha solution consisting of a 3:1 combination of sulphuric acid and 30% hydrogen peroxide was used for the removal of organic residues from the glass cell (used in electrochemical interrogations) and quartz cuvettes between experimental procedures.

4.4. Materials

Menzel® 'Superfrost' twin frosted-end microscope slides were purchased from Fisher Scientific (Loughborough, Leicestershire, UK) and were used for the construction of glass cells used in initial electrochemical interrogations.

Epoxy resin (Araldite®) and Acheson Electrodag® (1415M) silver conductive paint were purchased from AGAR Scientific Ltd. (Stansted, Essex, UK) and used in the production of glass cells and for the construction of counter electrodes.

Stainless steel gauze was purchased from Fine Mesh Metals (Brierley Hill, West Midlands, UK) and was used as a counter electrode during electropolymerisations.

Silver wire was purchased from J. Blundell & Sons Ltd. (Holborn, London, UK) and glass rods purchased from Fisher Scientific (Loughborough, Leicestershire, UK) were used for the construction of pseudo silver/silver chloride (Ag/AgCl) reference electrodes.

An assortment of magnetic fleas were purchased from Fisher Scientific (Loughborough, Leicestershire, UK) and used in buffer solution production and chronoamperometric interrogations.

All wires and crocodile clips were purchased from Maplin Electronics (Luton, Bedfordshire, UK) and used for the construction of reference and counter electrodes.

The screen-printed carbon electrodes were obtained from Microarray (Manchester, UK) and comprised of a 3-electrode system with a carbon ink working and counter electrode and with a silver/silver chloride reference electrode, as depicted in Figure 4.2. Screen-printed carbon ink doped with cobalt phthalocyanine transducers used for the screen-printing of sensors were also obtained from Microarray. These were purchased in sheets of 45 (Figure 4.1) and were used individually (Figure 4.2). Sensors were trimmed prior to use in electrochemical interrogations.

Figure 4.1 - A sheet of screen-printed carbon electrodes as received from Microarray (Manchester, UK)

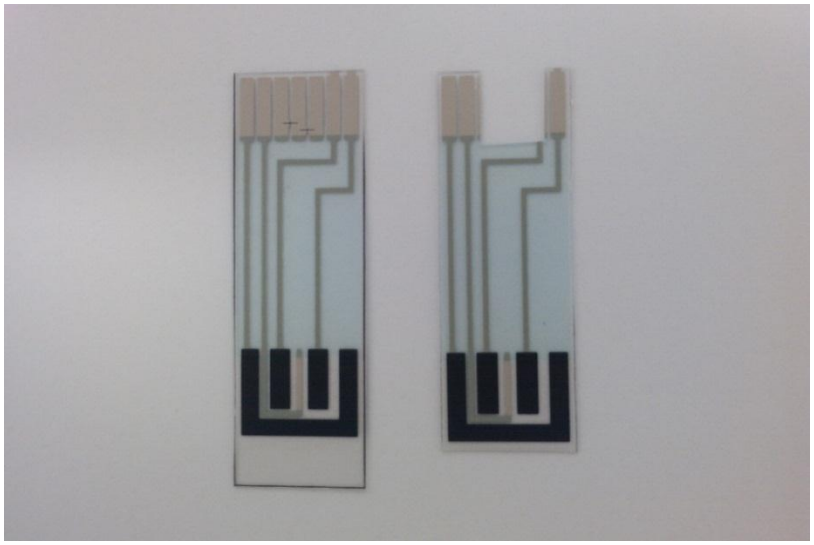

Figure 4.2 - An individual screen-printed sensor alongside a sensor trimmed in preparation for use

4.5. Experimental apparatus

Potentiostats:

An analytical electrochemical workstation (PG580) from Uniscan Instruments (Buxton, UK) was used for all electrochemical studies (see Figure 4.3). The current/charge outputs resulting from sensor interrogation were recorded with the relevant software supplied with the workstation.

Figure 4.3 - PG580 Uniscan hand-held potentiostat

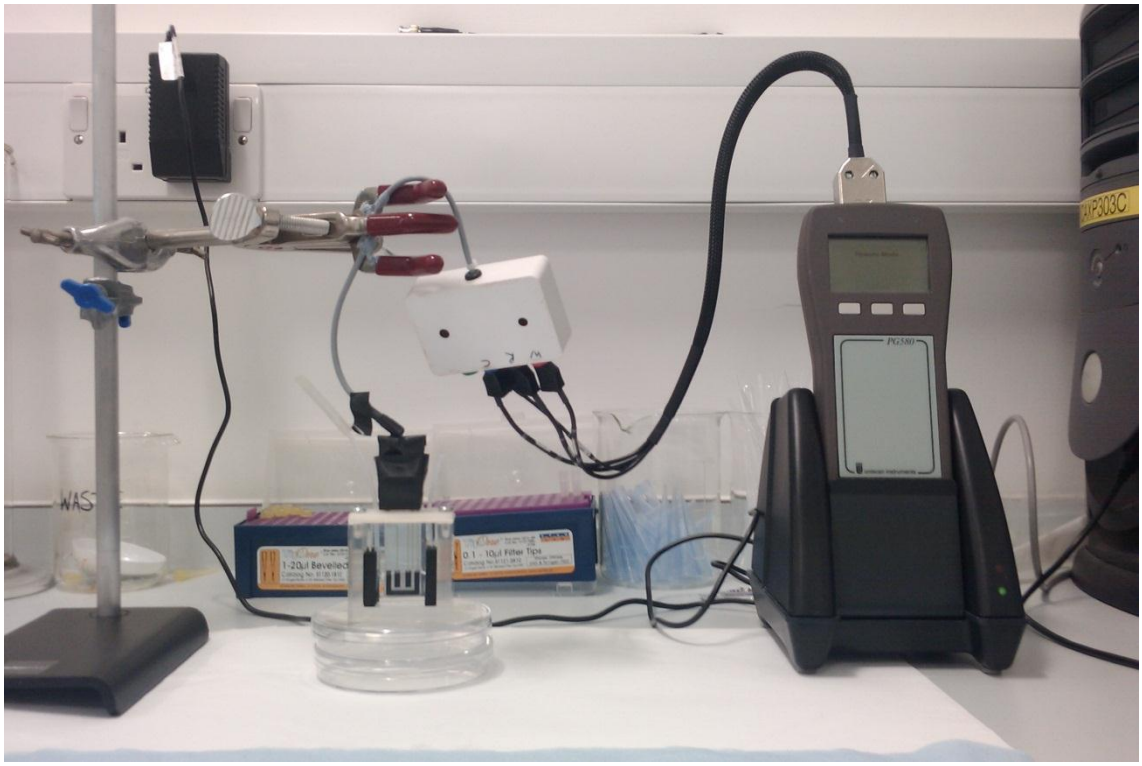

Figure 4.4 - Experimental set-up for electrochemical interrogations

Spectrophotometer:

Perkin Elmer UV dual spectrophotometer “Lambda 650” was used for examination into the efficacy of the enzyme nitroreductase prior to its use in electrochemical interrogations.

Ultrasonic devices:

An Ultrawave (model number U100), 30-45 kHz, ultrasonic bath with a 1.5 litre capacity from Ultrawave (Cardiff, Wales, UK) was used for the ultrasonic ablation of individual sensors.

Figure 4.5 - UltrawaveU100 ultrasonic bath

A Kerry Miniprobe 40 ultrasonic horn was used in examinations to attempt to improve the quality of the polymer coating gained by removing the surface bubbles prior to electropolymerisation, purchased from Kerry Ultrasonics Ltd, (Hitchin, Hertfordshire, UK).

Figure 4.6 - A Kerry Miniprobe ultrasonic horn

Sealed electrochemical cell:

A sealed electrochemical cell prototype was initially designed in-house and produced by Soham Scientific (Ely, Cambridge, UK) for use in all electrochemical studies. This was subsequently redesigned to remedy leakage caused by the capillary effect and the build-up of pressure due to the narrow glass cell and pressurised gas used during deoxygenation, leading to the final design depicted below (Figure 4.7), again manufactured by Soham Scientific.

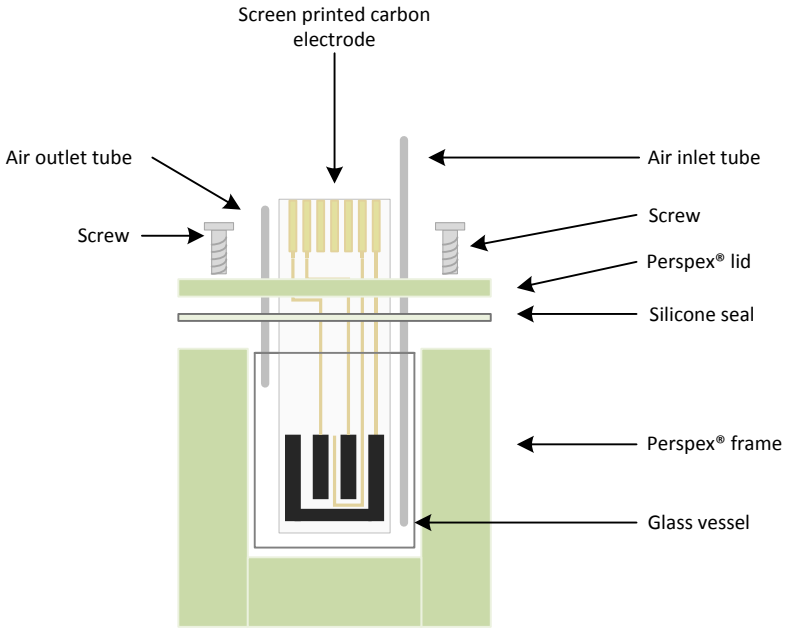

Figure 4.7 - Schematic representation of the cell developed and used for most electrochemical interrogations

A photograph of the above custom designed cell can be seen below, Figure 4.8

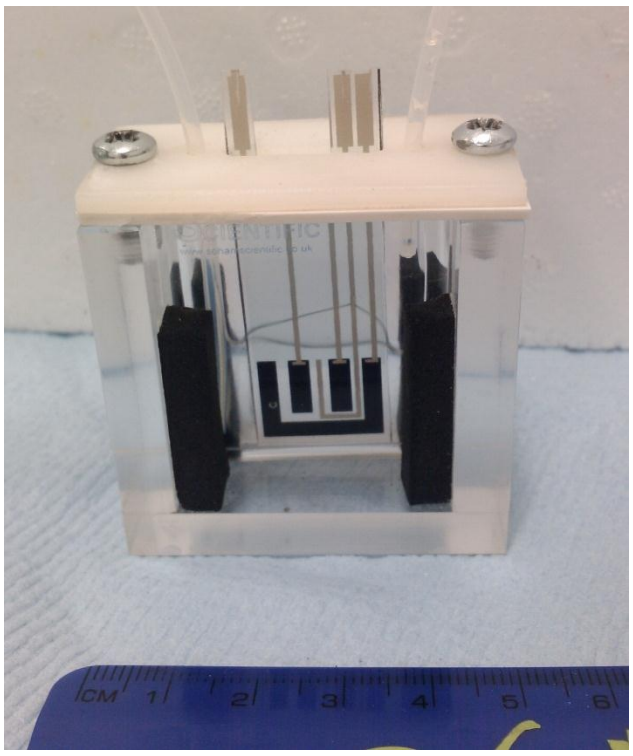

Figure 4.8 - The custom designed cell used for most electrochemical interrogations

Magnetic stirrer

A LTE Scientific (Lancashire, UK) magnetic stirrer was used for the production of buffer solutions and in all chronoamperometric interrogations.

Water purification:

An ELGA LabWater Purelab UHQ II (Vivendi Water Systems, High Wycombe, Buckinghamshire, UK) was used to provide all distilled water, with water quality of ≥18 MΩ cm^{-1}.

Air sampling system

An air sampling system was used for all collection studies of airborne particles, the Coriolis®μ from Berkin Technologies, France.

Figure 4.9 - The Coriolis®μ air sampling system

4.6. Experimental procedures

The following section will present the principle experimental procedures followed throughout this research.

4.6.1. Electrochemical interrogation with a screen-printed carbon sensor

Electrochemical interrogations were undertaken with either plain carbon screen-printed electrodes, cobalt phthalocyanine-doped screen-printed carbon electrodes or the microelectrode array sensors produced via electropolymerisation/ultrasonic ablation throughout this work. The electrochemical interrogation was performed with the PG580 potentiostat using the cyclic voltammetry program where the voltage is swept from one point to another and then reversed, unless otherwise stated.

Cyclic voltammetric techniques were performed on the screen-printed electrodes in the presence of TNT (and when required in the presence of TNT with the enzyme nitroreductase and the cofactor NADPH) in a sealed glass cell (as described in section 4.5). The solutions of TNT, NTR and NADPH were made up in the pH 7.0 phosphate buffer previously described. Prior to electrochemical interrogation, the cell was purged of oxygen by bubbling argon from a BOC Pureshield argon cylinder through gently for ten minutes.

The cyclic voltammetric investigation of nitro compounds was performed by sweeping the potential between -0.8 and +0.8 V (vs. Ag/AgCl) and back for one cycle. Unless otherwise stated, the scan rate for all interrogations was 20 mVs^{-1}.

4.6.2. UV spectrophotometry for the examination of the enzyme system

An assay solution containing the enzyme nitroreductase (20 units in 40µl), 0.1 mM NADPH and the nitroaromatic compound (TNT – initial concentration of 200µM) in pH 7.4 phosphate buffer was used for an assay to assess enzyme activity. NTR was added to the assay solution one minute into the scan using a pipette and the solution was

drawn into and released from this pipette several times to equilibrate the components. A reference solution containing all the elements except the enzyme was also recorded as a baseline.

Spectra were recorded with a spectrophotometer at a scan rate of 500 nm min^{-1} between 220 and 500 nm. Interrogations were performed at room temperature (25 °C) and pH 7.4 phosphate buffer as a supporting solution were utilised to recreate laboratory conditions. This assay was carried out both with and without degassing with argon to eliminate oxygen effects on the mechanism.

For reaction rate examinations, a kinetic run on the spectrophotometer at 340nm was performed (as this is where the identifying NADPH peak was positioned) to establish the change in absorbance over time and therefore the rate at which the NADPH was oxidised. The enzymatic activity was monitored in solution through the oxidation of NADPH by measuring the change in its absorbance peak at 340nm.

4.6.3. Electrode preparation

A pseudo silver / silver chloride (Ag/AgCl) reference electrode was used for electropolymerisation techniques. This was produced by attaching a silver wire to a multi-core copper wire with silver conducting paint. Once dried this is inserted within a glass capillary tube and fixed in place with epoxy resin to add mechanical strength and to stop solution ingress (Figure 4.10). This silver wire was pre-anodised at +1 V for ten minutes in a solution of saturated potassium chloride (>3 M) to enable a layer of silver chloride to develop on the surface. Periodically the coating of Ag/AgCl was removed with fine grade glass paper and the electrodeposition step was repeated to ensure a consistent response over time.

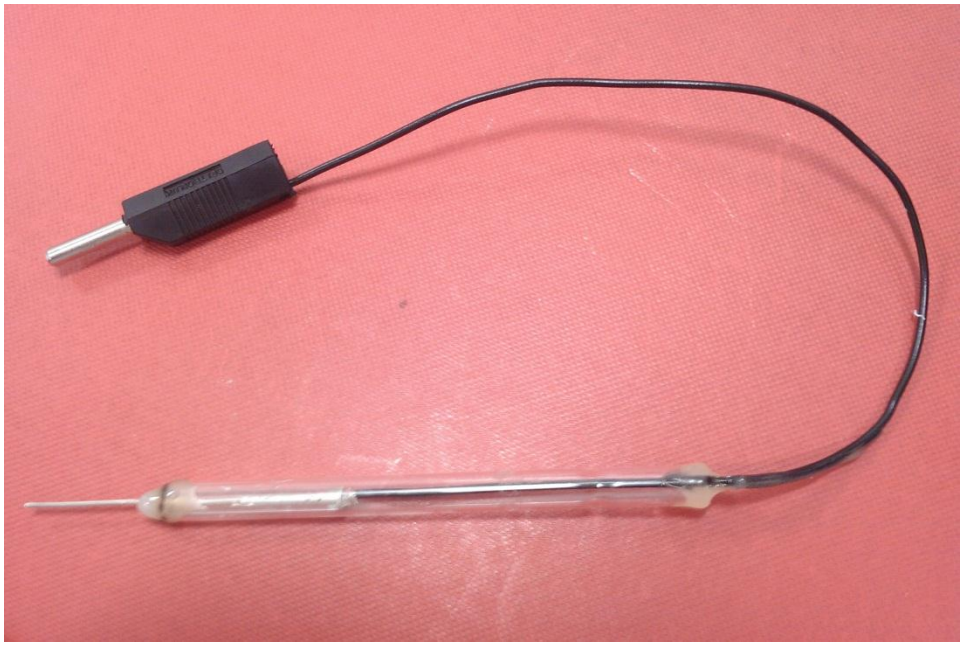

Figure 4.10 - A pseudo silver/silver chloride reference electrode produced for use in electropolymerisation techniques

Stainless steel gauze was used as a counter electrode during electropolymerisation. This constituted a section of stainless steel gauze (25 x 40 mm) attached to a copper multi-core wire via a crocodile clip.

4.6.4. Electropolymerisation of poly(*o*-phenylenediamine) on carbon screen-printed electrodes

Plain carbon screen-printed electrodes possess an inherent hydrophobicity causing the adherence of bubbles to the surface of the sensor. It has been established (Gornall et al., 2009) that exposure to ultrasound for between 30 and 60 seconds can displace these bubbles thus allowing a homogenous layer of the insulating polymer to be permitted during the electrodeposition process. This was omitted for the electrodeposition of *o*-phenylenediamine on the cobalt phthalocyanine sensors as it was found to adversely affect the insulating film deposition

The electrodeposition of the insulating film, poly(*o*-phenylenediamine), upon the surface of carbon and cobalt phthalocyanine screen-printed sensors was performed as follows: a 5 mM or a 10 mM solution of *o*-phenylenediamine was prepared with a pH 7.4 phosphate buffer solution as a supporting electrolyte immediately prior to use. A

3-electrode system was utilised, comprising the working electrode present within the screen-printed sensor, a stainless steel gauze counter electrode and a silver/silver chloride pseudo reference electrode (produced as described in section 4.6.3). Electropolymerisation was performed through sequentially scanning the working electrode potential from 0 V to +1 V (vs. Ag/AgCl) for 50 cycles using a PG580 potentiostat. Studies into the optimal scan rate were investigated (see chapter 10) and a scan rate of 10 mVs^{-1} was employed once the studies had been undertaken. Once the electrodeposition process was complete, the screen-printed sensor was rinsed in deionised water to remove excess *o*-phenylenediamine solution, allowed to air dry naturally and stored in a clean Petri dish at ambient temperature.

4.6.5. Ultrasonic ablation of poly(*o*-phenylenediamine) film

Ultrasonic ablation was performed on the screen-printed sensors within the Ultrawave U100 bench top ultrasound bath. The reservoir was filled with 1.5 litres of deionised water and the screen-printed sensor was positioned in a beaker of deionised water at the centre of the ultrasonic bath suspended such that the water level of beaker matched that of the reservoir. It has been previously reported (Barton et al., 2004) that a 20 s sonication time allows for the formation of microelectrode arrays which exhibit good stir independent behaviour. This is because sensors sonicated for longer periods have a larger population density of pores; the hemispherical diffusion profile associated with these pores can overlap – the consequence of this is the loss of the microelectrode behaviour (Barton et al., 2004). A study was performed to establish the optimum sonication time under the experimental conditions used throughout this work and a sonication period of 10 s would appear to provide the optimal caviational density (see chapter 10) and so, sonication was performed at 30 KHz for 10 seconds.

When ultrasound is passed through a solvent, such as water, it can cause thermal agitation and localised hotspots. These hotspots cause superheated bubble formation which, as they cool, implode ejecting jets of the solvent. These jets, on contact with the surface of the coated electrode, cause ablations through the relatively soft polymer coating down to the surface of the electrode. These cavitations, or pores,

may then act as nucleation sites for further bubble formation and their subsequent implosions (Suslick, 1990).

4.6.6. Electropolymerisation of a conducting polymer film – with and without the immobilisation of the enzyme nitroreductase

The electrodeposition of the conducting polymer film, polyaniline (PANI) in its emeraldine form, upon the surface of carbon and cobalt phthalocyanine screen-printed sensors was performed as follows: 0.2 M solution of PANI was prepared in a pH 4.0 acetate buffer (Myler et al., 1997) or a pH 7.0 phosphate buffer. A 3-electrode system was once again utilised, comprising the working electrode present within the screen-printed sensor, a stainless steel gauze counter electrode and a silver/silver chloride reference electrode (produced as described in section 4.6.3). Electropolymerisation was performed through sequentially scanning the working electrode potential from -0.2 V to +0.8 V (vs. Ag/AgCl) and back to the initial potential for 10 cycles using a PG580 potentiostat at a scan rate of 50 mVs^{-1}.

The PANI film, when deposited over the sonochemically ablated microelectrode array, generates protrusions from the micropores in the insulating polymer. The electrodeposition of the conducting polymer film with the co-entrapment of the enzyme nitroreductase was performed in much the same manner – in a solution of 0.2 M aniline as previously described with varying amounts of nitroreductase.

Once the electrodeposition process was complete, the screen-printed sensor was rinsed in deionised water to remove excess unpolymerised monomer solution and allowed to air dry naturally for immediate use.

4.6.7. Electrochemical characterisation

All electrochemical characterisation of the planar and microelectrode array sensors were performed using a PG580 potentiostat unless otherwise stated. All cyclic voltammetric interrogations for characterisation were performed using a reversible redox couple. The sensors were examined through the potential cycling between -0.2

and +0.6 V (vs. Ag/AgCl) in a solution of 5 mM ferrocenemonocarboxylic acid at a scan rate of 20 mV/s.

Visual assessment of cavitation sites was performed with scanning electron microscopy.

4.6.8. Stir-independence study of microelectrode arrays

To assess the stir-independent properties of the cavity microelectrode arrays chronoamperometric experiments were performed with a magnetic stirrer from LTE Scientific (Lancashire, UK). The potential was held at a relevant value for 300 seconds, during which time stirring was introduced at 60 s and terminated at 180 s and the current response measured as a function of time. The potential for interrogations involving ferrocenemonocarboxylic acid was held at 0.35 V and for TNT interrogations -0.50 V.

4.6.9. The cyclone collection system

The Coriolis®μ air sampling device was set to run for 2 minutes at the maximum collection setting, 300 litres per minute. A 10 ml solution of pH 7 phosphate buffer was used as the collection fluid – this volume was specified in the instruction booklet as required to enable the development of a vortex when the device was in operation. A spray bottle was used to aspirate the sample (ferrocenemonocarboxylic acid or TNT) in the vicinity of the air inlet value. One injection was performed every 10 seconds for the entire 2 minutes. The resulting sample, collected in the collection fluid, was interrogated electrochemically as previously described with an unmodified CoPc sensor, a microelectrode cavity array and a microelectrode protrusion array.

5. Electrochemistry of nitro compounds on bare carbon screen-printed electrodes

5.1. Introduction

Some of the important aims of this work were to develop a biosensing device that was easy to use, sensitive and selective and inexpensive to produce and utilise; one simple solution to this would be through a disposable sensor platform upon which characterisations can be performed. This approach may provide a commercially viable option for the widespread detection of nitro compounds for use, for example, in the prevention of terrorist attacks with such materials. Electrochemical techniques have long been recognised as an approach offering the potential for remote and portable analyses and to couple this process with a disposable sensor would appear to satisfy many of the needs as highlighted above.

Thick film screen-printed sensors provide the opportunity for mass production of a reliable, highly reproducible and inexpensive sensing platform (Hart and Wring, 1997). Screen-printing has become increasingly popular for electrode fabrication due to the ease at which complete sensors can be produced en mass at low unit cost – a estimate of the cost of one sensor when in mass production is estimated to be £0.05.

Screen-printing essentially involves forcing the paste or ink through a fine screen mesh, where the pattern of the required electrode or sensor has been included, and onto a substrate surface. When a finer resolution is necessary, the mask can be produced with etching. This film can then be cured through the application of heat or solvent evaporation (Kissinger, 1990).

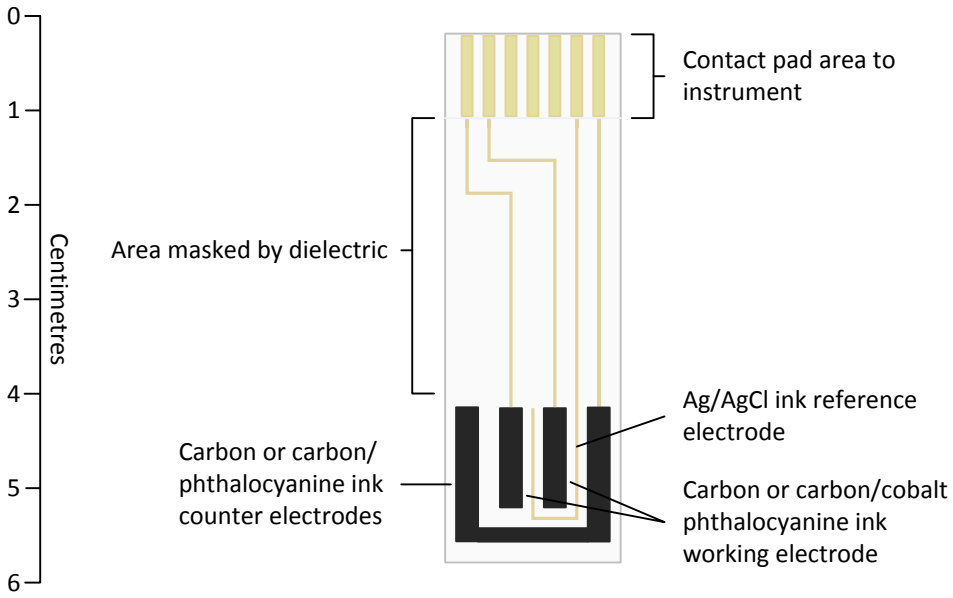

Figure 5.1 – Schematic representation of a screen printed carbon or carbon/cobalt phthalocyanine electrode

The popularity of electrochemical sensing has increased over recent years due to the advantages associated with this type of analysis, such as low cost of apparatus, low power requirements and because its small size enables hand-held, field-deployable devices. The use of screen-printed sensors in conjunction with advances in electrochemical analytical devices has increased, and the opportunity to purchase a wide variety of sensors, both of plain carbon within various matrices and carbon with the inclusion of mediators to improve electroactivity, is now a commercial reality (Fanjul-Bolado et al., 2008).

5.2. Classification of screen-printed carbon electrode activity

The plain carbon electrodes used throughout this work were designed and supplied by Microarray Ltd. Prior to use as the basis for nitro-species detection, these sensors were first electrochemically characterised to assess the suitability for use within further studies.

A common redox couple was utilised for the task of characterising the carbon screen-printed electrodes. The surface morphology and charge transfer properties of screen-printed sensors can differ greatly between different manufacturers, the size and loading of graphite particles within the carbon ink can have an effect on the electron transfer reactivities and the overall analytical performance of the sensor (Wang, 1997). The surface topography of the carbon screen-printed electrodes used in this study, for example, is shown in Figure 5.2.

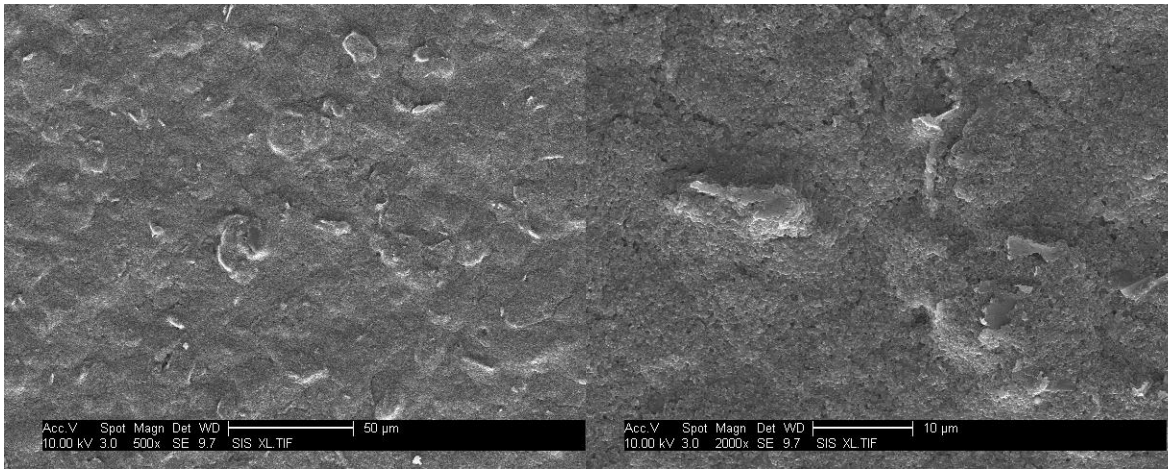

Figure 5.2 - An SFEG scanning electron micrograph of a bare carbon screen-printed electrode surface at 500x and 2000x magnification (after sputter coating with gold palladium)

The formulation and composition of the inks used in screen-printed sensors are regarded as propriety information by manufacturers and so it is unlikely that two sensors from different sources will provide the same electrochemical activity (Wang, 1997). It Is due to this that the charge transfer properties of the screen-printed electrodes intended for use in subsequent electroanalysis should be assessed (Fanjul-Bolado et al., 2008). Ferrocenemonocarboxylic acid [$Fc(CO_2H)^{3+/2+}$] (FeCA) displays clear single peaks in both the anodic and cathodic directions when the potential is

cyclically swept between -0.2 to +0.65 V (vs. Ag/AgCl), as the compound is first electrochemically oxidised into its $Fc(CO_2H)^{3+}$ form before being electrochemically reduced back to $Fc(CO_2H)^{2+}$, see Figure 5.3.

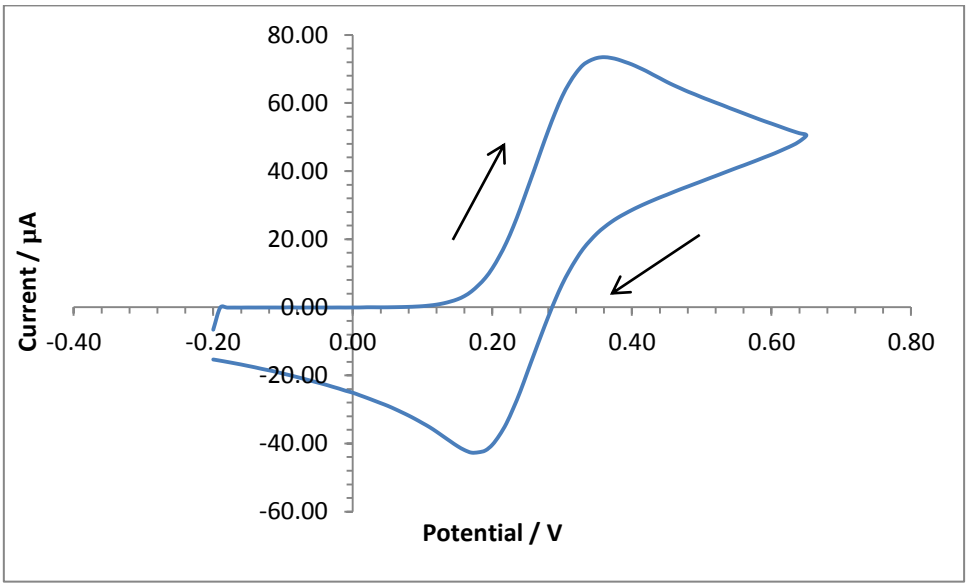

Figure 5.3 - Ferrocenemonocarboxylic acid interrogated electrochemically with a screen-printed carbon electrode between -0.2 and +0.65 V (with phosphate buffer as supporting electrolyte, at a scan rate 20 mVs^{-1} vs. Ag/AgCl)

A set of oxidative and reductive peaks were observed when the potential was cycled between two values as described corresponding to the one-electron oxidation from ferrocenemonocarboxylic acid to its ferricinium state. The peak separation, anodic peak potential and the anodic peak current have been identified and collated in table form (Table 5.1) so that this data may be compared with future modifications to the sensor system to establish differences in electrode kinetics and current output.

Peak separation	Anodic peak potential	Anodic peak current
ΔE_p	E_{ia}	i_{pa}
150 mV	360 mV	73.46 µA

Table 5.1 - Table illustrating the peak separation, anodic peak potential and anodic peak current of ferrocenemonocarboxylic acid interrogation with a carbon screen printed electrode

Although the cyclic voltammogram obtained here through, the electrochemical interrogation of ferrocenemonocarboxylic acid, demonstrates relatively good electron kinetics, as displayed through the peak separation data, a Nernstian reaction has not been illustrated – where a fast reversible reaction has taken place a peak separation of

59/*n* mV is expected, *n* denotes the number of electrons involved in the electron transfer process (Bard, 2001). This decrease in the electron-transfer rate may be due, in part, to the binder of the screen-printed electrode (Wang et al., 1998). As stated previously the surface morphology, for example: the graphite loading, size and position of particles and functionality of the graphite, of the electrode surface can also influence the electron transfer kinetics as can the hydrophobicity associated with the carbon surface (Fanjul-Bolado et al., 2008). As such, an idealised electrode system might not be expected of a screen-printed sensor (Pritchard et al., 2004).

The anodic/cathodic peak current ratio (I_a/I_c) for a completely reversible system should be close to 1, in this instance the ratio was found to be almost double this at 1.8 – from this it may be said that this reaction exhibits quasi-reversible rather than reversible electron transfer reactivities (Bard, 2001). This may be due, in part, to the non-homogeneous composition of graphite particles on the surface of the electrode which can affect the analytical performance. As a consequence, electrochemical interrogations using a screen-printed sensor may not exhibit the same responses as might be expected from a more traditional three electrode system where the working electrode is not constrained in this manner, for example, those made from more electroactive materials such as gold or platinum. Despite this, it has been demonstrated that this system is capable of electrochemical measurement for both reductive and oxidative interactions albeit in a non-idealised manner.

The above demonstration of the electrochemical interrogation of ferrocenemonocarboxylic acid has established that the carbon screen-printed electrode system may be an effective basis for electrochemical examination of other electroactive compounds in solution. This redox couple will be utilised again throughout this work to display the differences between planar electrodes (the system described above) and microelectrode arrays which are be examined in chapter 11. Further to this, the ferrocenemonocarboxylic acid redox couple will also be used to highlight any differences when screen-printed carbon electrodes doped with the electroactive species cobalt phthalocyanine are employed in the place of the plain un-doped carbon sensor (chapter 10)

5.3. Electrochemical characterisation of nitro-aromatic compounds with the screen-printed electrode

Initial investigations into the detection of nitro-explosives, in particular TNT and DNT, firstly involved a baseline measurement with pH 7.0 phosphate buffer solution alone, and then following this with the inclusion of the explosive substances within this control solution to establish any electrochemical properties attributed to the TNT / DNT that may interfere with the results obtained when the enzyme mediated interrogations are undertaken. Cyclic voltammograms were recorded of the interrogation of the pH 7.0 phosphate buffer control solution (Figure 5.4), TNT in pH 7.0 phosphate buffer solution (see Figure 5.5 and Figure 5.6) and DNT in pH 7.0 phosphate buffer solution (Figure 5.7 and Figure 5.8).

The voltammograms obtained of TNT and DNT demonstrate two reductive peaks and one oxidative peak; the anodic and cathodic redox peaks are present at the potential positions of +0.3, -0.3 and -0.72 V for TNT and +0.20, -0.35 and -0.77 V for DNT (vs. Ag/AgCl) – see Figure 5.6 and Figure 5.8.

As can be seen, when a potential sweep is performed on a phosphate buffer solution without nitroaromatic compounds present, this results in a voltammogram devoid of any obvious redox peaks (Figure 5.4). There is no visible evidence of peaks in a position that may influence those observed for the nitroaromatic compounds.

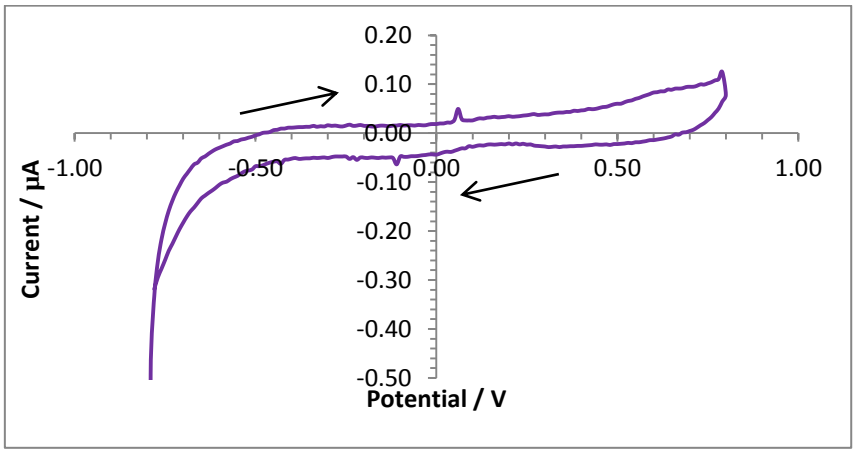

Figure 5.4 - Cyclic voltammogram of pH 7.0 phosphate buffer solution on bare carbon screen printed electrode at a scan rate of 20 mVs^{-1}

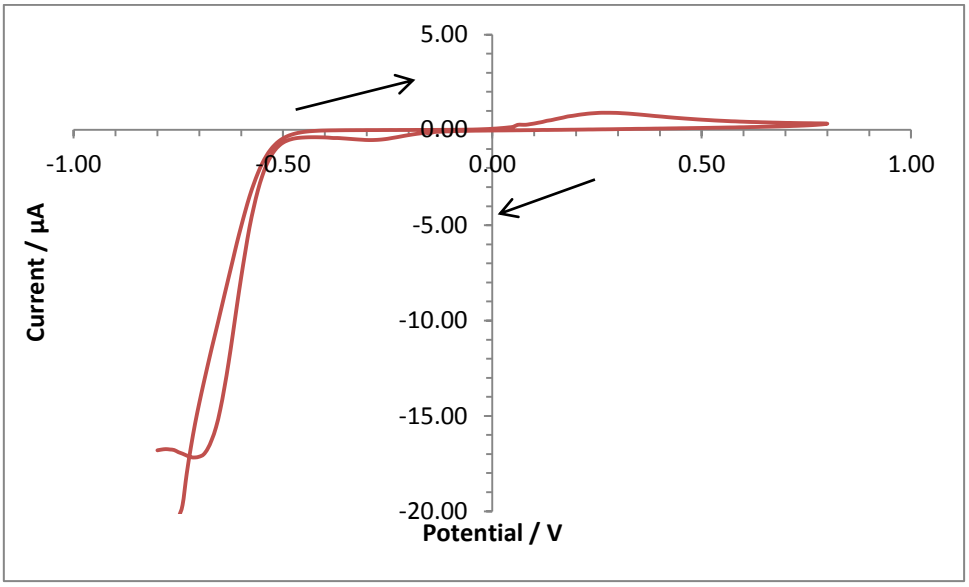

Figure 5.5 - A cyclic voltammogram of 200 µM TNT in a solution of pH 7.0 phosphate buffer solution (vs. Ag/AgCl) at a scan rate of 20 mVs^{-1}

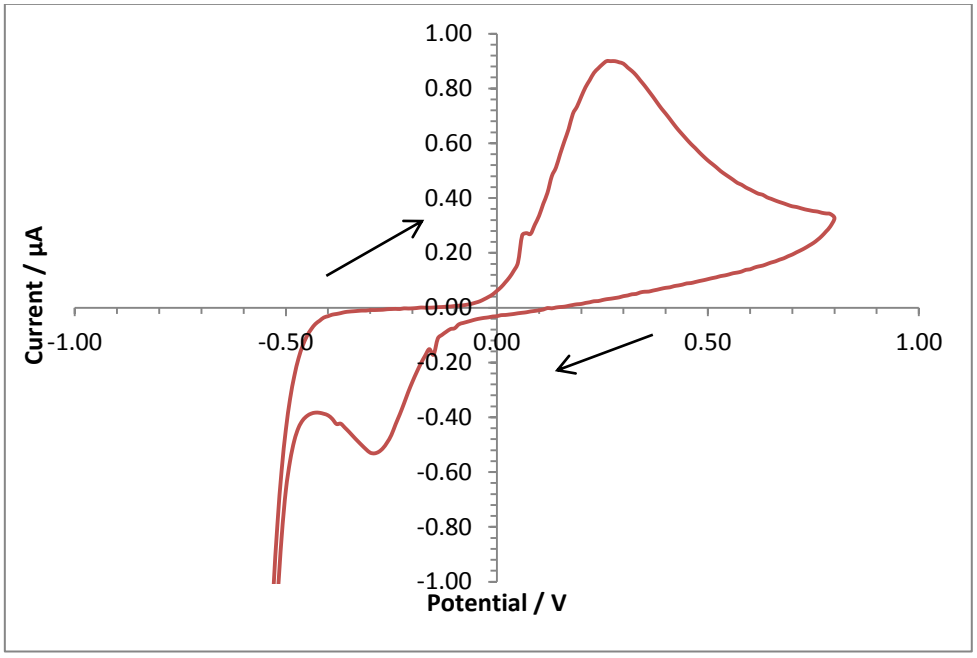

Figure 5.6 - The cyclic voltammogram of 200 µM Trinitrotoluene in a solution of pH 7.0 phosphate buffer solution at a scan rate of 20 mVs^{-1} (vs. Ag/AgCl) cropped to show the anodic and cathodic peaks

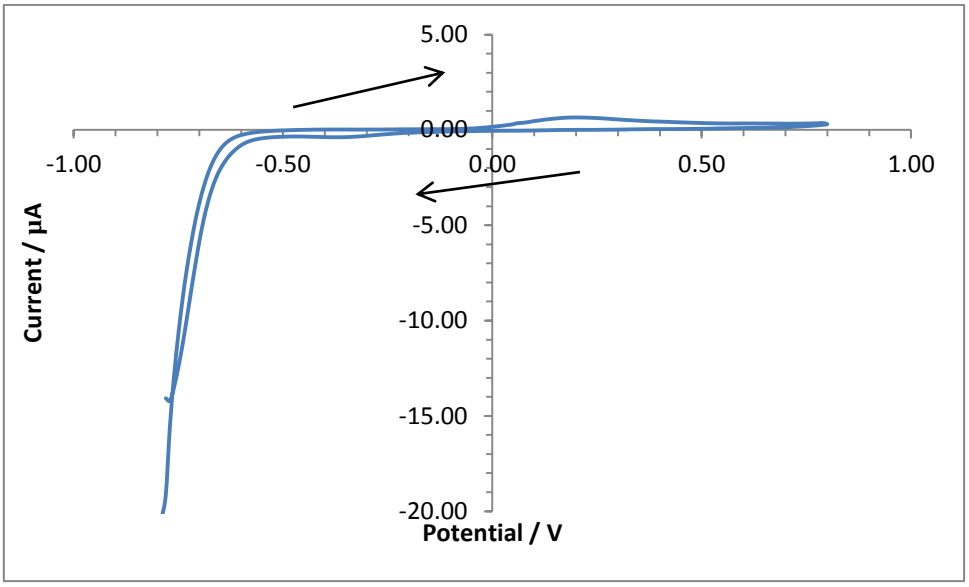

Figure 5.7 - A cyclic voltammogram of 200 µM Dinitrotoluene in a solution of pH7.0 phosphate buffer solution (vs. Ag/AgCl) at a scan rate of 20 mVs^{-1}

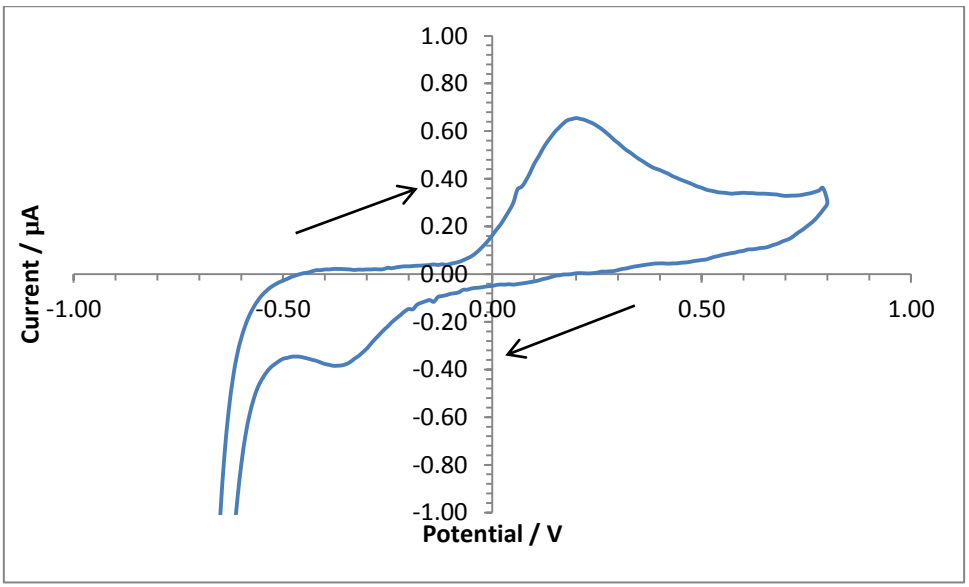

Figure 5.8 - The cyclic voltammogram of 200 µM Dinitrotoluene in a solution of pH 7.0 phosphate buffer at a scan rate of 20 mVs^{-1} (vs. Ag/AgCl) cropped to show the anodic and cathodic peaks

When a potential sweep is applied to the electrode between -0.8 and +0.8 V (vs. Ag/AgCl) within a solution containing 200 µM TNT or DNT (Figure 5.5), there is a significant observed change in the current response. Forward and reverse peaks are apparent indicating both oxidative and reductive reactions are taking place. Nitroaromatics can be observed to be electroactive compounds (Wang, 2007b; Wang

et al., 1998; Bratin et al., 1981) due to the inherent redox activity caused by the easily reducible nitro groups behaving as an electron acceptor.

Taking the electrochemical profile of TNT first (Figure 5.6), the reductive peak present at a potential of -0.72 V (vs. Ag/AgCl) is indicative of the electrochemical reduction of the nitro groups on the TNT molecule as a result of a sequential four-electron reduction of each nitro group to its hydroxylamine derivative, see Equation 5.1 (Chen et al., 2006).

$$NO_2 + 4e^- + 4H^+ \longrightarrow NHOH + H_2O$$

Equation 5.1

The mechanism by which this reduction takes place on polynitro-aromatic compounds depends on several factors including the number of nitro groups, their relative position on the ring, the nature of other substituents on the ring and the solution pH (Bratin et al., 1981). The electron deficient nitrogen on the nitro groups acts as an electron acceptor thus enabling the four-electron reduction to take place at each nitro group (Figure 5.9).

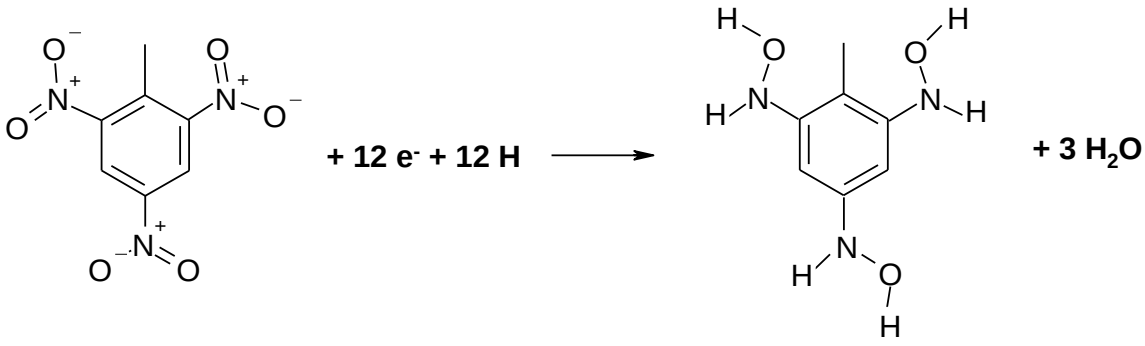

Figure 5.9 - Four-electron reduction of nitro groups on TNT

Once the reduction from nitro to hydroxylamine has taken place a reversible second step, from hydroxylamine to amine occurs with a two-electron reduction, this can be observed as an anodic and cathodic peak redox couple at +0.25 and -0.3 V (vs. Ag/AgCl).

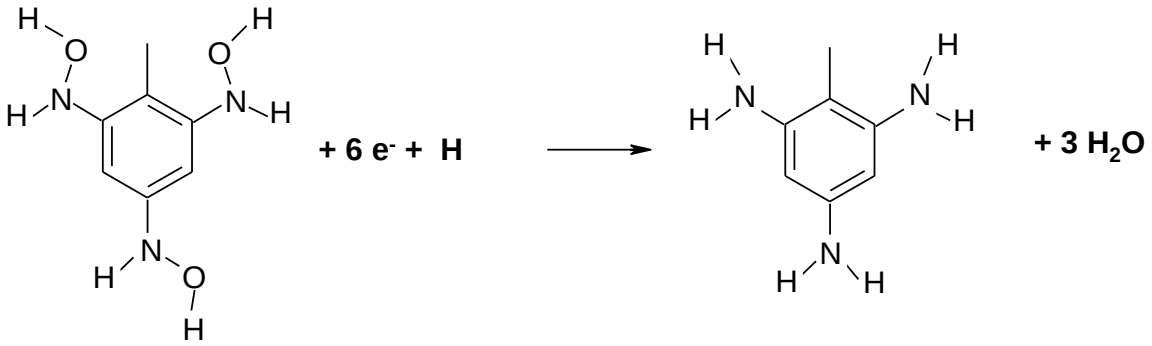

Figure 5.10 - Two-electron reduction of TNT's nitro groups from hydroxylamine to amine

For DNT, the mechanism of reduction is largely the same - with the two nitro groups being reduced first to hydroxylamine and then reversibly to amine moieties. It is interesting to note that DNT is less easily reduced than TNT and so the position of the reduction peaks should occur at a more negative potential (Wang, 2007a).

It can be seen that the peak positions of DNT and TNT are similar but not in precisely the same position – there is a 0.05 V (vs. Ag/AgCl) shift in the cathodic direction in the DNT voltammograms when compared to those obtained of TNT (Table 5.2). There is also a difference in the peak height of the two nitroaromatic compounds as one might expect because of the difference in nitro groups present on the central structure. This difference in peak height, and therefore current response, roughly equates to a 3:2 ratio of TNT and DNT, respectively, at the redox peak couple.

	E_{ia}	i_{pa}	E_{ic}	i_{pc}	E_{ic}	i_{pc}
TNT	+0.30	0.89	-0.30	0.53	-0.72	17.16
DNT	+0.20	0.65	-0.35	0.38	-0.77	14.2

Table 5.2 - Peak position (E_i) in volts and height data (i_p) in µA for both TNT and DNT to enable comparison, all performed with a carbon SPE at a scan rate of 20 mV/s (vs. Ag/AgCl)

Throughout the rest of this work the main reductive peak will be termed R1 and the redox couple observed for both TNT and DNT will be termed R2 and O1.

5.4. The influence of dissolved oxygen on the electrochemical reduction of nitroaromatics

The removal of oxygen from the solution under investigation can be advisable in systems where the interrogative parameters are near to where the electrochemical reduction of oxygen occurs. When the oxygen has been removed it is possible to analyse the reactions that take place free of influence of any oxygen in the system. Oxygen may be electrochemically reduced via two separate two-electron steps (Wang, 2006). The first involves the reduction of oxygen to hydrogen peroxide:

$$O_2 + 2H^+ + 2e^- \rightarrow H_2O_2$$

Equation 5.2

And the second step is the further reduction of the hydrogen peroxide:

$$H_2O_2 + 2H^+ + 2e^- \rightarrow 2H_2O$$

Equation 5.3

To eliminate any oxygen influence on the electrochemistry of the reduction of TNT, the solution was purged via a stream of argon for varying amounts of time. To assess the amount of time that was adequate for future electrochemical interrogations, a study was conducted, increasing progressively the time the solution was purged and tested by running a CV of a 100 μM TNT solution, between -0.8 and +0.8 V (vs. Ag/AgCl).

The effect of dissolved oxygen on the electrochemical system can cause issues when the intention is to produce a field-deployable device capable of analysing small sample volumes (Honeychurch et al., 2003). Under these circumstances it may not be possible to remove oxygen from the system prior to analysis and so the effect of having this oxygen present needs to be examined. During this work, the oxygen will be removed so that analysis of the reactions independent of oxygen influence can be undertaken. Where appropriate, investigations without deoxygenation will be included for completeness and with the final utilisation of the system in mind.

As can be seen in Figure 5.11, when increasing the time the solution is purged the main reductive peak at -0.72 V diminishes with the most significant drop occurring within

the initial 2 minute degassing period. At the 4 minute and above degassing time there is little difference in the loss of current response and the difference between 10 and 20 minutes was minimal (see Figure 5.12). Accordingly a degassing time of 10 minutes was subsequently utilised for all electrochemical interrogations unless otherwise stated.

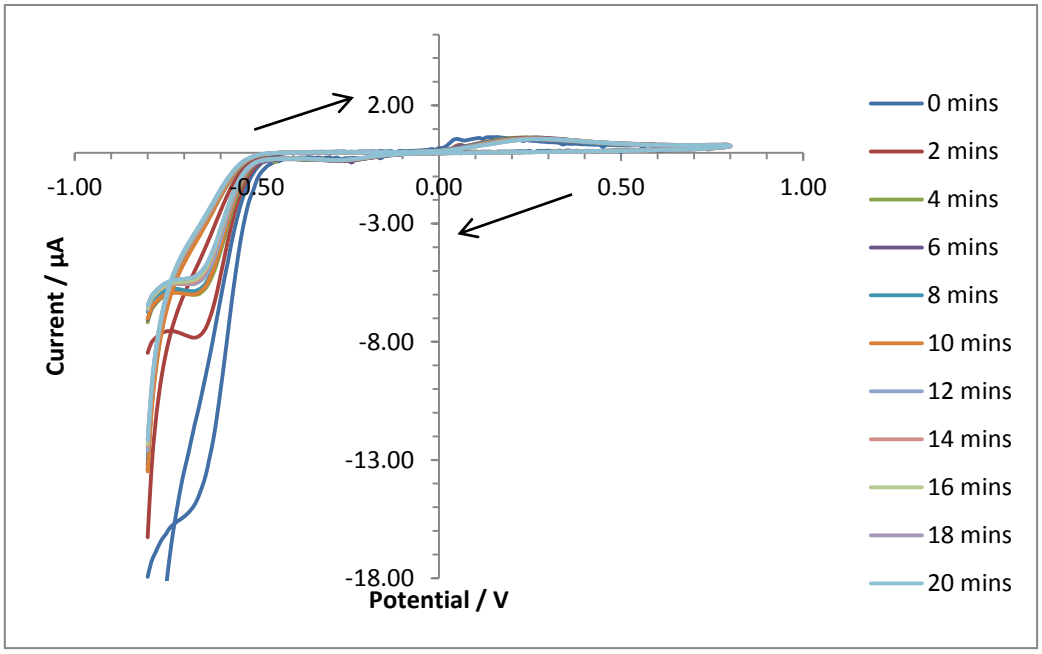

Figure 5.11 - Cyclic voltammograms representing the increase in argon purging time and the influence this has on the oxidative and reductive peaks of 100 µM TNT (in phosphate buffer at a scan rate of 20 mVs^{-1} vs. Ag/AgCl)

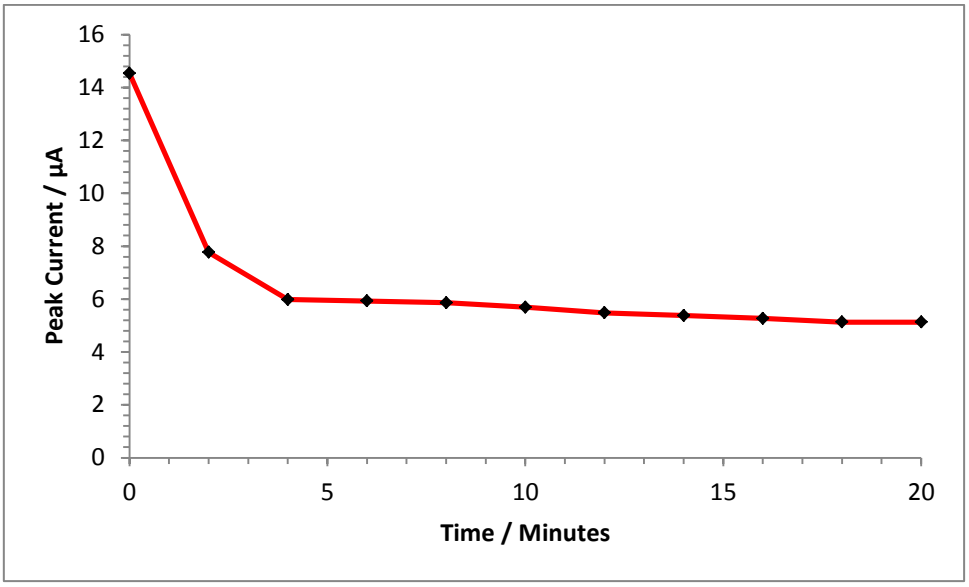

Figure 5.12 - A plot of the diminishing peak current with increasing periods of deoxygenation taken from maximum peak R1 (at scan rate of 20 mVs^{-1} vs. Ag/AgCl)

It is interesting to note that whilst the main reductive peak, R1, diminishes with increasing deoxygenation, the oxidative and reductive redox couple present actually increases slightly with the increasing degassing time period, see Figure 5.13 for the oxidative peak O1.

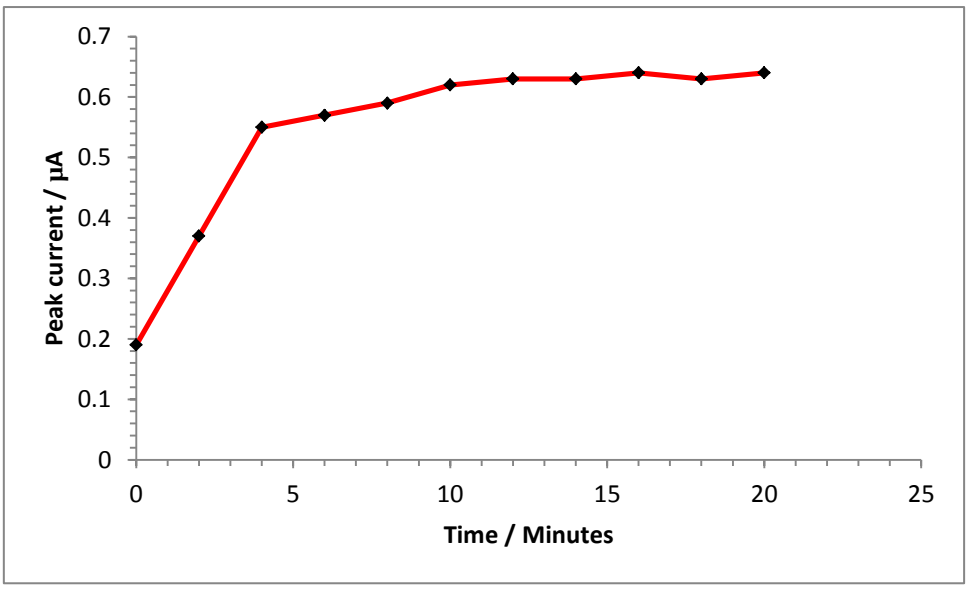

Figure 5.13 - A plot of the increasing peak current with increasing periods of deoxygenation taken from the maximum peak current at peak O1 (at scan rate of 20 mVs^{-1} vs. Ag/AgCl)

It is possible that the nitroaromatic and oxygen reduction peaks in the more cathodic region are overlapping and so with the removal of the dissolved oxygen there is a

removal of this influence. The redox peaks R2 and O1 are not situated in this region but are influenced by oxygen in another way – it seems that the dissolved oxygen may be acting as an electron acceptor which may compete with the electrochemical breakdown of the nitroaromatic compound, removal of this competitive process enables an increase in the electrochemical interrogation of the nitroaromatic – resulting in an increased current response in this area.

5.5. The effect of concentration increase on the current response

When increasing the concentration of the nitroaromatic compound present in the phosphate buffer solution it would be expected that the resulting current response would also increase. To investigate whether this increase of the substance under investigation did influence the current response a progressively stronger concentration of the nitroaromatic compounds, TNT and DNT, were interrogated electrochemically as described earlier (see section 4.6.1). The cyclic voltammogram profiles for this can be seen in Figure 5.14.

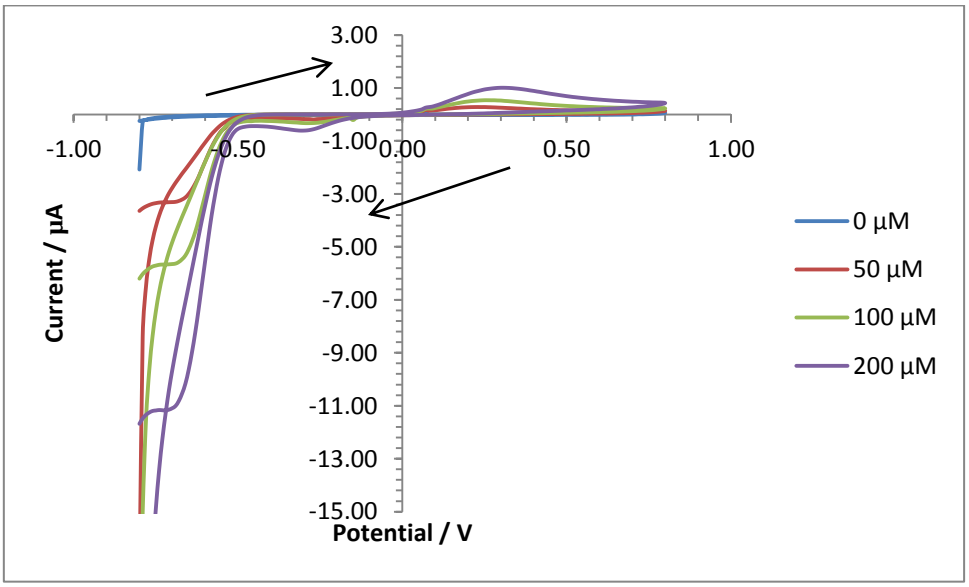

Figure 5.14 - Cyclic voltammograms of increasing concentrations of TNT in phosphate buffer solution (scan rate 20 mVs^{-1} vs. Ag/AgCl)

It can be observed that with the increasing concentrations of TNT there is a corresponding increase in current response. This is shown graphically in the form of a calibration plot, see Figure 5.15. The data for this calibration chart was taken from the main reductive peak, R1, observed at a potential of -0.72 V (vs. Ag/AgCl). This peak is indicative of the reduction of the nitro groups on the aromatic ring to form hydroxylamine moieties as discussed earlier (section 5.3).

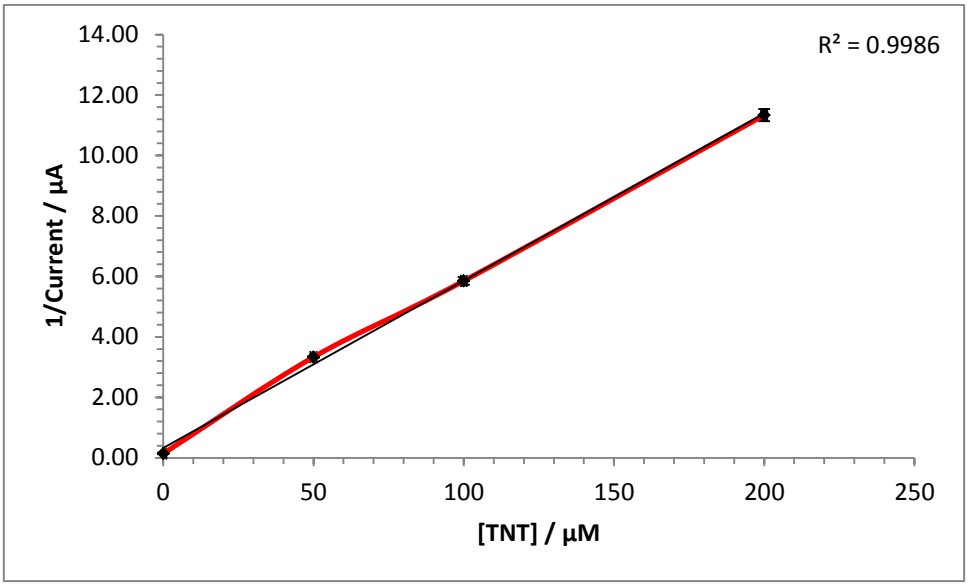

Figure 5.15 - Calibration plot for TNT in phosphate buffer solution on a screen-printed carbon electrode taken from the reductive peak in position at -0.72 V (vs. Ag/AgCl) – error bars are shown

There were two other peaks present in the voltammograms in Figure 5.14 – one oxidative peak, O1 at +0.3 V and one reductive, R2, at -0.3 V (vs. Ag/AgCl). This anodic peak is the result of the re-oxidation of the hydroxylamine moieties to form nitrosamine groups (Honeychurch et al., 2003). The reductive peak present at -0.35 V would correspond to the reduction of these nitrosamine groups back to the hydroxylamine form.

Calibration data representing these reactions can be seen in Figure 5.16 and Figure 5.17. The oxidative peak provides a quasi-linear calibration plot that has an R^2 value of 0.9995 up to the 100 µM solution concentration position before the influence of the concentration of TNT to the current response begins to level off. The error bars are included in the calibration profile and represent one standard deviation, calculated from the average of the population, either side of the data point. Figure 5.17 presents the peak height data from the reductive peak at -0.3 V (vs. Ag/AgCl) – here the increasing concentrations of TNT provide a linear calibration profile and the size of the error bars demonstrate that the electrochemical reduction of TNT in this manner is a reproducible process.

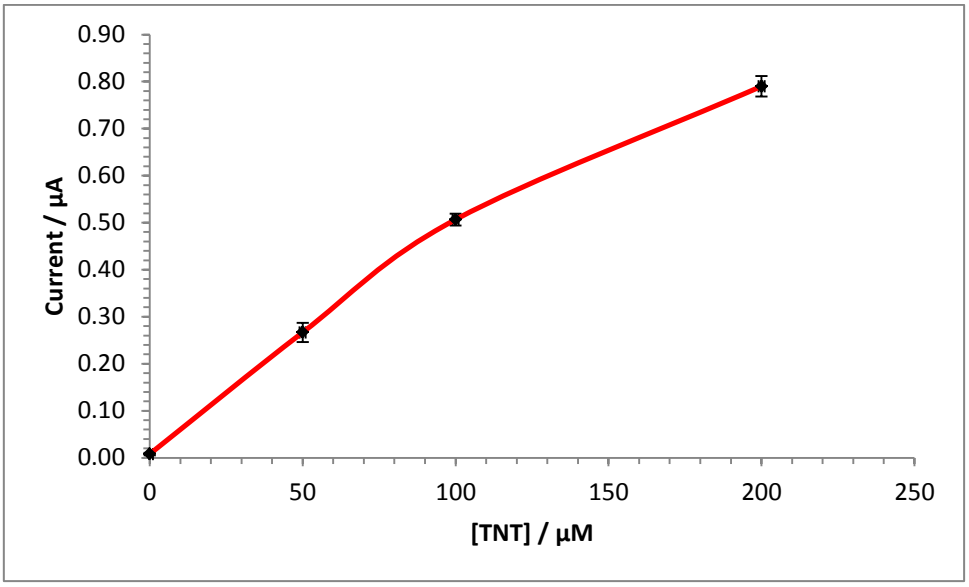

Figure 5.16 - Calibration plot for TNT in phosphate buffer solution on a screen-printed carbon electrode taken from the oxidative peak in position at +0.3 V (vs. Ag/AgCl)

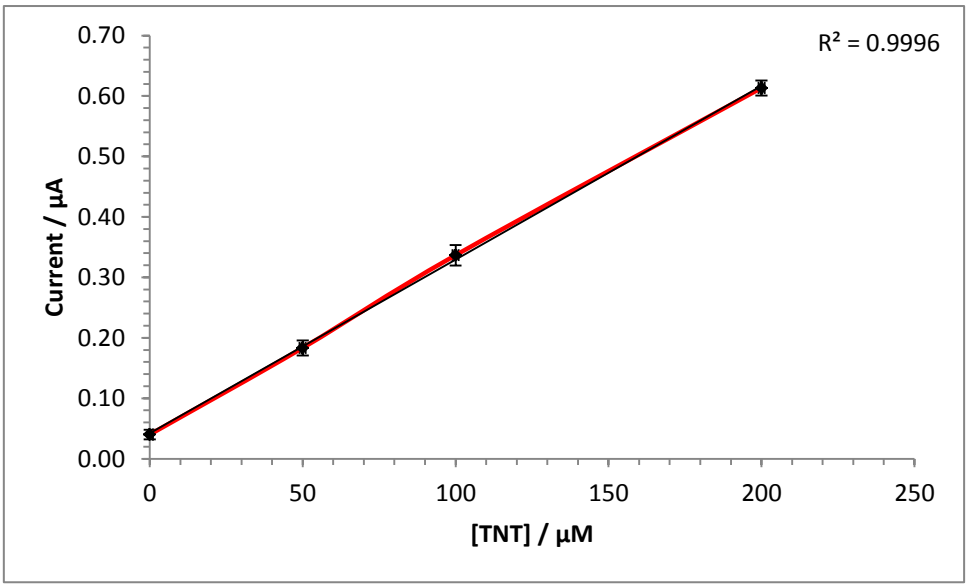

Figure 5.17 - Calibration plot for TNT in phosphate buffer solution on a screen-printed carbon electrode taken from the reductive peak in position at-0.30 V (vs. Ag/AgCl)

Calibration data can be seen in Figure 5.15 to Figure 5.17, however the actual current response output with screen-printed carbon electrode was found to be fairly low which may restrain the lower detection limits for this sensor. This was found to be the case as the concentration of TNT was decreased, the magnitude of response can be observed to be in the low microampere region.

A similar study was undertaken using DNT to assess the linearity when altering the concentration. As mentioned earlier (section 5.3), the breakdown of DNT and the resulting current profile occurs in a similar manner to TNT; with the reductive and oxidative peaks occurring in a more cathodic position due to the redox reactions taking place more readily with TNT than with DNT (Wang, 2007a). Calibration profiles for both the two reductive peaks (Figure 5.18 and Figure 5.19) and the oxidative peak (Figure 5.20) are provided below.

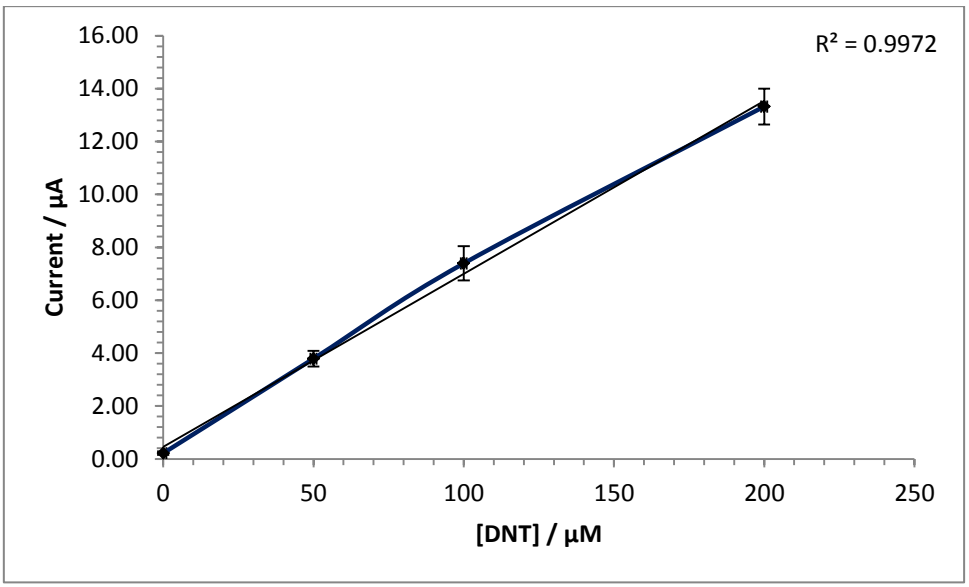

Figure 5.18 - Calibration plot for DNT in phosphate buffer solution interrogated with a screen-printed electrode taken from the reductive peak in position -0.77 V (vs. Ag/AgCl)

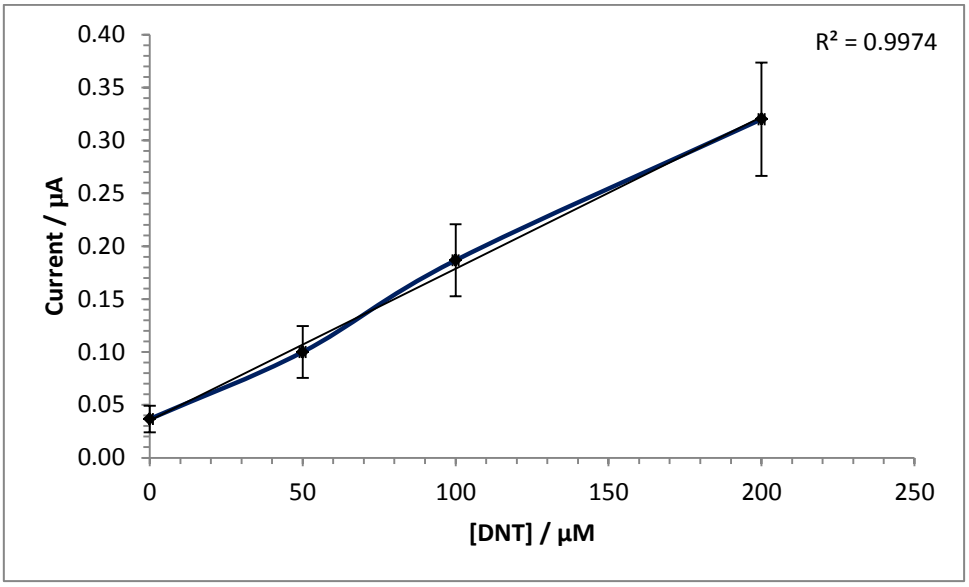

Figure 5.19 - Calibration plot for DNT in phosphate buffer solution interrogated with a screen-printed electrode taken from the reductive peak in position -0.35 V (vs. Ag/AgCl)

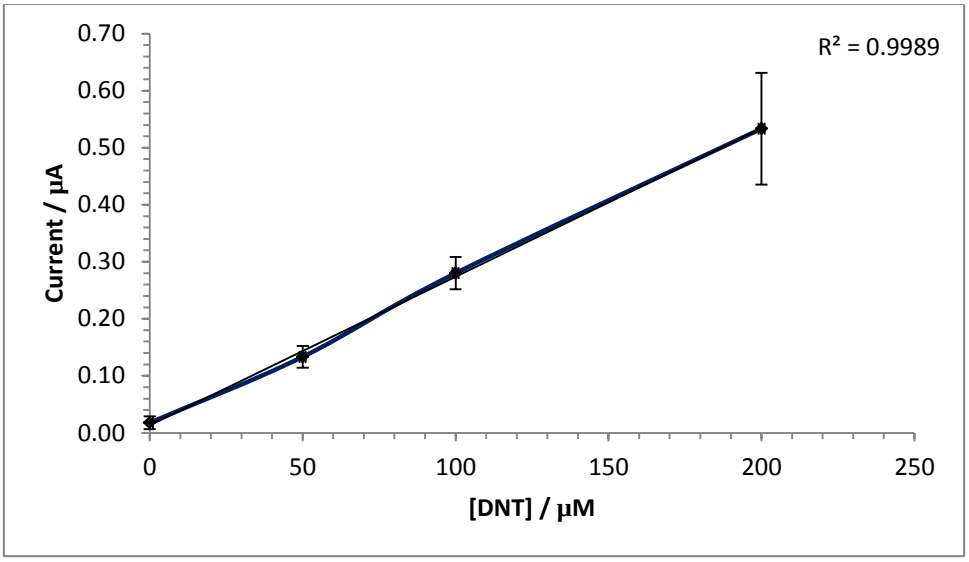

Figure 5.20 - Calibration plot for DNT in phosphate buffer solution interrogated with a screen-printed electrode taken from the oxidative peak in position +0.2 V (vs. Ag/AgCl)

It can be observed that there is a clear linear relationship of increasing current response with increasing concentrations of DNT and all peaks provided high R^2-values. This provides promise that a screen-printed sensor technique for detection of nitroaromatics is a feasible option if the magnitude of the current response can be improved.

5.6. The detection limit of the screen-printed carbon electrode system for nitroaromatic compounds

Other electrochemical detection technologies for nitroaromatic compounds have been reported in the literature with detection limits in the nano mole range, for example: Alizadeh et al, 2009, report a voltammetric carbon paste sensor chemically modified with molecularly-imprinted and non-imprinted polymers for the detection of TNT with a detection limit of 1.5 nM (Alizadeh et al., 2010). Mesoporous silica microspheres functionalised with amino groups aligned upon the surface of a glassy carbon electrode surface has been reported for the electrochemical detection of TNT using square-wave voltammetry with the limit of detection reported as 0.5 nM (Fu et al., 2010). It was therefore, important that the LOD of this electrochemical system was assessed to enable comparisons with future modifications.

The theoretical baseline current was determined through electrochemically interrogating a phosphate buffer solution, without the presence of any nitro compounds, with ten sensors. This baseline current was then used to calculate the limit of detection (based on three times the standard deviation, n=10). These limits of detection are provided in Table 5.3 for TNT and DNT.

	TNT			DNT		
Peak position, V	0.25	-0.30	-0.72	0.20	-0.35	-0.77
Detection limit, µA	0.06	0.04	0.15	0.06	0.06	0.17

Table 5.3 - Detection limits as calculated from three times the standard deviation of the mean current of a blank solution (n=10) taking peak positions from those associated with TNT and DNT (see Table 5.2)

Calibration profiles were produced for both TNT and DNT at low concentrations to establish the limit of quantification that this system is capable of, at present, providing for analysis of nitroaromatic compounds. Lower concentrations of TNT are demonstrated in the calibration plot below (Figure 5.21). Error bars are present and represent one standard deviation either side of the point, this was devised from the average of the population.

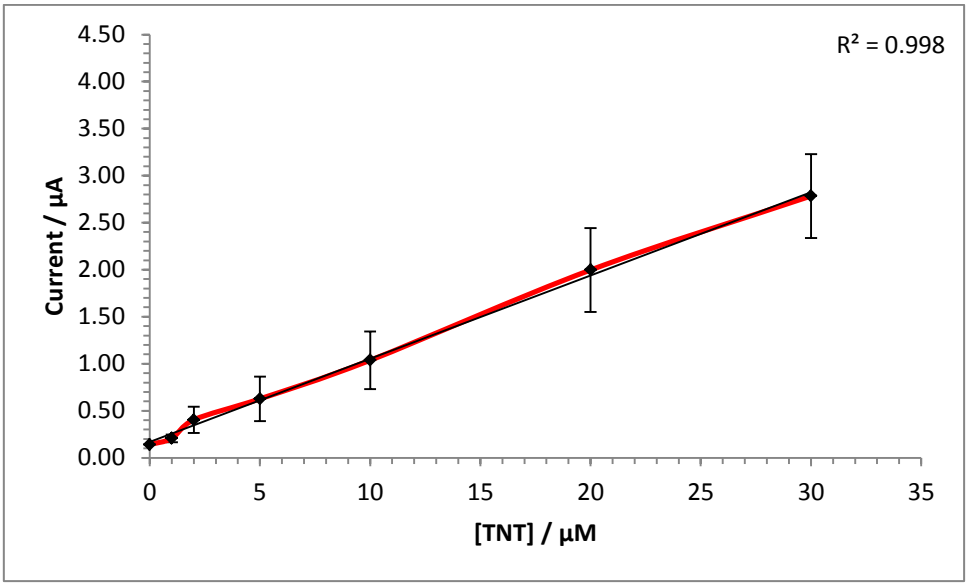

Figure 5.21 - Calibration plot representing the lower detection limits of TNT taken from the peak at a potential of 0.72 V (vs. Ag/AgCl)

The peak position of -0.72 V (vs. Ag/AgCl) for TNT has a baseline current demonstrated to be 0.15 µA. It can be calculated from the calibration plot that the minimum quantity of TNT that this system can reliably detect using the main reductive peak at potential -0.72 V is 0.4 µM. This value was obtained using the baseline figure as the limit of quantification and establishing, by assessing where this current value crosses the line within the calibration plot and reading the corresponding concentration value. The linear calibration plot is demonstrated through the high R^2 value, which adds support to the reliability of this result.

This technique was repeated with the second reductive peak at -0.30 V (Figure 5.22) and the oxidative peak at +0.30 (Figure 5.23) using the calibration profiles related to lower concentrations of TNT. It should be noted, however, that there is a greater variability in the results at these two peaks as demonstrated by the larger error bars displayed on the chart area, especially on the calibration plot of the oxidative peak.

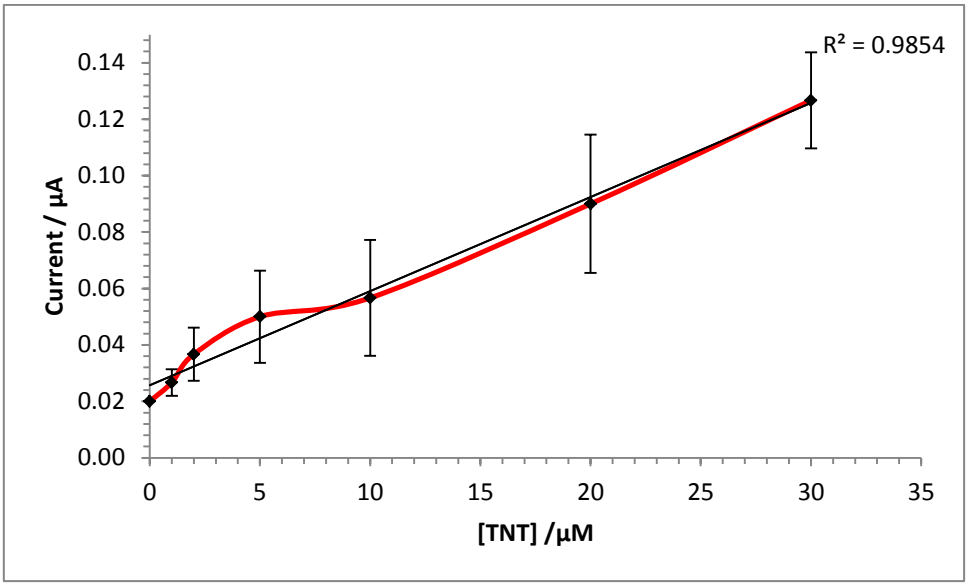

Figure 5.22 - Calibration plot representing the lower detection limits of TNT taken from the peak at a potential of -0.30 V (vs. Ag/AgCl)

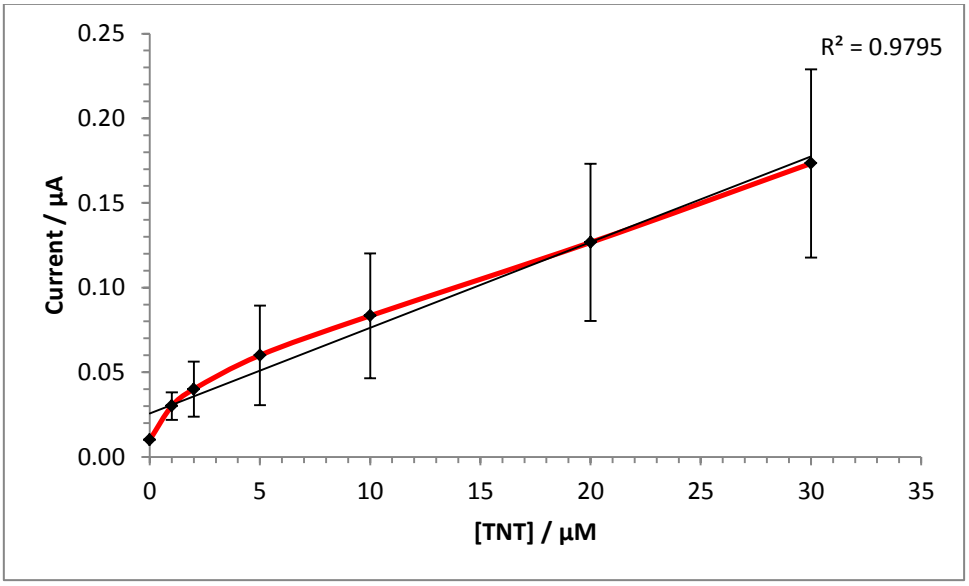

Figure 5.23 - Calibration plot representing the lower detection limits of TNT taken from the peak at a potential of +0.3 V (vs. Ag/AgCl)

Using the baseline data collected it is possible to give the limit of detection for TNT using the reductive peak at -0.30 V as 2.6 µM and using the oxidative peak at +0.30 V as 5 µM. It may be the case that, due to the error demonstrated in the oxidative peak, this potential might not be suited for reliable, low concentration analysis of TNT.

The same process was carried out with DNT to establish the limit of detection for this substance using the screen-printed carbon electrode system as described above. The

calibration profiles for the DNT current response peaks at low concentrations are provided below (Figure 5.24, Figure 5.25 and Figure 5.26).

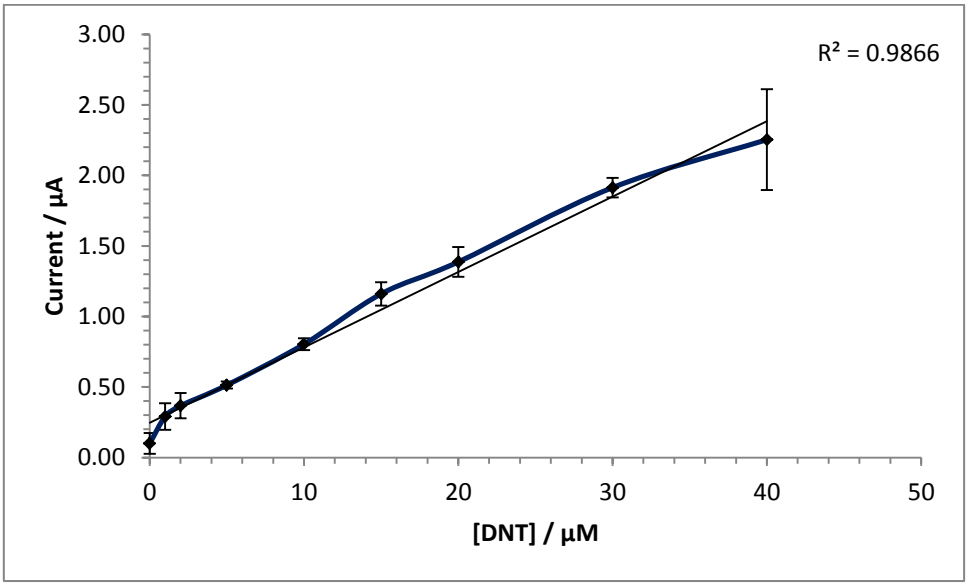

Figure 5.24 - Calibration plot representing the lower detection limits of DNT taken from the peak at a potential of -0.77 V (vs. Ag/AgCl)

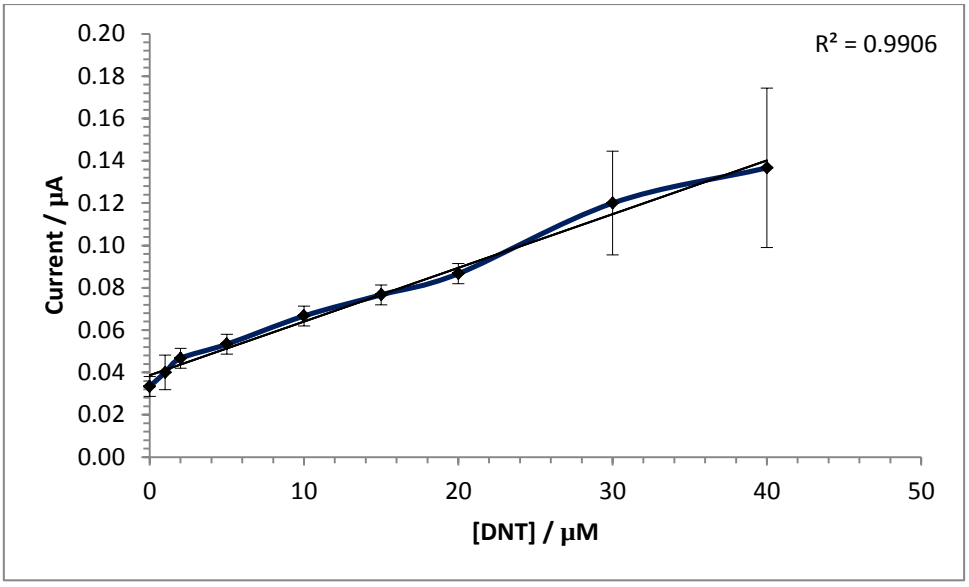

Figure 5.25 - Calibration plot representing the lower detection limits of DNT taken from the peak at a potential of -0.35 V (vs. Ag/AgCl)

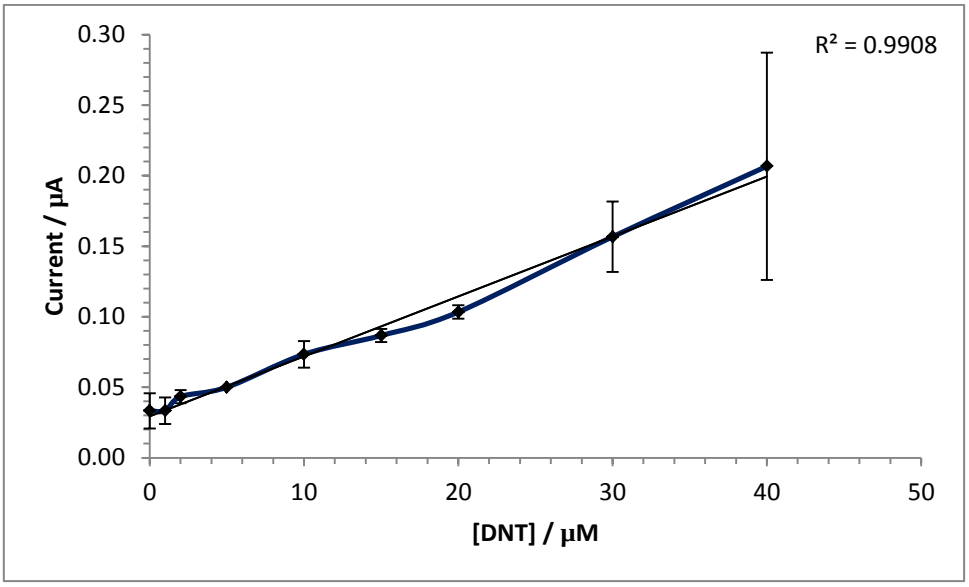

Figure 5.26 - Calibration plot representing the lower detection limits of DNT taken from the peak at a potential of +0.20 V (vs. Ag/AgCl)

Using the baseline data acquired earlier (Table 5.3) the limit of detection was devised at each visible peak in the DNT current profile. At the main reductive peak, present at -0.77 V, the baseline was indicated to be 0.17 µA and from this value the limit of detection was determined to be 0.7 µM. For the second reductive peak at potential -0.35 V the baseline was established as 0.06 µA and the limit of detection is thus 7.5 µM. The oxidative peak at +0.20 V also has a baseline associated with that potential of 0.06 µA and this equates to a limit of detection of 7 µM. These LODs and those for TNT are presented together in Table 5.4.

	Detection limit in µM		
	R1	**R2**	**O1**
Trinitrotoluene	0.4	2.6	5.0
Dinitrotoluene	0.7	7.5	7.0

Table 5.4 - Limits of detection for TNT and DNT using a calculated baseline and low concentration calibration profiles

Detection limits were demonstrated in this section to be in the order of micro moles, however, this detection limit would need to be improved to compete with other, similar, portable devices reported in the literature, as mentioned earlier.

It would appear, for example, that the development and inclusion of nanotechnology in electrochemical systems has enabled a great improvement in detection limits of

explosive compounds whilst retaining the ease of use and relatively low unit costs associated with an electrochemical sensing system. Synthetic copolypeptide-doped polyaniline nanofibers have been demonstrated to provide a detection limit for TNT of 100 nM when interrogated with adsorptive stripping voltammetry (Wang et al., 2009). Rezaei and Damiri, 2010, report a detection limit of 25 nM for the explosive RDX using multi-walled carbon nanotubes immobilised on the surface of glassy carbon electrodes (Rezaei and Damiri, 2010).

Work towards the miniaturisation and portability of other detection techniques has also advanced over recent years, with a focus on reducing energy consumption, improving usability and integrating a system into a self-contained unit (Capitán-Vallvey and Palma, 2011). Caron et al, 2010, report the ultra-trace detection of explosives in air or present in trace amounts on objects with a portable fluorescent detector. Detection limits for TNT were reported as 0.75 ppbv (Caron et al., 2010b).

5.7. Conclusions

The suitability of the screen-printed carbon electrodes designed and supplied from Microarray Ltd. was assessed using the common redox couple, ferrocenemonocarboxylic acid. This species displays clear single peaks in the anodic and cathodic directions representing its oxidation into the ferricinium state before reduction back to its original form. This was displayed in Figure 5.3. The peak separation using the screen-printed electrodes for analysis, although not demonstrating a truly reversible system, did illustrate a reliable technique for electroanalytical interrogations. It should not be expected that this system will have the same electron transfer reactivities or current response as an electrode system based on a more electroactive material, such as gold or platinum, however this system has the advantage of decreased cost and sensor disposability.

Initial investigations with the explosive TNT took place without prior deoxygenation. These investigations demonstrated the inherent electroactivity of TNT; three peaks were present in the voltammogram, one anodic and two cathodic representing the electrochemical reduction of each of the nitro groups on the aromatic ring first to a hydroxylamine and then, reversibly, to an amine group. DNT was demonstrated to have a similar profile but the two reductive peaks and one oxidative peak are present in a more cathodic position. This is because DNT is less easily reduced than TNT, hence the peaks occurring at a more negative potential.

The influence of dissolved oxygen on the system has been demonstrated – this is of importance as a portable device may not have the capacity for removal of oxygen prior to analysis of sample solutions. It was interesting to note that while the main reductive peak at -0.72 and -0.77 V, for DNT and TNT respectively, diminished with increasing deoxygenation periods; the oxidative and reductive peak couple actually increased with deoxygenation time. This may be a factor when deciding which peak to base analysis on for a portable system – the improved size of the main reductive peak when not deoxygenated may be a desirable aspect in this circumstance.

It has been proven that a carbon screen-printed electrode for the detection of nitro compounds is a feasible option. Detection limits were demonstrated in section 5.5 to be in the low micro molar region; however, this detection limit would need to be improved to compete with similar, portable devices already reported in the literature. There was also good linearity demonstrated at low concentration limits when using the more cathodic reductive peak R1 (at -0.72 and -0.77 V for TNT and DNT, respectively) as a reference point. This can be seen in section 5.5 where R^2 values were 0.9985 and 0.9906 for TNT and DNT, respectively. A linear relationship between concentration and current response was also demonstrated at greater concentrations of the nitroaromatic compounds.

The addition of a recognition agent to the solution may provide an improvement in both the response and the selectivity of this system for the detection of explosive nitroaromatic compounds. Biological entities such as antibodies and enzymes have widely been used in this manner in previous work in other area, for example, glucose oxidase sensors for the continuous monitoring of glucose levels in the blood (Vashist et al.,) or the detection of organophosphate pesticides (Skládal, 1991). There has also been significant work using biological entities in the detection of explosive compounds (Singh, 2007; Yinon, 2002; Larsson et al., 2006a).

The advantages of a biosensor system based on a screen-printed carbon electrode is still the minimal costs required for purchase and maintenance, with an added element of disposability as the chip can be discarded and replaced when necessary. Ease of use of such a device would limit the time and money required to train personnel to operate the system. As such, it is necessary to attempt improvement to the current response as far as possible to provide for a device that is more commercially viable.

The *E. coli* oxygen-insensitive nitroreductase enzyme has the ability to reduce nitroaromatic compounds independent of external reductive means – electrochemical interrogation, for example (Yin et al., 2005). The use of a nitroreductase enzyme in the electrochemical system described above may, therefore, have the ability to significantly improve the current response with the possible additional advantage of increasing the selectivity of the proposed sensor. As such, work progressed in this

direction – with the inclusion of a commercially available nitroreductase enzyme, to remain dedicated to the production of a low cost and disposable sensor, and included the appropriate cofactor, β-nicotinamide adenine dinucleotide 2-phosphate.

6. Characterisation of the activity of the nitroreductase and co-factor system

6.1. Introduction

The metabolism and degradation of nitroaromatic and nitroheterocyclic compounds receives considerable attention due to the environmental and health risks associated with these compounds. Nitro-substituted compounds can be found in many areas, such as the manufacturing of dyes and pigments, as anti-microbial agents, in explosives, in pharaceuticals, and can also be associated with many by-products such as, for example, diesel exhausts (Whiteway et al., 1998; Bryant and DeLuca, 1991).

The biological degradation of nitroaromatic explosives, such as TNT, also receives much consideration due to the toxic and mutagenic properties of TNT itself and its metabolites (Kim et al., 2002). The metabolisation of TNT may be performed in two ways; firstly through the reduction of the nitro groups on the aromatic ring to nitroso and hydroxylamine intermediates before further reduction to various amino-substitued metabolites (Whiteway et al., 1998). The second pathway involves removing the nitro groups as nitrite ions after the ring is first attacked with a hydride compound (Kim and Song, 2005).

The use of a nitroreductase enzyme in the degradation of nitro-substituted compounds has been well documented (Yin et al., 2005; Esteve-Núñez et al., 2001; Klausmeier et al., 2001) and there are many examples of nitroreductase enzymes that are capable of the metabolism of TNT (Esteve-Núñez et al., 2001). Nitroreductase enzymes are classified with reference to the manner in which they catalyse the reduction of nitro-compounds; nitroreductases may be oxygen sensitive or oxygen insensitive. Nitroreductase from *Escherichia Coli* is known to be found in both the oxygen insensitive and sensitive forms, known as NfsA and NfsB, respectively. The NfsA gene is a flavin mononucleotide (FMN) containing protein that can only use NADPH as an electron donor whilst the NfsB strain, also containing a FMN, can use either NADH or NADPH, β-nicotinamide adenine dinucleotide 2-phosphate, as an electron source

(Whiteway et al., 1998). A diagram of the NfsA nitroreducatse enzyme from *Escherichia Coli.*

A commercially available NfsA nitroreductase from *E. Coli*, purchased from Sigma-Aldrich UK, was utilised in this work due its availablity and with the consideration of producing an explosive detection system that is a commerically viable, mass producible device.

The NfsA nitroreductase from *E. Coli* and the cofactor NADPH are an enzyme system that has been reported to catalyse the reduction of nitroaromatic compounds such as TNT. The nitroreductase catalyses the reduction of nitro groups on the TNT molecule in a two-electron sequential fashion utilising the NADPH as the electron donator (Zenno et al., 1996) utilising the NADPH as the electron donator. The mechanism by which the enzyme facilitates this reduction reaction is a ping-pong Bi-Bi catalysis mode (Naal et al., 2002), where one substrate binds and one product is released before a second substrate can bind and subsequently release a second product, this is also known as a two-step transfer or double displacement (Dixon, 1979).

The enzyme is first reduced by the cofactor, NADPH, into its activated reduced form (Equation 6.1); it is then able to reduce electron withdrawing nitro groups on the nitroaromatic compound, see Equation 6.2.

$$\text{Enzyme} + \text{NADPH} \longrightarrow \text{enzyme}_{(red)} + \text{NADP}^{+}$$

Equation 6.1

$$\text{Enzyme}_{(red)} + \text{nitroaromatic} \longrightarrow \text{enzyme}_{(ox)} + \text{nitroaromatic}_{(red)}$$

Equation 6.2

The enzymatic reduction of the nitro compounds may be observed through the diminishing absorbance at 340 nm associated with the NADPH when observed using UV spectroscopy.

6.2. Characterisation of the enzyme system using UV spectroscopy

The use of a biological species in the bioremediation of nitro compounds has been well documented. Kim et al, 2002, describe this process with a *Klebsiella* strain isolated from activated sludge which is capable of the reduction of TNT and DNT via two different pathways (Kim and Song, 2005). Bryant and DeLuca, 1991, describe the purification of a nitroreductase from intestinal microflora, Enterobacter cloacae, and the characterisation with a nitrofurazone reduction (Bryant and DeLuca, 1991). A review describing many of the biological degradation mechanisms such as, for example, the anaerobic and aerobic bacterial metabolism and the fungal breakdown mechanisms of TNT can be found in the literature. This review mentions 36 enzymes capable of TNT degradation or transformation through various transformation pathways (Esteve-Núñez et al., 2001). Most papers relating to the enzymatic breakdown of TNT procure the enzymes through cloning and expression in-house. As this work is aimed towards the detection system as a whole rather than the specific enzymology that would be required to undertake this development and characterisation, the enzyme was purchased from a scientific supplies company. The use of this nitroreductase and the necessary cofactor was, therefore, characterised for suitability within this project using UV visible spectroscopy.

As previously discussed, the nitroreductase enzyme from *Escherichia Coli* is known to reduce nitro groups on aromatic compounds, such as TNT, using the cofactor NADPH as an initiating step. This reaction can be observed through monitoring the drop in absorbance at 340 nm over time with a UV spectrometer as the enzyme is introduced to a cuvette containing the cofactor, and the species to be reduced, in this case TNT. The measurable species at this wavelength is the NADPH and so the reaction being monitored is the reduction of NADPH to $NADP^+$, see Figure 6.1.

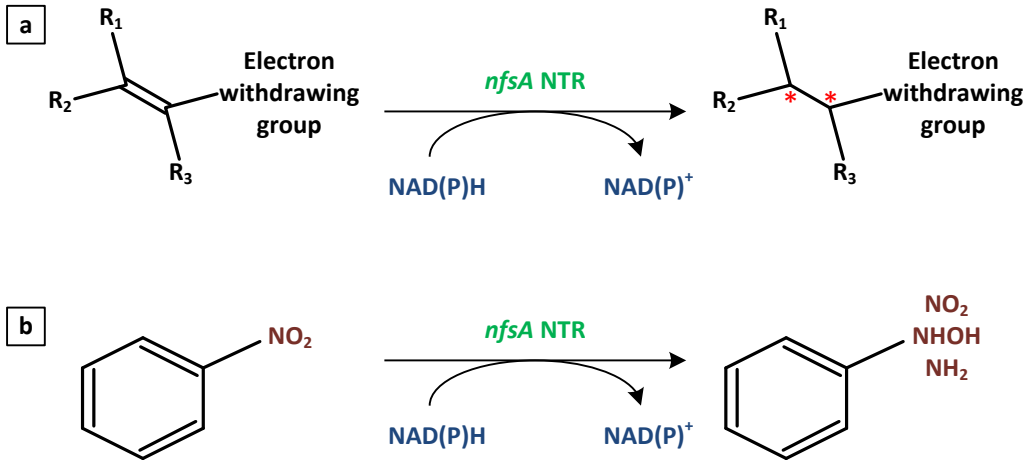

Figure 6.1 - Schematic demonstration of a). the reductive pathway of the nitroreductase enzyme with the cofactor NADPH and b). an example of this nitroaromatic reduction mechanism

This study of the enzyme system is to assess the compatibility of an NfsA nitroreductase and NADPH as a technique to reduced nitro aromatic species. As such, the UV visible spectroscopy investigation is aimed towards confirming this suitability and assessing the performance of the enzyme under conditions necessary for subsequent aspects of this project.

6.2.1. Assessing the functionality of the NfsA *E. Coli* nitroreductase

To assess the functionality of the nitroreductase enzyme, NTR, purchased from Sigma-Aldrich, UK, an enzyme assay was performed using a UV visible spectrometer. The literature reports that the NTR cofactor, NADPH, exhibits absorbance at a wavelength of 340 nm (Gwenin et al., 2007; Smets et al., 2007). A scan was performed between 700 and 300 nm and the absorbance was recorded to confirm the presence and magnitude of this absorbance peak with varying concentrations of NADPH and 100 µM of TNT present in the cuvette but without the enzyme present in pH 7.0 phosphate buffer. A blank cuvette was included in analysis with a phosphate buffer solution.

A 0.1 mM concentration of NADPH was used initially as this concentration has been used previously with an NfsA nitroreductase enzyme from *E. Coli* (Zenno et al., 1996). A clear absorbance peak can be observed at 340 nm which corresponds to the presence of NADPH; TNT is not visible in this region and can only be measured after a pre-treatment step with, for example, sodium hydroxide (Qasim et al., 2009).

The first UV spectra obtained included a 0.1 mM solution of NADPH, Figure 6.2

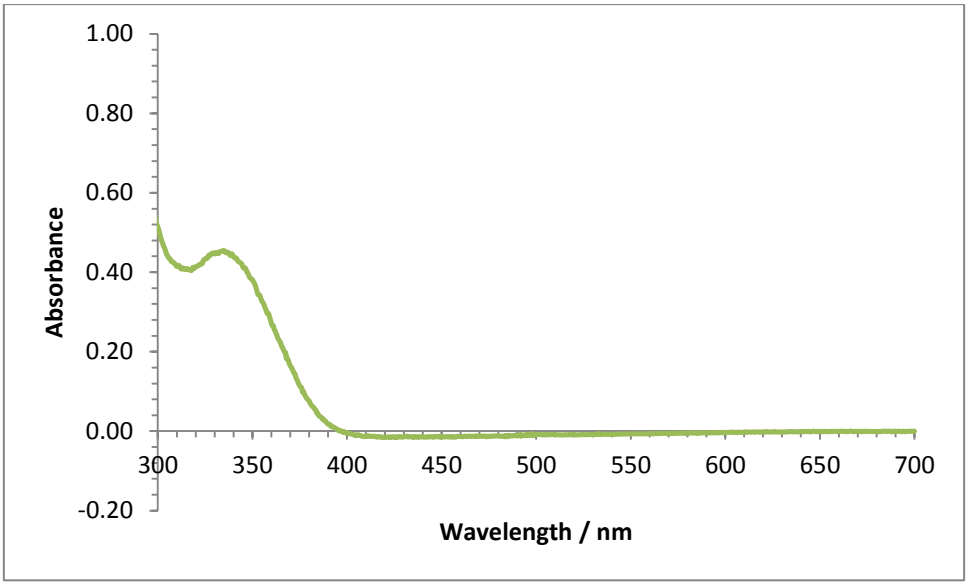

Figure 6.2 - UV visible absorbance spectrum scanned between 700 and 300 nm with an absorbance peak observed at 340 nm which can be related to the amount of NADPH present [0.1 mM]

To assess the influence of increasing NADPH concentrations on the resulting absorbance spectra a further three spectral analyses were performed increasing the

concentration of NADPH to 0.2, 0.3 and 1.0 mM whilst maintaining the concentration of all other factors. The absorbance spectra can be seen in Figure 6.3 and Figure 6.4 below. The analysis of 1.0 mM NADPH produced a large absorbance peak at 340 nm in the same manner as those for the lower concentrations but, due to the magnitude of the obtained peak, suffered significant noise and so is not presented here.

It can be seen that when the concentration of NADPH is increased, there is a corresponding increase in the magnitude of the absorbance at 340 nm. The absorbance peak present at 0.1 mM NADPH provided an absorbance of 0.45; when this was increased to 0.2 mM the absorbance was 0.84 and with 0.3 mM NADPH the absorbance increased further to 1.44. This is an approximate linear increase with each additional concentration increase.

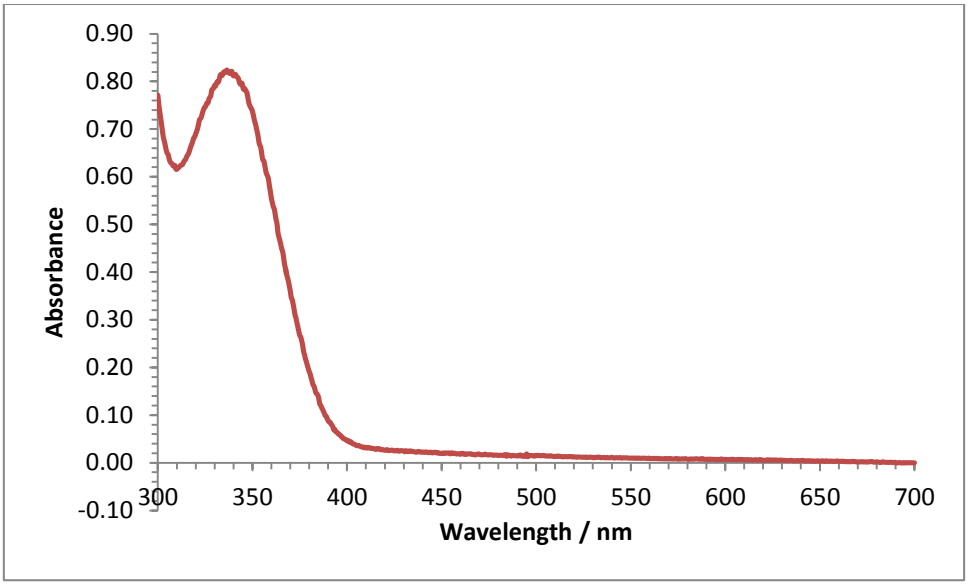

Figure 6.3 - UV visible absorbance spectrum scanned between 700 and 300 nm with an absorbance peak apparent at 340 nm which corresponds to the amount of NADPH present [0.2 mM]

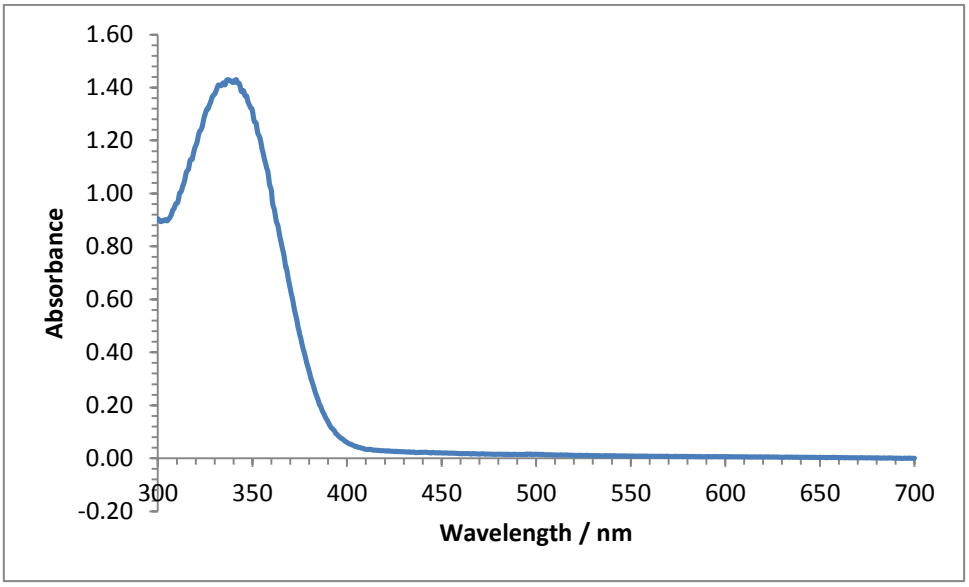

Figure 6.4 - UV visible absorbance spectrum scanned between 700 and 300 nm with an absorbance peak apparent at 340 nm which corresponds to the amount of NADPH present [0.3 mM]

To examine the properties of the system, and to confirm the activity of the enzyme and cofactor for the reduction of TNT, a time scan was performed with each of the concentrations of NADPH. The scan was allowed to run for one minute to allow the system to reach a stable baseline before the enzyme was added (see Section 4.6.2.) to activate the reaction process. This stage can be observed in the resulting spectra as a sharp initial drop before returning to the baseline prior to the characteristic absorbance drop due to the oxidation of the NADPH species by the enzyme.

In all cases, the introduction of the enzyme into the sample cuvette activated a steady drop in absorbance. This can be directly related to the decline in the reduced form of the cofactor as it initiates the enzymatic reduction of TNT through the prior reduction of the enzyme, see Figure 6.5 to Figure 6.7.

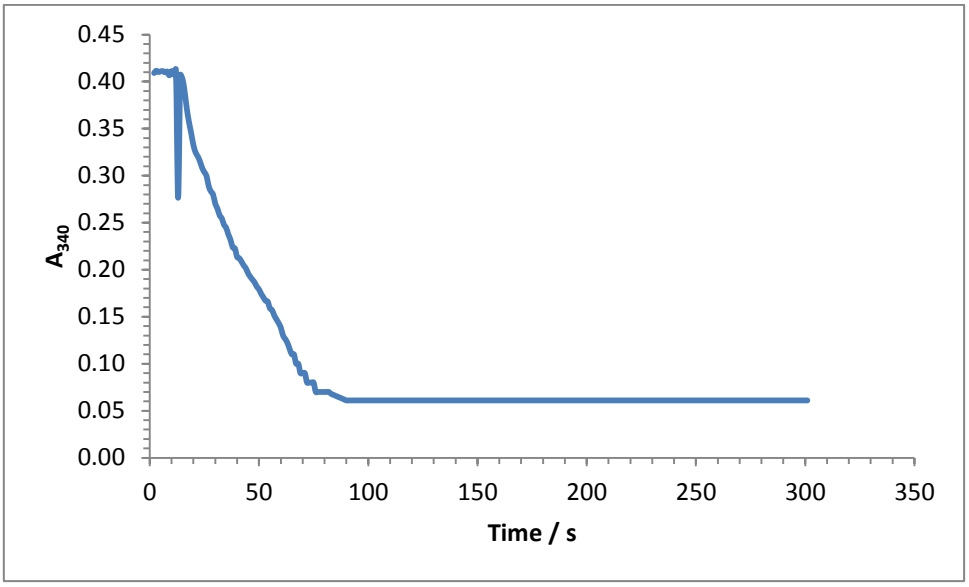

Figure 6.5 - Plot demonstrating the diminishing absorbance over time at a wavelength of 340 nm when one unit of the enzyme nitroreductase was added to the cuvette containing 0.1 mM NADPH and 100 µM TNT under analysis in the UV visible spectrometer

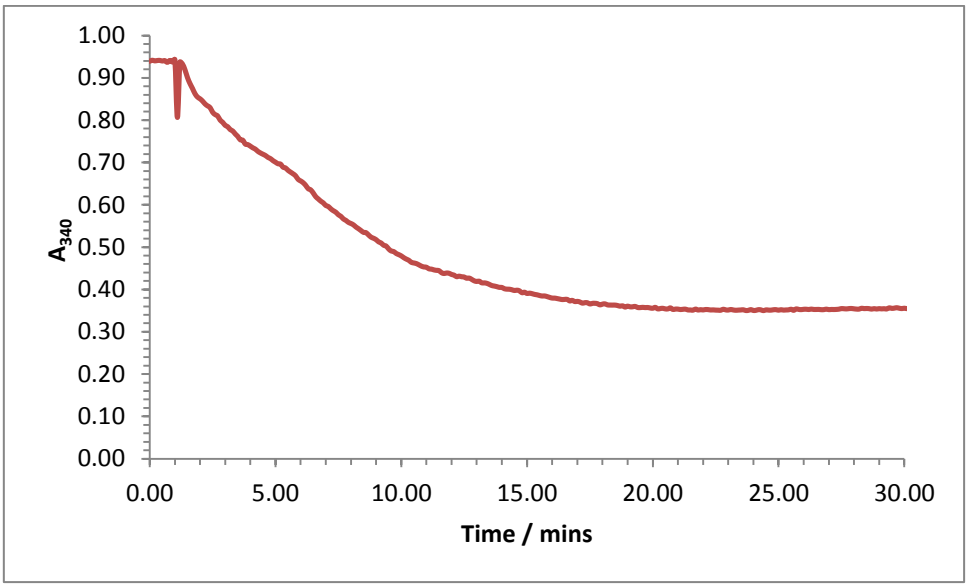

Figure 6.6 - Plot demonstrating the diminishing absorbance over time at a wavelength of 340 nm when one unit of the enzyme nitroreductase was added to the cuvette containing 0.2 mM NADPH and 100 µM TNT under analysis in the UV visible spectrometer

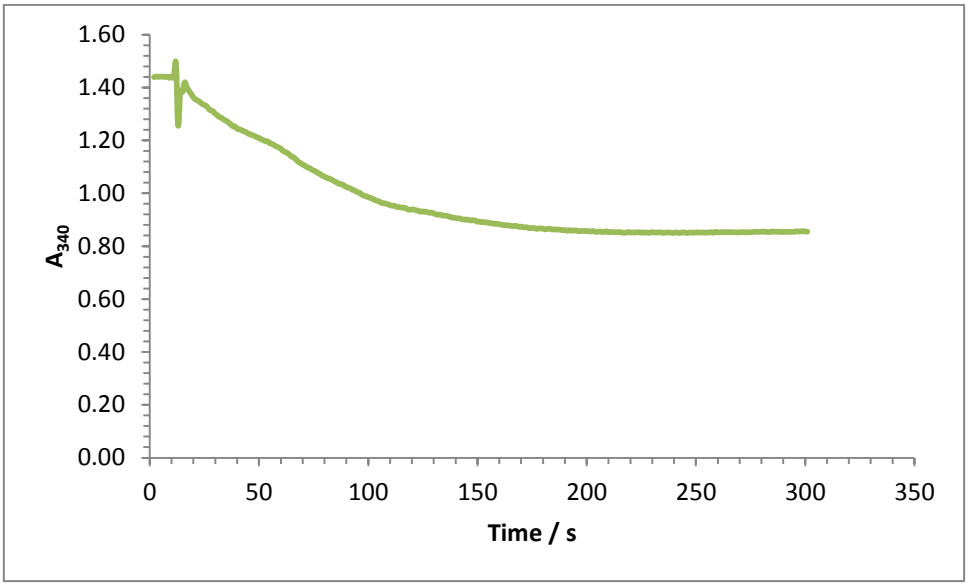

Figure 6.7 - Plot demonstrating the diminishing absorbance over time at a wavelength of 340 nm when one unit of the enzyme nitroreductase was added to the cuvette containing 0.3 mM NADPH and 100 µM TNT under analysis in the UV visible spectrometer

The percentage drop in absorbance from the baseline position at the initiation of the enzymatic process to the stage at which the reaction has completed and a stable baseline has been reached once more was found to be 64, 63 and 65 % for 0.1, 0.2 and 0.3 mM, respectively.

The use of a minimal amount of substrate for explosive detection was highlighted as one of the routes by which a research objective associated with this project will be satisfied; this objective is the production of a low-cost sensor device. As such, despite the greater absorbance presented with increasing concentrations of NADPH, initial electrochemical studies will be performed with the minimal amount of NADPH assessed that enables a functioning enzyme system (0.1 mM).

6.2.2. The effect of pH on the enzyme system

The temperature and pH conditions of the enzyme can have dramatic effect on the resulting activity of that enzyme. All experimental work within this project will be carried out at room temperature and pressure – therefore the UV spectrometry investigations in section 6.2.1 and subsequent analyses of this work have taken this aspect into account. The pH of the solution in which not only the enzyme but also the cofactor is present will affect the activity of both species. The stability of NADPH has been demonstrated previously to be significantly affected by temperature and pH changes (Wu et al., 1986). The activity of the NADPH decreases progressively as the solution within which it is being analysed becomes more acidic; this affect is also observed at an extreme alkaline pH.

The electrodeposition of aniline monomers into a conductive polyaniline film on the surface of a screen-printed carbon sensor can be accomplished at various pH levels, however, the more conductive forms of polyaniline are electrodeposited at a low pH. Polyaniline can be found in one of three states: emeraldine, leucoemeraldine and pernigraniline. To achieve the most conductive form of the polymer during electrodeposition a low pH of the solution need to be maintained as acidic conditions are required for the formation of the most highly conductive form of PANI; this environment does not naturally lend itself to the immobilisation of biological entities, such as enzymes, as many enzymes simply cannot survive in these acidic conditions.

Previous work into the immobilisation of enzymes into the conducting PANI matrix on a screen-printed sensor completed within this group used a pH 4.0 phthalate buffer as the solution into which the aniline monomer solution was prepared which enabled some retention of the conducting properties of PANI whilst preserving the activity of the enzyme immobilised (Barton et al., 2004; Barton et al., 2004; Myler et al., 1997; Pritchard et al., 2004). The enzyme in these instances was glucose oxidase – well known for its stability under a variety of conditions and able to function in the pH range of 2-8 (Wilson and Turner, 1992).

As it would be advantageous in this context to have an enzyme capable of withstanding short periods of time at a pH lower than neutral pH, a study was undertaken using the UV visible spectrometer assessing the diminishing absorbance signal over time with the inclusion of the enzyme into a sample cuvette containing the cofactor and 100 µM TNT at various pH levels. Using a phosphate buffer solution, solutions of NADPH were made up at pH 1.15, 2, 3, 6.2 and 7. The NADPH solution within a phosphate buffer at various pH levels was produced directly before use to limit the time at which it was held at this pH. A time period of 5 minutes was chosen as the maximum reaction time as this is the approximate period necessary for the electrodeposition of polyaniline. The resulting absorbance drop plots can be seen in Figure 6.8.

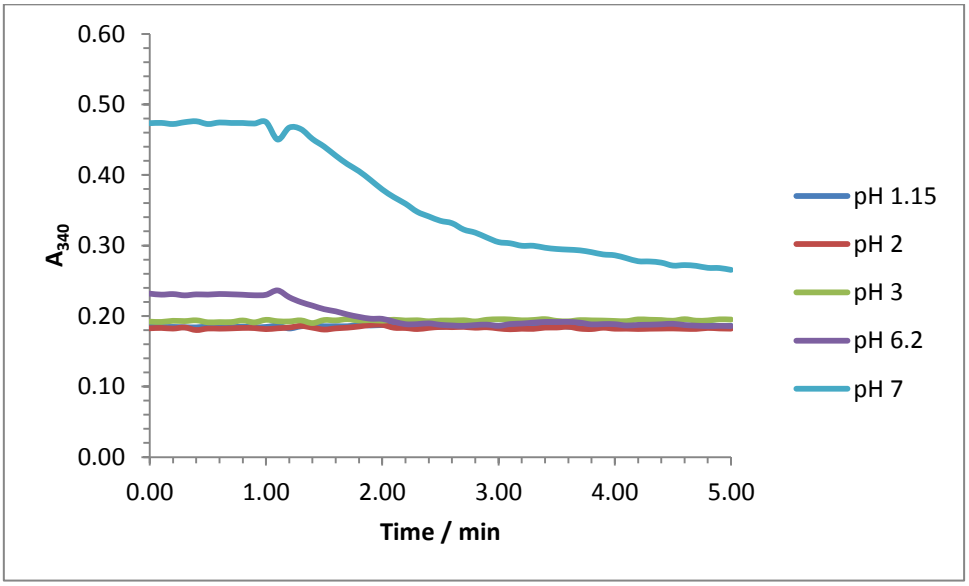

Figure 6.8 - Plot demonstrating the diminishing absorbance over time at a wavelength of 340 nm when one unit of the enzyme nitroreductase was added to the sample cuvette containing 0.1 mM NADPH and 100 µM TNT at various pH levels under analysis in the UV visible spectrometer

The absorbance drop at pH 7.0 can be seen to occur in much the same manner as presented above, at the 5 minute point it had not reached a baseline level but the reaction had begun to slow. The NADPH solution produced at pH 6.2 did produce a reaction with the addition of the enzyme into the cuvette containing the nitro species and the NADPH, however, this reaction is markedly diminished when compared to that gained at the more neutral pH. At the more acidic pH levels, there was no observable

reaction, as would be witnessed by a change in absorbance, when the enzyme was introduced into the system. These results confirm that for the enzyme to be immobilised on the surface of a screen-printed sensor, in this instance the optimal pH is pH 7.0. Whilst there is some activity retained at pH 6.2, it is unlikely that the enzymes immobilised in a PANI matrix at this pH would be effective as an enzyme modified biosensing device.

It is also interesting to note the decline in the initial absorbance as demonstrated by the initial baseline level for each pH. It is probable that this can be related to the effect of the pH on the NADPH. As mentioned previously, the stability of the NADPH is significantly affected by pH and so this diminished absorbance signal is an observable effect of this instability (Wu et al., 1986). This factor supports the conclusion that for the optimum retention of enzyme activity during immobilisation within a PANI matrix, the aniline solution would need to be at a neutral pH of 7.

6.3. Conclusions

The reductive pathway for the degradation of nitro-aromatic compounds with a nitroreductase enzyme and NADPH as a cofactor was discussed and the characterisation of this process was demonstrated using UV visible spectroscopy. An absorbance peak was apparent at a wavelength of 340 nm when various concentrations of NADPH were investigated. The magnitude of the peak at this wavelength was found to increase in a near linear fashion with increasing concentrations of the cofactor.

A time scan was then performed at each of the NADPH concentrations with the addition of one unit of the enzyme NfsA nitroreductase from *E. Coli* purchased from Sigma-Aldrich. The addition of the enzyme took place after the system had been allowed to reach a settled baseline (approximately one minute) and the resulting drop in absorbance can be attributed to the reduction of the enzyme by the cofactor, therefore it is the reduced species of the cofactor that is detected at this wavelength. The reaction was found to take approximately 20 minutes before the system reached a baseline once more. These analyses demonstrated that the enzyme system operates well and that a 0.1 mM concentration of NADPH might be a suitable starting point of studies into the electrochemical detection of nitro-compounds with the addition of the enzyme and cofactor.

A subsequent examination was undertaken to assess the effect of pH on both the enzyme and the cofactor. This aspect is important for the electrodeposition of a conducting polymer, polyaniline, onto a screen-printed sensor to immobilise the enzyme and cofactor near to the surface. When the NADPH was made up into various pH levels there was a significant effect on the initial absorbance in those solutions more acidic than the pH 7.0 solution. This can be attributed to the effect that pH modification has on the NADPH. The inclusion of the enzyme into the cuvette should have initiated a measurable response; this was apparent with the pH 7.0 and, to some extent, pH 6.2 solutions. At more acidic pH levels, however, there was no observable

change when the enzyme was introduced into the system. This had a consequence in the immobilisation of polyaniline in later stages of this project.

7. The *E. Coli* nitroreductase enzyme and the comparable electrochemical reduction of nitro compounds

7.1. Introduction

The use of biologically modified electrochemical sensors to improve the selectivity and sensitivity of sensing devices has been applied to a variety of research areas, for example: sensors utilising glucose oxidase for monitoring the blood-glucose level in insulin deficient diabetes patients (Wang, 2008; Jaffari and Turner, 1995)) detection of organophosphate pesticides (Collyer et al., 2010; Somerset et al., 2007; Wu et al., 2011) and organophosphorus nerve gases (Pohanka et al., 2009; Du et al., 2009; Arduini et al., 2007) and for the detection of pathogens in food (Liao et al., 2007; Mathew and Alocilja, 2005; Pividori et al., 2006) to name but a few examples in this vast field of research.

The biological entity used in biosensing devices can be based on a variety of approaches, such as the utilisation of one or more enzymes, affinity ligand-based sensing using antibodies or the use of nucleic acids such as DNA.

The approach that this work will follow will be the utilisation of the enzyme nitroreductase and the relevant cofactor NADPH to attempt to improve the response gained when interrogating nitroaromatic compounds electrochemically both in the resulting current output and in the selectivity of the completed system. This will help to improve the prospects of producing a viable nitro-explosive detector.

Nicotinamide adenine dinucleotide phosphate, or NADPH, was discovered by Warburg and Christian in 1931 as a coenzyme of glucose-6-phosphate dehydrogenase. NADPH differs from NADH in that it possesses an extra phosphate group and is used as a cofactor that acts as an electron donor in the reduction of various enzymatic reactions (Dixon, 1979).

The activity of the enzyme nitroreductase is based on its interaction with the cofactor NADPH. The oxidised form of the enzyme is reduced by the cofactor and it is this

reduced form that interacts with the nitro constituents on the TNT or DNT molecules (Figure 6.1).

As the nitro substituent is reduced by the enzyme, the nitroreductase reverts back to the original oxidative state and the process may continue in this manner.

It may be observed that this reduction of the nitro moieties is equivalent to the electrochemical reduction of nitro compounds discussed earlier (chapter 5). Here too, the nitro substituents are reduced first into their hydroxylamine derivative before the subsequent reversible reduction into amine groups.

7.2. Electrochemical characterisation of a nitro compound with the screen-printed sensor and enzyme system

The electrochemical interrogation of both TNT and DNT were performed with a planar screen-printed carbon electrode system as described in chapter 5 in which a current output could be related to the reduction and partial re-oxidation of the nitro groups present. The mechanism for this has been discussed previously (chapter 5). The same screen-printed carbon sensor will be used for these electrochemical interrogations in a matrix containing the enzyme and the cofactor.

The inclusion of an enzyme system into the sample matrix was performed with the intention to assess whether this would provide an element of selectivity to the electrochemical system and to investigate whether any improvements in signal occurred.

Control interrogations of pure phosphate buffer solution, the nitroreductase in the phosphate buffer, NADPH in a phosphate buffer and both NTR and NADPH in a phosphate buffer solution were performed first to assess the electrochemical profile for these solutions before subsequent examinations in the presence of TNT (Figure 7.1).

A 0.1 mM NADPH solution (Zenno et al., 1996) containing 200 µM of TNT, a 20 unit addition of the enzyme nitroreductase (known from this point as NTR) within a phosphate buffer as the supporting electrolyte was interrogated electrochemically and the resulting voltammogram can be seen below, Figure 7.2.

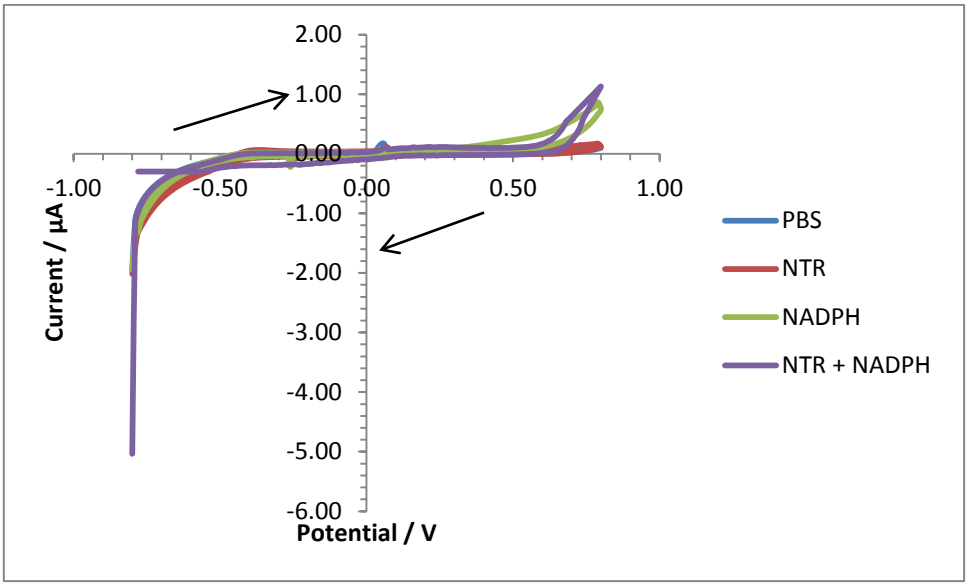

Figure 7.1 - Cyclic voltammograms of the control solutions interrogated at a scan rate of 20 mVs^{-1} vs. Ag/AgCl

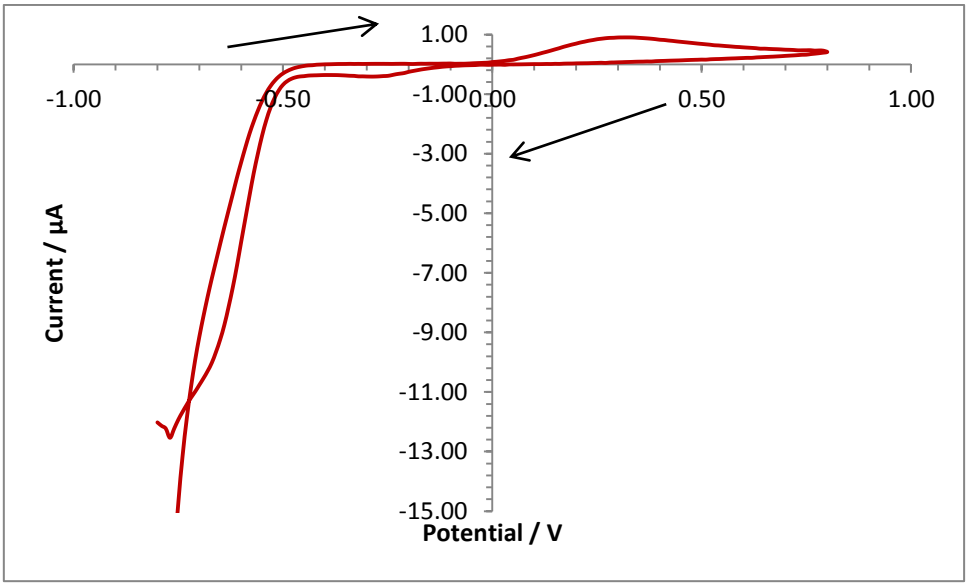

Figure 7.2 - Cyclic voltammogram of a 200 µM TNT, 0.1 mM NADPH and 20 unit NTR solution within a phosphate buffer as the supporting electrolyte performed with a screen-printed carbon sensor (at a 20 mVs^{-1} scan rate vs. Ag/AgCl)

The peak potentials of the interrogated TNT solution containing both the enzyme and cofactor are located in a similar position to that gained when TNT is electrochemically interrogated by a plain screen-printed electrode system (see Table 7.1).

	E_{ia}	i_{pa}	E_{ic}	i_{pc}	E_{ic}	i_{pc}
SPCE	*+0.30*	0.9	*-0.30*	0.41	*-0.72*	11.20
SPCE+NTR	*+0.30*	1.01	*-0.30*	0.63	*-0.72*	11.57

Table 7.1 - Peak position (Ei) in volts and peak height (ip) in µA for both TNT in a phosphate buffer solution and for TNT in a solution containing the enzyme and cofactor (after 10 minute deoxygenation at 20 mVs^{-1} scan rate vs. Ag/AgCl)

As such, it may be observed that the voltammogram obtained from a solution containing the enzyme and cofactor is almost identical to that attained without the enzyme and cofactor present (see Figure 7.3, Figure 7.4 and Figure 7.5).

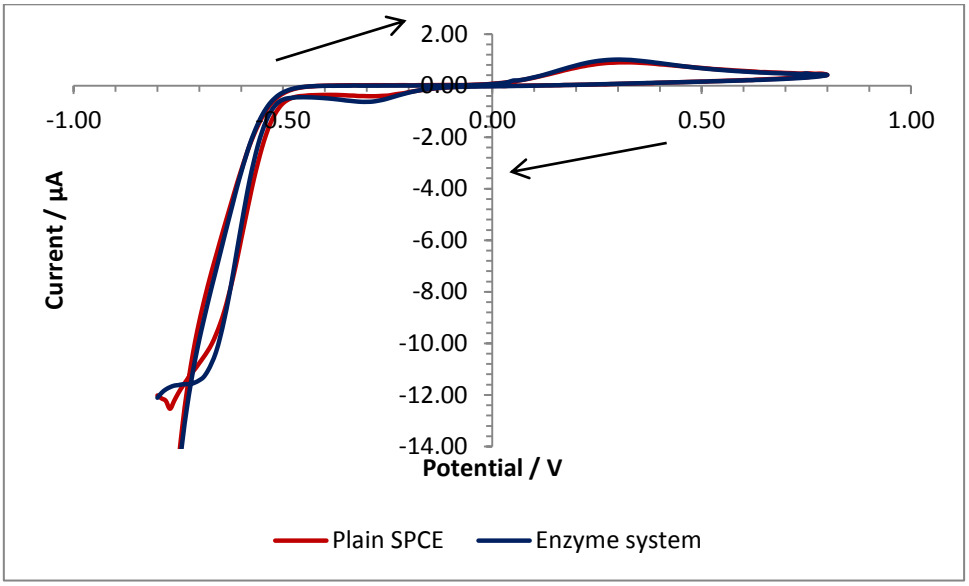

Figure 7.3 - Cyclic voltammograms of 200 µM solutions of TNT either with or without the enzyme system (scan rate of 20 mVs^{-1} vs. Ag/AgCl)

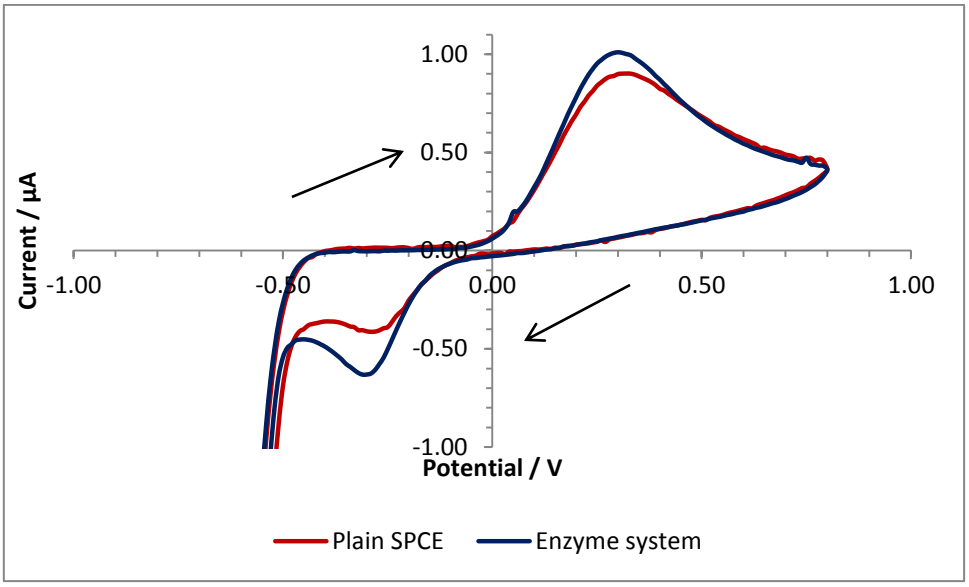

Figure 7.4 - Cyclic voltammograms of 200 µM solutions of TNT either with or without the enzyme system (scan rate of 20 mVs^{-1} vs. Ag/AgCl)

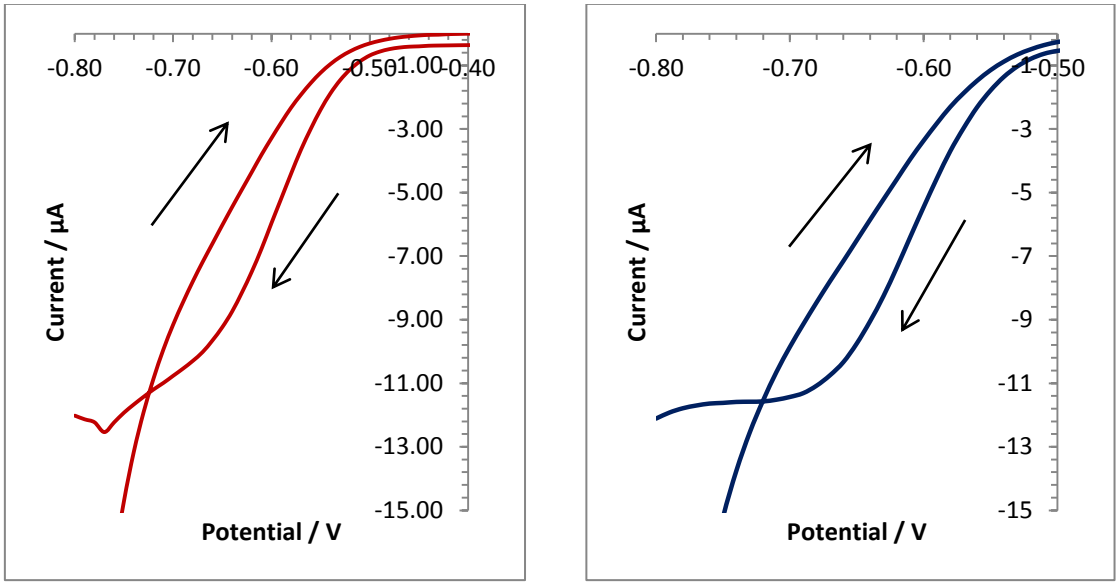

Figure 7.5 - Cyclic voltammograms of 200 µM solutions of TNT either with (red line) or without (blue line) the enzyme system (scan rate of 20 mVs^{-1} vs. Ag/AgCl)

Once more, the breakdown of TNT can be attributed to the same mechanism as described in chapter 5 and in the introduction to this chapter. Briefly, the nitro groups are first reduced into a hydroxylamine (peak R1) before being further reversibly reduced to an amine (R2 and O1).

7.3. The effect of concentration increase on the current response

Following the results gained for increasing nitroaromatics in Chapter 5, it might be the case that increasing the concentrations of TNT would increase the resulting current responses. In Chapter 5, this outcome was obtained, with most of the calibration plots demonstrating a near linear relationship with an incremental increase in available TNT or DNT. The same process was followed in this instance to demonstrate any linearity achieved with the SPCE in a solution containing the enzyme and co factor.

A set of voltammograms with increasing concentrations of TNT and including the enzyme and cofactor are seen below in Figure 7.6.

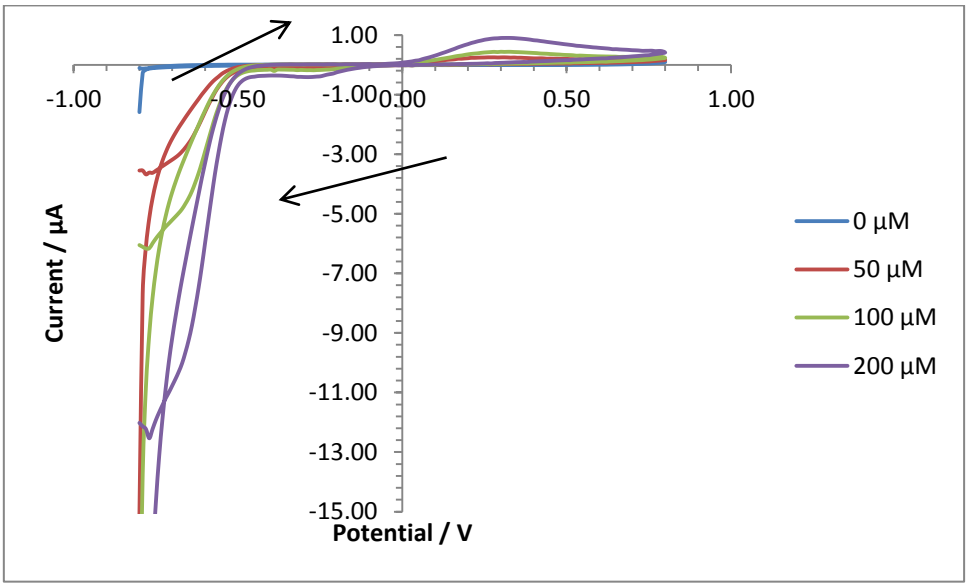

Figure 7.6 - Cyclic voltammograms of increasing concentrations of TNT with 20 units NTR and 0.1 mM NADPH in a supporting phosphate buffer (at scan rate 20 mVs^{-1} vs. Ag/AgCl)

The increasing concentrations of TNT provide an increase in the peak current as seen previously (Chapter 5). This again occurs in a near linear fashion – this is especially the case when the reductive peaks known previously as R1 and R2 are analysed. The current response at the main reductive peak, R1, at a peak potential of -0.72 V (vs. Ag/AgCl) is shown below in Figure 7.7.

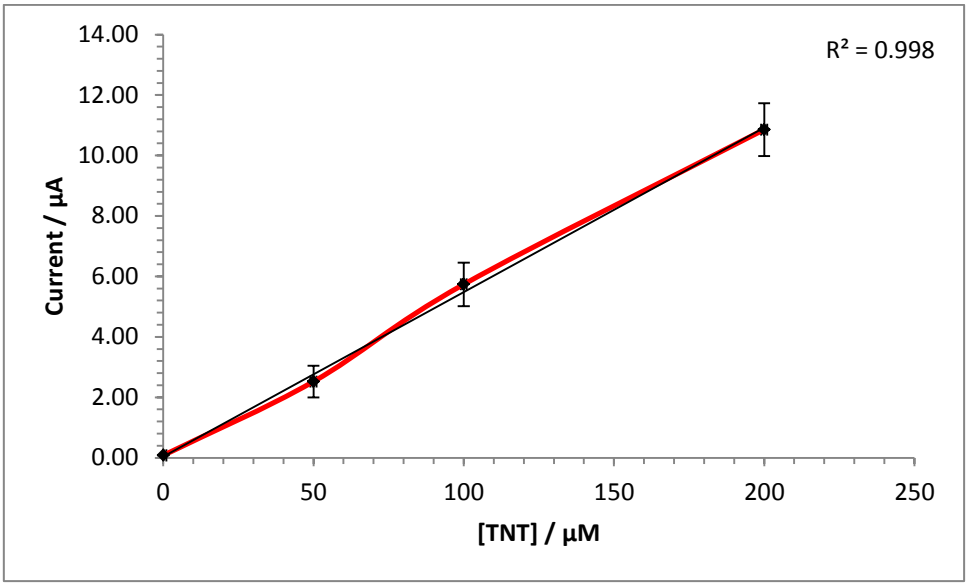

Figure 7.7 - Calibration plot of increasing TNT concentrations with 20 units NTR and 0.1 mM NADPH (taken from peak position -0.72 V vs. Ag/AgCl at a scan rate of 20 mVs^{-1})

As described earlier the R1 peak represents the reduction of the nitro groups on the aromatic ring to their hydroxylamine form, with this reduction being present both in a system without the enzymatic species and one including an enzyme.

It was demonstrated in chapter 6 that the enzyme and cofactor are capable of reducing the nitroaromatic molecules without the necessity for an electrochemical interrogation. As such, the task of separating the reductive activity of the enzyme from that of the simple electrochemical reduction of TNT may form a challenge. It may be that case that an assumption be made that any additional electroactivity gained when using the enzyme system be attributed to the inclusion of the enzyme/cofactor.

There is, however, a greater amount of error due to the spread of data between one run and another in the system containing the enzyme and cofactor. This may simply be due to the fact that there is more scope for variability in the system including the enzyme due to, for example, slight differences between batches of the enzyme and even batches of the cofactor. These are factors that would not affect the simple electrochemical reduction of TNT as they were not present.

The second reductive peak, R2, shows more variability than R1 but still has an R^2 value above 0.9. A calibration plot for R2 can be seen below in Figure 7.8.

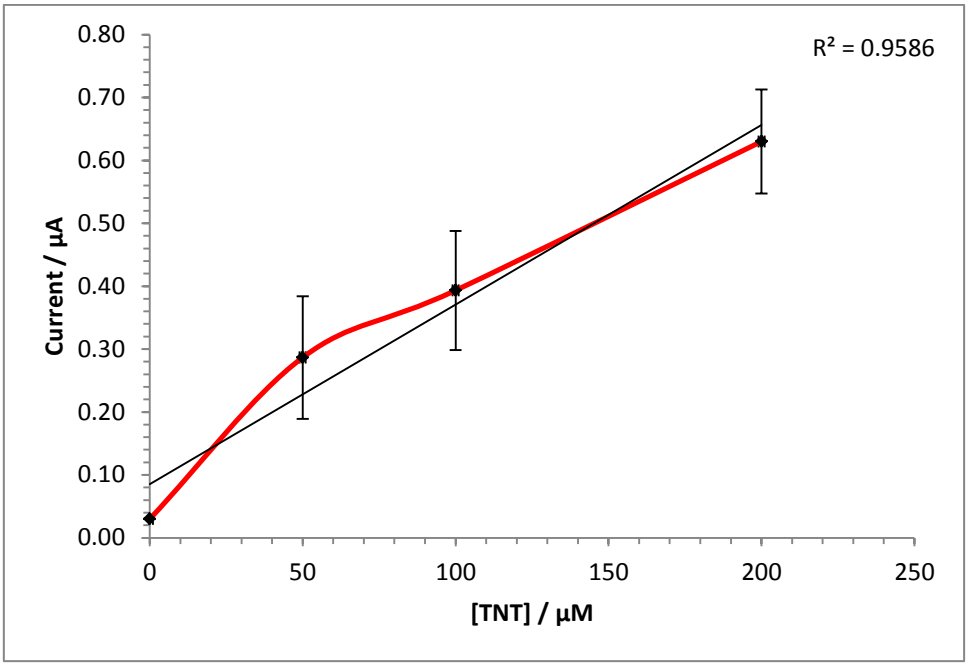

Figure 7.8 - Calibration plot of increasing TNT concentrations with 20 units NTR and 0.1 mM NADPH (taken from peak position -0.3 V vs. Ag/AgCl at a scan rate of 20 mVs^{-1})

The oxidative peak, O1, that relates to the re-oxidation of some of the amine groups back to their hydroxylamine moieties (Honeychurch et al., 2003) can also be seen to be significantly larger than the O1 peak without the enzyme present. The resulting calibration plot (see Figure 7.9) forms what seems similar to a traditional enzyme progress curve; where the initial response is fairly linear before, due to the depletion of the substrate, the curve tends to a plateau before finally reaching this plateau (this final stage is not observable in this instance).

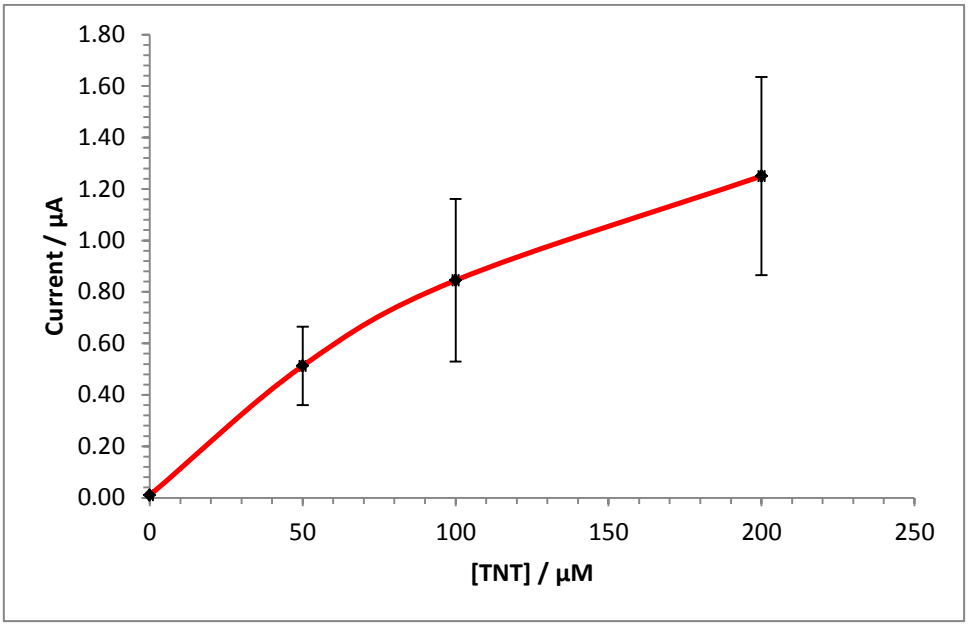

Figure 7.9 - Calibration plot of increasing TNT concentrations with 20 units NTR and 0.1 mM NADPH (taken from peak position +0.30 V vs. Ag/AgCl at a scan rate of 20 mVs^{-1})

7.4. Detection limit of the screen-printed sensor with the enzyme system for nitro compounds

The theoretical baseline for the system was calculated in the same manner as described in section 5.6. Briefly, a phosphate buffer solution containing the enzyme and cofactor was interrogated electrochemically using cyclic voltammetry between -0.8 and +0.8 V (vs. Ag/AgCl) and ten replicate measurements were obtained. The set of baseline currents from these interrogations were then used to calculate the theoretical limit of detection (three times the standard deviation where n=10). The limits of detection are provided for the three peak positions associated with the electrochemical breakdown of TNT, see Table 7.2.

	TNT peak positions		
Peak position / V	+0.3	-0.3	-0.72
Detection limit / µA	0.10	0.06	0.16

Table 7.2 - Theoretical detection limits for TNT as calculated from three times the standard deviation of the mean current of a solution containing NTR and NADPH but no TNT (n=10)

Calibration plots were produced for TNT at lower concentrations for the peaks referred to previously as R1, R2 and O1. R1 represents the main reductive peak at -0.72 V and the calibration plot relating to this reductive peak can be seen in Figure 7.10.

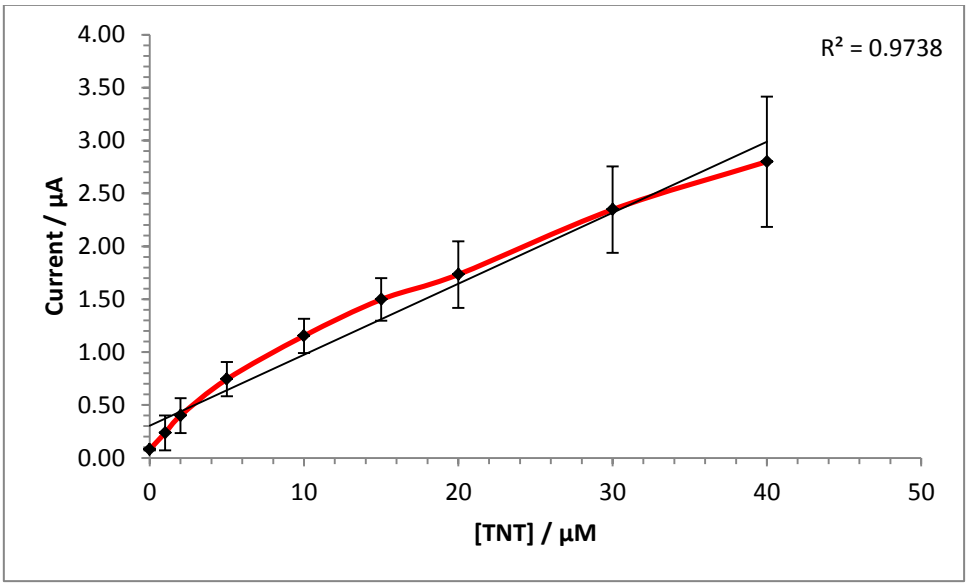

Figure 7.10 - Calibration plot representing the lower detection limits of TNT taken from the peak -0.72 V (scan rate 20 mVs^{-1} vs. Ag/AgCl)

The error bars present in all calibration plots found in this section represent one standard deviation in each direction as calculated from the average of the interrogations (n=3). Using the theoretical baseline calculated earlier (see Table 7.2) the limit of detection for this system at each of the peaks was assessed by evaluating the concentration of TNT at this baseline current using the calibration plot. At peak R1, the baseline was calculated to be 0.16 µA (see Table 7.2); using this value the limit of detection was shown to be 0.5 µM. This is similar to that gained with the plain carbon sensor without the enzyme and cofactor present, this value was 0.4 µM. It was postulated in Section 5.6 that this peak was perhaps the most suitable for further electrochemical study due to the low detection limits and linearity of the data; it may be the case that this supposition holds with the inclusion of the enzyme system.

The calibration plot of lower concentrations at the peak R2 is seen below, Figure 7.11 where R2 represents the reduction peak at -0.3 V.

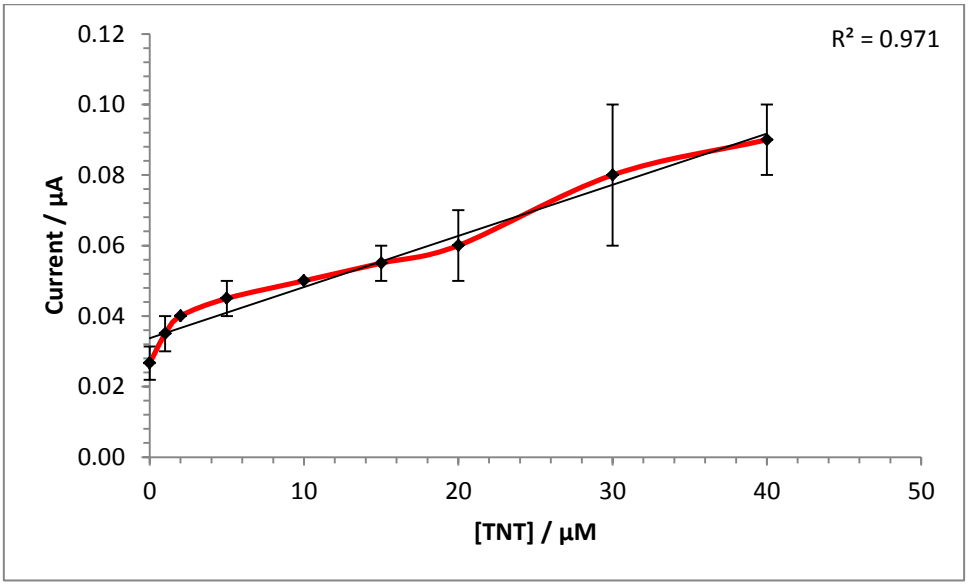

Figure 7.11 - Calibration plot representing the lower detection limits of TNT taken from the peak -0.30 V (scan rate 20 mVs^{-1} vs. Ag/AgCl)

The baseline at this peak potential (from Table 7.2) is 0.06 µA. The limit of detection at peak R2, if using this baseline, would be 20 µM; this is in contrast to the detection limit of 2.6 µM gained when using a carbon screen-printed electrode without the presence of the enzyme and cofactor. It would seem to be that case that this reduction peak

would not present as a suitable peak for further analyses – and again that the main reductive peak R1 provides a more suitable peak in this sense.

The calibration plot of lower TNT concentrations measured at the oxidative peak O1 is seen in Figure 7.12.

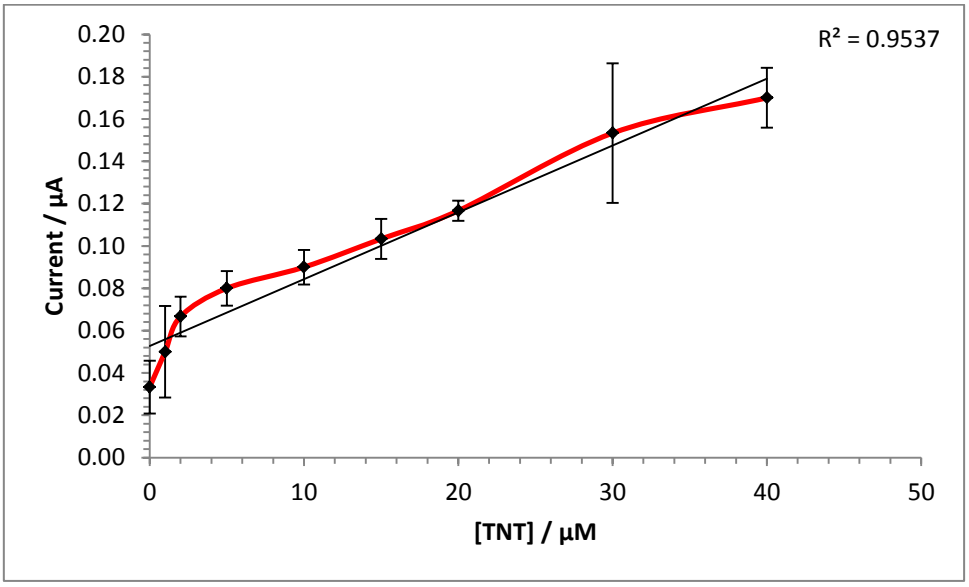

Figure 7.12 - Calibration plot representing the lower detection limits of TNT taken from the peak +0.30 V (scan rate 20 mVs-1 vs. Ag/AgCl)

Using the same method, the limit of detection for TNT at the oxidative peak can be assessed. The baseline (from Table 7.2) was 10 µA - this leads to a minimum detection level of 15 µM. When compared to the limit of detection found in the same manner but when a solution of TNT was interrogated without the presence of the enzyme and cofactor, a value of 5 µM, this addition of the enzyme system has not enabled a decrease in the lower limits of detection.

The detection limits with a screen-printed sensor both with and without the enzyme system present can be seen in Table 7.3 where despite the increase in current response at higher concentrations, the limits of detection are found to be lower without the inclusion of the enzyme in the sample matrix.

	Detection limit in μM		
	R1	**R2**	**O1**
SPCE	0.4	2.6	5.0
SPCE/NTR+NADPH	0.5	20.0	15.0

Table 7.3 - Limits of detection for TNT interrogated with a SPCE and a SPCE with the enzyme and cofactor using a calculated baseline and low concentration calibration profiles

From these analyses it is possible to highlight the peak R1 as the best peak with which to conduct analyses in this matrix – including the enzyme and cofactor in the solution. This was found to be the case where TNT was interrogated in a matrix of just the supporting phosphate electrolyte solution too.

In the case of the TNT interrogations without the enzyme system, the level of error was slightly less, as demonstrated by the size of the error bars (displayed as one standard deviation each side of the data point from the measured signal output). As such, although the peak R1 can still be highlighted as the optimal choice for analyses, it seems the system without the enzyme and cofactor provides more reproducible results at the lower end of the concentration scale, possibly due to the variability inherent in different batches of the enzyme and cofactor.

7.5. Conclusions

It has been established (section 7.2) that the addition of the enzyme, nitroreductase, and the coenzyme, NADPH, into the solution matrix prior to electrochemical interrogations with a screen-printed carbon electrode has increased the resulting signal magnitude at both of the reductive peaks and the oxidative peak at higher concentrations of TNT. The improvement can be seen to mainly occur about the redox couple at +0.3 and -0.3 V but there is also a slight increase at the main reductive peak.

The effect of increasing the concentration of TNT was the same as the system without the enzyme and cofactor present, with the increasing magnitude of current response related to this increased concentration. A near linear calibration plot was gained for peak R1; whereas peak R2 displayed more variation in the results. The oxidative peak, O1, seemed to be beginning to demonstrate a characteristic enzyme progress curve, with a sharp linear response before approaching a plateau.

The baseline, devised from the interrogation of a solution containing the enzyme and cofactor but without any TNT present, presented a baseline that is similar to that gained of the phosphate buffer solution interrogated in chapter 5. This would illustrate that any response achieved is due to the electrochemical breakdown of TNT and not to any inference from the enzyme system.

The limit of detection for TNT was assessed at all three peaks and was observed to be 0.5 μM for the reductive peak R1 and 15 μM for the oxidative peak O1; the second reductive peak did not provide as low a detection limit, with the lowest concentration of TNT this system is able to detect at this peak being 20 μM. The value for R1 corresponds to the detection limits gained when no enzyme was present in the sample solution, in these analyses the detection limit was 0.4 μM for R1.

8. The electrochemistry of nitro compounds on a cobalt phthalocyanine-doped screen-printed carbon electrode

The contents of this chapter are being prepared for publication

8.1. Introduction

Phthalocyanines are macrocyclic compounds that are capable of forming coordination molecules when complexed with over 70 metal ions; displaying high thermal and chemical stability. They feature a central structure of 4 pyrrole units linked with methane or azamethine bridges to form a circular structure. Within this circular structure a central atom may coordinate with the nitrogen groups on the pyrrole units.

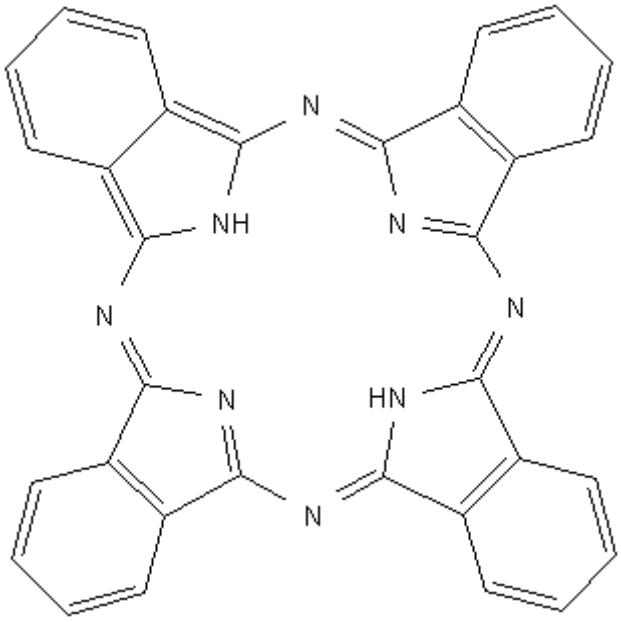

Figure 8.1 - Molecular diagram of an un-complexed phthalocyanine molecule

Metallophthalocyanine complexes have been used in many different ways. They are perhaps most well known in the capacity of industrial dyes due to the vivid blue-green colour and the intense absorption displayed at wavelengths of 650-700 nm (Contakes, 2000). They have been utilised more recently as the photo-conducting material in laser printers and as the photo-sensitisers in laser cancer therapy. More relevant to this study, metallocyanines, in particular cobalt phthalocyanine, have also found use as

electrocatalysts in many oxidative (see Equation 8.1and Equation 8.2) and reductive reactions

$$[CoPc] - e \rightleftarrows [CoPc]^{+}$$

Equation 8.1

$$[CoPc]^{+} + target \longrightarrow [CoPc] + oxidised\ target$$

Equation 8.2

These include, but are not limited to: the oxidation of nitrites (Caro et al., 2002), the oxidation of glucose with the enzyme glucose oxidase (Crouch et al., 2005), the reduction and oxidation of nitrous oxide (Nyokong and Vilakazi, 2003) and the oxidation of citric acid (Hart and Hartley, 1994).

The use of cobalt phthalocyanine at a modified electrode can act as an electrocatalyst which can enable the resulting oxidation to occur at considerably lower voltages (Hart and Hartley, 1994). This lowered working potential has the advantage of eliminating the appearance of some interfering reactions as the reactive range is narrowed within the resulting voltammograms (Pchelintsev and Millner, 2008) and can allow an increase in response and sensitivity (Shaidarova et al., 2003).

8.2. Characterisation of the CoPc-doped screen-printed electrode activity

An observed increase in the electrochemical activity gained when utilising a cobalt phthalocyanine-doped screen-printed electrode when compared to the response obtained with a plain carbon screen-printed electrode (i.e. undoped) is postulated to be due to the inherent mediating activity of the CoPc species. Cobalt phthalocyanine, CoPc, can act as an electrocatalyst when adsorbed onto carbon electrodes (Maree and Nyokong, 2000) enabling reactions such as oxygen reduction, carbon dioxide reduction and the oxidation of thiols to be catalysed by the presence of the metallophthalocyanine complex.

An examination of the surface topography of a cobalt phthalocyanine screen-printed carbon electrode revealed the presence of particles of the CoPc clearly within the electrode matrix. When comparing the surface to the plain carbon sensors (Figure 8.2b) there are clear differences in the CoPc sensor image, with areas of greater conductivity, as demonstrated by the greater luminescence around the edges of these particles, and the mostly featureless topography of the carbon surface, see Figure 8.2a.

a).

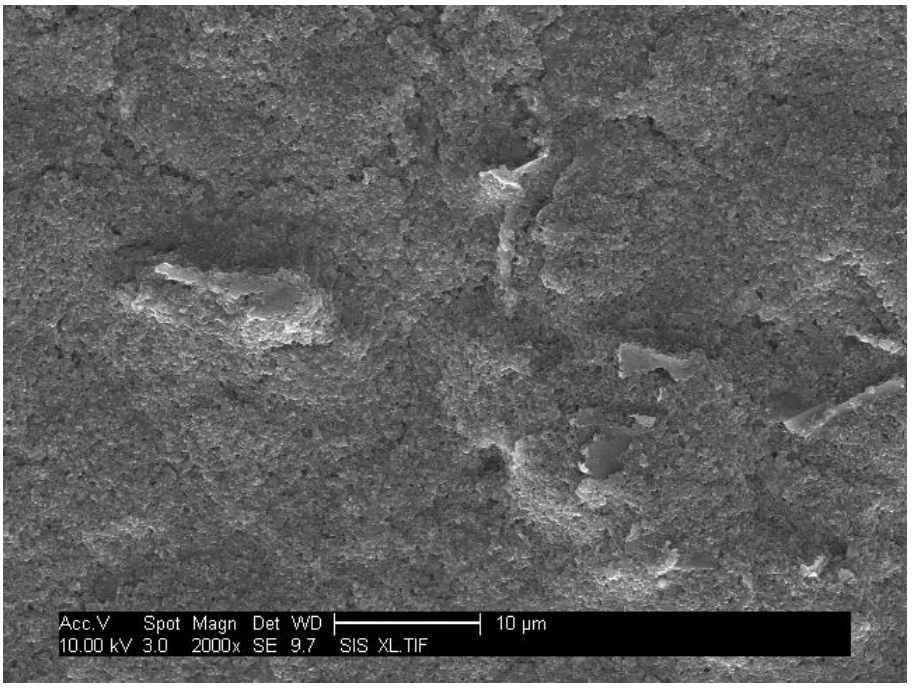

b).

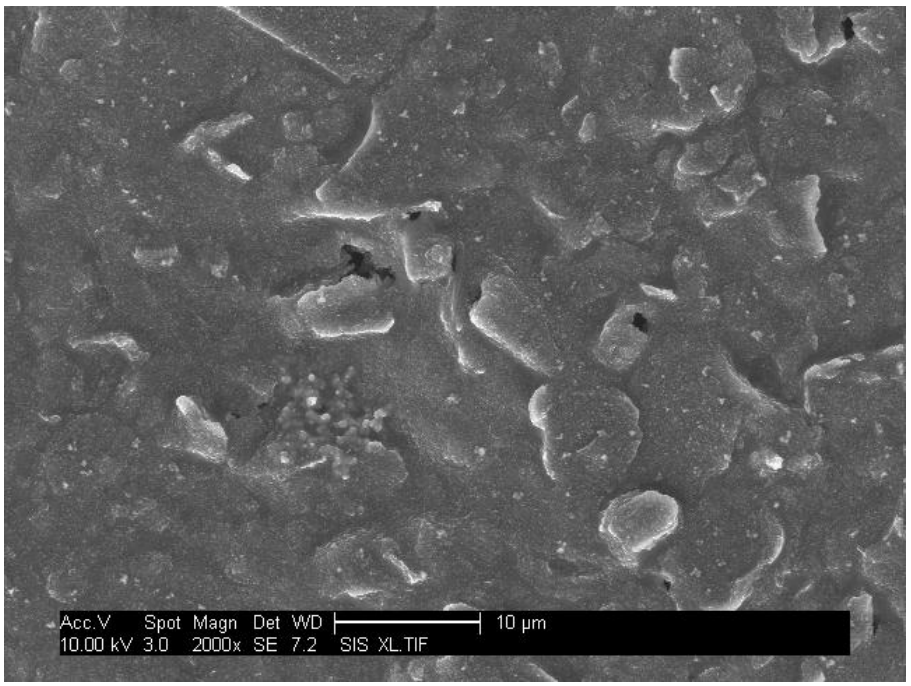

Figure 8.2 - An SFEG scanning electron micrograph of a). a bare carbon and b). a cobalt phthalocyanine-doped screen-printed electrode surface at 2000x magnification (after sputter coating with gold palladium)

To analyse the differences in the charge-transfer reactivities of a cobalt phthalocyanine sensor over that attained with a plain carbon screen-printed electrode, the system was

tested in a solution of 5 mM ferrocenemonocarboxylic acid as described in section 4.6.7 and the resulting voltammograms are observed below in Figure 8.3.

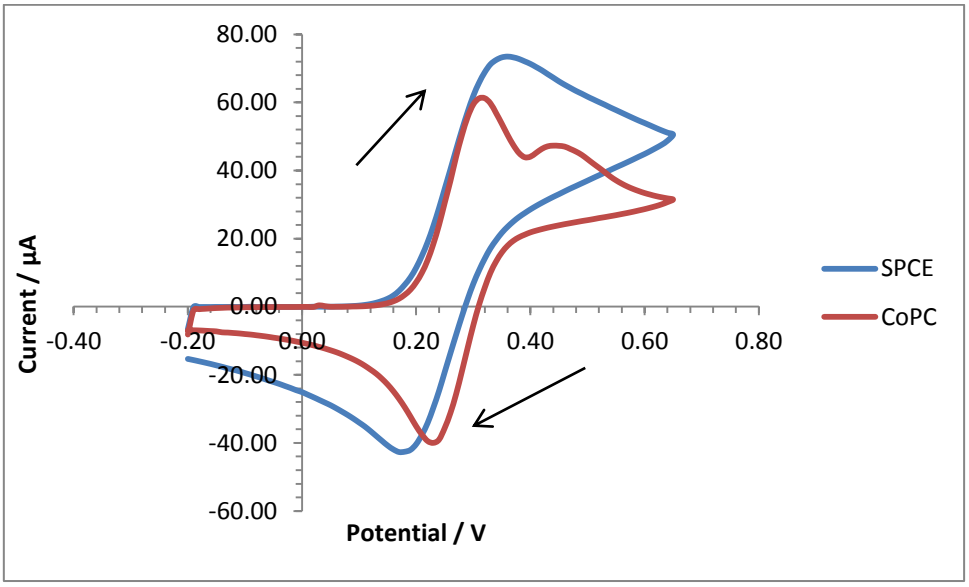

Figure 8.3 - A cyclic voltammogram of 5 mM ferrocenemonocarboxylic acid performed with a plain carbon (blue line) and a CoPc screen-printed sensor (red line) (in a pH 7.0 phosphate buffer at a scan rate of 20 mV s^{-1} vs. Ag/AgCl)

The most obvious difference between this CoPc-doped sensor voltammogram of ferrocenemonocarboxylic acid and that attained using a plain carbon screen-printed electrode is the double oxidative peak present. The peak separations (ΔE_p) and the differences in the anodic peak potential (E_{ip}) and current (i_{pa}) of a plain carbon and a CoPc screen-printed sensor can be seen in Table 8.1. The CoPc sensor produced two anodic peaks, hence the two peak potential and current values.

Peak separation		Anodic peak potential		Anodic peak current	
ΔE_p		E_{ia}		i_{pa}	
Plain Carbon	**CoPc**	**Plain Carbon**	**CoPc**	**Plain Carbon**	**CoPc**
150 mV	70 mV	360 mV	300 mV	73.46 µA	60.02 µA
			410 mV		53.97 µA

Table 8.1 - Table illustrating the peak separation, anodic peak potential and anodic peak current of ferrocenemonocarboxylic acid interrogated with a plain carbon and a CoPc-doped screen-printed carbon electrode

It can be observed that although there is not an improvement in the peak current response gained when compared to that obtained interrogating ferrocenemonocarboxylic acid with a plain carbon screen-printed electrode (in that instance the anodic peak current was actually greater at 73.46 μA) there is an improvement in the peak separation bringing this value of 70 mV closer to that expected when a Nernstian reaction has occurred where the peak separation is 59/*n* mV (Bard, 2001) whereas the peak separation for the plain carbon sensor was more than double this value at 150 mV.

The cathodic peak potential positions and current output from the plain carbon and CoPc sensors are also different; with the plain carbon sensor inducing the reductive reaction at a potential of 170 mV, current response of 42.68 μA, and the CoPc at 230 mV, with the current response at 39.98 μA (vs. Ag/AgCl). The reductive peak for the CoPc sensor occurs first on the reverse scan in the cathodic direction during the cyclic voltammetry interrogation. This may be due to the enhanced mediation effects due to the electroactivity of the cobalt phthalocyanine within the carbon ink.

The anodic/cathodic peak current ratio (I_a/I_c) was calculated to be 1.5 – although this is closer to the value of 1 that represents a reversible system than the anodic/cathodic peak ratio gained for the plain carbon SPE (1.8), this value is still representative of a quasi-reversible rather than reversible system.

The increase in electron transfer rate demonstrated by the reduced peak separation potential may indicate that this CoPc-doped screen-printed sensor can lend this characteristic to the improved electrochemical interrogation of nitroaromatic compounds. The mediating attributes of CoPc can facilitate the electron transfer between the active centres of an enzyme and a transducer (Shaidarova et al., 2003) and are known to decrease the working potential required in oxidative and reductive processes (Pchelintsev and Millner, 2008).

8.3. Trinitrotoluene interrogated with a CoPc-doped screen-printed sensor

The electrochemical interrogation of TNT with a plain carbon sensor platform yielded a current response due to the electroactivity of TNT itself. The mechanism by which this occurs, a four electron reduction of each nitro group to hydroxylamine followed by a two electron reduction from hydroxylamine to amine, has been described earlier in section 5.3. The motivation for utilising the cobalt phthalocyanine-doped sensors was that an improvement in current response and limits of quantification might be demonstrated in the presence of TNT and this would improve the applicability of this technique in the sphere of explosive detection.

A pH 7.0 phosphate buffer solution was used as a control and was interrogated as described previously (see section 4.6.1). A reductive peak was observed at around -0.47 V, this can be observed in Figure 8.4.

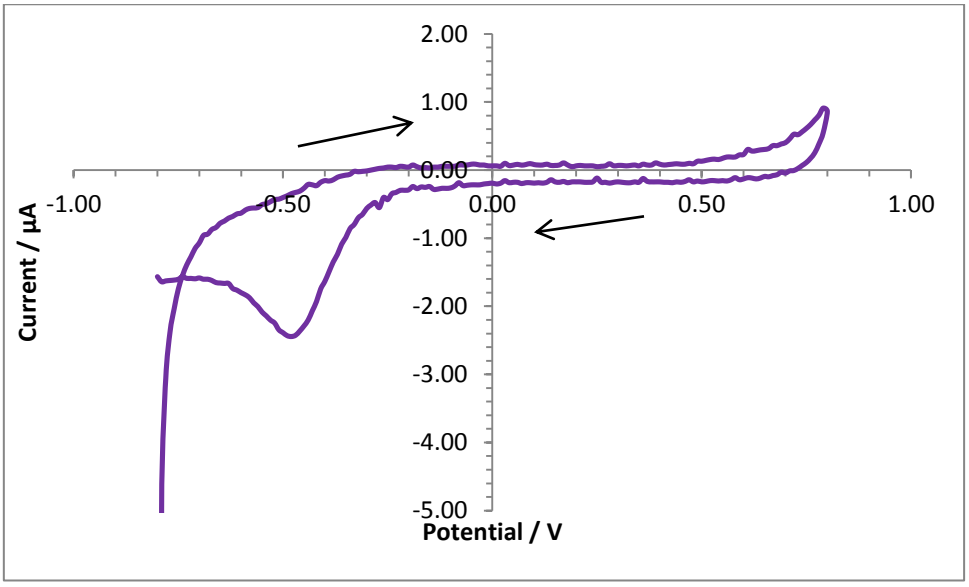

Figure 8.4 - Cyclic voltammogram of pH 7.0 phosphate buffer solution on a CoPc doped screen-printed carbon sensor (at a scan rate of 20 mVs^{-1} vs. Ag/AgCl without deoxygenation)

The interrogation of pH 7.0 phosphate buffer solution with plain carbon SPEs presented no such peak (see Figure 5.4) – it might be assumed, therefore, that this peak can be related to the mediator, cobalt phthalocyanine. It has been demonstrated in the literature that a reductive process occurring in the macrocyclic CoPc molecule

produced a reductive peak at -0.3V [ref: Hart and Hartley, 1994]. The reductive peak observed in the voltammogram obtained from the phosphate buffer solution is closer to -0.47 V rather than -0.3 V, however, the explanation for the existence of this peak may be attributed to the electrochemical reduction of cobalt.

$$Co^{2+} + e^{-} \rightarrow Co^{+}$$

Equation 8.3

A phosphate buffer solution with 200 µM TNT was interrogated using cyclic voltammetry and the CoPc-doped screen-printed electrodes, Figure 8.5.

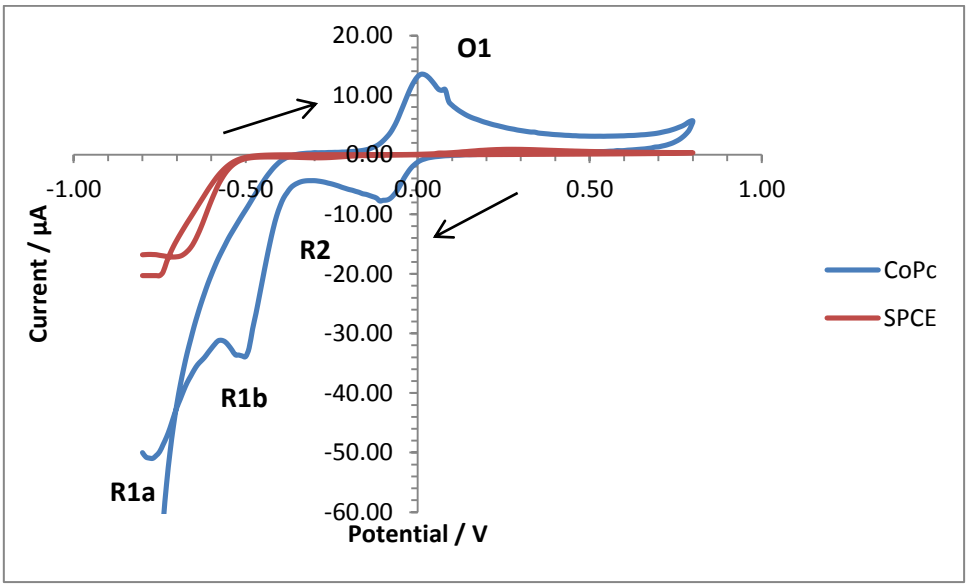

Figure 8.5 - Cyclic voltammogram of 200 µM TNT on a plain carbon (red line) and a CoPc-doped sensor platform (blue line) at a scan rate of 20 mVs^{-1} (vs. Ag/AgCl without deoxygenation) from peak R1a

The voltammogram obtained here (Figure 8.5) is similar to that obtained for a plain carbon screen-printed electrode, also presented here in red. There is a redox couple present about the 0 V potential position (at +0.01 and -0.11 V vs. Ag/AgCl) which can be related to those gained at +0.30 and -0.30 V, known as O1 and R2, when TNT is interrogated with a plain carbon SPE system, although this is not clear in this figure due to the difference in the magnitude of response it can be seen more clearly in Figure 5.6.

There are also significant reductive peaks present in the cathodic region at positions -0.5 and -0.77 V. This aspect differs from the voltammograms gained on plain carbon where there is only one reductive peak present in this region, R1 at -0.72

V. It is postulated that the mediating effect from the CoPc-doped sensor has not only significantly increased the current response, as seen in Figure 8.5, but has also enabled the splitting of the peaks within this reductive region to a form that better represents the electrochemical reduction of the nitro groups on the TNT molecule into hydroxylamine groups (Wang et al., 2009).

A comparison of peak positions and responses of plain carbon and CoPc-doped screen-printed electrodes are provided below, see Table 8.2.

Table 8.2a

SPCE	O1 E_{ia}	O1 i_{pa}	R2 E_{ic}	R2 i_{pc}	R1 E_{ic}	R1 i_{pc}
TNT	+0.3	0.89	-0.3	0.53	-0.72	17.16

Table 8.2b

CoPc	O1 E_{ia}	O1 i_{pa}	R2 E_{ic}	R2 i_{pc}	R1b E_{ic}	R1b i_{pc}	R1a E_{ic}	R1a i_{pc}
TNT	+0.01	13.50	-0.11	7.77	-0.5	33.79	-0.77	50.96

Table 8.2 - Table a). provides data from nitroaromatics interrogated with a SPCE and table b). provides comparison data of nitroaromatic compounds interrogated with a cobalt phthalocyanine-doped screen-printed electrode. Peak potential (E_i) is in volts and peak current (i_p) is in μA.

A further examination, increasing the concentration of TNT present in the phosphate buffer solution was performed to establish whether an increase in peak current is observed for increasing concentrations of the nitroaromatic TNT, see Figure 8.6.

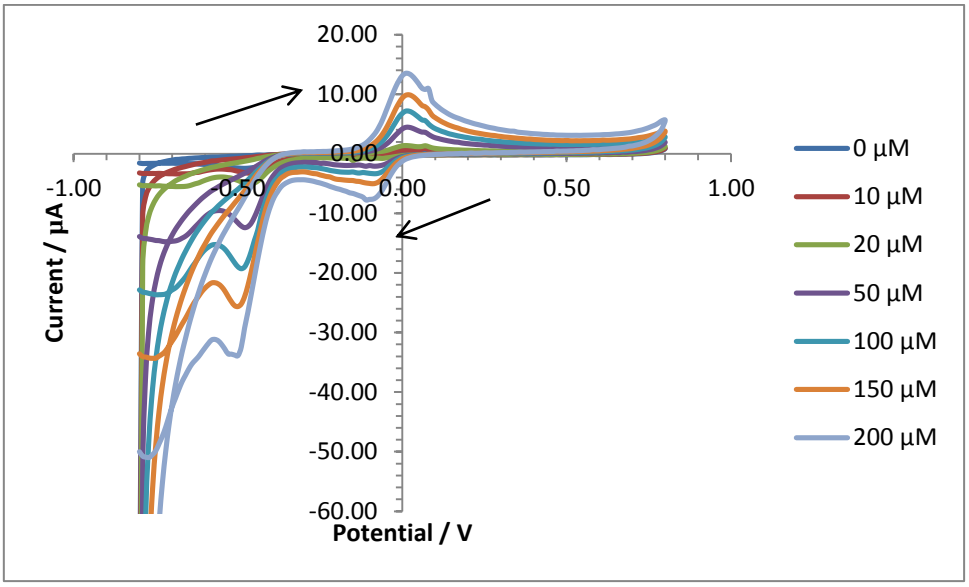

Figure 8.6 - Increasing concentration of TNT interrogated with a CoPc doped screen-printed electrode system (in a pH 7.0 phosphate buffer solution at a scan rate of 20 mVs^{-1} vs. Ag/AgCl without prior deoxygenation)

It can be observed that with increasing concentrations of TNT there is a corresponding increase in the current response when the solution is electrochemically interrogated with a CoPc-doped sensor. This can be observed in the calibration plot provided below taken from the reductive peak R1 at the potential position of -0.77 V for CoPc and -0.72 V for SPCE. The calibration data gained by the interrogation of TNT with a plain carbon screen-printed sensor is included for comparison (blue line) and the significant increase in the magnitude of response is apparent, see Figure 8.7.

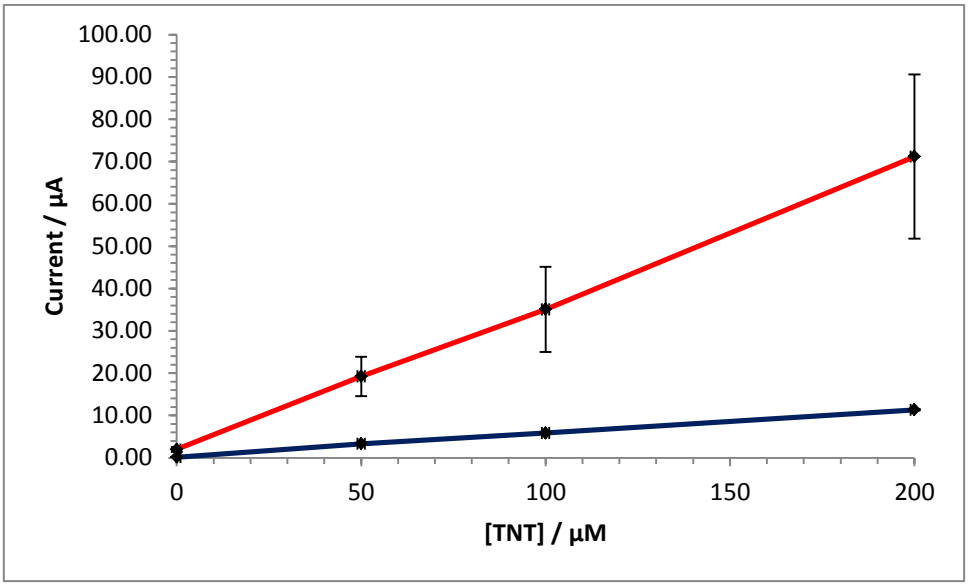

Figure 8.7 - Calibration plot for TNT interrogated with a CoPc sensor (red line) and a plain carbon sensor (blue line) after interrogation in a pH 7.0 phosphate buffer solution at a scan rate of 20 mVs^{-1} vs. Ag/AgCl taken from the reductive peak R1 (-0.77 for CoPc and -0.72 for plain carbon)

This calibration plot demonstrates the improved response when interrogating a solution containing TNT with the CoPc mediated sensor. This improvement should lend itself to improved lower limits of detection and can be seen to improve the peak clarity of the system.

8.4. The influence of dissolved oxygen on the electrochemical interrogations with a cobalt phthalocyanine sensor

The influence of dissolved oxygen on the electrochemical interrogation of nitro compounds using a plain screen-printed carbon sensor was examined previously. As mentioned in section 5.4 the removal of oxygen from the solution under investigation can be advisable in systems where the interrogative parameters are near to the region where electrochemical reduction of oxygen occurs. The mechanism by which oxygen is electrochemically reduced is discussed fully in section 5.4. The result of purging with argon the plain carbon SPE electrochemical system containing TNT was that the main reductive peak present at -0.72 V diminished; and the redox couple increased slightly with increasing deoxygenation periods. This is discussed fully in chapter 5.

To eliminate any oxygen influence on the electrochemistry of the reduction of TNT on the CoPc electrodes, the solution was again purged via a stream of argon for varying amounts of time in the same manner as described earlier (section 5.4). The study was conducted by increasing progressively the time the solution was purged and tested by running a CV of 100 µM TNT between -0.8 and +0.8 V (vs. Ag/AgCl) the results of which can be seen in Figure 8.8.

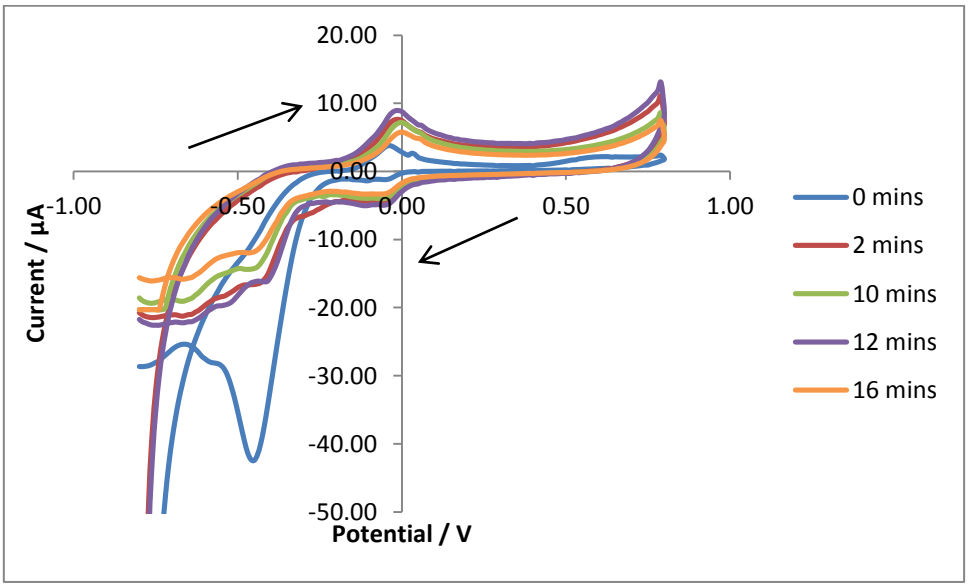

Figure 8.8 - Voltammograms demonstrating the influence of increasing deoxygenation periods on a 100 µM TNT solution in a phosphate buffer solution (at a scan rate of 20 mVs^{-1} vs. Ag/AgCl)

It can be observed that the oxidative and reductive peaks behave in the same manner as previously discussed – with the large reductive peak in the cathodic region, R1a, diminishing in size with each increasing deoxygenation period whilst the redox couple (O1 and R2) can be observed to increase with increasing deoxygenation periods.

The new reductive peak, R1b, at -0.5 V is observed to behave in the same manner as reductive peak R1a. The reasons for this were discussed fully in Chapter 5.4 but, briefly, may be associated with the electrochemical breakdown of the dissolved oxygen in the system which can occur at a similar potential; when this effect is removed, the peak remaining may be directly related to the electrochemical breakdown of TNT. The redox couple, as the increased response with increasing deoxygenation time is the same as that observed previously on plain carbon screen-printed electrodes, may see an increased response due to a competitive process whereby the oxygen dissolved in the system is acting as a competitive electron accepter, thus diminishing the opportunity for the nitroaromatic compound to be reduced. All interrogations with the CoPc sensors from this point onwards will be, unless otherwise stated, presented with a 10 minute deoxygenation period.

8.5. The effect of concentration increase on current response with CoPc sensors

Once more, the effect of increasing the concentration of TNT has been examined to establish whether the use of a cobalt phthalocyanine-doped carbon sensor in the place of a bare carbon screen-printed sensor has a detrimental effect on the linear responses gained previously (see section 5.5). When plain carbon screen-printed sensors were used to interrogate increasing concentrations of TNT the resulting calibration plots, taken from the three peaks present in the voltammograms, demonstrated good linearity and reproducibility through high R^2 values and the minimal error bars presented; for DNT the linearity was also good, with the lowest R^2 value at 0.997, however the error did increase somewhat.

Through the use of cobalt phthalocyanine-doped sensors, and the increased electroactivity associated with this experimental change, the magnitude of the current response has already been demonstrated to increase, see Figure 8.7. The linearity at each of the peaks, including the peak present at -0.5 V (vs. Ag/AgCl), is now examined as is the level of error associated with using this sensor in the electrochemical reduction of TNT.

The calibration plots for the two reductive peaks found in the cathodic region (R1a and R1b) can be observed in Figure 8.9 and Figure 8.10.

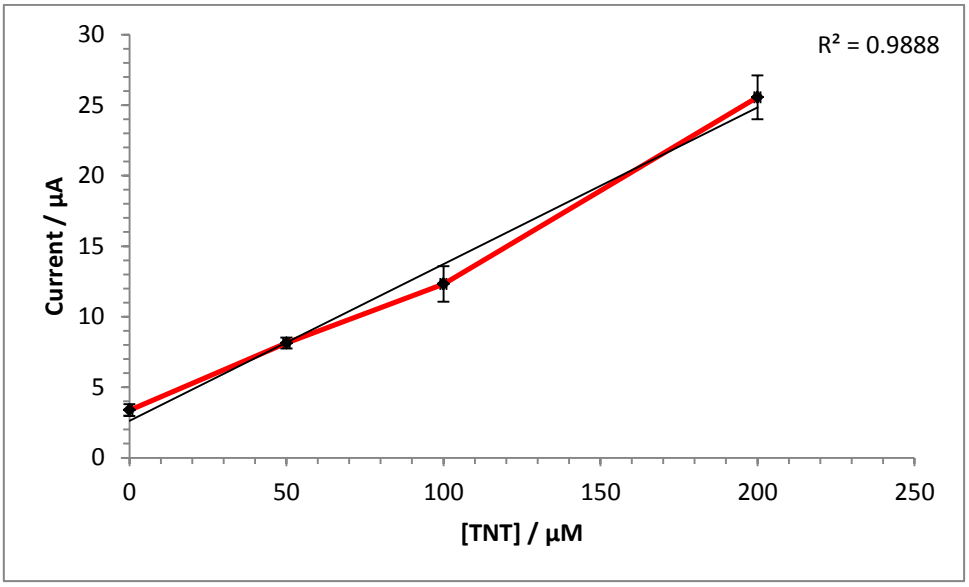

Figure 8.9 - Calibration plot taken from the reductive peak R1a at a potential position of -0.77 V from the voltammogram of TNT in a pH 7.0 phosphate buffer (at a scan rate of 20 mVs^{-1} vs. Ag/AgCl)

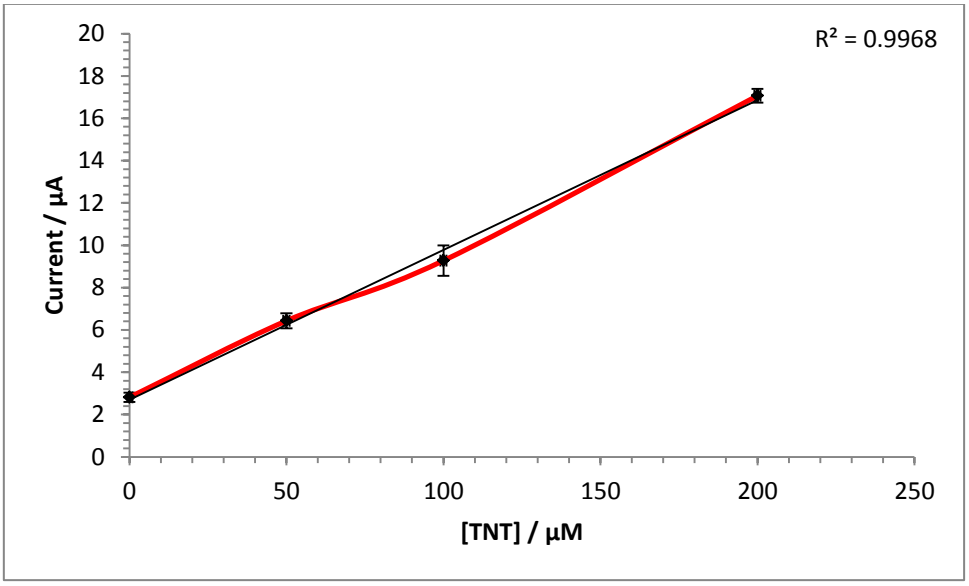

Figure 8.10 - Calibration plot taken from the reductive peak R1b at a potential position of -0.5 V from the voltammogram of TNT in a pH 7.0 phosphate buffer (at a scan rate of 20 mVs^{-1} vs. Ag/AgCl)

It can be seen that a clear linear relationship is demonstrated between the increase in concentration and the corresponding increase in current response.

The calibration plot for the redox couple, O1 and R2, are displayed in Figure 8.11 and Figure 8.12.

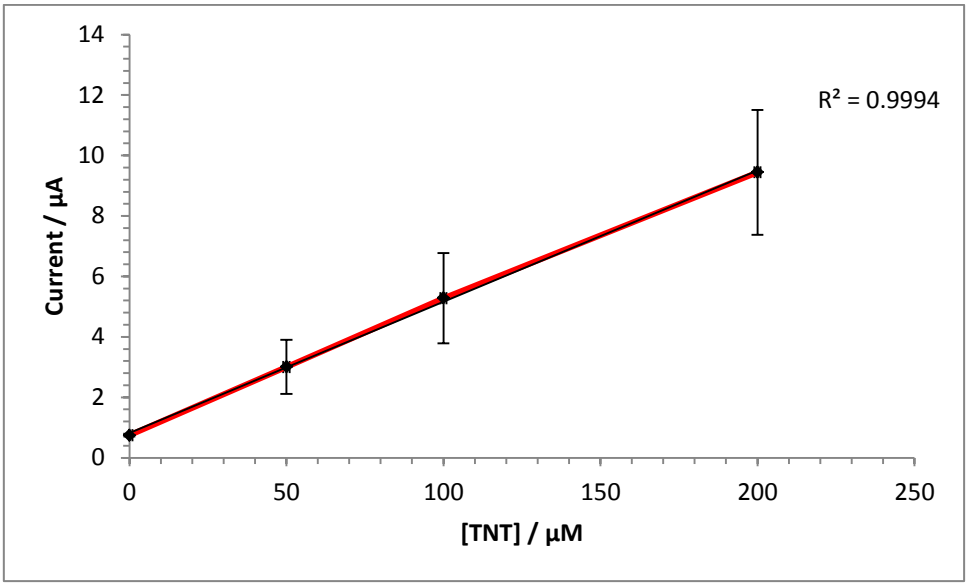

Figure 8.11 - Calibration plot taken from the oxidative peak O1 at a potential position of +0.01 V from the voltammogram of TNT in a pH 7.0 phosphate buffer (at a scan rate of 20 mVs^{-1} vs. Ag/AgCl)

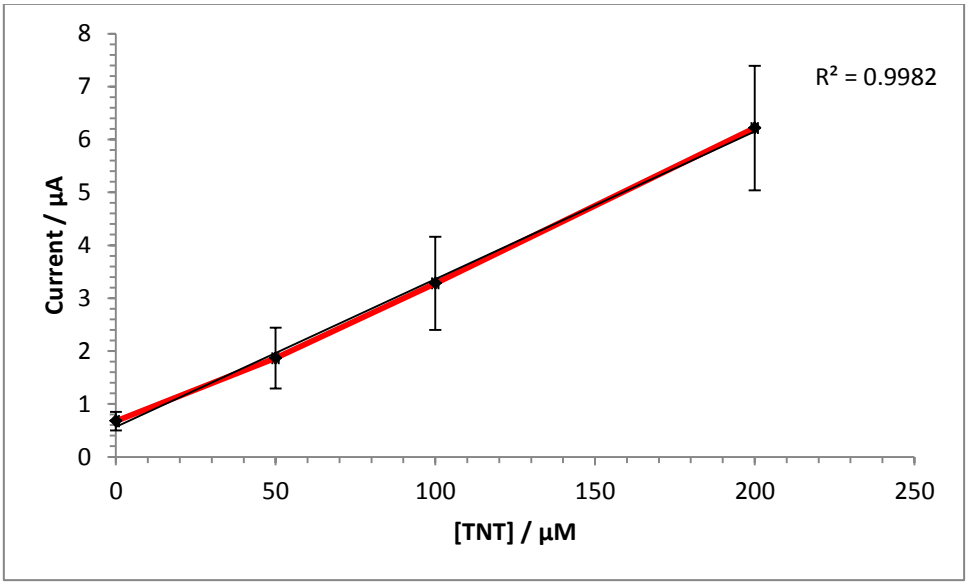

Figure 8.12 - Calibration plot taken from the reductive peak R2 at a potential position of -0.11 V from the voltammogram of TNT in a pH 7.0 phosphate buffer (at a scan rate of 20 mVs^{-1} vs. Ag/AgCl)

The redox peaks from which the data for these calibration plots were taken represent the reversible reduction of the hydroxylamine moiety to its amine form. The linearity, as with the reductive peaks R1a and R1b, has also been demonstrated to be satisfactory; from this it might be possible at this stage to use any of the peaks apparent in the voltammogram gained through the electrochemical breakdown of TNT as an option for subsequent interrogations.

8.6. The detection limit of the cobalt phthalocyanine-doped screen-printed electrode system for nitroaromatic compounds

The theoretical baseline current for the system was determined through the electrochemical interrogation of a phosphate buffer solution without the presence of any nitro compounds. For this analysis a solution containing the enzyme and cofactor in pH7.0 phosphate buffer was interrogated in the same manner as for subsequent work – by performing a forward and reverse potential scan between -0.8 and +0.8 V (vs. Ag/AgCl). Ten replicate measurements were performed and the current response at the potential of +0.01, -0.11, -0.5 and -0.77 V (corresponding to O1, R2, R1b and R1a, respectively) were used to establish the theoretical baseline (based on three times the standard deviation of the average baseline current, n=10) as these are the peak positions identified on the voltammograms obtained when interrogating TNT electrochemically (see Table 8.2). This data is presented in Table 8.3.

	TNT			
	O1	**R2**	**R1b**	**R1a**
Peak position, V	0.01	-0.11	-0.5	-0.77
Detection limit, µA	0.16	0.22	2.9	1.9

Table 8.3 - Theoretical detection limits for TNT as calculated from three times the standard deviation of the mean current of a blank solution (n=10)

The calibration plots corresponding to the redox couple O1 and R2 in peak positions +0.01 and -0.11 V (vs. Ag/AgCl) can be seen below in Figure 8.13 and Figure 8.14.

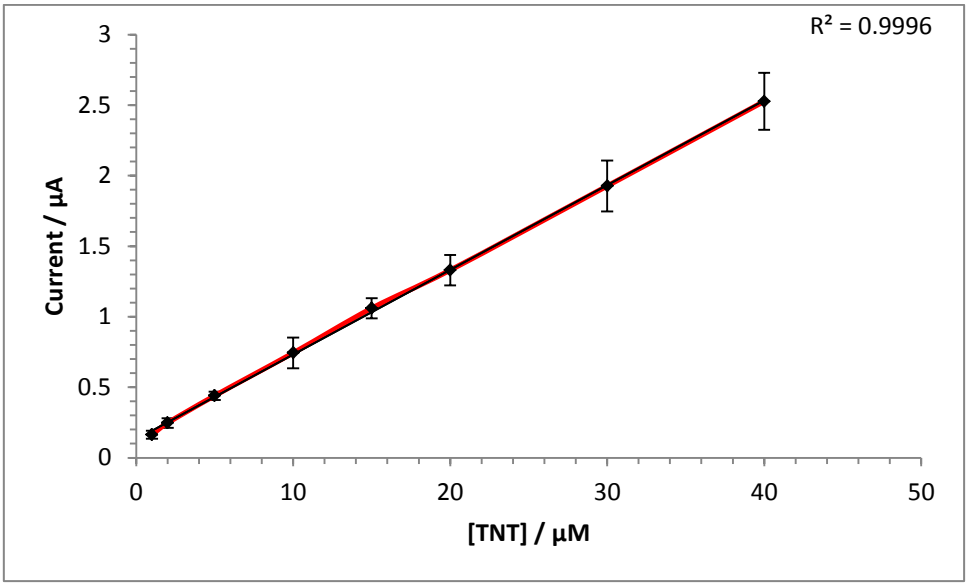

Figure 8.13 - Calibration plot of TNT in pH 7.0 phosphate buffer solution at peak O1, +0.01 V (at scan rate 20 mVs^{-1} vs. Ag/AgCl)

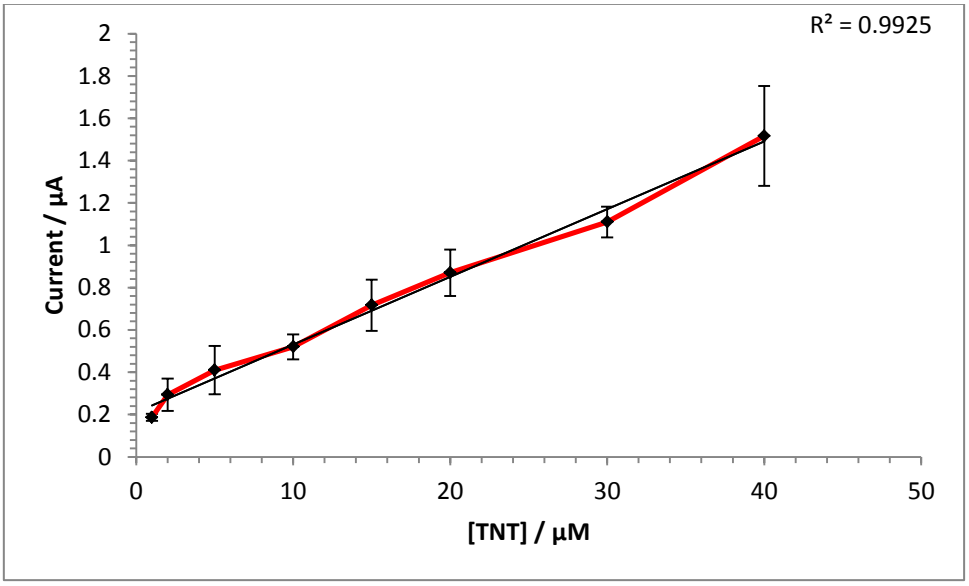

Figure 8.14 - Calibration plot of TNT in pH 7.0 phosphate buffer solution at peak R2, -0.11 V (at scan rate 20 mVs^{-1} vs. Ag/AgCl)

It can be observed that the lower concentrations of TNT interrogated with a CoPc sensor exhibit linear responses with good R^2 values at the redox couple of O1 and R2, with the oxidation peak in particular demonstrating exceptional linearity with increasing concentrations of TNT, $R^2 = 0.9996$. The error observed when interrogating at this peak is also low, with relatively small error bars. The reductive peak R2 also displays respectable linearity and although the error is slightly greater at this peak

position it is not severe. It would appear from these calibration plots that both of these peaks would be suitable for detection of TNT at lower concentrations, with the O1 peak demonstrating particular suitability due to the high linearity and low error. The detection limits for these peaks, using the baseline data in Table 8.3, were found to be 1µM the oxidative peak O1 and 0.3 µM the reductive peak R2.

The calibration plots for the two peaks now present in the cathodic region, R1a and R1b, are displayed below in Figure 8.15 and Figure 8.16.

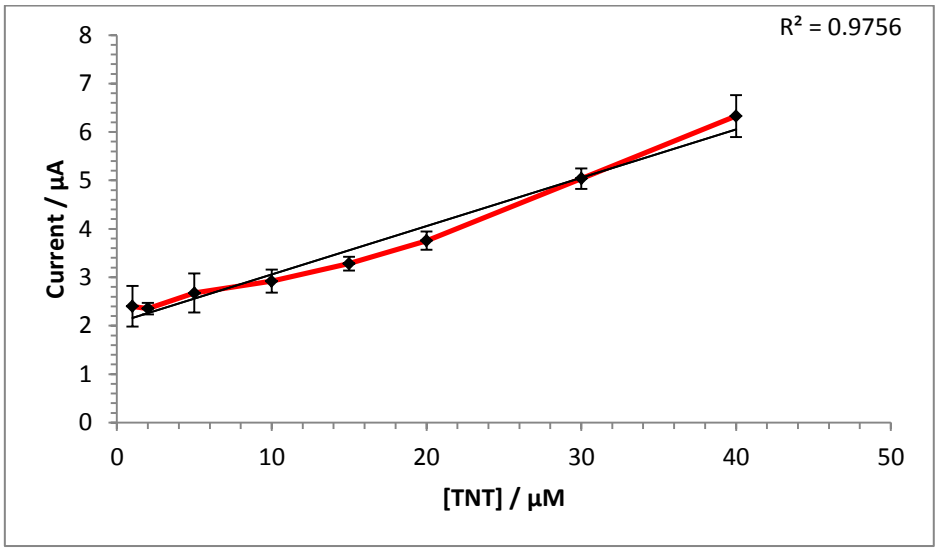

Figure 8.15 - Calibration plot of TNT in phosphate buffer solution at peak R1b, -0.5 V (at scan rate 20 mVs^{-1} vs. Ag/AgCl)

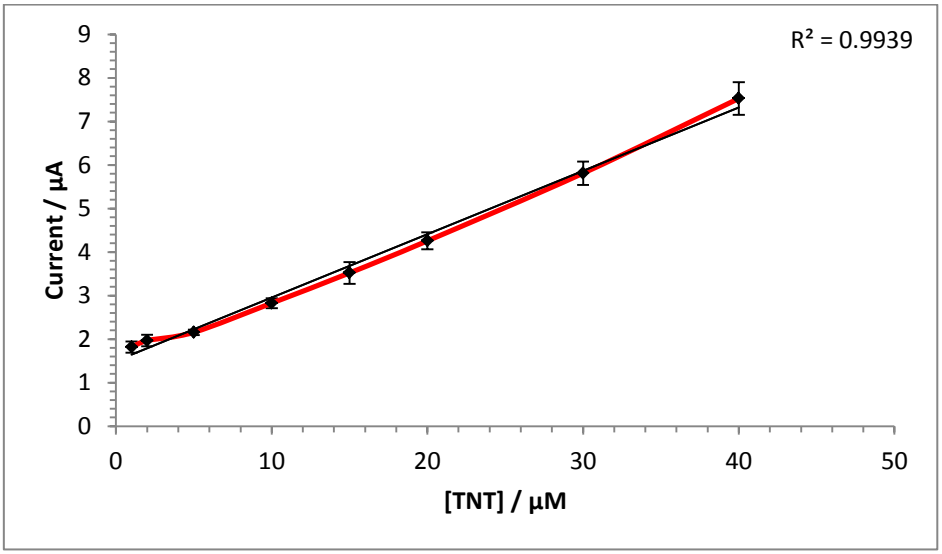

Figure 8.16 - Calibration plot of TNT in phosphate buffer solution at peak R1a, -0.77 V (at scan rate 20 mVs^{-1} vs. Ag/AgCl)

Once more the calibration plots demonstrate good linearity – this is most apparent with the larger reductive peak, R1a, at the potential position of -0.77 V. The error in these two reductive peaks has also been demonstrated to be limited as can be observed with the minimal error bars present. Again the peak R1a has consistently low error in the system which may lend this peak to further electrochemical interrogations. This was also the case when lower concentrations of TNT in phosphate buffer solution were interrogated with the plain carbon sensors; however, the error in that system was much greater than seen here as demonstrated in Figure 8.17.

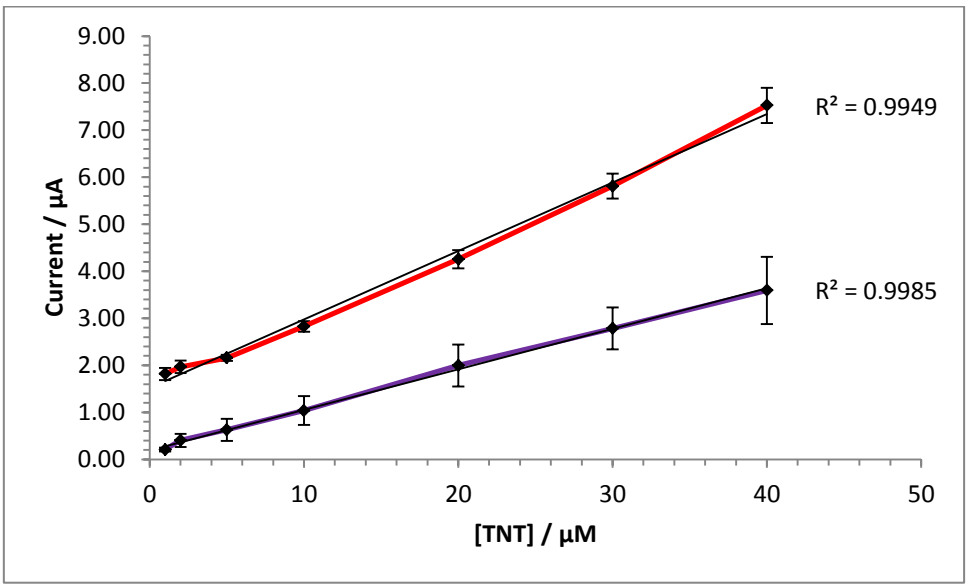

Figure 8.17 - Comparison calibration plots of TNT in phosphate buffer solution to demonstrate the improvement in current magnitude and error in the system between the plain carbon (purple line) and CoPc (red line) sensors

The lower limits of detection at these two peaks, R1a and R1b, using the baseline data from Table 8.3 were 2.7 µM and 9 µM, respectively

It can be seen from the calibration data presented here that the use of a CoPc-doped screen-printed sensor has significantly improved the magnitude of the current response as compared to the plain carbon sensors in chapters 5 and 7, particularly at the lower levels of concentration, although this has not translated into improved lower limits of detection. The inclusion of the enzyme system may, as with the plain carbon sensors, enhance this current response further still.

8.7. Conclusions

A visual examination of the topography of the plain carbon and cobalt phthalocyanine sensors was possible using SEM imaging at 2000x magnification. There were significant differences between the two surfaces, with the plain carbon sensors possessing a fairly featureless topography whilst the CoPc sensors showing flakes of what is postulated to be the cobalt phthalocyanine within the carbon ink matrix.

The cobalt phthalocyanine sensors were first characterised through the interrogation of a solution of 5 mM ferrocenemonocarboxylic acid, as the plain carbon sensors were previously. Comparison of the two sensor platforms demonstrated a slightly diminished peak height when interrogating with the CoPc sensors, but a considerable improvement in the peak separation, from 150 mV with plain carbon to 70 mV with CoPc sensors, demonstrating the reaction took place in a more ideal system. The peak positions were also found to differ from those obtained with the plain carbon sensors; it is postulated that the CoPc sensors provide a mediating effect on the redox reaction, thus enabling the oxidation and reduction to take place before it might with the plain carbon.

A system for the detection of TNT on CoPc sensors has been demonstrated here with a different current response profile when compared to plain carbon screen-printed sensors. The use of cobalt phthalocyanine sensors has improved response when using the main reductive peak R1a as a means for comparison, increasing the current response significantly. This peak is present in interrogations both with plain carbon and CoPc-doped screen-printed sensors, although the peak has become broader with more distinguishable features with the CoPc sensors. This may be due to the mediating effect of the cobalt phthalocyanine on the system.

It was interesting to note that when a phosphate buffer solution was interrogated electrochemically with the CoPc sensors there was a reductive peak present at -0.5 V (vs. Ag/AgCl) which was not apparent when interrogated with the plain carbon sensors. This peak is attributed to the electrochemical reduction of cobalt on the macrocyclic molecule.

The effect of dissolved oxygen on the CoPc system is very much the same as observed when the nitroaromatic compounds were interrogated with the plain carbon sensors. Those reductive peaks in the far cathodic positions were observed to diminish with increasing deoxygenation periods whilst the redox couple at +0.01 and -0.11 V were seen to increase. The same reasons were suggested for this as described previously, these being that the cathodic peaks may have been influenced by the electrochemical reduction of any oxygen within the system and when this residual oxygen was removed the peaks in this region were diminished appropriately. The redox couple had peaks that increased with increasing deoxygenation periods, thought to be the result of oxygen behaving as a competing electron acceptor, thus its removal would increase the available electrons required in the reduction of the hydroxylamine groups on the aromatic ring.

The lower detection limit at the redox couple R2 and O1 was found to be 1 µM in both cases. This is an improvement on that gained with the plain carbon sensors, where the detection limits were found to be 2.6 and 5 µM for peak R2 and O1, respectively. Due to the drop observed between the current response gained from the lowest TNT concentration examined, 1 µM, and the baseline current, it is not possible with this data to give a definitive detection limit – subsequent interrogations with concentrations lower than 1 µM are likely to demonstrate a discord with relation to the linearity already presented in these calibration plots.

9. The influence of nitroreductase on the electrochemical reduction profile of TNT using CoPc sensors

The contents of this chapter are being prepared for publication

9.1. Introduction

It has been illustrated previously, (Section 6.1) that the enzyme system of nitroreductase and NADPH facilitates a reduction of TNT through a mechanism similar to the electrochemical reduction of TNT. This was visualised with the depletion of the NADPH absorbance demonstrated when the reaction takes place in a UV visible spectrometer (Chapter 6). From this fact, the enzyme was introduced to the solution of TNT and interrogated with a plain carbon screen-printed electrode with the aim of improving the sensitivity and the current response in the presence of TNT, as presented earlier (Chapter 7). This theory, however, was found not to be upheld– the inclusion of the enzyme and cofactor into the TNT solution and subsequent electrochemical interrogation produced cyclic voltammograms that were similar both in the presence of the enzyme system and without it. It would seem that the electroactivity of the TNT compound during these interrogations was such that any influence the enzyme and cofactor had on the system was masked.

A mechanism for the possible rectification of this trend would be to improve the enzyme activity through the addition of a mediator. Cobalt phthalocyanine has been used in this fashion previously (Shaidarova et al., 2003; Hart et al., 2004) and screen-printed sensors with the inclusion of CoPc have already, in this study, shown promise in enhancing the signal response for TNT, it was postulated that they would again facilitate an increased signal response when used in conjunction with the enzyme/NADPH system. As such, this appears to be an elegant solution to this challenge if the proposed hypothesis holds.

9.2. The influence of dissolved oxygen on electrochemical interrogations with a CoPc sensor platform and enzyme system

The influence of dissolved oxygen on the electrochemical interrogation of nitro compounds using a plain screen-printed carbon sensor was examined previously in section 5.4 and again for cobalt phthalocyanine screen-printed sensors in section 8.4. To assess whether there is any difference when the enzyme and co-factor are also included in the system this stage was completed once more in the same manner as previously described.

To eliminate any oxygen influence on the electrochemistry of the reduction of TNT on the CoPc electrodes with nitroreductase and NADPH present, the solution was purged via a stream of argon for increasing time periods and tested by running a CV of 50 µM TNT between -0.8 and +0.8 V (vs. Ag/AgCl) and then 100 µM TNT in the same manner.

It can be seen (Figure 9.1) that as the deoxygenation time period increases, the predominant reduction peak in the region of -0.77 V (vs. Ag/AgCl) diminishes; with the greatest drop in response of 27% found after the initial deoxygenation period of two minutes. After 10 minutes and above deoxygenation the majority of the peak definition is seen to disappear.

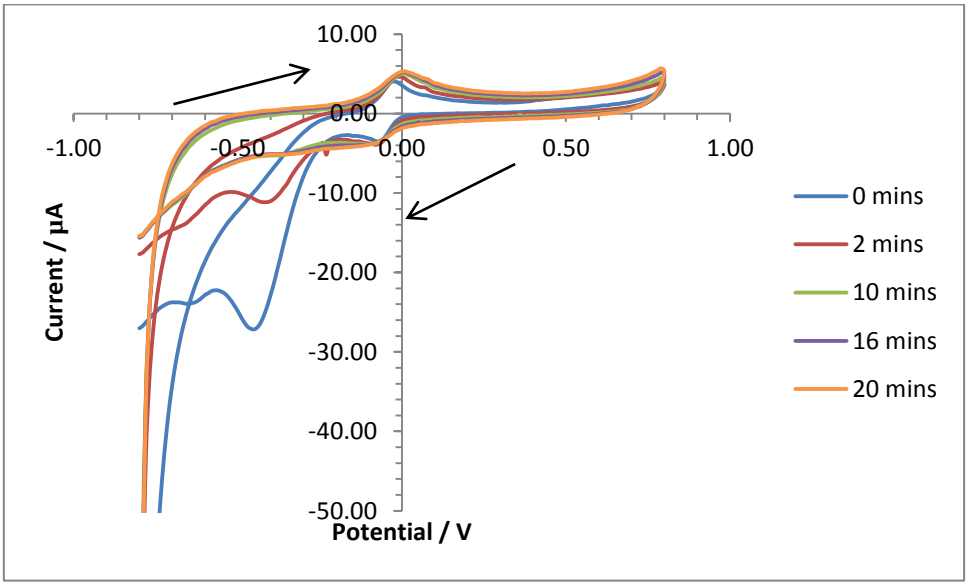

Figure 9.1 - Cyclic voltammogram illustrating the influence of increasing deoxygenation periods on the current response - 50 µM TNT with 2 units NTR and 0.1 mM NADPH

It is apparent that there is little difference in response between the deoxygenation periods of 10, 16 and 20 minutes – this is better illustrated in Figure 9.2.

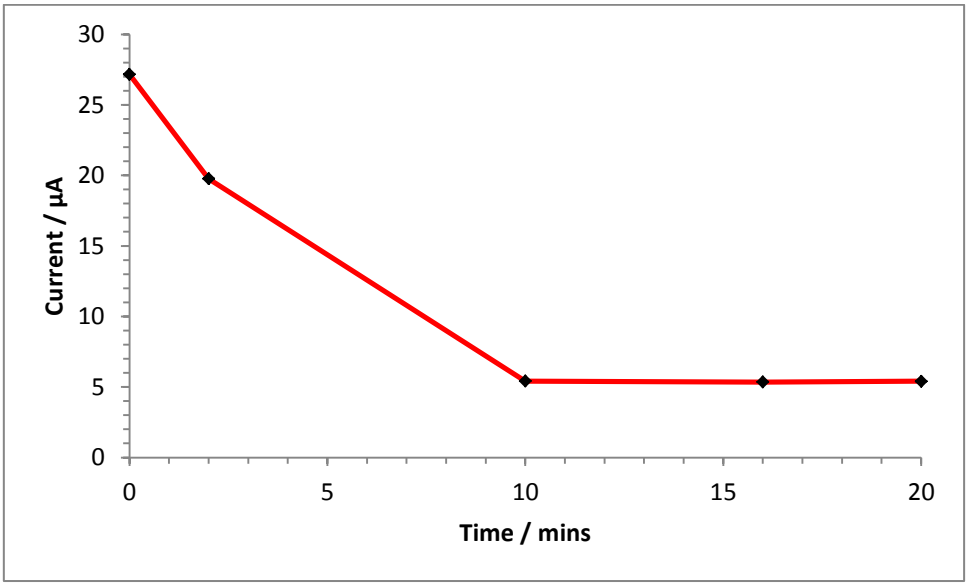

Figure 9.2 - A plot of the diminishing peak current with increasing periods of deoxygenation taken from maximum peak current at R1a (at scan rate of 20 mVs^{-1} vs. Ag/AgCl)

It can also be observed that the oxidation and reduction peaks in the proximity of 0.0 V (vs. Ag/AgCl) actually show a slight increase with increasing degassing periods, with the greatest improvement in response again being that following zero and two minutes (+35%), Figure 9.3. This may be due to the oxygen within the system acting as an electron acceptor in the electrochemical reduction of the nitroaromatic compound. The fact that this trend was also observed with plain carbon sensors would appear to discount this phenomenon being caused by the increase electroactivity of the sensor due to the cobalt phthalocyanine present.

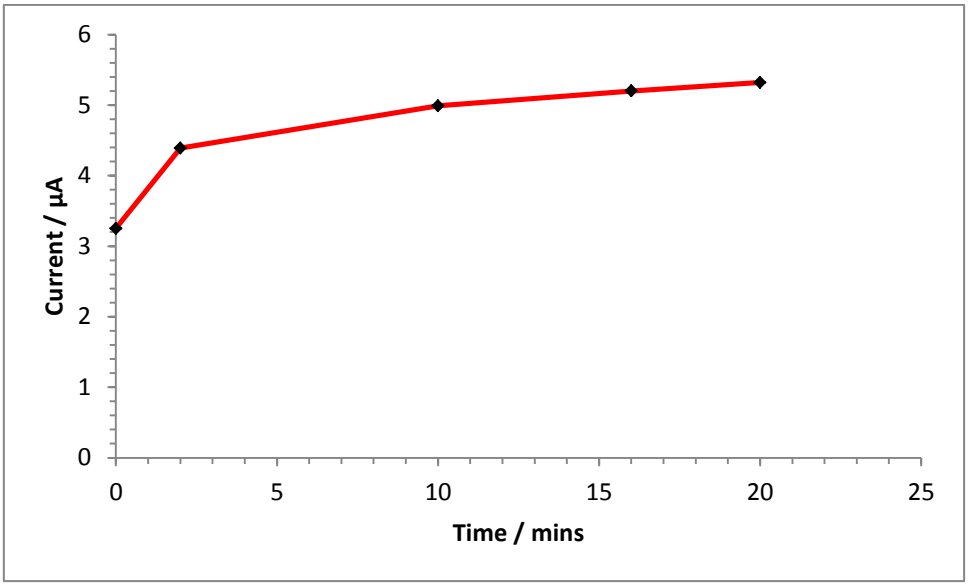

Figure 9.3 - A plot of the increasing peak current with increasing periods of deoxygenation taken from the maximum peak current at peak O1 (at scan rate of 20 mVs^{-1} vs. Ag/AgCl)

These trends can be observed when the electrochemical interrogation is performed in the presence of an increased concentration of TNT (100 µM), see Figure 9.4, although with greater concentrations of TNT the current responses observed for 2 minutes and above deoxygenation periods are also negligible.

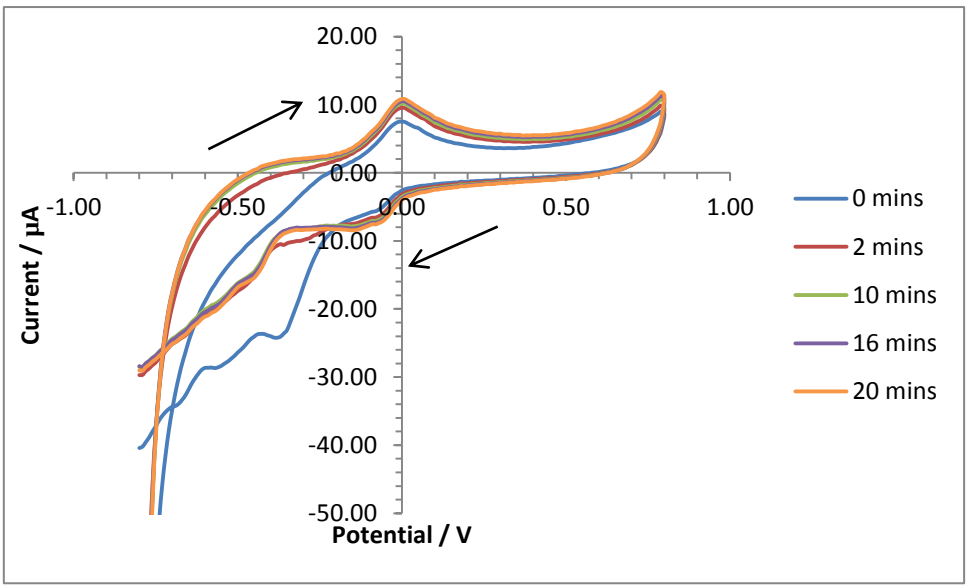

Figure 9.4 - Cyclic voltammogram illustrating the influence of increasing deoxygenation periods on the current response - 100 µM TNT with 2 units NTR and 0.1 mM NADPH (in phosphate buffer solution at scan rate 20 mVs^{-1})

A further investigation was undertaken to narrow the deoxygenation period utilised to establish if there was an obvious period of optimal deoxygenation where the decrease

in the reduction peak at around -0.5 V (vs. Ag/AgCl) and the increase in oxidation/reduction peaks around 0.0 V. This would lead to an optimal degassing period to be applied to all subsequent work with the CoPc sensors, see Figure 9.5, and a cropped section of this voltammogram is presented to greater visualise the differing current response with increasing deoxygenation periods, Figure 9.6.

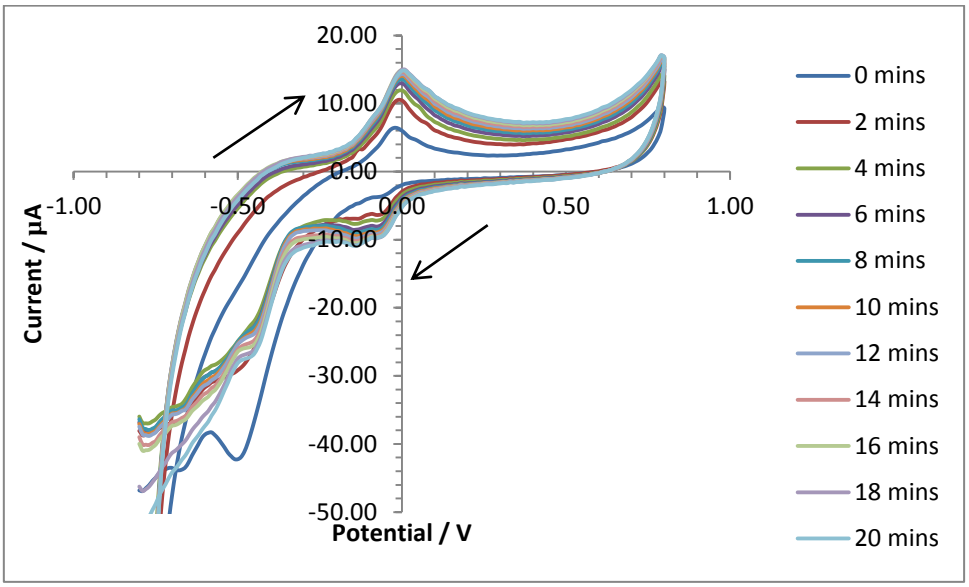

Figure 9.5 - Cyclic voltammogram illustrating the influence of increasing deoxygenation periods on the current response - 100 µM TNT with 2 units NTR and 0.1 mM NADPH (scan rate 20 mVs^{-1} vs. Ag/AgCl)

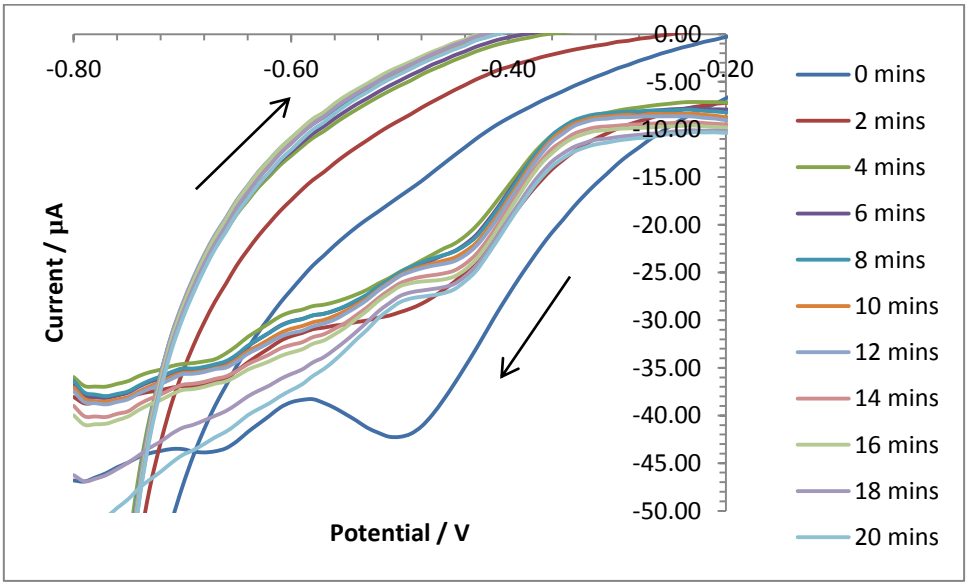

Figure 9.6 - Cropped section of cyclic voltammogram to illustrate the diminishing response with increasing deoxygenation periods (from Figure 9.5)

Once again, it can be observed that the greatest drop in current response at peak -0.5 V is between 0 to 2 minutes; and it has been established once more that between 10 minutes and above deoxygenation periods there is very little change in peak current response. At this point it can be observed that the sealed electrochemical system has been optimally deoxygenated and any further deoxygenation would be deemed time consuming and relatively unnecessary. This is the same outcome as was observed in plain carbon sensors and, as such, all subsequent interrogations were performed both with and without a 10 minute deoxygenation period however, for brevity, only the deoxygenated results are be shown unless otherwise stated.

9.3. Interrogation of TNT with the enzyme system and cobalt phthalocyanine-doped sensor

Cyclic voltammetric interrogations were carried out with the CoPc-doped sensors in the presence of the enzyme and cofactor in a pH 7.0 phosphate buffer solution, with increasing concentrations of TNT as described earlier (section 4.6.1). Interrogations were performed using a minimal concentration of the enzyme nitroreductase, initially 2 units, and with a 0.1 mM concentration of the cofactor NADPH for the same reasons mentioned in the earlier section 7.2 (Zenno et al., 1996). An increasing concentration of TNT produces a corresponding increase in terms of response in the same manner as illustrated earlier with the plain carbon screen-printed sensor system (Figure 9.7).

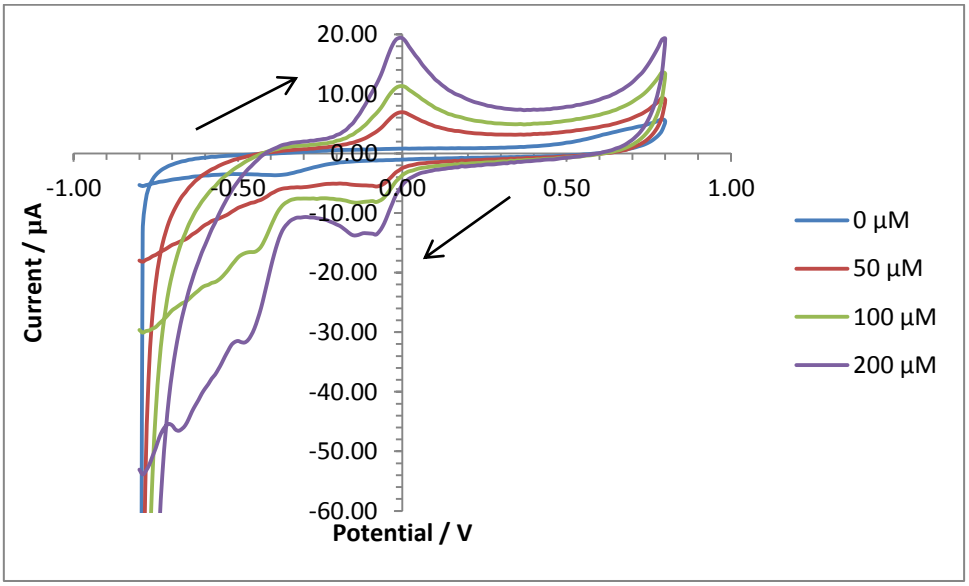

Figure 9.7 - Cyclic voltammograms of increasing concentrations of TNT in the presence of 2 units of NTR and 0.1 mM NADPH performed with a CoPc-doped SPE (20 mVs^{-1} vs. Ag/AgCl) with a 10 minutes deoxygenation period

This current profile includes peaks at a similar potential as found earlier in interrogations without the presence of the enzyme and cofactor (see Table 8.2), which coincides with the systematic breakdown of each nitro group on the TNT molecule; first into a hydroxylamine and then an amine as previously described (Section 5.3). The position of the peaks, in terms of peak potential, are similar however there appears to be increased electrochemical activity in the cathodic region – where the peaks are not as sharp but there does seem to be an additional peak present. This may

be related to the increased electroactivity of the CoPc-doped sensor and also the improved activity related to the additional enzyme system which enables the splitting of the peaks into the three reductive reactions associated with the initial reduction of the nitro groups on the aromatic ring. The peak positions for the interrogation of TNT within both a phosphate buffer solution and the enzyme system is given in Table 9.1 alongside those peak positions gained for the interrogation of TNT with a plain carbon screen-printed electrode with the enzyme and cofactor.

TNT	**R1a**	**R1b**	**R1c**	**R2**	**O1**
Plain carbon NTR/ NADPH	-0.72	*N/A*	*N/A*	-0.3	+0.3
CoPc in PBS	-0.77	-0.5	*N/A*	-0.11	+0.01
CoPc with NTR/NADPH	-0.79	-0.5	-0.70	-0.11	0.00

Table 9.1 - Peak position data of TNT interrogated with a plain carbon sensor, a cobalt phthalocyanine sensor in both a simple phosphate buffer and with the enzyme system for comparison

The increasing concentration of TNT and the resulting increase in current response can be visualised more effectively with the calibration data found below, the first set of which are taken from the three reductive peaks R1a-c (present between -0.5 and -0.79 V vs. Ag/AgCl) (Figure 9.8).

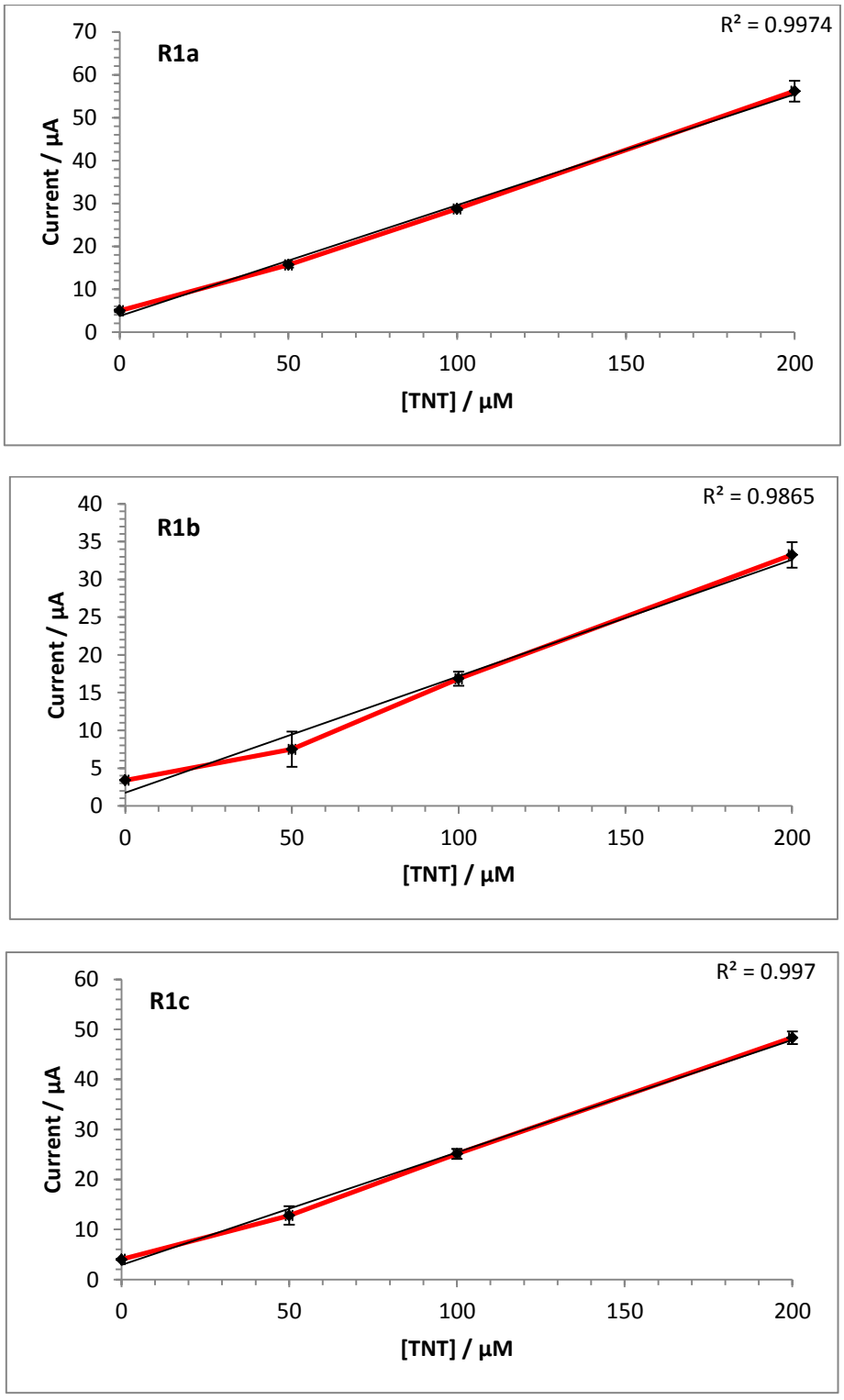

Figure 9.8 - Calibration data illustrating the result of increasing the concentration of TNT on the three R1 reductive peaks; where peak positions were R1a= -0.79, R1b= -0.50 and R1c= -0.7 V (in the presence of 2 units NTR and 0.1 mM NADPH in phosphate buffer at a scan rate of 20 mVs^{-1} vs. Ag/AgCl)

In all cases a relatively linear plot is apparent demonstrating a reproducible trend of increasing current response with increasing concentrations of TNT. These three reductive peaks present in the cathodic region of the voltammograms correspond, once more, to the breakdown of the nitro groups on the aromatic ring of TNT into their hydroxylamine moieties, as shown in section 5.3. The fact that there are now three peaks present in this region does not dispel the earlier explanation of the electrochemical reduction of TNT (see section 5.3 for this explanation in greater detail) as it would appear that the improved electroactivity attributed to the cobalt phthalocyanine sensors and the addition of the enzyme system have improved not only the current magnitude, but also the signal differentiation in the voltammograms gained.

To assess the improvement in current magnitude in a more concise manner a set of calibration curves is seen below, with the peak in the most cathodic position (between -0.72 and -0.79 V vs. Ag/AgCl) exploited as this peak is present in all systems.

The calibration plots for the redox couple at 0.00 and -0.11 V (vs. Ag/AgCl) can be seen below in Figure 9.9 and Figure 9.10. These peaks displayed excellent linearity when increasing concentrations of TNT were interrogated electrochemically. This was also seen in the three reductive peaks R1a, R1b and R1c. This linearity presents all of these potential peak positions as possibilities for use in steady state voltammetric examinations – useful for a handheld system. The peak R1a perhaps demonstrates the most promise, due to the consistently good linearity and the proximity away from the inherent CoPc peak demonstrated in phosphate buffer solution.

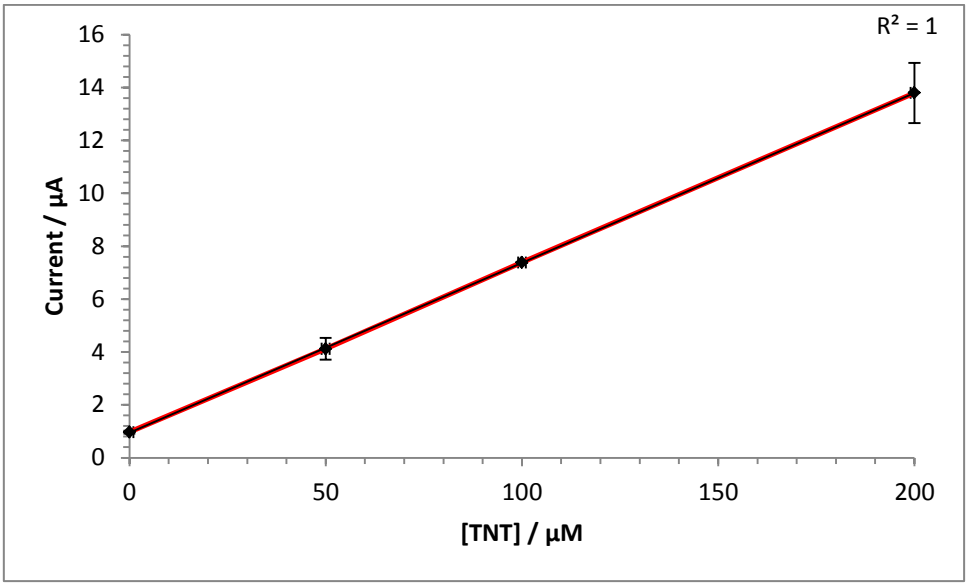

Figure 9.9 - Calibration plot for the peak at position -0.11 V, known as R2, from the electrochemical interrogation of TNT with 2 units NTR and 0.1 mM NADPH in a phosphate buffer (scan rate 20 mVs^{-1} vs. Ag/AgCl)

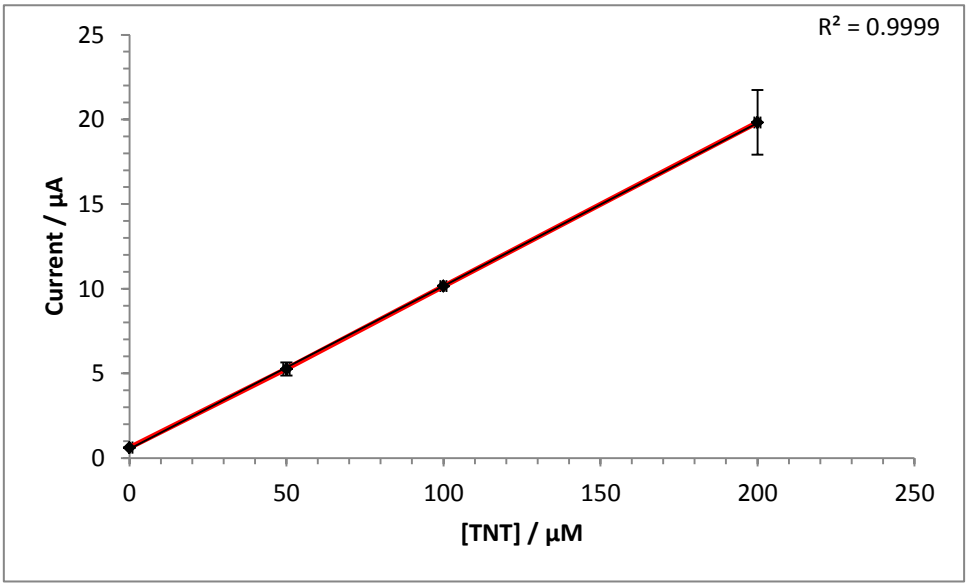

Figure 9.10 - Calibration plot for the peak at position -0.00 V, known as O1, from the electrochemical interrogation of TNT with 2 units NTR and 0.1 mM NADPH in a phosphate buffer (scan rate 20 mVs^{-1} vs. Ag/AgCl)

The actual current response is not any greater with the inclusion of the enzyme and cofactor than when these were not present. It may be the case that the electroactivity of the CoPc-doped sensor is such that any additional response attributed to the enzyme system is simply overshadowed by the magnitude of this CoPc signal response.

9.3.1. Increasing the enzyme available in the system

To assess whether an increase in the quantity of the enzyme present improves the resulting magnitude of current response the interrogation of TNT in the same manner described in section 9.3 was repeated with a ten-fold increase in the available nitroreductase, from 2 units to 20 units, Figure 9.11.

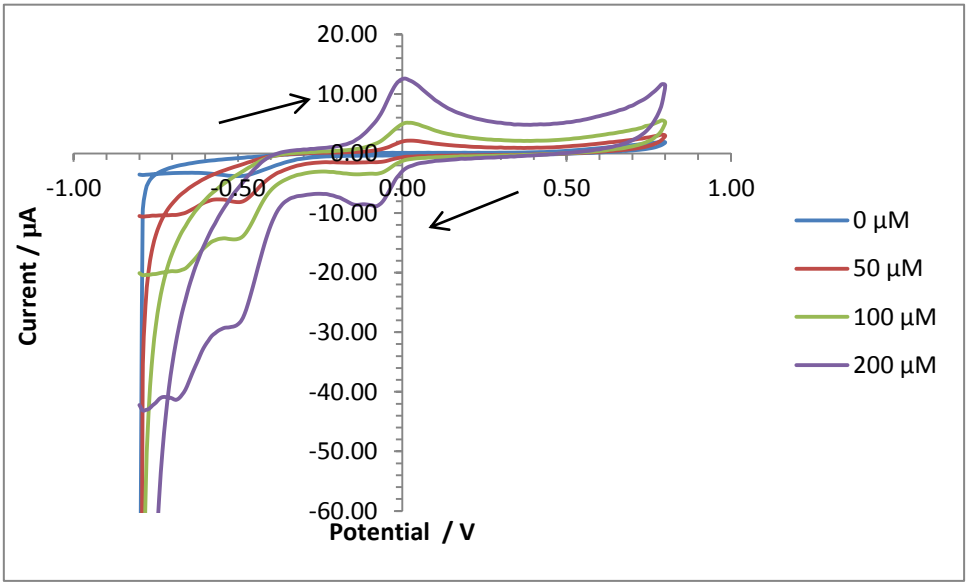

Figure 9.11 - Cyclic voltammograms of increasing TNT concentrations when electrochemically interrogated in the presence of 20 units NTR and 0.1 mM NADPH on CoPc-doped SPE (at a scan rate of 20 mVs^{-1} vs. Ag/AgCl)

Whilst increased quantity of enzyme appears to have had very little influence on the peak positions it does, however, cause the magnitude of response to decrease (Figure 9.12). There does seem to be an enhancement in the peaks obtained in terms of more differentiated peaks occurring in the reductive region at peak position -0.70 V in the voltammograms where 20 units as opposed to those with 2 units of NTR when interrogating with a CoPc.

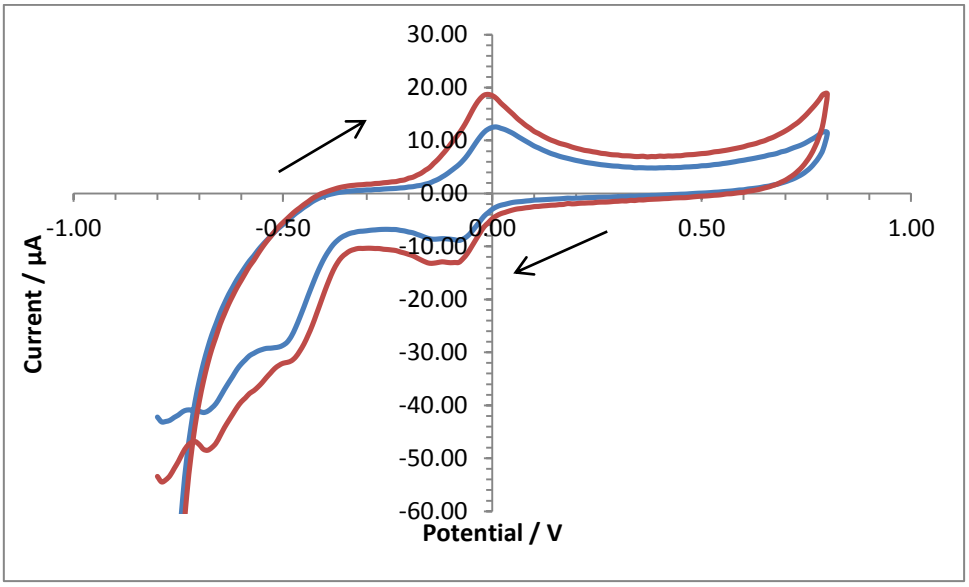

Figure 9.12 - 200 µM TNT in phosphate buffer with either 20 units (blue line) or 2 units (red line) of nitroreductase and 0.1 mM NADPH (scan rate 20 mVs^{-1} vs. Ag/AgCl)

The calibration plot below confirms that there is a decrease in current response when increasing the concentration of the enzyme – this is not as expected and may be attributed to some hindrance effect caused by the increase in enzyme in the bulk solution, see Figure 9.13. The linearity was demonstrated to be excellent in both cases, with both R^2 values over 0.99. The greater current response in the system with less enzyme present was somewhat surpassed by the improvement in peak clarity, this is best seen at peak position -0.5V (vs. Ag/AgCl).

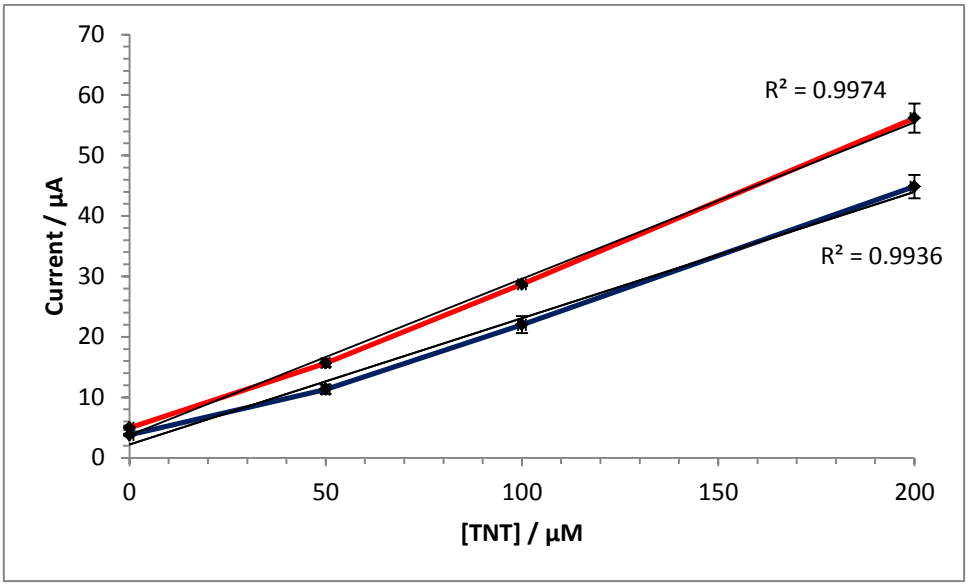

Figure 9.13 - Calibration data illustrating the increasing concentration of TNT in the presence of 20 units (blue line) and 2 units (red line) of NTR and 0.1 mM NADPH in phosphate buffer taken from the peak position at -0.79 V (scan rate of 20 mVs^{-1} vs. Ag/AgCl)

Despite the fact that there is not an improvement in current response with the increase in nitroreductase, the enhancement of peak clarity would suggest that an increase in the enzyme provides a more desirable system as the improved clarity of the peak lends itself to better identification of the nitroaromatic present through more clearly defined peaks which may be associated directly with the analyte under examination, and the identification of an optimal potential can be performed for steady state chronoamperometry.

9.3.2. Increasing the coenzyme available in the system

The quantity of the cofactor NADPH was initially set following previous work using the NfsA form of nitroreductase (Zenno et al., 1996) for the reduction of nitro groups; however, a subsequent investigation into the inclusion of additional NADPH to the system was performed to ascertain if an increased quantity will improve the magnitude of response and the clarity of the peaks.

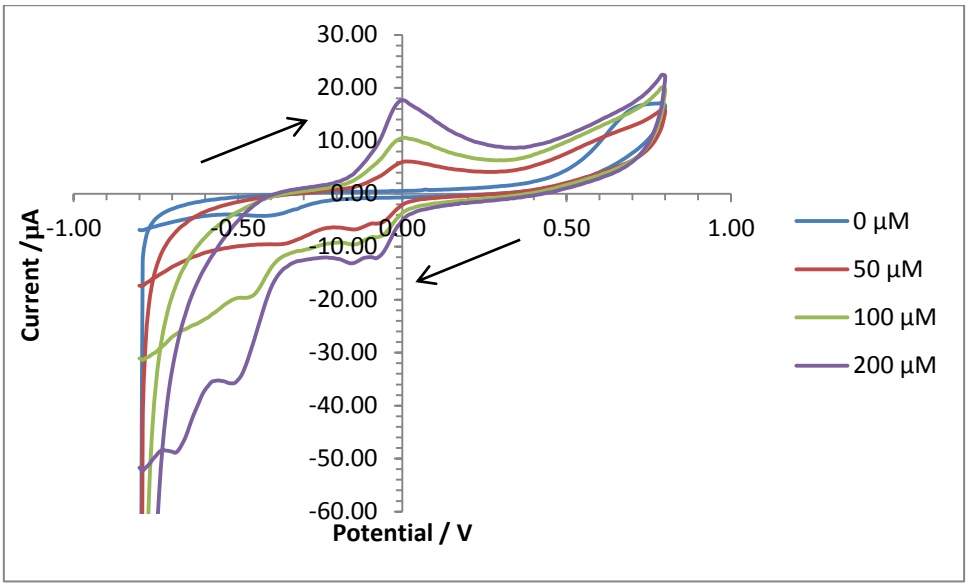

Figure 9.14 - Cyclic voltammograms of increasing concentrations of TNT in the presence of 20 units of NTR and 1 mM NADPH performed with a CoPc-doped SPE (vs. Ag/AgCl) with a 10 minutes deoxygenation period

Once more, the general response profile is similar to those gained previously with very little difference between this set of voltammograms and those gained with only 0.1 mM NADPH present. This can be better observed in Figure 9.15 below which includes a voltammogram showing the interrogation of 200 µM of TNT in a phosphate buffer solution with 20 units of nitroreductase and either 0.1 mM or 1.0 mM NADPH. The peak positions and current magnitude are very similar – in this case the 1.0 mM NADPH voltammogram demonstrates a slightly greater current response at peak R1a, however, when calibration data was taken from three full sets of concentration interrogations the average responses were consistent or, in some cases, slightly lower. This can also be seen below in Figure 9.16.

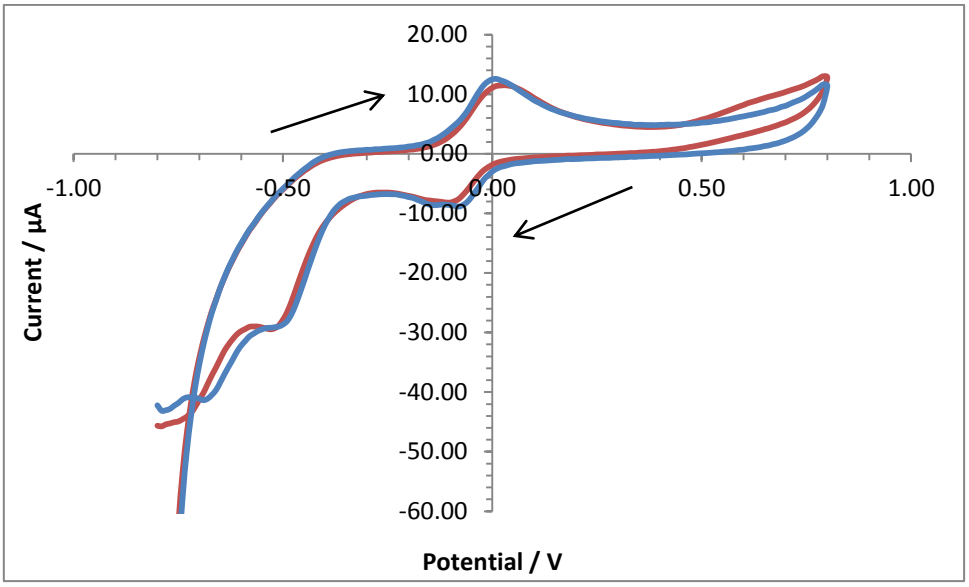

Figure 9.15 - 200 µM TNT in phosphate buffer with 20 units of nitroreductase and either 0.1 mM (blue line) or1 mM (red line) of NADPH (scan rate 20 mVs^{-1} vs. Ag/AgCl)

The calibration data below, Figure 9.16, confirms this observation. The data gathered from the electrochemical interrogations with an increased concentration of NADPH does not provide any improvement in the observed current response – at lower TNT concentrations the current magnitude is almost identical and at a higher concentration of TNT the 0.1 mM NADPH provides a slightly greater response. There is also more error apparent in those interrogations with the increased concentration of NADPH as demonstrated by the greater error bars, better seen in Figure 9.17.

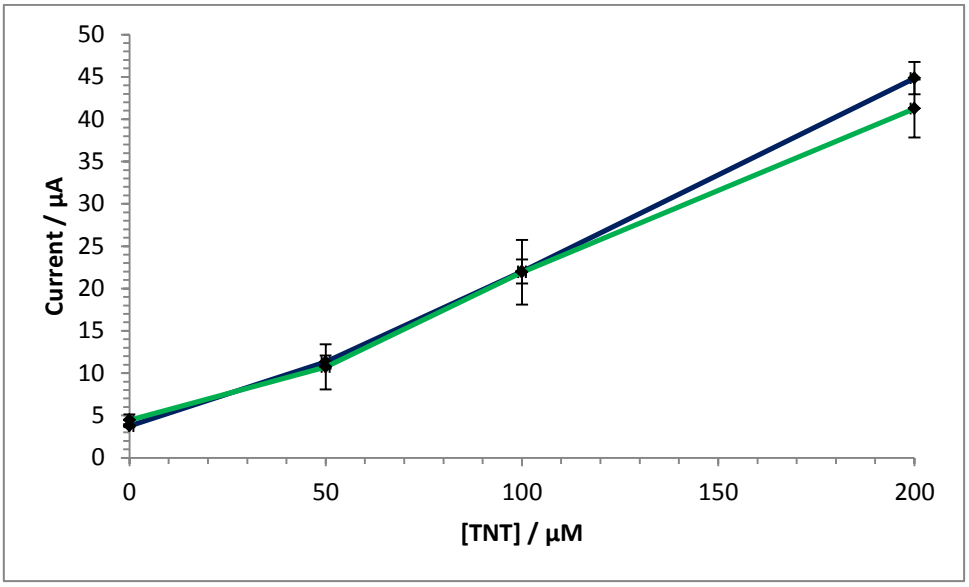

Figure 9.16 - Calibration data illustrating the increasing concentration of TNT in the presence of 20 units of NTR and either 0.1 mM (blue line) or 1.0 mM (green line) of NADPH in phosphate buffer taken from the peak position at -0.79 V (scan rate of 20 mVs^{-1} vs. Ag/AgCl)

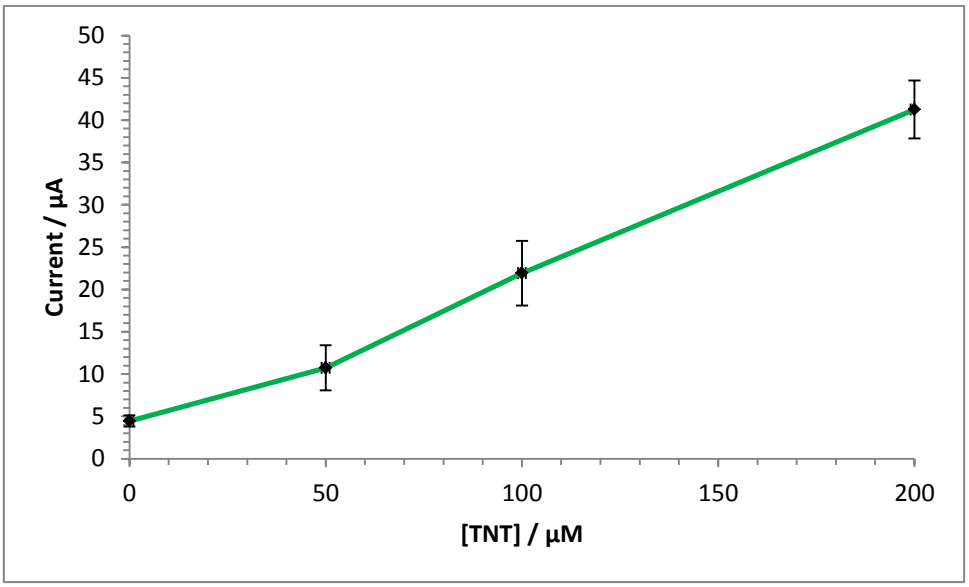

Figure 9.17 - Calibration data illustrating the increasing concentration of TNT in the presence of 20 units of NTR and 1.0 mM of NADPH in phosphate buffer taken from the peak position at -0.79 V (at a scan rate of 20 mVs^{-1} vs. Ag/AgCl)

It would seem that the increase in cofactor present brings no additional benefits to the system, in terms of there being no observable increase in the magnitude of current response or an improvement in the reproducibility of the system. Indeed, the error seems to increase with the increase in NADPH. It may be that case that this lower concentration of NADPH is the optimal quantity to provide full initiation of the enzyme

reaction during analysis within the bulk solution and any additional NADPH available is simply wasted. As such the original concentration of 0.1 mM will be utilised for the remainder of interrogations performed with the CoPc sensor platform this is due to the reasons provided above and to maintain the ideal of a low cost device.

9.4. The detection limit of nitroaromatics using the mediated sensor including the enzyme and cofactor

An analysis of the baseline of the system was completed with a solution containing the enzyme and cofactor in pH7.0 phosphate buffer interrogated in the same manner as for subsequent work – by performing a forward and reverse potential scan between -0.8 and +0.8 V (vs. Ag/AgCl). Ten replicate measurements were performed each with a new sensor and the current response at the potentials of +0.00, -0.11, -0.5, -0.70 and -0.79 V (corresponding to O1, R2, R1b and R1a) were used to establish the theoretical baseline (based on three times the standard deviation of the average baseline current, n=10). This was undertaken as these are the peak positions identified in the voltammograms obtained when interrogating TNT electrochemically and as such could each be used as an interrogation method for sensor response. This data is presented in Table 9.2.

	TNT				
Peak position, V	0.00	-0.11	-0.50	-0.70	-0.79
Detection limit, µA	0.2	0.7	0.61	0.80	0.69

Table 9.2 - Theoretical detection limits for TNT as calculated from three times the standard deviation of the mean current of a blank solution (n=10)

Calibration plots were produced using amperometric interrogations for TNT at lower concentrations (0-40 µM) to establish the limit of detection that the system is capable of reliably recording. The calibration plots were produced at the peak potentials previously identified during the electrochemical interrogation of TNT (Table 8.2). The calibration plot of TNT for peak O1 at a peak potential of +0.00 V (vs. Ag/AgCl) can be seen below, Figure 9.18.

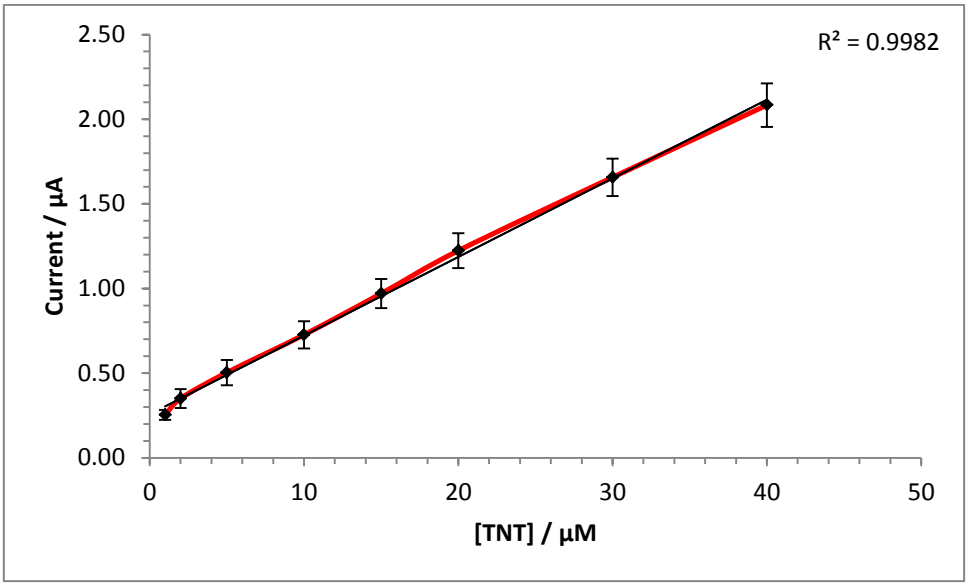

Figure 9.18 - Calibration plot representing the lower detection limits of TNT taken from a potential of +0.00 V (at scan rate 20 mVs^{-1} vs. Ag/AgCl) after 10 minutes deoxygenation

As the baseline has been calculated within this region to be at a current of 0.2 µA (Table 8.3), the lowest concentration that is above this baseline figure is 1 µM.

This technique was followed with the reductive peak, R2, at -0.11 V that forms part of the redox couple in the electrochemical profile of TNT representing the reversible reduction of the hydroxylamine groups to their amine moiety, see Figure 9.19. Here it can be observed that the baseline current was calculated as 0.7 µA (Table 9.2) which can be used to identify the value of 12 µM as the lowest concentration of TNT that may be identifiable over the baseline

.

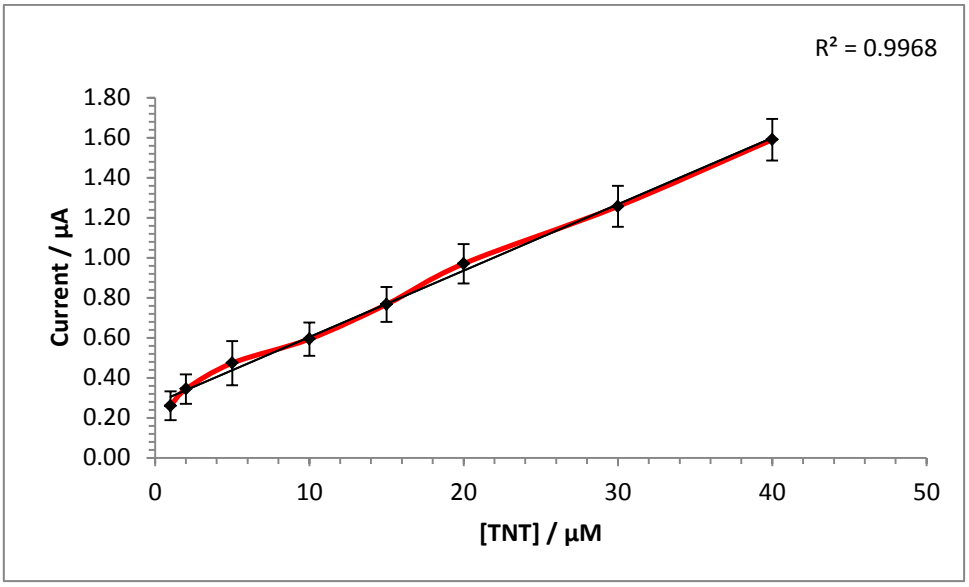

Figure 9.19 - Calibration profile representing the lower detection limits of TNT taken from the peak at a potential of -0.11 V (at 20 mVs^{-1} vs. Ag/AgCl) after ten minutes deoxygenation

The relatively shallow calibration plot obtained from the potential position at -0.5 V (Figure 9.20) may be due, in part, to any influence from the reduction of cobalt phthalocyanine in the doped carbon ink. This reductive reaction has been illustrated to occur at a potential of -0.5 V within this system, see Figure 8.4.

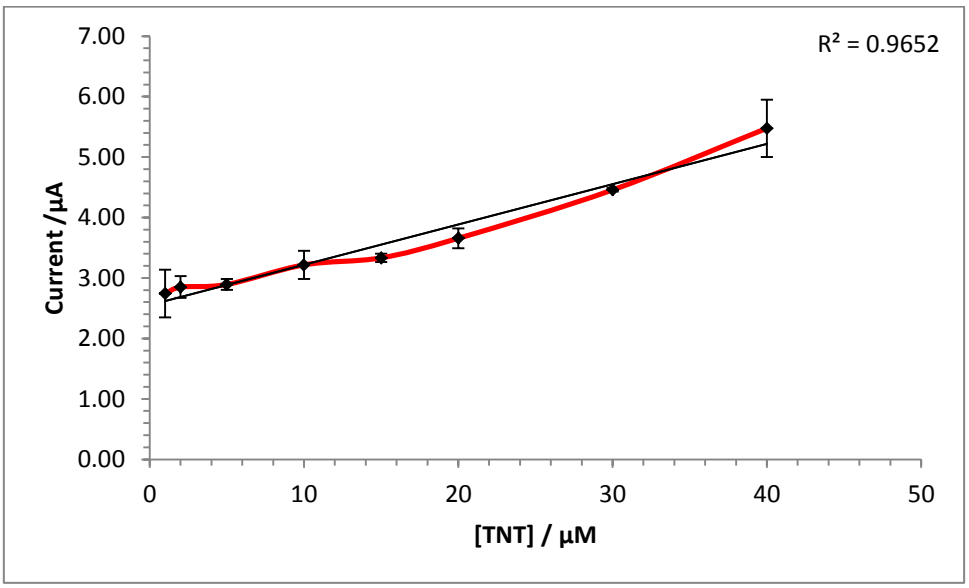

Figure 9.20 - Calibration profile representing the lower detection limits of TNT taken from a potential position of -0.5 V (at scan rate 20 mVs^{-1} vs. Ag/AgCl) after ten minutes deoxygenation

Utilising the baseline current of 0.61 µA, obtained from Table 9.2, the lowest concentration of the TNT that can be observed to give a response above this baseline at peak R1b (potential position -0.5 V) value is 30 µM.

The reductive peak R1c calibration plot can be seen below in Figure 9.21 which demonstrates a linear profile with little error. From the baseline data, the lowest current value above which a signal can be reliably reported is 0.80 µA. This would mean that a concentration of 4 µM can be given as the limit of detection.

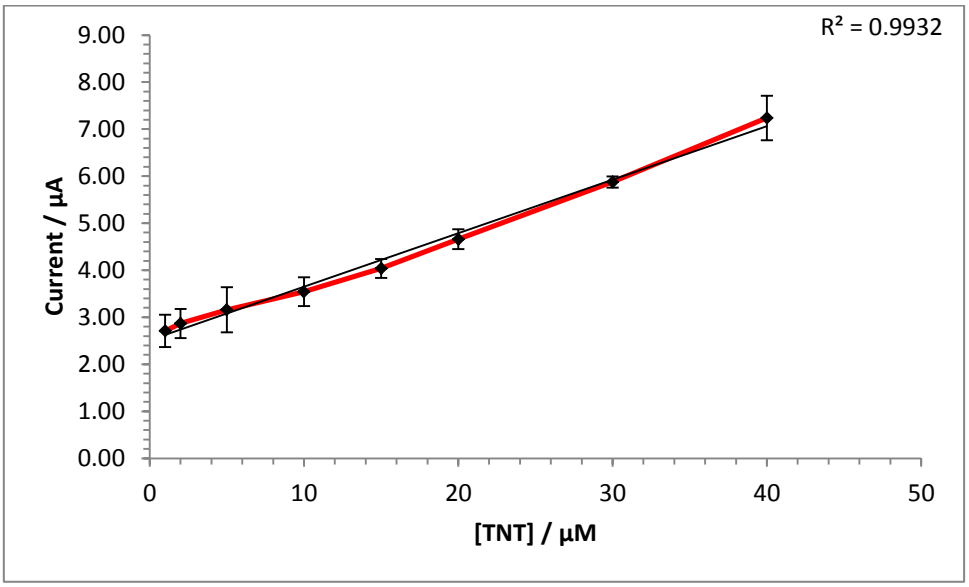

Figure 9.21 - Calibration plot representing the lower detection limits of TNT taken from a potential position of -0.70 V (at scan rate 20 mVs^{-1} vs. Ag/AgCl)

The data related to the peak at potential of -0.79 V (R1a) defines the baseline at this potential to be 0.69 µA. When this is the case the limit of detection of TNT, using the calibration plot gained for this potential position presented below in Figure 9.22, can be identified as 14 µM.

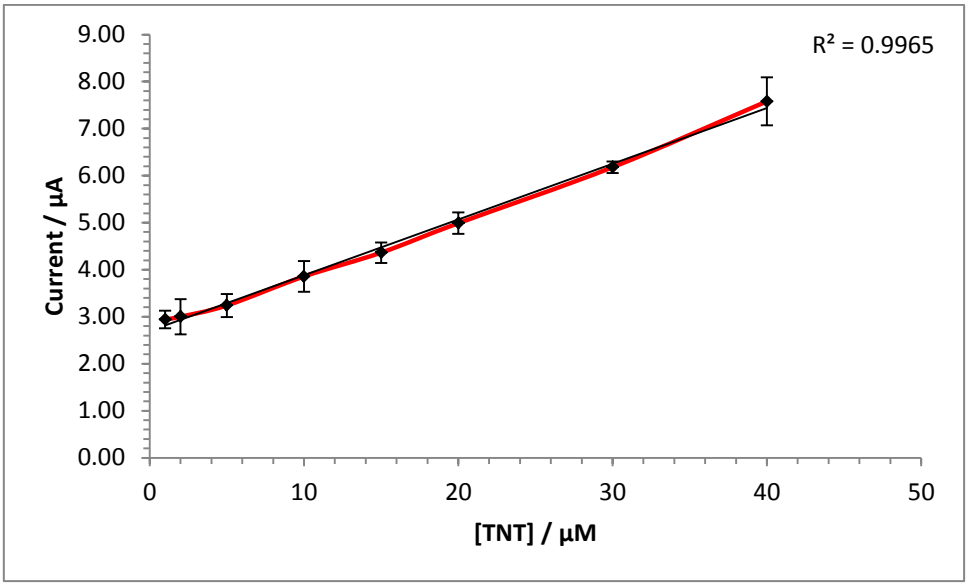

Figure 9.22 - Calibration plot representing the lower detection limits of TNT taken from the potential position of -0.79 V (vs. Ag/AgCl) after a ten minute deoxygenation period

From this assessment of the lower detection limits of the CoPc sensor and the enzyme/coenzyme system it is possible to note that the detection limits have been reduced considerably from those gained with a plain carbon screen-printed sensor both with and without the enzyme system present. As such, these sensors have been demonstrated to be not only suitable for subsequent analyses but a significant improvement in current responses. Perhaps the most suitable peak for sensor analysis is peak R1a – this peak is sufficiently far from the peak associated with the electroactivity of the CoPc sensor itself and, although there is an influence caused by dissolved oxygen prior to deoxygenation, this influence may be taken into account in a portable sensor and the system zeroed to include it. Both with and without the deoxygenation stage the peak in this position demonstrates good clarity and differentiation. Further work was undertaken using these CoPc sensors primarily but with the plain carbon sensors sometimes used in interrogations for comparison where appropriate.

9.5. Conclusions

An investigation into the influence of the enzyme system, nitroreductase and NADPH, found that there was little improvement on the current response gained with the addition of NTR and its cofactor. This may be due to the significant electroactivity of the CoPc sensor itself overshadowing any reactions associated with the enzyme and cofactor. Although the peak height and position remained largely the same, the clarity of the peaks seemed to be improved (Figure 9.11). When the amount of enzyme in the system was increased, this clarity too increased (Figure 9.14), with three separate shoulders apparent on the reductive peak found within the cathodic region. It may be the case that these shoulders represent each nitro group undergoing the reduction into hydroxylamine – this type of electrochemical profile has been demonstrated with adsorptive stripping voltammetry (Wang et al., 2009) and using carbon fibre electrodes with cyclic voltammetry (Agüí et al., 2005).

A similar investigation into the influence of NADPH on the system found there to be little difference between 0.1 and 1 mM concentrations of the cofactor. It may be the case that at a concentration of 0.1 mM this is already optimal for the amount of enzyme available in the system; any subsequent NADPH would, therefore, not be utilised. The resulting calibration plots were remarkably similar with the 0.1 mM NADPH concentration only deviating at the 200 μM concentration of TNT where a better response was obtained. The level of error in the system was also greater with the higher concentration of NADPH. As such 0.1 mM was determined as the concentration for subsequent interrogations.

The limits of detection for this sensor platform was found to be 30 μM of TNT at -0.5 V for both a system with and without the inclusion of the enzyme – this was determined using the baseline calculations (section 9.4) as a limit and undertaking a study into lower concentrations of TNT. At concentrations below 30 μM, the current response of the potential peak in position -0.5 V (vs. Ag/AgCl) was below the baseline peak of 4.45 μA. It would be advantageous to improve this detection limit further to increase the commercial viability of this system.

10. Cobalt phthalocyanine poly(*o*-phenylenediamine) coated and sonochemically treated cavity carbon electrodes

10.1. Introduction

The use of a microelectrode, as discussed in section 2.6.2, offers many possible advantages over that of a planar electrode such as, for example, the smaller electrode surface allowing the accumulation of a smaller charging current near the surface. This charging current influences the dispersal of ionic species which can cause a masking effect on the reaction being investigated. The smaller charging current associated with a microelectrode will obviously help to alleviate this effect. Microelectrodes are also known for their stir-independent properties which allow for their use in fluidic systems, hence their use within *in vivo* monitoring of living organisms.

The advantages of microelectrodes are, however, negated somewhat by the very factor that makes them advantageous – their small size. Due to the significantly smaller electroactive area associated with microelectrodes, the resulting signal size is also significantly smaller in magnitude. To obviate this factor the use of many microelectrodes connected in parallel in the form of an array can enable the increase in response while retaining the microelectrode properties that are desirable.

Microelectrode arrays have been produced using many different techniques such as, for photolithography, laser ablation and micro-machining approaches.

In this work, the microelectrode array will be fabricated in the same manner as described previously in (Myler et al., 1997) where an insulating polymer is electropolymerised at the conductive electrode surface to form an insulting thin film where the thickness is not greater than 40 nm. This insulated electrode surface may then be submerged into an ultrasonic bath where, as the ultrasound is passed through the solvent, thermal agitation and localised hotspots occur. These hotspots cause superheated bubble formation which, as they cool, implode ejecting microjets of the solvent; these jets impact on the surface of the insulated electrode causing microscopic ablations through to the conducting surface. These exposed areas, or

cavities, can act as a microelectrode due to their size, and the collection of many cavities can function as a microelectrode array. These techniques are described in sections 4.6.3, 4.6.4 and 4.6.5 in the materials and methods chapter.

10.2. Optimising the electrodeposition of poly(*o*-phenylenediamine) upon cobalt phthalocyanine screen-printed electrodes

10.2.1. Electrodeposition of the polymer film onto cobalt phthalocyanine-doped screen-printed electrodes

Poly(*o*-phenylenediamine), PoPDA, was electropolymerised onto the surface of planar cobalt phthalocyanine, CoPc, screen-printed electrodes as described in section 4.6.4. Briefly, the screen-printed sensors with an external counter and reference electrode were placed in a 5 mM solution of *o*-phenylenediamine / pH 7.4 phosphate buffer and initially scanned between 0 and +1000 mV (vs. Ag/AgCl) for 20 potential cycles. The electropolymerisation of PoPDA occurs via a $2e^-$ process (Myler et al., 1997) and forms a stable insulating film onto the electrode substrate (Yano, 1995).

The voltammogram gained displays a large irreversible anodic peak area on the first scan – with two distinct peaks occurring at a potential of +0.35 and +0.55 V (vs. Ag/AgCl). This large oxidative peak is followed in successive scans by a decreasing anodic current; this may be attributed to the inherent insulation taking place at the electrode surface and also the fact that oxidation of the monomer units upon the surface of the already coated electrode takes place less readily than that on the bare carbon surface. The cyclic voltammogram corresponding to the electrodeposition of the PoPDA is shown in Figure 10.1.

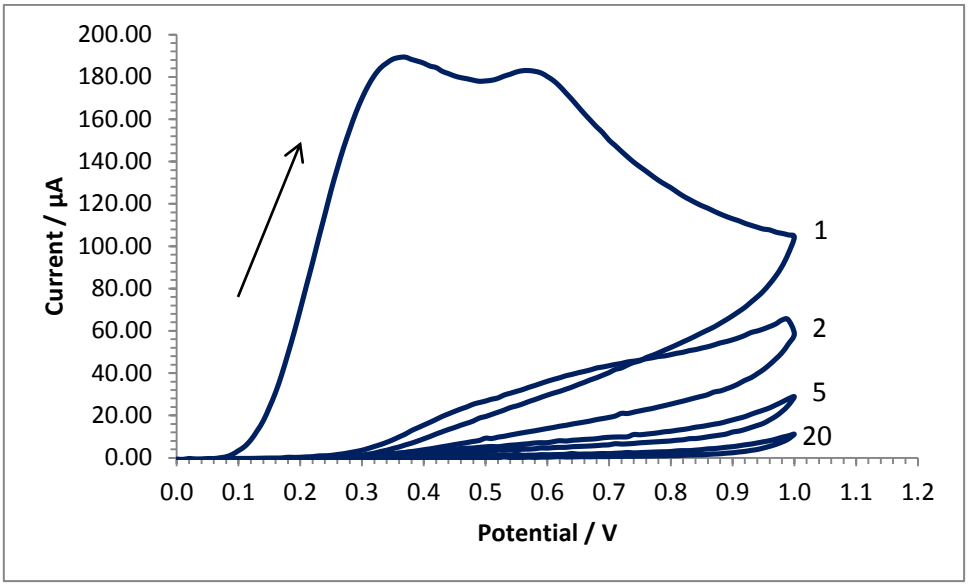

Figure 10.1 - Cyclic voltammograms for the polymerisation of poly(o-phenylenediamine) thin films at a cobalt phthalocyanine-doped screen-printed electrode (scan rate 20 mVs^{-1} vs. Ag/AgCl)

As the electrode surface becomes more insulated, the anodic peak can be observed to diminish further still until, at sweep 20, it appears to have decreased almost to background level as described by (Gornall et al., 2009). The electrochemical polymerisation of PoPDA is essentially a self-limiting process since the polymer is insulating; it follows that as the electrode surface becomes fully insulated no further deposition can take place. It should be noted at this point that although this self-limiting behaviour has been demonstrated previously an electrode surface will never be entirely coated in this way. Yano, 1995, reported that film thickness did not increase when cycling was continued after the 1000^{th} sweep; however, a very small peak current was still observed after this point (Yano, 1995). As such, it should be expected that a low peak current will be observed in this work even after the insulating stage has been performed.

10.2.2. Pre-treatment of electrodes

The electrodeposition technique of the insulating polymer PoPDA upon plain carbon screen-printed electrodes has been previously optimised (Gornall et al., 2009) with the inclusion of an ultrasonic pre-treatment to dispel any microbubbles adhering to the surface of the electrode prior to electrodeposition due to the hydrophobicity of carbon ink (see section 4.6.4 for a full description). This technique was carried out and tested to establish the necessity of this step in the electropolymerisation on the CoPc-doped screen-printed electrodes used in this work, see Figure 10.2.

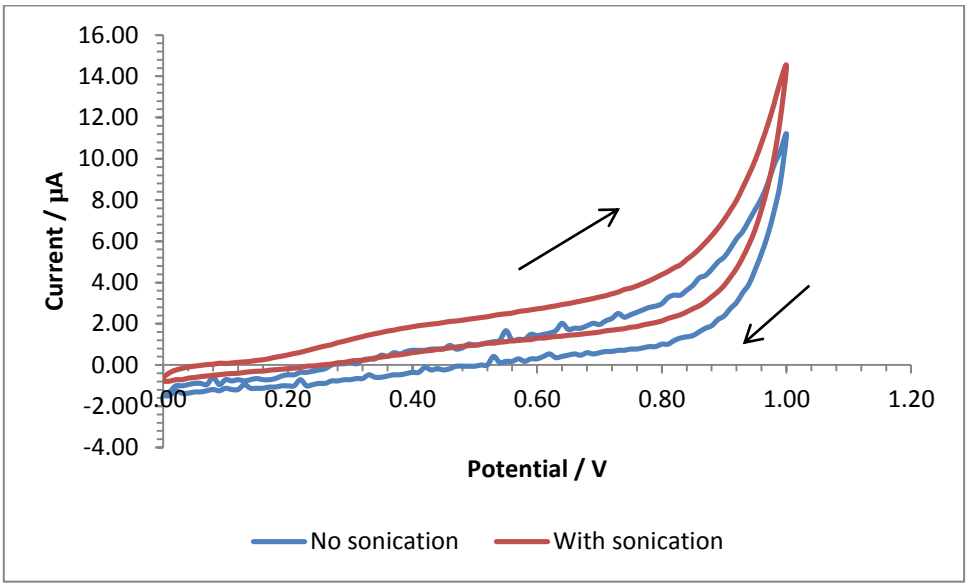

Figure 10.2 - Cyclic voltammograms obtained of the final sweep during the electrodeposition of 5 mM PoPDA upon cobalt phthalocyanine screen-printed electrodes, where the red line represents a prior ultrasonic pre-treatment and the blue line corresponds to no prior ultrasonic pre-treatment (scan rate 20 mVs^{-1} vs. Ag/AgCl)

It can be observed in Figure 10.2 that contrary to the well-established technique of sonochemical pre-treatment prior to the electrodeposition of PoPDA on carbon electrodes, when using a CoPc-doped sensor this pre-treatment does not provide an improvement on the thin-film deposition process.

The addition of the sonochemical pre-treatment step has not provided an improved insulating effect when PoPDA is polymerised on the CoPc electrode surface. This can be observed by the slightly greater current profile gained from the pre-treated sensor (taken from the final potential sweep of 20) when compared to the untreated sensor

(Figure 10.2). These sensors, when used to interrogate ferrocenemonocarboxylic acid electrochemically, can be seen to present a different current profile when compared to a bare CoPc sensor interrogated in the same manner (Figure 10.3).

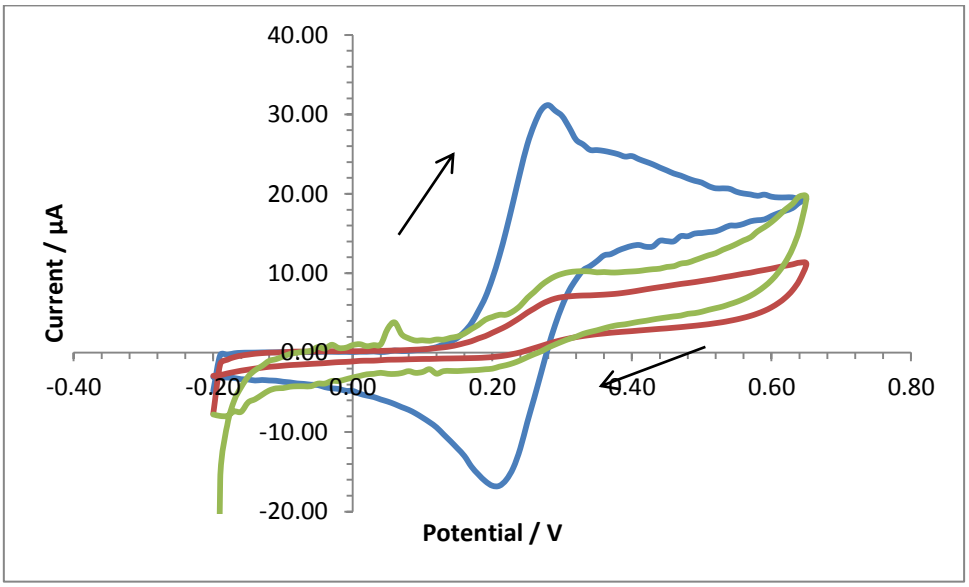

Figure 10.3 - Cyclic voltammograms of ferrocenemonocarboxylic acid interrogated with a bare (blue), PoPDA insulated without pre-treatment (red) and PoPDA insulated with sonochemical pre-treatment (green) (scan rate 20 mVs^{-1} vs. Ag/AgCl)

It can be seen in Figure 10.3 that there is a significant insulation effect apparent with both sensors, and that the sensor without the sonochemical pre-treatment can be seen to impart a slightly more insulated profile than that gained with the pre-treatment.

There are two possibilities that might contribute to this effect. The first may be that the ultrasonic pre-treatment actually dislodges some of the CoPc particles within the carbon ink matrix thereby exposing more conductive carbon. A second contributory explanation could be that the CoPc carbon electrodes offer a more hydrophilic surface than untreated carbon and so there is less tendency for dissolved gases to come from solution and adhere to the surface of the electrodes in the first instance. As the electrodeposition has been demonstrated to occur more favourably without this pre-treatment step, from this stage it was omitted.

10.2.3. Number of potential cycles required for optimum deposition of poly(*o*-phenylenediamine) on cobalt phthalocyanine sensors

Previous literature has reported that when a gold screen-printed sensor is coated with the insulating polymer PoPDA using 20 potential sweeps, the resulting electrode surface become essentially totally insulated (Myler et al., 1997). It can be seen, however, that with a cobalt phthalocyanine sensor as the base substrate there is still a considerable voltammetric profile when used to interrogate ferrocenemonocarboxylic acid (Figure 10.3). As such, a study was undertaken to establish the optimum number of potential cycles to achieve the best insulation of the CoPc sensor (Figure 10.4).

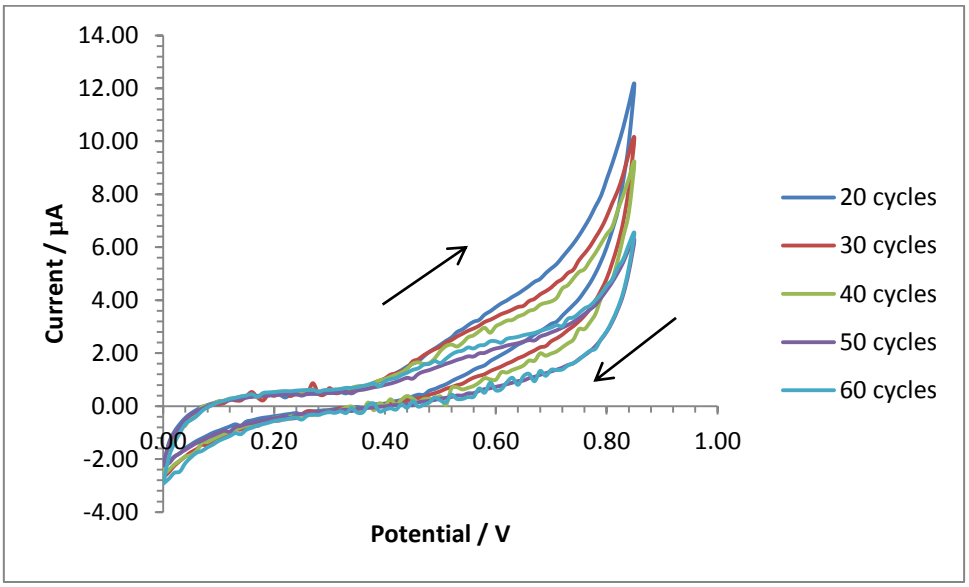

Figure 10.4 - The final potential cycle gained from the electrodeposition of 5 mM PoPDA on the surface of a CoPc sensor after various numbers of potential cycles (20 mVs^{-1} vs. Ag/AgCl)

It can be observed with the final cycle figure above (Figure 10.4) that when the final voltammograms of each insulated sensor are compared there is a distinct difference between the voltammogram representing the sensor insulated with 20 cycles and each of the other sensors insulated with a greater number of insulating cycles – this would indicate that the sensor was not sufficiently insulated with 20 cycles and that further electrodeposition is desirable to provide a surface as insulated as practical before sonochemical treatment and the development of conducting polymer microarrays. The current response progressively decreases with each additional 10 cycles until the

50 cycle electrodeposition; at this stage the difference between 50 and 60 cycles is negligible, shown below for improved clarity within Figure 10.5.

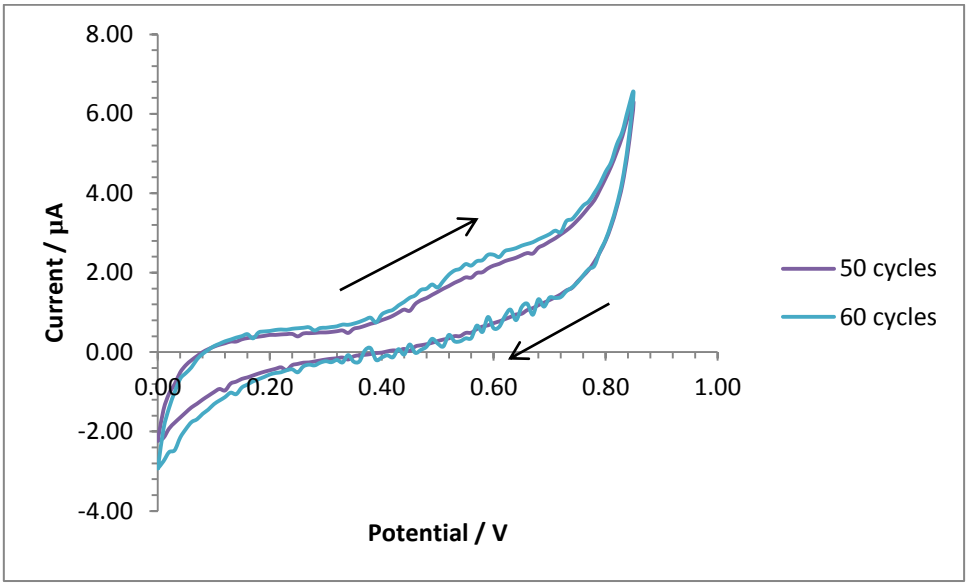

Figure 10.5 - The final potential cycle gained from the electrodeposition of PoPDA on the surface of a CoPc sensor after 50 and 60 potential cycles (20 mVs^{-1} vs. Ag/AgCl)

It would be desirable that the final cycle might have as small as possible a current profile at this stage. The difference between the sensor insulation after sequentially cycling for 50 and 60 scans, demonstrated in Figure 10.5, can be observed to be sufficiently negligible enough that 50 potential cycles will be used in all PoPDA electrodeposition processes from this stage unless otherwise stated.

This is apparent in a more recent study (Gornall et al., 2009; Collyer et al., 2010) where an optimum deposition period of 50 sweeps was found to fully insulate a batch of 100 inter-connected screen-printed carbon electrodes. It is postulated here that an analogous result is found due to the electroactivity of the CoPc sensor, and the electroactivity of the 100 sensor batch, when compared to a single plain carbon screen-printed electrode. In both circumstance, to achieve a more homogeneous insulating layer, increased sweeps (and therefore increased PoPDA) are required to fully insulate the sensor surfaces.

10.2.4. The scan rate required for optimum deposition of poly(*o*-phenylenediamine) on cobalt phthalocyanine sensors

The production of sonochemically fabricated microelectrode arrays, as pioneered by our group, through the electrodeposition of PoPDA has been described in the literature and as such the scan rate used during the development of these microelectrode arrays has in most instances been reported as 50 mVs^{-1} (Myler et al., 1997; Barton et al., 2004; Pritchard et al., 2004). It has been established, however, that a slower rate of potential cycling may produce a more uniform thin film deposition in the surface of the electrode (Mădăraş and Buck, 1996).

The scan rate used for the initial work in this chapter was 20 mVs^{-1}, and a study was carried out to assess the suitability of several other scan rates based on their propensity to insulate the electrode well and the time required to complete the insulation of each sensor. This factor can be important when considering the commercial viability of future devices in terms of processing time.

In addition to the 20 mVs^{-1} scan rate electrodeposition, 10 and 5 mVs^{-1} scan rates were assessed for the insulating capacity provided through sequentially cycling the electrode in a 5 mM PoPDA solution. The resulting cyclic voltammograms are shown for cycles 1, 2, 5 and 20 in Figure 10.6a-c.

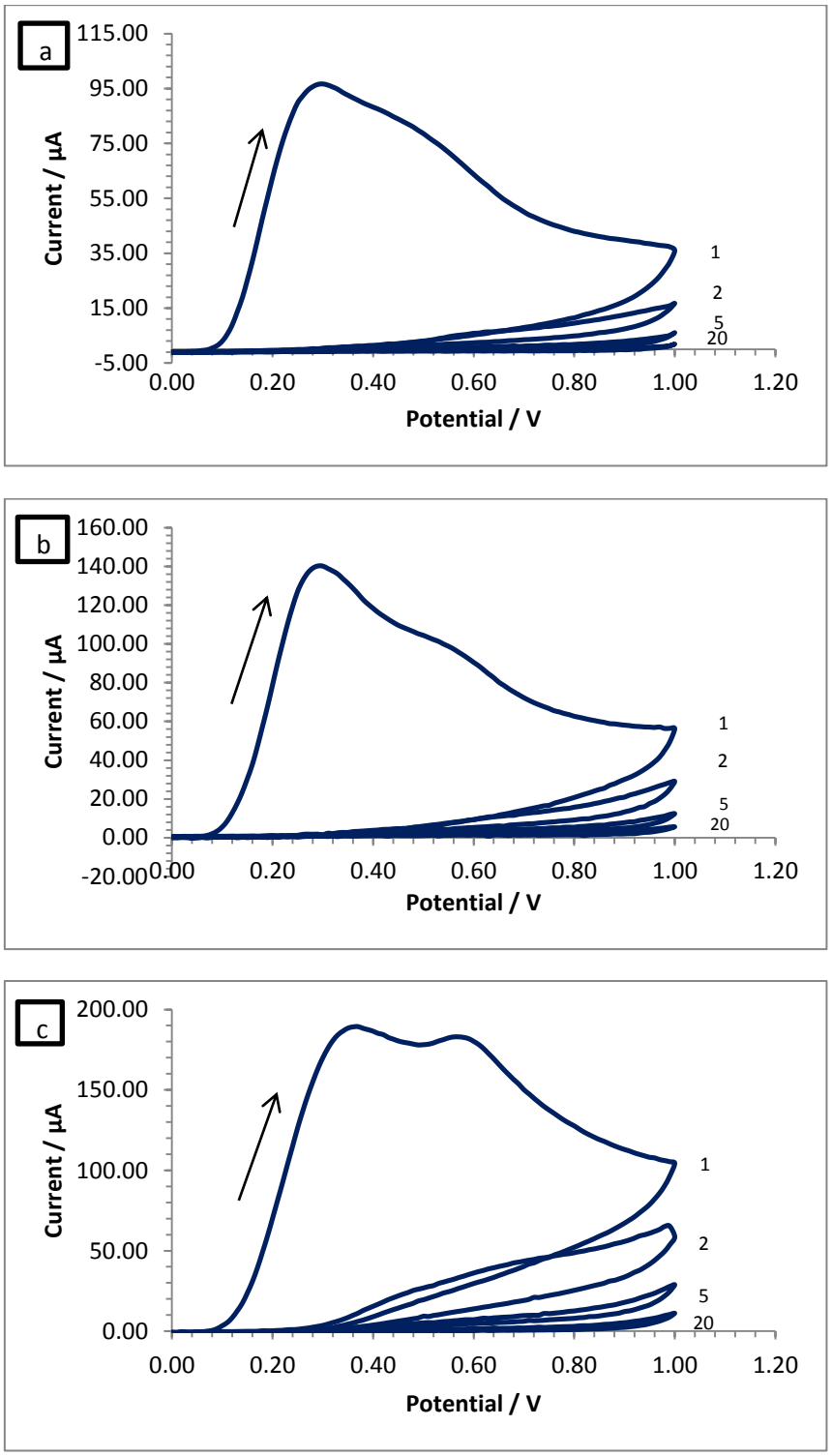

Figure 10.6 - Cyclic voltammograms of the electrodeposition of PoPDA at a). 5 mVs^{-1}, b). 10 mVs^{-1} and c). 20 mVs^{-1} scan rates

Through the examination of the final cycle (i.e. the 20th deposition sweep) from each of the electrodepositions described earlier (scan rates 5, 10 and 20 mVs^{-1}) it is possible to compare the degree by which the electrodes have become insulated by reference to the current levels in this final sweep. This can be observed in Figure 10.7.

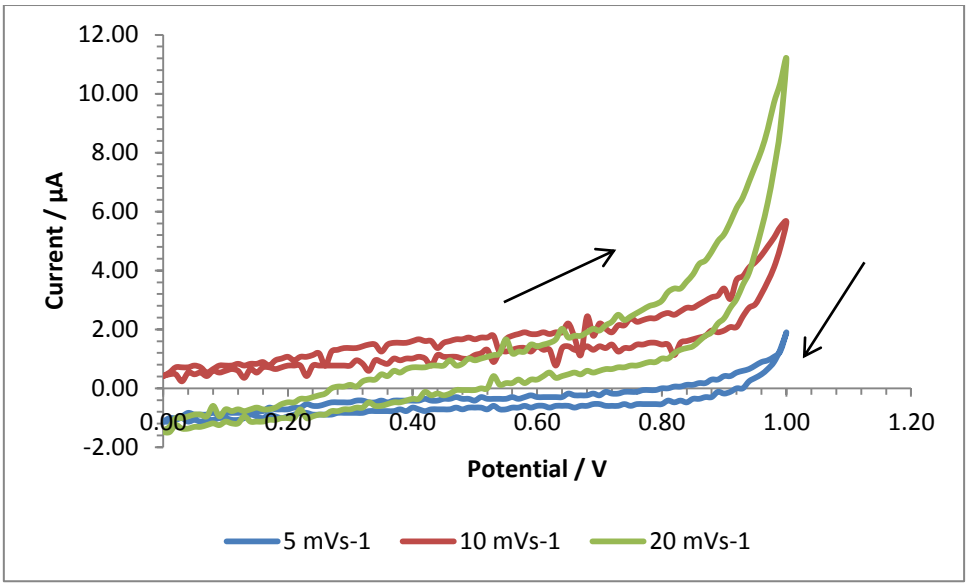

Figure 10.7 – Voltammograms of the final cycle of 20 in the electrodeposition of PoPDA at a scan rate of 5 (blue), 10 (red) and 20 (green) mVs^{-1} vs. Ag/AgCl

It can be seen that the scan rate of 5 mVs^{-1} provides the greatest insulating effect on the sensor since the current output after the 20th cycle is lower than that gained with both the 10 and 20 mVs^{-1} scan rate. This is in close agreement with a similar study on plain carbon screen-printed electrodes (i.e. without doped CoPc) where a scan rate of 5 mVs^{-1} was proven to yield the optimum insulating effect (Gornall, D. D., PhD Thesis, 2004). When a solution containing the redox couple ferrocenemonocarboxylic acid was interrogated with each of these sensors this insulation effect can be demonstrated further as shown in Figure 10.8.

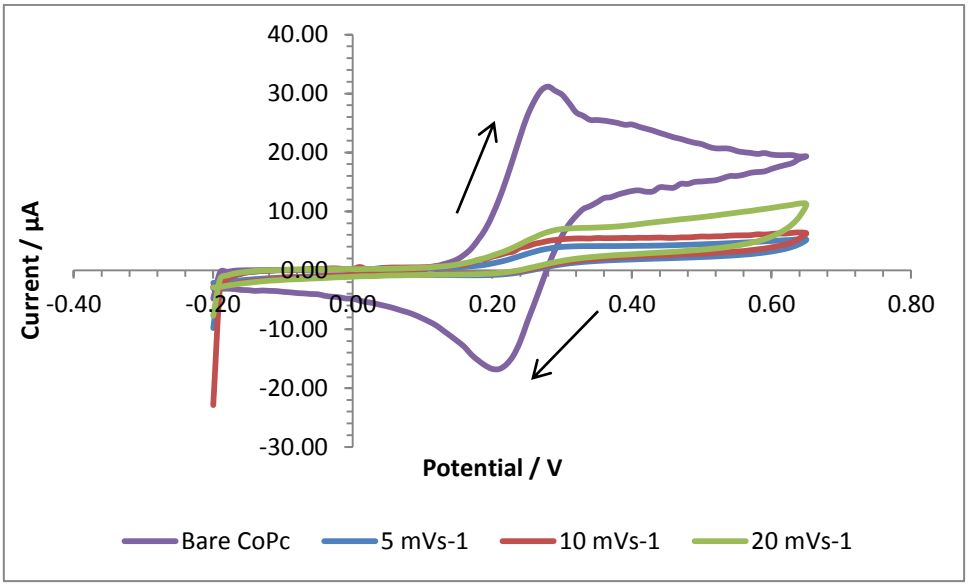

Figure 10.8 - Ferrocenemonocarboxylic acid interrogated with CoPc sensors coated through electropolymerisation with PoPDA at various scan rates for 20 cycles and with a bare, uncoated CoPc sensor for reference

Once more it can be observed that the 5 mVs^{-1} scan rate has given rise to the greatest insulating effect on the CoPc sensors as demonstrated by the low current magnitude in the voltammetric profile in Figure 10.8. It may also be seen, however, that the difference between the 5 and 10 mVs^{-1} scan rate deposition of the polymer is not sufficiently great as to discount using this faster scan rate.

It was reported in the previous section (section 10.2.3) that the number of potential cycles to produce a well-insulated CoPc electrode was 50; to complete this electrodeposition using a scan rate of 5 mVs^{-1}, the time required per sensor would be 5½ hours. The time required to insulate a sensor at a 10 mVs^{-1} scan rate is, consequently, 2¾ hours which halves the time taken to perform this fabrication step with a relatively small effect on the insulation of the sensor. For these reasons within this work a 10 mVs^{-1} scan rate for 50 cycles was performed to coat the sensors with a thin insulating film.

10.2.5. Microscopic examination of the surface topography

The insulated effect can be demonstrated through microscopic examination of the topography of both the bare (Figure 10.9) and PoPDA insulated (Figure 10.10) electrode surface.

The surface topography of the bare CoPc electrode indicates the presence of raised regions which would likely be attributed to the cobalt phthalocyanine particles within the carbon ink matrix. This supposition can be upheld when contrasting this image with that gained from a plain carbon screen-printed electrode where the absence of these raised particulate areas is observed, see Figure 8.2.

It might be expected that the electrodeposition of the insulating thin film would occur in a uniform fashion as reported for plain carbon screen-printed electrode surfaces (Tolan et al., 1996) with the irregularities on the bare surface being observed through the thin film deposited. In this case, however, it can be observed that the PoPDA film has been deposited as 'flake-like' accumulations upon the electrode surface. It may be the case that the raised regions of cobalt phthalocyanine, and therefore the increased electroactivity associated with these areas, have induced a *pseudo*-gel point mechanism. In general, the current at the outer edge of a planar electrode can always be observed to be slightly greater than that in the centre (Liu et al., 2008). As such, it can often be observed that the gel-point is reached around the edges first, inducing film formation from the monomer solution to occur here before deposition initialises in the centre. This can cause a slight irregularity in thin film deposition but is generally overcome with subsequent potential sweeps.

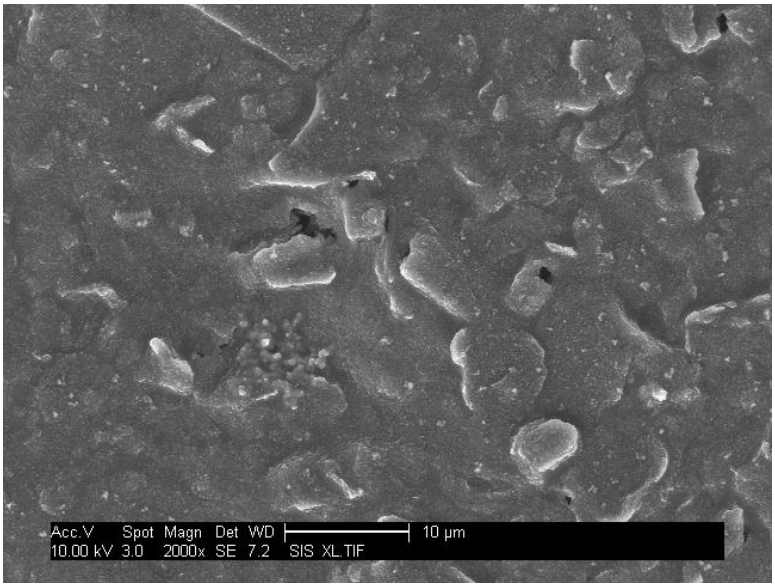

Figure 10.9 - An SFEG scanning electron micrograph of a bare cobalt phthalocyanine screen-printed electrode (at 2000x magnification after sputter coating with gold palladium)

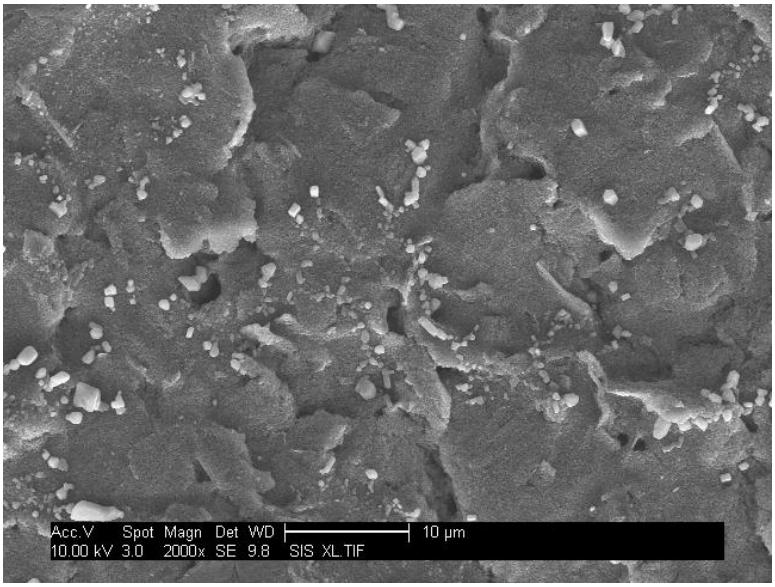

Figure 10.10 - An SFEG scanning electron micrograph of a poly(*o*-phenylenediamine) coated cobalt phthalocyanine screen-printed electrode (at 2000x magnification after sputter coating with gold palladium)

The deposition of PoPDA upon the CoPc-doped screen-printed electrode surface does not seem to retain the observable features on the surface as has been reported with the electrodeposition of polymer films on plain carbon sensors (Barton et al., 2004). The irregularities observed on the surface of the insulated CoPc electrode (Figure 10.10) do not correspond with those on the bare surface of the CoPc electrode (Figure 10.9). The initiation of the polymer formation may have taken place, as postulated

earlier, through a *pseudo*-gel point mechanism where the initiation occurs at the location of the highly electroactive cobalt phthalocyanine particles within the carbon ink and propagates from these areas of high electroactivity rather than the edge of the electrode. This might explain the surface profile observed in Figure 10.10.

The micrograph gained for the CoPc coated electrode surface also illustrates small (approximately 0.5 µm) particles present in the image. As these sensors were sputter-coated with a gold palladium film prior to imaging this may be evident in the images. It may also be the case that these illuminated particles are caused by surface contamination associated with the electrodeposition process or the subsequent washing with first a pH 7.0 phosphate solution and then deionised water. Salt particles remaining on the surface due to washing with the phosphate solution might correspond to this.

10.3. Sonochemical ablation of the insulating polymer to form microelectrode arrays

The electropolymerisation of poly(*o*-phenylenediamine) provided an insulated thin film on the CoPc sensors (as described in section 10.2). The microelectrode array was prepared on these insulated sensors through the ablation caused by exposing them to ultrasound at a frequency of 25 kHz (Myler et al., 1997), see Figure 10.11.

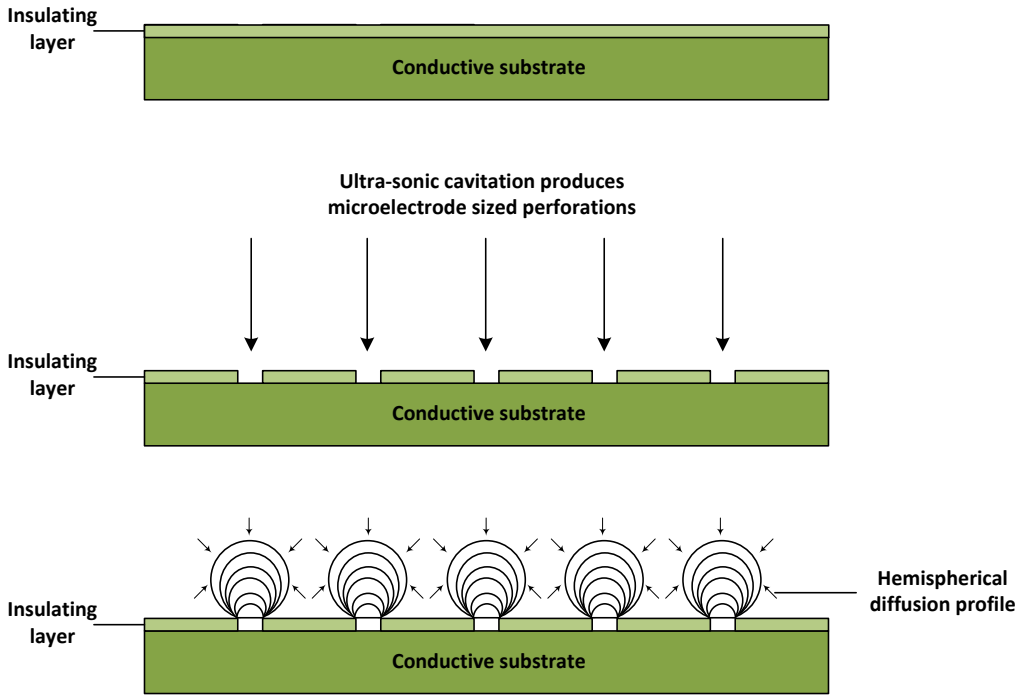

Figure 10.11 - The sonochemical formation of microelectrode array and the resulting hemispherical diffusion profile

Ultrasound when passed through a solvent, such as water, can cause thermal agitation and localised hotspots. The hotspots can be attributed to the rapid compression of gases and vapours; the temperatures associated with this compression have been estimated to be as high as 5000 °C (Flint and Suslick, 1991; Didenko et al., 1999). As these bubbles are small in comparison to the volume of solvent, the overall temperature of the solvent is often unaffected and this causes a rapid cooling of the

bubbles to take place which in turn causes the collapse of these bubbles (Suslick, 1986).

Where there is a solution-surface interface, such as that between the insulated electrode and the solvent (in this instance DI water), the bubbles will collapse asymmetrically and there is an implosion; drawing-in solvent on the side opposite the surface which is then forced out in a micro-jet in the direction of the surface at speeds of up to 100 ms^{-1}(Leighton, 1994). These jets, on contact with the surface of the coated electrode, cause ablations through the relatively soft polymer coating down to the significantly more rigid surface of the carbon ink.

These cavities may then act as nucleation sites for further bubble formation and their subsequent implosions within the confines of the original cavity. These cavities may develop in this manner until a critical size has been achieved and the nucleation of subsequent bubbles becomes favoured less (Suslick, 1990).

10.3.1. Study into the optimal sonication time period

The optimal sonication period for the production of sonochemically fabricated microelectrode arrays has been reported previously as 20 seconds (Barton et al., 2004). Increasing the period at which the sensor was exposed to ultrasonic ablation was demonstrated to increase the population density of the microscopic pores in a near linear fashion, however, the signal variance during stirring was found to significantly increase at periods greater than 20 s (Barton et al., 2004). The microelectrode arrays reported in the literature demonstrated that a 20 second sonication period provided a microelectrode array that demonstrated the characteristic sigmoidal shaped cyclic voltammogram when interrogating a reversible redox couple such as ferrocenemonocarboxylic acid.

To examine whether a 20 second sonication period also provided the optimal microelectrode behaviour when using a PoPDA insulated CoPc sensor a study was performed where sensors sonicated for a variety of lengths of time were used to interrogate a 5 mM solution of ferrocenemonocarboxylic acid. The resulting voltammograms, alongside that gained from an unmodified CoPc sensor, are seen in Figure 10.12.

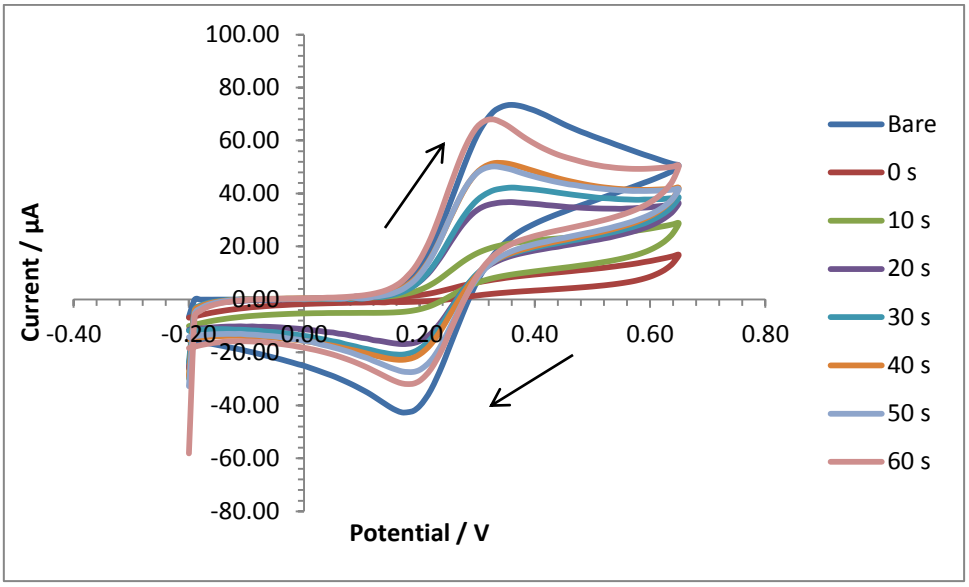

Figure 10.12 - Voltammograms gained of ferrocenemonocarboxylic acid interrogated with a bare CoPc sensor and with CoPc sensors insulated with 5 mM PoPDA (50 scans at 10 mVs^{-1}) and sonicated for varying time periods (at a scan rate of 20 mVs^{-1} vs. Ag/AgCl)

It can be observed in Figure 10.12 that an insulated CoPc sensor that had not been sonicated displays very little voltammetric response when compared to a bare sensor (see the red line – 0 s) which confirms that insulation of the electrode surface has taken place. When an insulated sensor has been sonicated for a 10 s period a sigmoidal shaped profile is observed, where the reductive and oxidative current profiles in a reversible reaction lie very close to one another. This can be indicative of the sensor demonstrating microelectrode behaviour and, therefore, that a microelectrode array has indeed been formed. This can be better observed in Figure 10.13.

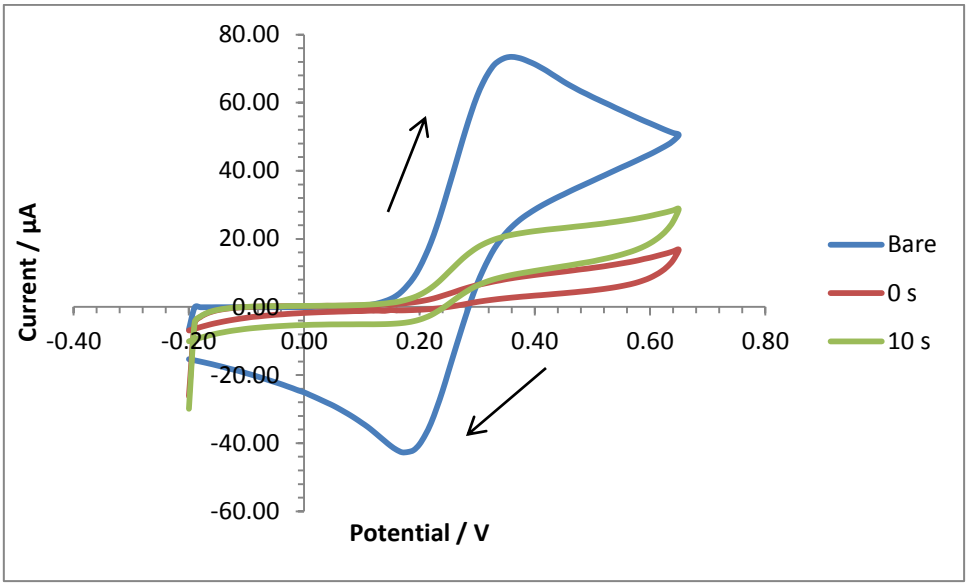

Figure 10.13 - Cyclic voltammograms of a bare, an insulated and an insulated with a 10 s sonication period CoPc sensor in 5 mM ferrocenemonocarboxylic acid (20 mVs^{-1} scan rate vs. Ag/AgCl)

With increasing sonication periods the voltammetric response profile of ferrocenemonocarboxylic acid interrogated with the various sensors can be seen to gradually become more like of a bare CoPc sensor (see dark blue line in Figure 10.12 and 10.13) as the size and number of cavities within the insulating polymer increase. As the population of the cavities increase, the hemispherical diffusional profiles associated with the individual microelectrodes within the array can begin to overlap; this causes the loss of the microelectrode effect and the array will begin to demonstrate characteristics more akin to a planar electrode surface.

As a 10 s sonication period appears to demonstrate this microelectrode effect, and those sensors with 20 s sonication periods have begun to lose the characteristic sigmoidal shaped voltammetric profile associated with microelectrodes, a ten second sonication period will be used for all further studies unless otherwise stated.

10.3.2. Microscopic examination of the microelectrode array

To better characterise the sonochemically fabricated microelectrode array, scanning electron microscopy was utilised so that visual confirmation of the pore structure on the surface of the CoPc sensor was performed. With a 10 second sonication period small cavities appear in the insulated surface of the sensor, see Figure 10.14. It can be seen that there is a random distribution of pores in the surface, which is as might be expected due to the chaotic cavitation process that takes place in the ultrasonic bath.

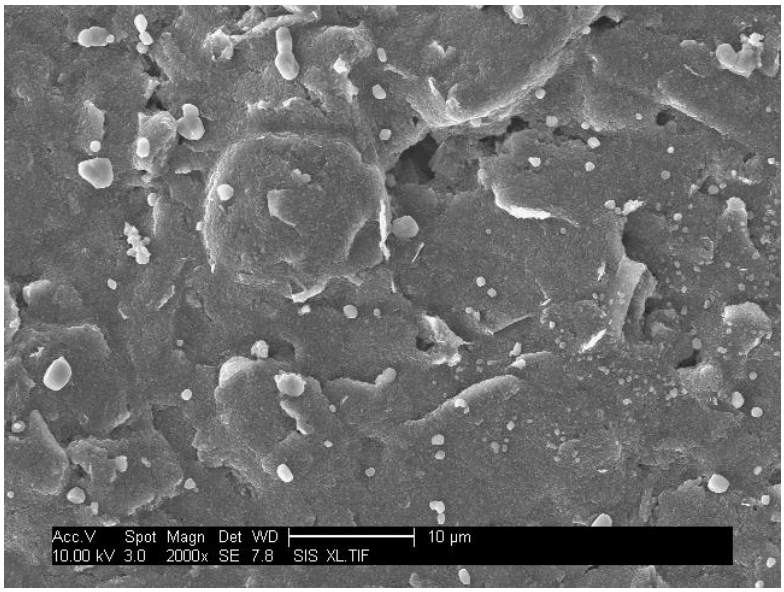

Figure 10.14 - An SFEG scanning electron micrograph of a poly(o-phenylenediamine) coated cobalt phthalocyanine screen-printed electrode microelectrode array produced after 10 seconds in a sonication bath (at 2000x magnification after sputter coating with gold palladium)

The cavities can be seen to vary in size, with the largest pore observed here possessing a diameter of approximately 3 µm. As mentioned previously, after initial cavitation caused by micro-jets of solvent from imploding superheated bubbles, further bubble formation can take place at these cavitation sites. This enlarges the initial pore until it reaches a size that no longer acts as a nucleation site. This explains the range of pore sizes observed in Figure 10.14.

An electron micrograph of the PoPDA insulated CoPc sensor and of the sensor with a 10 second sonication period is presented below at a greater magnification than in

Figure 10.14 which makes it possible to observe the cavity in more detail, see Figure 10.15.

Image a **Image b**

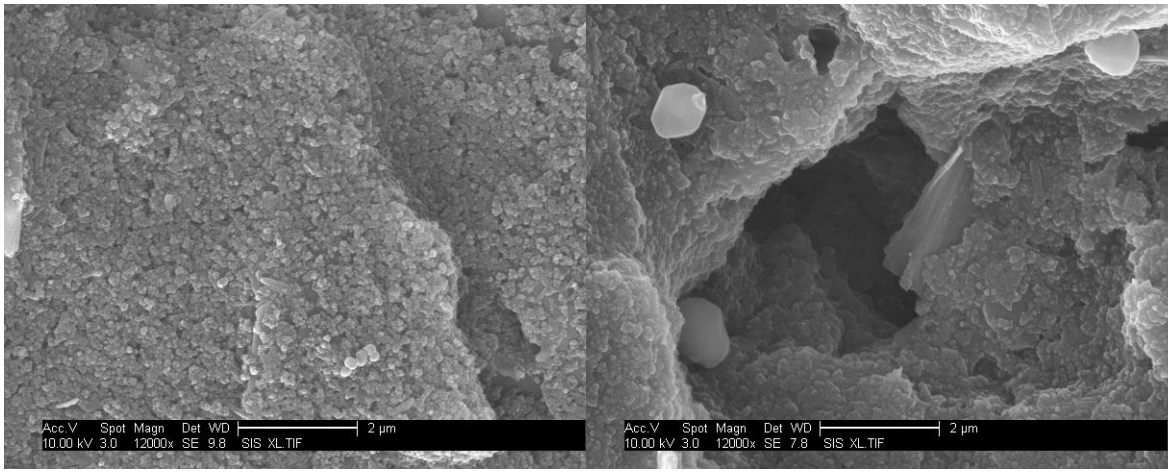

Figure 10.15 - An SFEG scanning electron micrograph of a). a poly(o-phenylenediamine) coated cobalt phthalocyanine screen-printed electrode and b). a cavity in the microelectrode array after 10 s sonication (at 12000x magnification after sputter coating with gold palladium)

Here, the difference between the insulated and the ultrasonically ablated sensor surface is clear, with a large cavity in the latter appearing to be punctured through the insulating polymer with the implication that it reaches the surface of the CoPc sensor, thus creating a microelectrode.

10.3.3. Study into the stir-independent characteristics of the sonochemically fabricated microelectrode array

The stir-independent properties offered by microelectrodes are one of the central advantages in the utilisation of microelectrode based arrays. The ability of microelectrodes in an array format to remain unaffected by the convection of a solution under analysis enables sensors incorporating this characteristic to be utilised in flowing systems such as, for example, *in vivo* analyses within living organisms or to enable detection within other analytical techniques such as high-performance liquid chromatography (HPLC) or capillary electrophoresis (CE') (Štulík et al., 2000).

Although in the context of this project the necessity for a stir-independent system is not an essential aspect, as the intention is not to produce a system required for use in a flowing environment, the analysis of the stir-independence provides another means to assess the presence and function of the microelectrode array.

The stir-independence associated with a single microelectrode can be related to the hemispherical diffusional profile which allows the rate of mass transportation of reactants and products to be significantly greater than that achieved with a planar electrode due to the increased area under the influence of the microelectrode's diffusional control. Other processes that might negatively affect a planar electrode, such as convection, are found to have less influence upon the microelectrode as the rate of diffusion is greater than the rate of convection and, as such, a steady state current response is maintained independent of the flow characteristics within the system.

This stir-independence may also be observed in microelectrode arrays where the centre to centre distance between each microelectrode in the array is sufficiently large that the hemispherical diffusional profile related to each does not overlap, leading to the individual fields merging, thus forming a linear diffusion layer analogous to macroelectrodes of the same total surface area.

To assess the stir-independent properties of the sonochemically fabricated microelectrode arrays on both plain carbon and CoPc-doped carbon sensors (produced

as described earlier in this chapter) chronoamperometric investigations were initially performed where the microelectrode array was polarised at +0.35 mV in a solution of 5 mM ferrocenemonocarboxylic acid or a pH 7.0 phosphate buffer solution for 300 seconds. After a quiescent time period of 60 seconds, convection was applied to the solution using a stirring plate (with a magnetic flea in the analyte beaker) and at 180 seconds the stirring was terminated. The results of this were compared to those from unmodified, planar electrodes analysed in the same manner.

It can be observed for both the bare carbon (Figure 10.16) and the bare CoPc-doped sensor (Figure 10.17) interrogations that there is a clear influence on the resulting current response when using these unmodified, planar electrodes once convection is applied to the system. Convection does not, however, display as great an influence on the microelectrode arrays formed on both of these systems. This can be clearly observed in Figure 10.16, where the introduction of stirring yields a negligible increase in current response when interrogating with a microelectrode array in comparison to a planar surface. The percentage change due to the application of convection can be calculated for both examples of the plain carbon sensors which was found to be 144 % and 20 % for the carbon planar sensor and the microelectrode array, respectively.

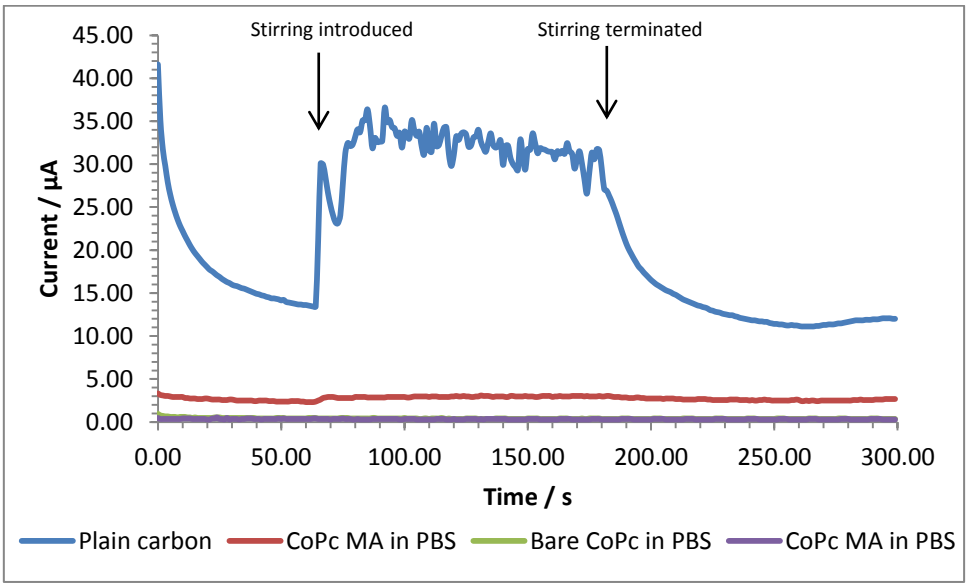

Figure 10.16 - Stir-independence study using carbon screen-printed sensors (where the bare sensor is the blue or green line and the microelectrode array is the red or purple line) in a 5 mM ferrocenemonocarboxylic acid solution or a pH7 phosphate buffer solution where the potential was held at +0.35 mV for 300 seconds and the stirring applied after 60 s and terminated at 180 s.

The stirring speed was set at a high speed (200 rotations per minute), greater than what might be expected in a real-life situation and whilst the microelectrode array has not negated the influence of convection completely, it has diminished its effect on the system considerably.

The CoPc sensors were found to perform in a similar manner as the plain carbon sensors when assessing the stir-independence in a steady-state chromoamperometric study (in FeCA). With the application of stirring there is again a demonstrated influence on the resulting current response achieved with a planar CoPc sensors (see Figure 10.17). It is worth noting here that the current response for CoPc microelectrode arrays, prior to solution agitation, is comparable to that obtained for an unmodified CoPc planar sensor. It is evident, however, that in the case of undoped carbon (Fig 10.16), this response is seen to decrease for MA's when compared to bare carbon, when tested in FeCA. As the direction of work is aimed towards utilising CoPc electrodes for the measurement of nitroaromatic species, all MA fabrication steps were aimed at producing the best MA's on CoPc-doped sensors. Whilst a current response is obviously evident for FeCA solutions tested on undoped carbon MA's the signal is lower than observed on a bare undoped carbon (Fig 10.16 red and blue plots, respectively). It is suggested here that an enhancement in signal response, whilst retaining stir-independent behaviour, for this system is achievable by further investigations into the fabrication of these undoped carbon MA's as has been undertaken on the CoPc doped version. It can be seen, however, that again in this instance, the percentage increase from the steady state baseline between 50 and 60 s and the current response during stirring (90 to 100 s) was 465 % for the planar electrode and only 19% for the microelectrode array.

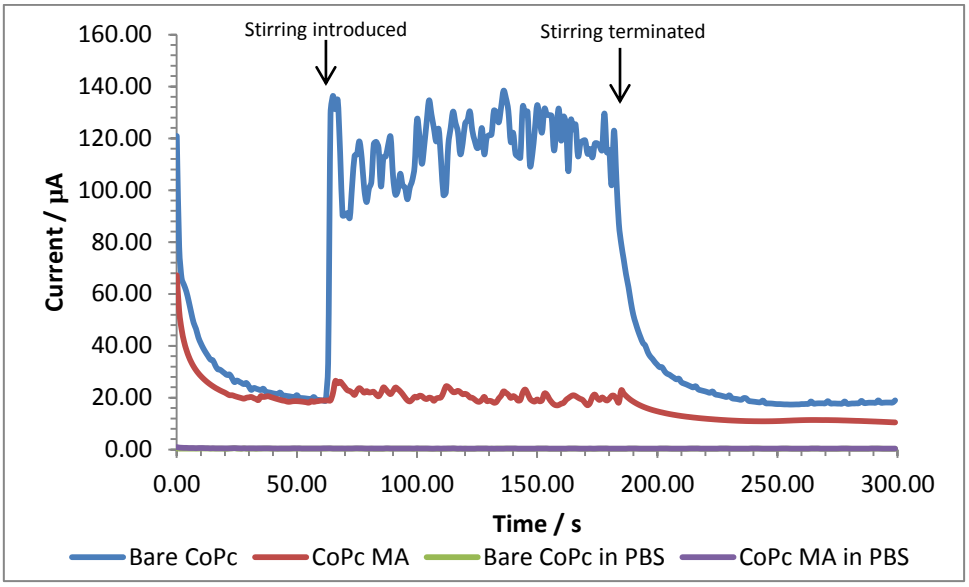

Figure 10.17 - Stir-independence study using the CoPc sensors (where the bare CoPc sensors are the blue and green line and the CoPc microelectrode arrays are the red or purple line) in a 5 mM ferrocenemonocarboxylic acid or pH 7.0 phosphate buffer solution where the potential was held at +0.35 mV for 300 seconds and the stirring applied after 60 s and terminated at 180 s.

As this work is aimed towards the electrochemical detection of nitroaromatic species, utilising CoPc microelectrode arrays for their detection and analysis, the stir-independence of these CoPc cavity microelectrode arrays was also analysed in a pH 7.0 phosphate buffer solution with 200 µM TNT. The potential was held at -0.50 V, corresponding to a reductive peak present in this region as observed previously in Section 8.3., all other experimental parameters were maintained as described above.

The planar CoPc sensor can again be observed to be influenced by convection (Figure 10.18). There is also an influence on the current response related to the microelectrode array caused by the initiation of stirring within the system, although it can be observed that this is not as pronounced as that with the planar electrode. The relative percentage change from the steady-state baseline (50-60 s) to the response under convection (90-100 s) was calculated to be 447 % and 109 % for the bare sensor and the microelectrode array, respectively.

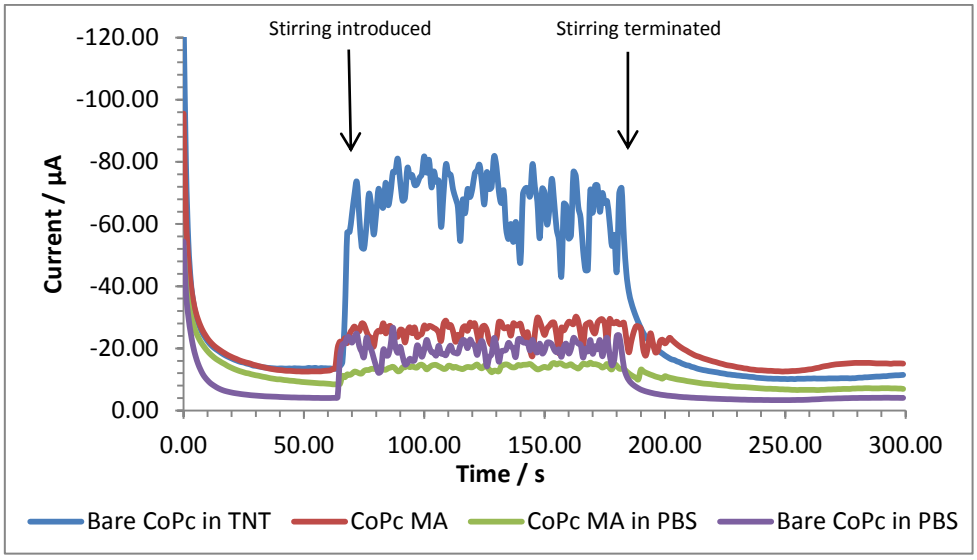

Figure 10.18 - Stir-independence study using the CoPc sensors (where the planar CoPc sensor is the blue line, CoPc microelectrode array is the red line) in a 200 µM TNT solution or a pH 7.0 phosphate buffer solution where the potential was held at -0.50 mV for 300 seconds and the stirring applied after 60 s and terminated at 180 s.

The steady-state transient chart for the interrogation of a solution of TNT does broadly correspond to the study undertaken with 5 mM FeCA. Convection again demonstrates a significant influence on the signal response gained from planar electrodes and a marked decrease in this influence is observed when stirring was introduced to the system containing the microelectrode array.

There is a significant difference between microelectrode arrays formed on a plain carbon electrode and a CoPc-doped electrode when investigating their stir-independence properties. The plain carbon microelectrode arrays are influenced much less by the application of convection; it is postulated that the electroactive nature of the CoPc particles within the carbon ink matrix of the CoPc-doped microelectrodes is such that the diffusional profiles are correspondingly greater. This may cause an overlap of these profiles. The inter-electrode distance has been suggested as the most critical aspect in the optimisation of microelectrode arrays (Morf, 1996). It may, therefore, be necessary to increase the distance between individual microelectrodes within the array through a reduced sonication period, or variations in the ultrasonic frequency applied (set at a fixed 25 kHz for all investigations due to tank limitations) to counteract this trend.

10.4. Trinitrotoluene detection with a microelectrode array

10.4.1. Interrogation of TNT with the cavity microelectrode array

Unless otherwise stated, all interrogations take place including 20 units NTR and 0.1 mM NADPH within the analyte solution.

Prior to the interrogation of TNT with the microelectrode array a baseline recording was performed which entailed the interrogation of a pH 7.0 phosphate buffer solution to establish any electrochemical properties that may appear in the resulting voltammogram, see Figure 10.19. The microelectrode array was fabricated as described above and, briefly, involved first the insulating of a CoPc sensor with PoPDA (50 scans at 10 mVs^{-1} vs. Ag/AgCl) before a 10 second sonication process within an ultrasonic bath.

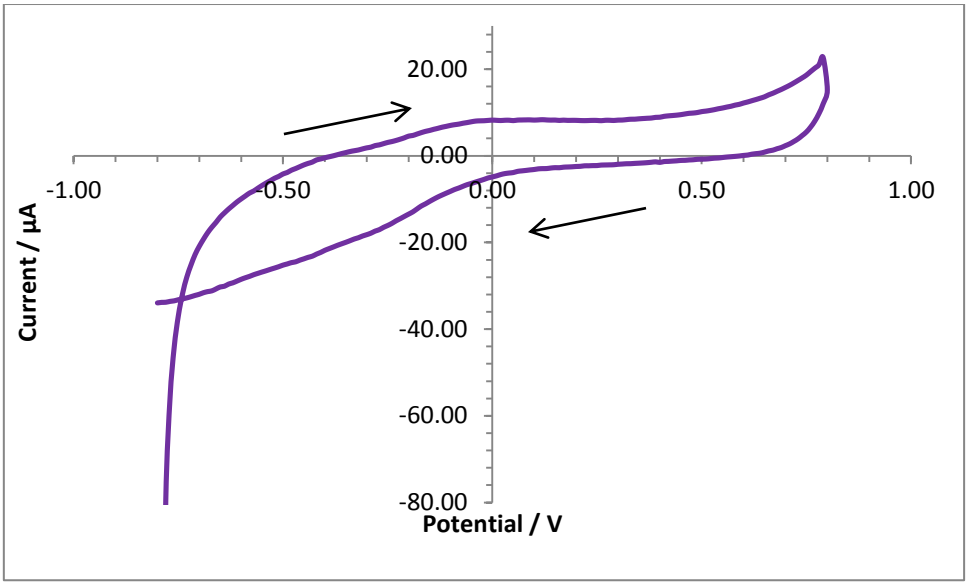

Figure 10.19 - Cyclic voltammogram of pH 7.0 phosphate buffer solution interrogated with a microelectrode array (developed as described previously) at a scan rate of 20 mVs^{-1} vs. Ag/AgCl

The resulting voltammetric profile is can be observed to be divergent from that gained with a plain CoPc sensor without prior pre-treatment or insulation (Figure 10.20). The peak that was observed in the latter interrogations at a potential position of -0.50 V (vs. Ag/AgCl) is not apparent as a definitive peak, but there is a large shoulder-like peak

present in the cathodic region of the voltammogram gained with the microelectrode array that may correspond to this.

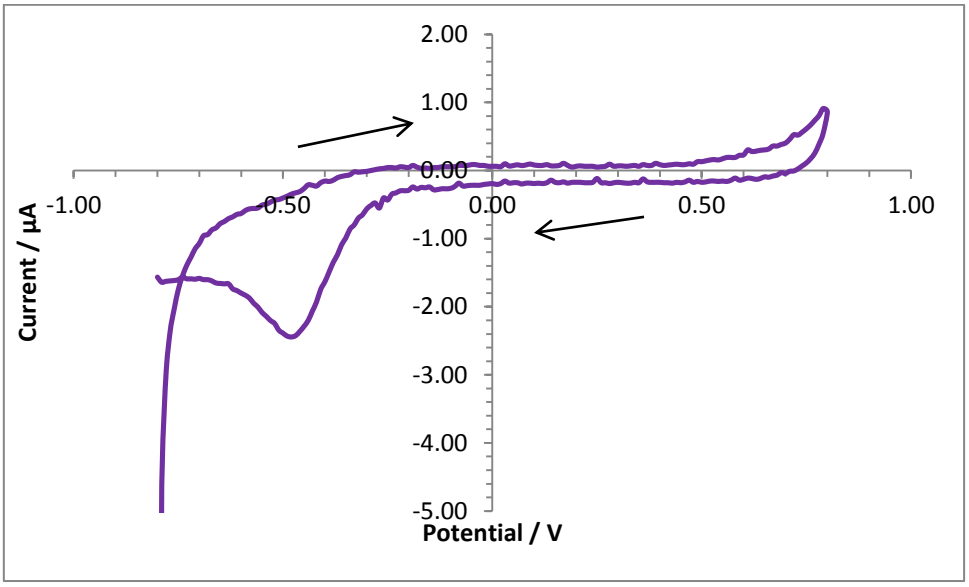

Figure 10.20 - Cyclic voltammogram of pH 7.0 phosphate buffer solution interrogated with an unmodified CoPc sensor at a scan rate of 20 mVs^{-1} vs. Ag/AgCl

Perhaps the most obvious feature to note is the significant increase in the magnitude of the current response gained with the microelectrode array. A comparison of the peak area from the cathodic region (-0.2 to -0.8 V vs. Ag/AgCl) found that while the peak current for a plain CoPc sensor was just 0.88 µA, for the same region with the microelectrode array the peak current was 15.11 µA. Individual microelectrodes offer only very small responses and, therefore, this substantial increase in the magnitude of the current response must demonstrate that a microelectrode array has been fabricated.

A phosphate buffer solution with 200 µM of TNT was subsequently interrogated in the same manner as described previously, briefly a voltammetric sweep was performed between -0.8 and +0.8 V. The recorded profile is shown in Figure 10.21.

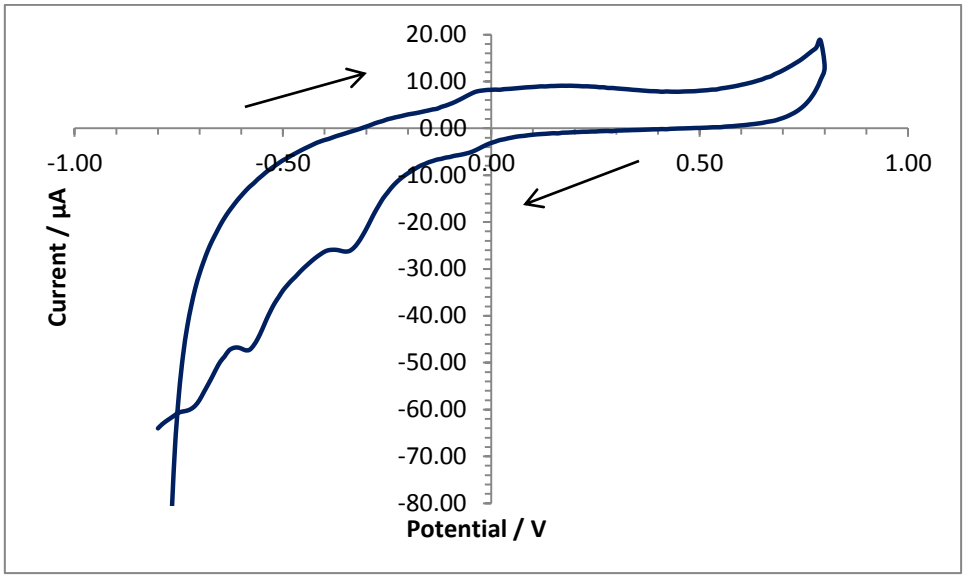

Figure 10.21 - Cyclic voltammogram of 200 µM TNT in phosphate buffer solution on a microelectrode array (developed as described previously) at a scan rate of 20 mVs^{-1} vs. Ag/AgCl without deoxygenation

The voltammetric profile gained when interrogating the TNT solution with the microelectrode array is similar to that gained for a plain CoPc sensor; the cathodic region contains a shoulder with three definitive reductive peaks present at -0.35, -0.60 and -0.72 V (vs. Ag/AgCl). A noticeable difference to the current profile gained with a plain CoPc sensor is the change in the redox peaks normally apparent at +0.01 and -0.11 V, see Figure 10.22. In the voltammogram obtained with the microelectrode array these clear peaks are not present, although there does seem to be a very slight oxidative and reductive peak present at -0.06 and -0.09 V, respectively. A comparison of the voltammogram obtained with a plain CoPc sensor and one modified into a microelectrode array can be seen below in Figure 10.22.

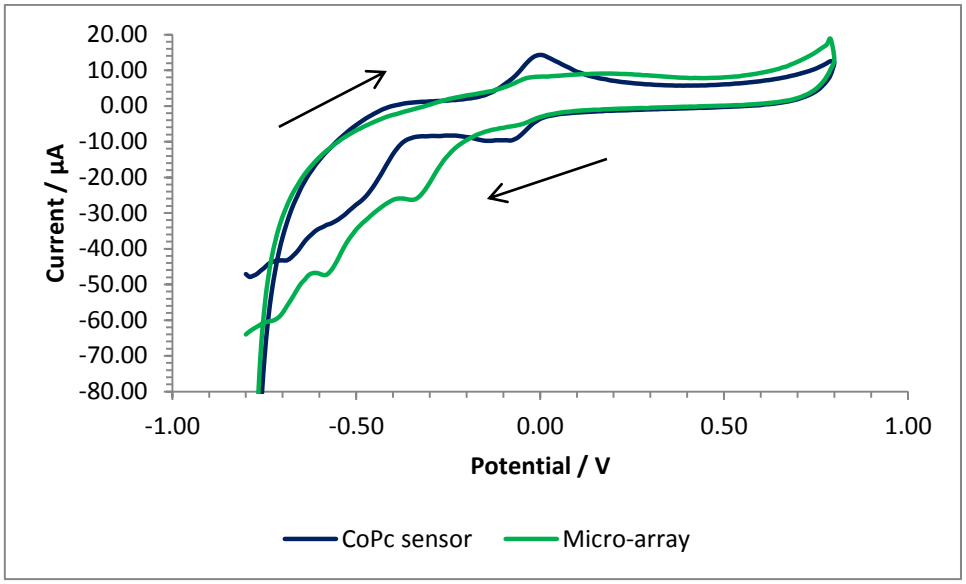

Figure 10.22 - Cyclic voltammogram of 200 µM TNT in phosphate buffer solution on a plain CoPc sensor (green line) and a microelectrode array (blue line) (developed as described previously) at a scan rate of 20 mVs^{-1} vs. Ag/AgCl without deoxygenation

The reductive peaks apparent in the cathodic region are, as stated previously, similar when the TNT solution is interrogated with a plain CoPc sensor and a microelectrode array (MA); the signal differentiation, however, can be seen to have improved significantly with the MA. There are definitive peaks at -0.45 and -0.60 V as opposed to a broader peak at -0.50 V on the unmodified CoPc sensor. Enhanced electrochemical characteristics afforded by the MA's have clearly defined the 3 TNT reductions (relating to each nitro group on the aromatic ring) by splitting the peak at -0.50 V into two distinct reduction peaks. The peak area of the cathodic region (from -0.2 to -0.8 V vs. Ag/AgCl) was calculated for both sensor system and was found to be 15.10 µA for the plain CoPc sensor and 21.74 µA for the microelectrode array demonstrating an improvement in response.

A voltammetric profile of 200 µM TNT with and without deoxygenation is provided below in Figure 10.23.

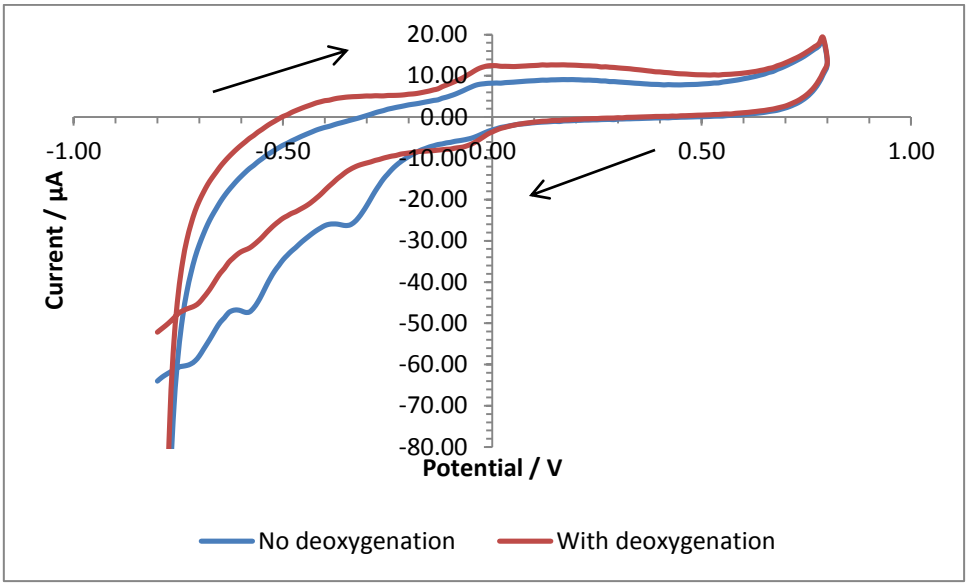

Figure 10.23 - A comparison between the voltammograms of 200 µM TNT in phosphate buffer solution gained with a microelectrode array either with deoxygenation for 10 minutes (red line) or without this deoxygenation period (blue line) at a scan rate of 20 mVs^{-1} vs. Ag/AgCl

It can be seen that the reductive peaks in the cathodic region begin to lose clarity and the magnitude of the current response diminishes with the ten minute deoxygenation step as seen in Figure 10.23. This was also the case when a deoxygenation process was applied in the plain CoPc and the plain carbon sensor interrogations. The reasons for this were given previously as being attributed to reduction of any dissolved oxygen in the solution overlapping with the reductive peaks present in the electrochemical reduction of TNT.

It is interesting to note that, as also described previously, the redox peaks at -0.01 and -0.10 V increase with the deoxygenation process; this was attributed to the oxygen in the system acting as an electron acceptor, thus competing with the reversible reductive reaction of the hydroxylamine groups on the aromatic compound to their amine moiety. The TNT voltammetric profile gained with the microelectrode array showed little evidence of these peaks, but following a deoxygenation step, they become apparent once the oxygen has been removed from the system.

The deoxygenation step, when interrogating the nitroaromatic compound with a microelectrode array, does not seem to offer any clear benefit other than the increased magnitude of the redox peaks; the reductive peaks seem to suffer

disproportionately with the removal of oxygen from the system – more so than with the plain carbon and CoPc sensors where the clarity of the peaks remained the same, it was only the magnitude of the current response that was diminished. As such, work undertaken with the microelectrode arrays will be done both with and without a deoxygenation period and both voltammograms will be included for comparison.

10.4.2. The effect of TNT concentration on the current responses gained with a microelectrode array

The increasing concentration of TNT has, in previous studies with the various screen-printed sensor systems, increased the magnitude of the current response (Chapters 5 and 7-10). This has been shown to exhibit a near linear response in all cases, both with and without deoxygenation, and with low error. This is demonstrated more so in a system that has undergone a deoxygenation step prior to interrogation.

The electrochemical interrogation of various concentrations of TNT in a phosphate buffer solution was performed with the microelectrode array fabricated as described in this chapter. This was performed both with and without prior deoxygenation as this step was found to diminish the peak clarity and magnitude (see section 10.4.1). A control demonstrating the interrogation of simply the phosphate buffer solution can be found in the previous section (see Figure 10.19) for comparison. Presented first is a set of voltammograms gained using cyclic voltammetry swept between -0.8 and +0.8 V (vs. Ag/AgCl) with increasing concentrations of TNT, see Figure 10.24, where part a). was performed without deoxygenation and part b). included a prior ten minute deoxygenation period with argon.

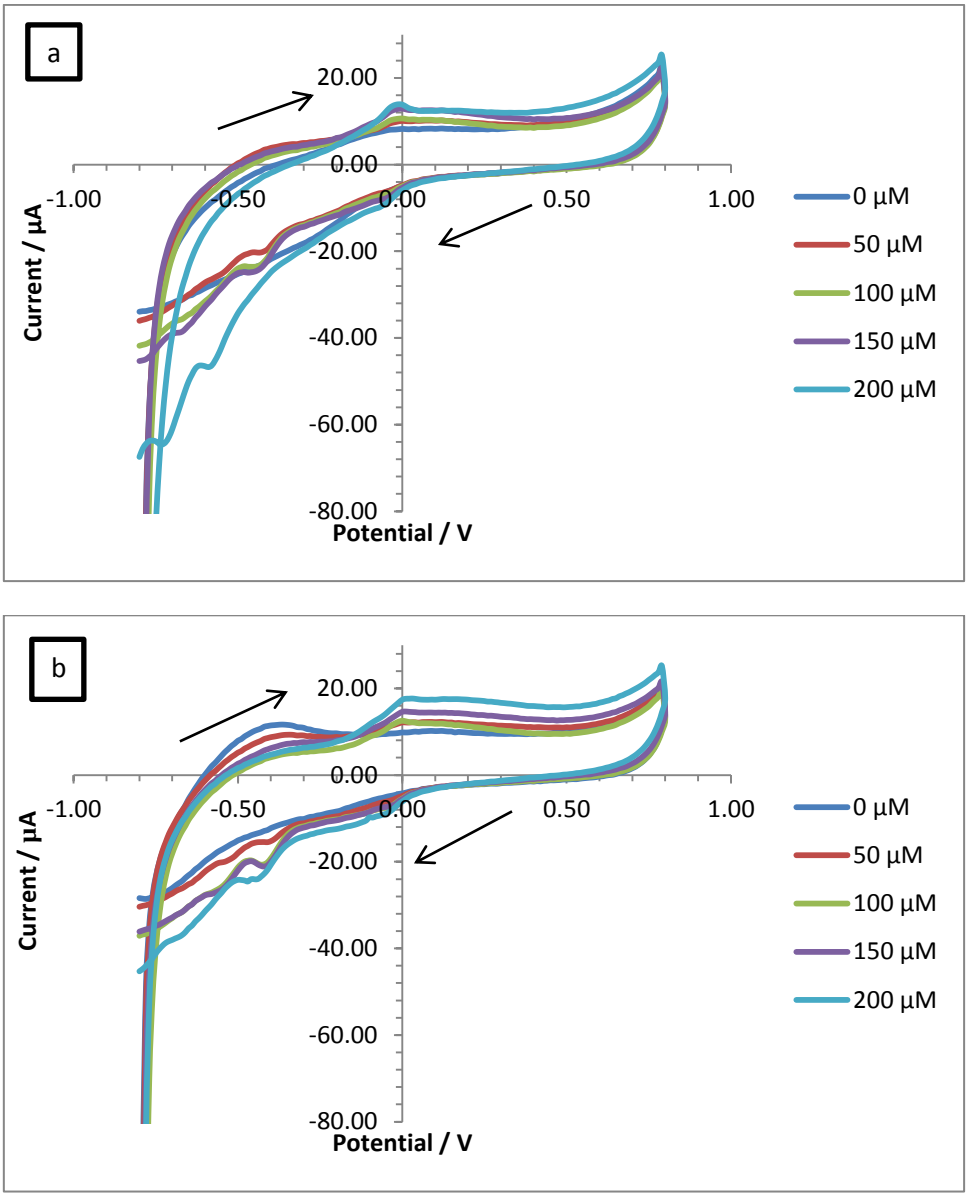

Figure 10.24 - Cyclic voltammograms demonstrating the increasing concentrations of TNT interrogated with a microelectrode array (produced as described previously) in a phosphate buffer where a). is without deoxygenation and b). is with a 10 minute deoxygenation period (scan rate 20 mVs^{-1} vs. Ag/AgCl)

Perhaps the most notable aspect to these voltammetric profiles is the magnitude of the current response observed for the phosphate buffer without the presence of TNT. It is also worth noting that previously there was a significant increase in current response with the increasing addition of TNT on plain carbon and CoPc-doped sensors which is not apparent when interrogated with the microelectrode array.

When the deoxygenation step was included, the clarity of the peaks, as mentioned previously, was diminished somewhat; as were the magnitude of responses in the

cathodic region. This does correspond to the consequences of deoxygenation when interrogation was performed with a planar, unmodified screen-printed sensor. The redox couple, representing the reversible electrochemical reduction of the hydroxylamine groups on the aromatic ring, can be observed to increase with the inclusion of deoxygenation with argon.

Calibration plots were produced to better examine the concentration profiles of TNT interrogated with the microelectrode array both with and without deoxygenation. From the possible five peaks present in the voltammetric profile, three peaks have been selected to study from both the deoxygenated and non-deoxygenated data. These three peaks, selected for their clarity in all interrogations performed, are those known as R1a (-0.72 V), R2 (-0.10 V) and O1 (-0.01 V) vs. Ag/AgCl.

The calibration plots for the largest reductive peak, R1a, can be observed below in Figure 10.25.

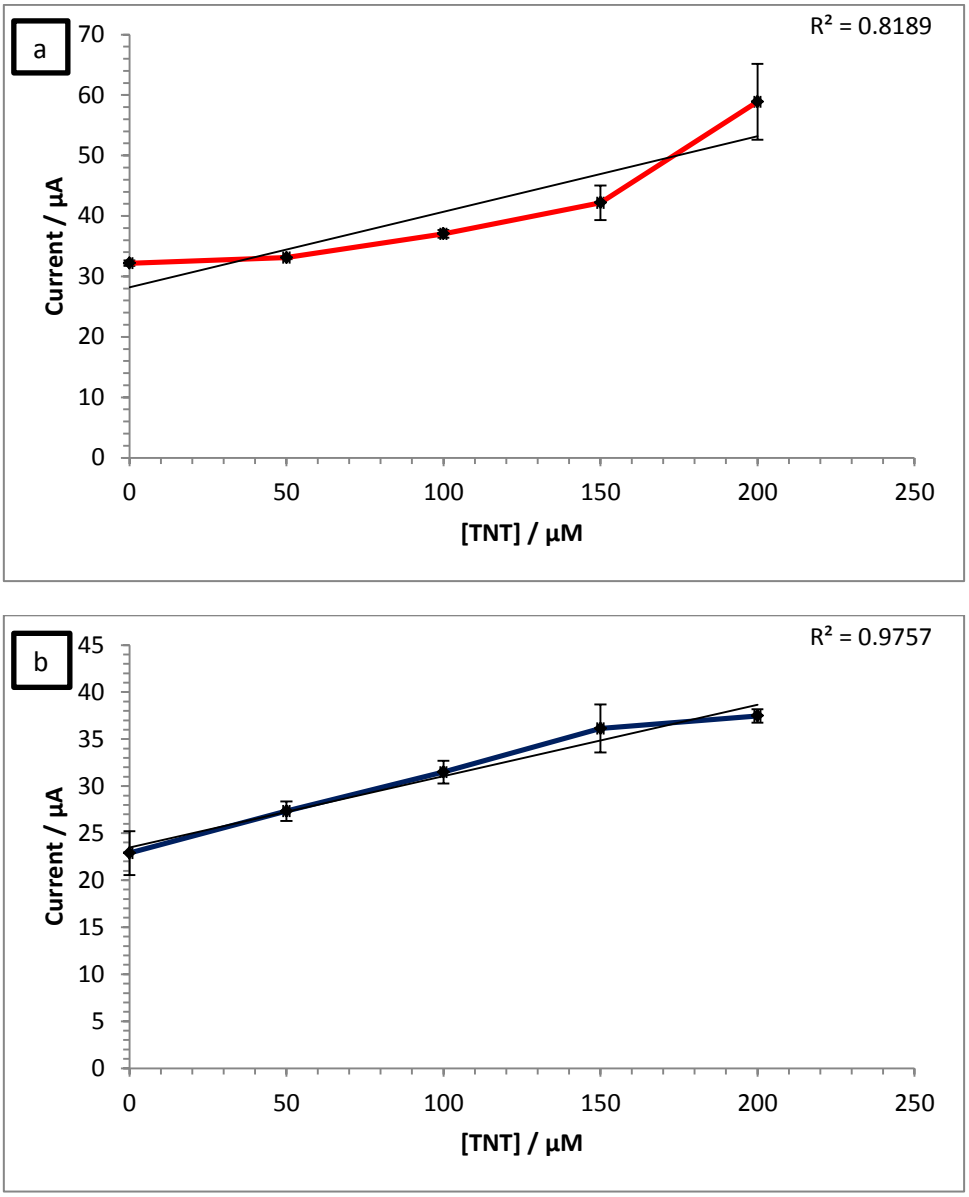

Figure 10.25 - Calibration plots taken from peak -0.72 V (R1a) where a). is without prior deoxygenation and b). has undergone a ten minute deoxygenation with argon (scan rate 20 mVs^{-1} vs. Ag/AgCl; n=3)

The R^2 value for the calibration plot gained from the voltammetric profiles produced without prior deoxygenation are quoted here for reference as it is clear to see that there is very little linearity and signal differentiation at lower concentrations demonstrated when interrogating a TNT solution with the microelectrode array. This statement can be supported through the relatively low error in terms of reproducibility as displayed through the small error bars – the RSDs for 0, 50 and 100 µM was 1.4, 0.8 and 1.8 %, respectively. This would indicate that these results are not due to one anomalous data point and therefore there must be another cause for the lack of

sensitivity at the lower concentration level – something that is not expected due to enhanced characteristics exhibited by the microelectrode arrays.

It may be the case that, as the microelectrode array is essentially comprised of many cavities within the polymer surface that once the sensor is submerged these cavities fill with TNT solution. This may cause a hindrance effect that prevents the free movement of the analyte of interest towards and away from the electrode surface in a static solution. This might explain or at least contribute to the relatively reproducible but low magnitude of current response.

The amount of enzyme available in the solution may also be a factor influencing the limited differentiation with increasing concentrations of TNT, at present only 20 units are available in a 1 ml solution – the dispersal of this enzyme is obviously random within the TNT solution, hence there possibly being areas in the vicinity of the microelectrode array without any enzyme present. Whilst TNT can be electrochemically reduced without the presence of the enzyme, the addition has been demonstrated previously to improve current magnitude (Chapter 7) and peak clarity (Chapter 9).

An examination of the calibration plots associated with the redox couple (at -0.01 and -0.10 V vs. Ag/AgCl) both with and without deoxygenation can be seen in Figure 10.26 and Figure 10.27.

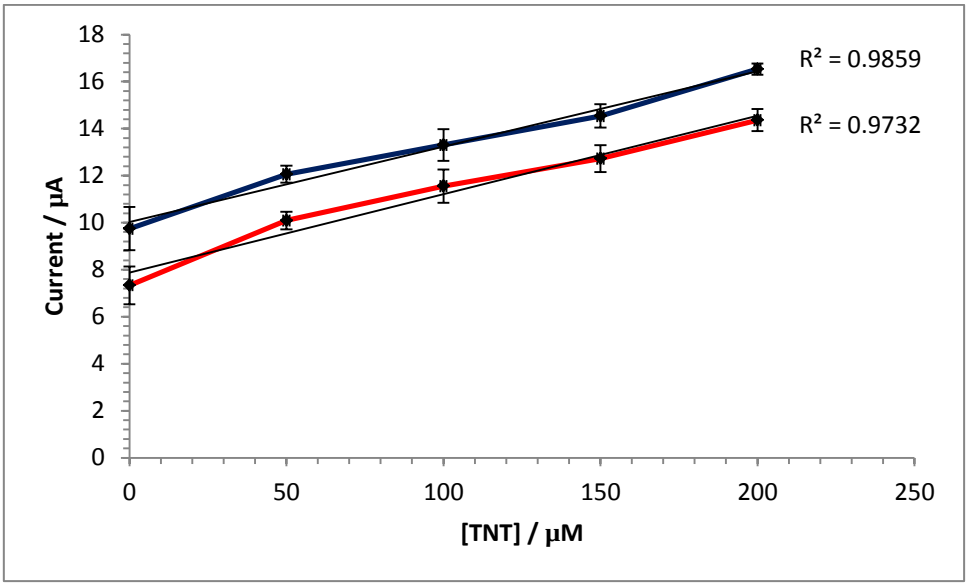

Figure 10.26 - Calibration plots of increasing TNT interrogated with the microelectrode array either with 10 minutes deoxygenation (blue line) or without this step (red line) taken from the oxidative peak at -0.01 V (scan rate 20 mVs^{-1} vs. Ag/AgCl)

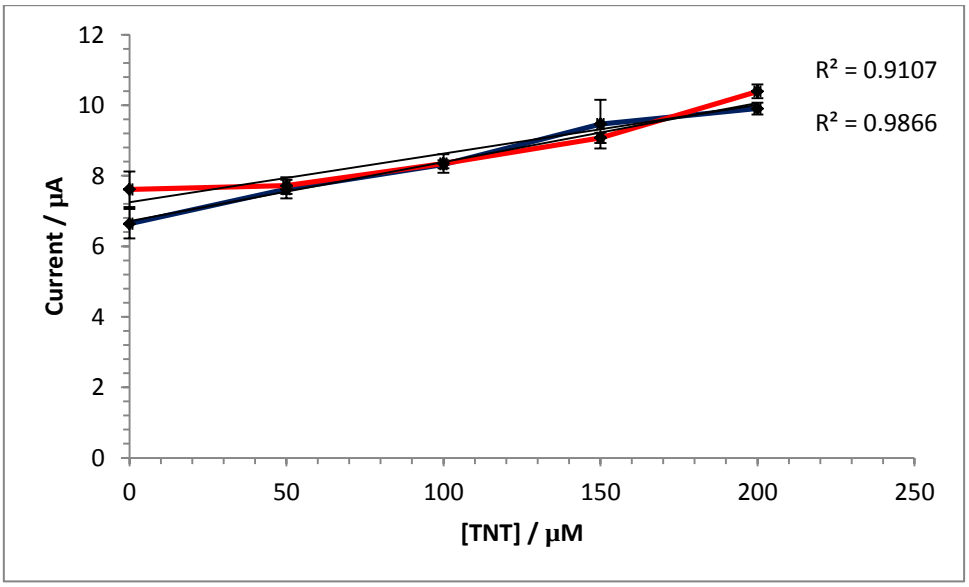

Figure 10.27 - Calibration plots of increasing TNT interrogated with the microelectrode array either with 10 minutes deoxygenation (blue line) or without this step (red line) taken from the reductive peak at -0.10 V (scan rate 20 mVs^{-1} vs. Ag/AgCl)

It can be observed in the calibration plots taken from the redox couple seen at approximately 0 V (-0.01 V for the oxidative and -0.10 V for the reductive peak) that the oxidative peak increases with the inclusion of a deoxygenation period whilst the reductive peak remains largely the same. This is in contrast to the outcome of the

deoxygenation period with planar electrodes where both redox peaks increased with the removal of oxygen as a competitive electron acceptor within the solution.

The reason for the increased current response associated with the oxidative peak might be, alongside those reasons postulated previously, that with the cavity electrode (Figure 10.15) array there is a pore essentially filled with reaction products. As many of the products of reaction will be the reduced amine species, and following the postulated theory that the cavities cause a build-up of reacted products unable to diffuse away from the surface with ease, it may be the case that a relatively greater quantity of the products required for the oxidative reaction of the amine to hydroxylamine species are available at the surface of the electrode.

It can be observed, once again, that the magnitude of the current response increases only marginally with the increasing concentrations of TNT available in the solution making the differentiation between concentration values limited. The magnitude of the current response when compared to an unmodified CoPc sensor is, however, considerably greater as can be seen in Figure 10.28.

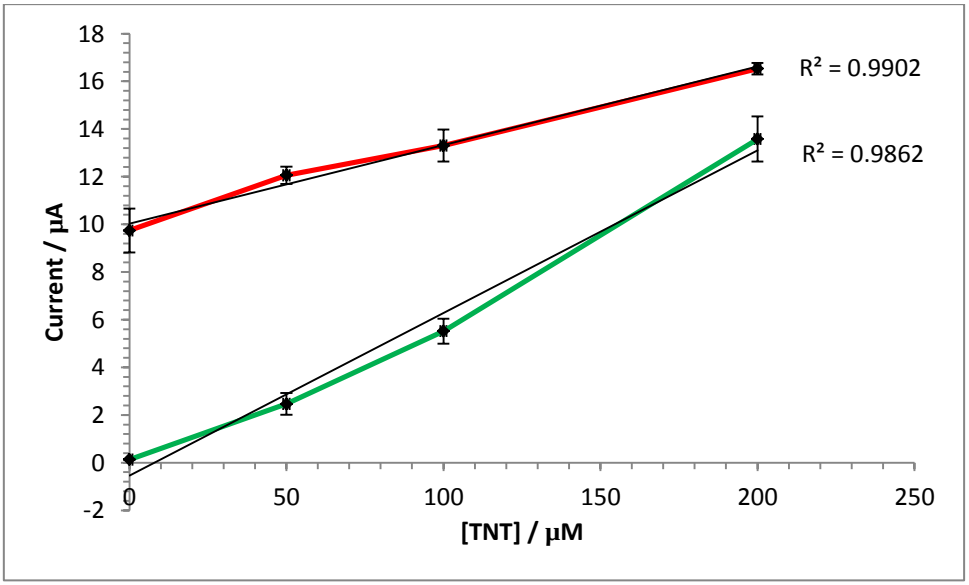

Figure 10.28 - Comparison calibration plots taken from the oxidative peak from an unmodified CoPc sensor (green line) and a microelectrode array (red line) after a ten minute deoxygenation period

The unmodified CoPc sensor and the microelectrode array can both be observed to display near linear profiles as can be seen in Figure 10.28. The amount of error both

sensors display appears to be relatively low – the actual error can be better compared using the RSD values, which are presented in Table 10.1.

	0 µM	50 µM	100 µM	200 µM
Unmodified CoPc	15.6	18.3	9.5	7.0
Microelectrode array	9.4	3.0	5.0	1.4

Table 10.1 - RSD values in % of each of the concentration data points for both an unmodified CoPc sensor and a microelectrode array

It can be observed that despite the limited differentiation between the increasing TNT concentrations with the microelectrode array, the amount of error in the system, and therefore the reproducibility of the results, has been substantially improved.

10.4.3. The detection limit of TNT interrogated with a cobalt phthalocyanine microelectrode array

The clarity of the voltammetric profile of TNT interrogated with the microelectrode array (fabricated as described previously in this chapter) was demonstrated to be optimal at a high concentration of TNT and without the deoxygenation step. Figure 10.21 provided the voltammetric profile with the greatest detail apparent – including the three peaks in the far cathodic region and the redox couple just evident at approximately 0.0 V. It follows that the interrogation of a lower concentration range of TNT, as carried out throughout this project, with the microelectrode array might not provide clear differentiations between the different concentrations of TNT in the system at the lower level.

A study was undertaken to establish the voltammetric profiles of a solution of TNT at varying low concentrations with the enzyme and cofactor present using cyclic voltammetry where the potential is swept between -0.8 and +0.8 V (vs. Ag/AgCl). A set of the resulting voltammetric profiles can be seen in Figure 10.29 where plot a) is without a deoxygenation period and plot b) is after a ten minute deoxygenation stage with argon gas.

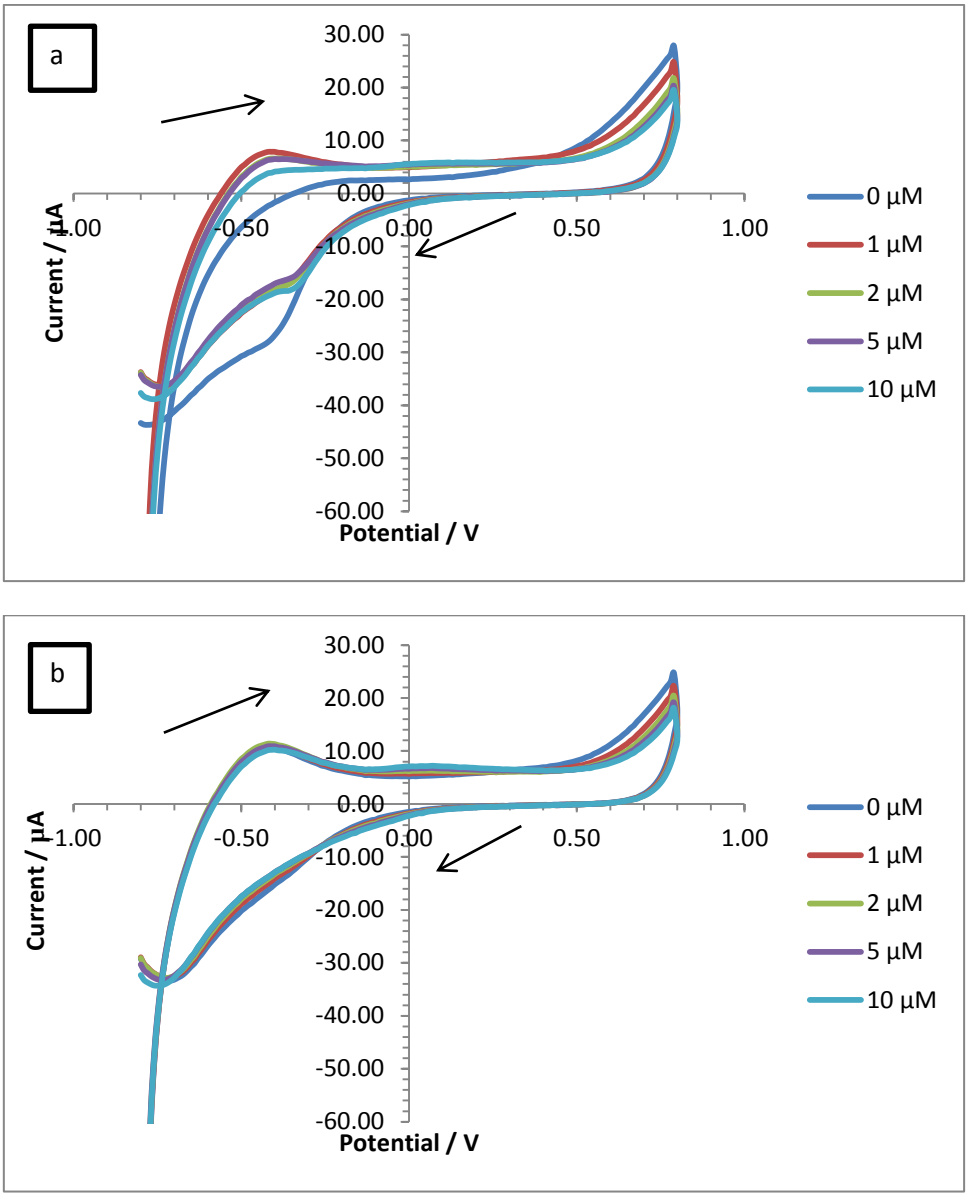

Figure 10.29 - Cyclic voltammograms representing the interrogation of lower concentrations of TNT with a microelectrode array where a). was no deoxygenated and b). was deoxygenated for a ten minute period (scan rate 20 mVs^{-1} vs. Ag/AgCl)

The characteristic peaks observed previously, see Figure 10.21 for example, have almost entirely receded in both the voltammetric profile with and without prior deoxygenation, with the exception of the R1a peak (-0.72 V). The deoxygenation step has caused a complete depreciation of signal response, leading to no distinguishable differences between a solution without any TNT present and one with 10 µM. Taking the potential position where a peak was apparent at higher concentrations, -0.72 V,

the similarity between the different concentrations of TNT can be better represented in the figure below, see Figure 10.30.

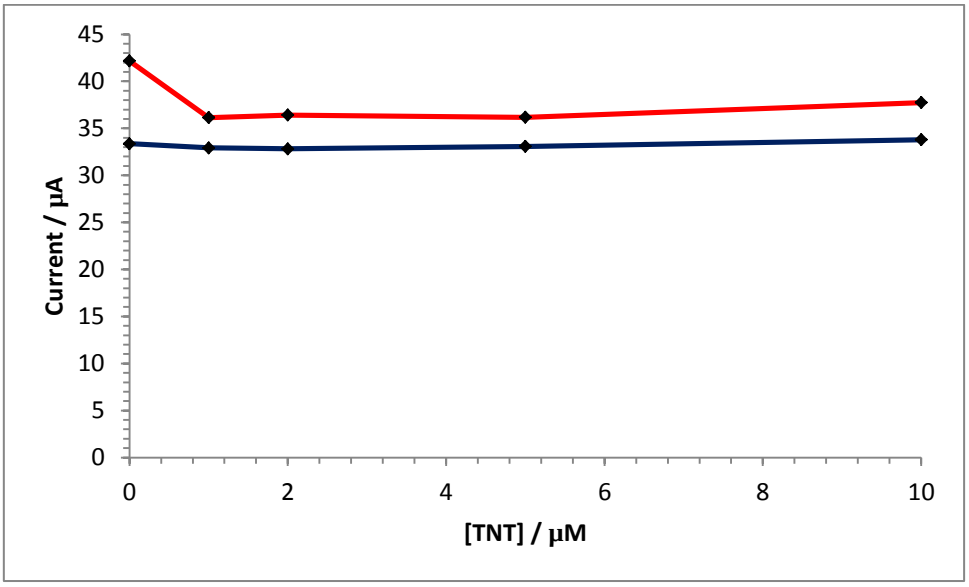

Figure 10.30 - A plot representing the similarities between increasing concentrations of TNT at a potential position of -0.72 V either with a ten minute deoxygenation period (blue line) or without this stage (red line) interrogated with a microelectrode array (scan rate 20 mVs^{-1} vs. Ag/AgCl)

It can be seen that the interrogation of a solution without TNT present has produced a greater magnitude of response than any of those with the lower concentrations of TNT present. As such, it would seem inappropriate to utilise this microelectrode sensor in its present format for the detection of low concentrations of nitroaromatic compounds.

10.5. Conclusions

A study was performed into the optimal conditions required to fabricate a microelectrode array on a CoPc sensor through the electrodeposition of an insulating polymer before sonochemical ablation. The conditions required for the optimal deposition of the polymer PoPDA were first investigated using previous work carried out within our group as a guideline.

Previous electrodepositions on a plain carbon electrode have benefited from a pre-treatment of the surface of the screen-printed sensor with an exposure to ultrasound. This disperses any gases adhering to the carbon surface due to the hydrophobicity of carbon and improves the deposition of the polymer film. A study into whether this was the case with the cobalt phthalocyanine sensors found that the insulating effect of the PoPDA was improved when this pre-treatment step was omitted. It was suggested that the reason for this might be twofold; firstly, that the application of ultrasound may dislodge some CoPc particles within the carbon ink matrix and, secondly, that the CoPc surface may be more hydrophilic and therefore less gasses would adhere to the surface eliminating the need to expel them.

The number of scans required to provide an adequately insulated sensor was examined, previously 20 scans were performed to provide an adequate insulation of a gold screen-printed sensor. The CoPc sensors were found to still produce a significant current response after 20 scans. A study into the optimal scan number found little difference between 50 and 60 and therefore 50 scans were assumed adequate for this project.

The scan rate was subsequently investigated – previously a scan rate of 50 mVs^{-1} was utilised but again this failed to adequately insulate the more electroactive CoPc-doped screen-printed sensor. The slowest scan rate examined, 5 mVs^{-1}, provided the best insulation, however, there was little difference between this scan rate and 10 mVs^{-1} in terms of insulated effect. As such, and to minimise fabrication times, the faster scan rate of 10 mVs^{-1} was utilised in subsequent electrodeposition stages.

Ultrasonic ablation of the insulated surface of the CoPc screen-printed sensor was performed at 25 KHz in an ultrasonic bath for various periods of time to establish the optimal duration to produce cavities through the polymer to the surface of the electrode whilst maintaining the properties of a microelectrode which are known to diminish when the pore population becomes too dense. A time period of 10 seconds was determined as optimal in maintaining the microelectrode characteristics whilst allowing for minimal signal response. This was confirmed using the redox couple ferrocenemonocarboxylic acid.

A simple study into the stir-independence of the microelectrode arrays was undertaken using chronoamperometry. It was demonstrated that the microelectrode array was significantly less affected by the introduction of convection than a bare, unmodified electrode. This can be related to the hemispherical diffusional profile associated with the microelectrode array.

Studies into the detection of TNT with the microelectrode array, developed as described above, were undertaken at both high and low concentrations of TNT in the presence of nitroreductase and NADPH. The peak profile of TNT interrogated with a microelectrode array was demonstrated to produce an extra peak in the cathodic region – this was attributed to the improved electroactivity due to the MA allowing clarification of this region and the splitting of the broad peak previously situated at -0.5 V into two distinct peaks. These three peaks were postulated to be indicative of the reduction of the three nitro groups on the aromatic ring. The magnitude of the current response was seen increase considerably with the microelectrode array, however, the differentiation between the different concentrations of TNT was shown to have diminished significantly. This was highlighted in the calibration plots in section 10.4.2 where the increasing TNT concentrations displayed only small incremental increases in current response. It was postulated that the cavity like pores comprising the microelectrode array may retain a quantity of the bulk solution throughout the electrochemical interrogations, thus diminishing the diffusion of reactants away from the electroactive surface. The quantity of enzyme within the solution bulk may also have an influence on the resulting voltammetric profiles.

At lower concentrations, the definition between various TNT concentrations was observed to decrease further and it became impossible to accurately define peaks with a quantity of TNT included from those without any – in some cases the voltammetric profile of a baseline solution (without the nitroaromatic) provided a greater response than those including the analyte of interest.

It may be advantageous to immobilise the enzyme near the electrode surface to improve the current responses both at high and low concentrations of TNT. The development of protrusions from the microelectrode array with an insulating polymer immobilising the enzyme within its matrix will be discussed within Chapter 11.

11. Microelectrode array of PANI mushroom shaped protrusions and the immobilisation of nitroreductase

11.1. Introduction

The immobilisation of enzymes and other biological entities within a conducting polymer matrix is a technique that has received significant attention due to the relative ease with which a biosensing device can be produced through this procedure (Bartlett and Whitaker, 1988). The entrapment of a biological species within a conducting polymer can be performed electrochemically using an electrodeposition technique where a monomer solution, within which is the biological requiring immobilisation, deposits a film on the conductive electrode surface through potential cycling or through fixed potential techniques (Bartlett and Birkin, 1993). As the thin conductive film coats the surface, the biological entity becomes trapped within it, thus immobilising the enzyme where the active site may be close to the conductive electrode surface (Foulds and Lowe, 1986).

Advantages of this entrapment process include the control over film thickness that electrodeposition holds; as the deposition is controlled by the electrode potential is it possible to control the polymer film thickness through the total charge passed (Bartlett and Birkin, 1993). Related to this regulation over the film thickness is the reproducibility that this control allows. It is also possible to build multi-layer structures with more than one type of enzyme or polymer associated with one electrode or a system of electrodes in an array (Bartlett and Birkin, 1993).

The entrapment of many different enzymes in a conducting polymer in this manner has been reported such as, for example, horseradish peroxidase (Kong et al., 2003; Rahman et al., 2004), glucose oxidase (Wilson and Turner, 1992; Liu et al., 2008; Fortier et al., 1990) and the lactate enzymes oxidase or dehydrogenase (Warriner et al., 1997; Pandey et al., 1994; Haccoun et al., 2004). There are various conducting polymers that may be used for this immobilisation, such as polypyrrole, polyacetylene and polyaniline (known as PANI) (Nicholson, 2006).

PANI can exist in three oxidation states: the fully reduced form, leucoemeraldine (poly-(paraphenyleneamine)), the fully oxidised form, pernigranilinine (poly-(paraphenyleneimine)) or the 50% oxidised form, emeraldine (poly-(paraphenyleneamineimine)) (Macdiarmid et al., 1987). The form most desirable for its conducting properties is the emeraldine form – at low pH levels (<pH 5.0) the oxidative polymerisation of aniline produces this conductive emeraldine salt. The generally accepted mechanism by which aniline may be electropolymerised involves firstly the oxidation of aniline to the radical cation followed by radical-radical coupling to form head-to-tail, head-to-head and/or tail-to-tail dimers. These dimers are then oxidised and undergo further coupling with either aniline monomers or other dimer molecules forming increasingly larger molecules in this fashion (Deng and Van Berkel, 1999). As mentioned earlier, while this is the generally accepted mechanism there is some speculation still associated with this as the polymerisation mechanism (Genies and Tsintavis, 1985).

The immobilisation of the enzyme, nitroreductase, and its cofactor NADPH onto the microelectrode array described in Chapter 10 was investigated as a means to improve the available enzyme in the system and to improve the resulting current response and differentiation when the sensor was used to detect TNT. The cobalt phthalocyanine cavity microelectrode array was found to display little differentiation between different concentrations of nitroaromatics within the system; this was particularly observed at the lower concentrations of TNT (below 50 μM). This issue was contrary to the microelectrode behaviour demonstrated when a sensor was used in electrochemical studies of ferrocenemonocarboxylic acid. The conductivity from the electrode surface enables, through the electrodeposition of polyaniline, the formation of protrusions from the cavities in the microelectrode array, see Figure 11.1. The rationale here is to produce protrusions from the surface of the electrode so as to prevent the need for the filling of cavities with an analyte solution.

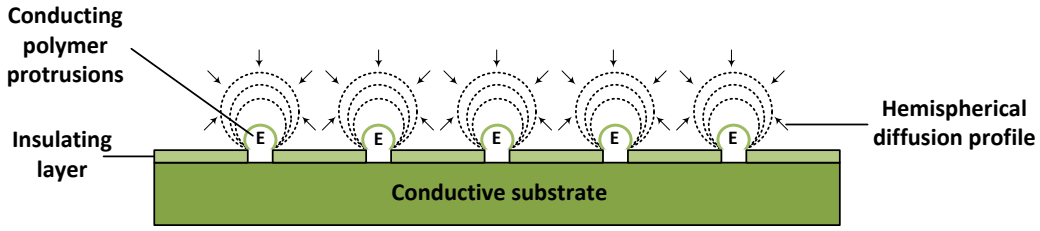

Figure 11.1 - Schematic representation of the polymer protrusions containing the immobilised nitroreductase and the resulting hemispherical diffusional profile due to the microelectrode array

This technique will form the basis of the immobilisation of the enzyme and cofactor.

11.2. Electrodeposition of polyaniline

The electropolymerisation of polyaniline from an aniline monomer solution has been discussed in section 11.1. This will be performed with the microelectrode arrays fabricated as described in Chapter 10 which involved, briefly, the electropolymerisation of *o*-phenylenediamine, an insulating polymer, onto the surface of a cobalt phthalocyanine screen printed electrode until the sensor is essentially insulated. This insulated sensor was then sonicated for 10 seconds in an ultrasonic bath, thus producing cavities through the insulating polymer down to the carbon surface of the working electrode. These cavities provide the basis for the array, and microelectrode properties were displayed through the stir independence and sigmoidal voltammetric profiles displayed by a common redox couple, ferrocenemonocarboxylic acid. All voltammetric interrogations within this chapter will be performed with the underlying microelectrode array system unless otherwise stated.

The conducting properties of polyaniline as a film applied through electrodeposition have been reported to rely on several factors, the most important of which are the concentration and the pH of the aniline monomer solution (Deng and Van Berkel, 1999). As such, to retain these desirable conductive properties, the electrodeposition of polyaniline is usually performed within an acidic aniline monomer solution (Barton et al., 2004; Myler et al., 1997).

The number of potential cycles can also be important, not only for the thickness of the film, but also as after 15 or more scans cracking can occur in the polymer film which can affect the flow of electrons and, therefore, the conductivity of the PANI film (Grennan et al., 2006).

As was previously ascertained, whilst some enzymes are capable of retaining their activity after short treatments within an acidic matrix, nitroreductase in the form commercially available and used throughout this project is not. To assess this, the nitroreductase enzyme and its cofactor NADPH were produced in phosphate buffers at a variety of pHs. These were subsequently checked for activity using a UV visible

spectrometer and while some limited activity was retained at pH 6.2, all solutions examined at a more acidic pH displayed zero change in absorbance with the introduction of the enzyme, see Chapter 6, this suggests that the enzyme is not active in these lower pH environments.

Due to this factor, it was postulated that the electrodeposition of polyaniline and the co-entrapment of the biological species should be carried out using a pH 7.0 monomer solution of aniline. It may be the case that at this pH the polymer is acting simply as a matrix for the immobilisation of the enzyme. However, to assess the difference in activity of the polymer at different pH levels a study was undertaken polymerising the aniline at pH 4.0 as well as pH 7.0 and checking the resulting activity in the redox couple used for all previous characterisations, namely FeCA.

The electropolymerisation was performed in a 0.2 M aniline solution by cycling the potential between -0.2 and +0.8 V (vs. Ag/AgCl) for 10 scans at 50 mVs^{-1} in the differing pH solutions The resulting voltammograms can be observed in Figure 11.2 for a pH 4.0 and Figure 11.3 for a pH 7.0 aniline solution for bare CoPc electrodes.

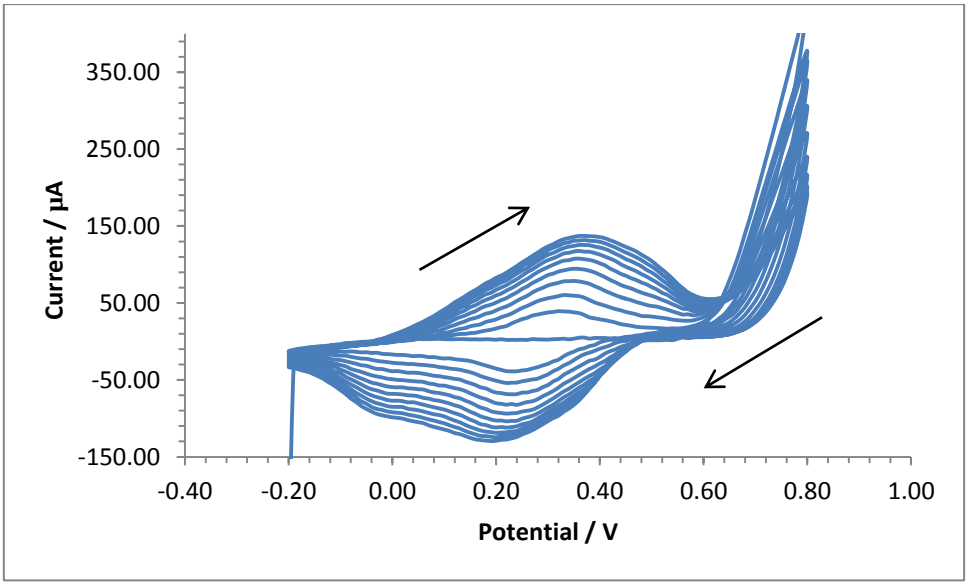

Figure 11.2 – The electropolymerisation of 0.2 M pH 4.0 aniline to form a thin film on an unmodified cobalt phthalocyanine screen-printed sensor (for 10 cycles at a scan rate of 50 mVs^{-1} vs. Ag/AgCl)

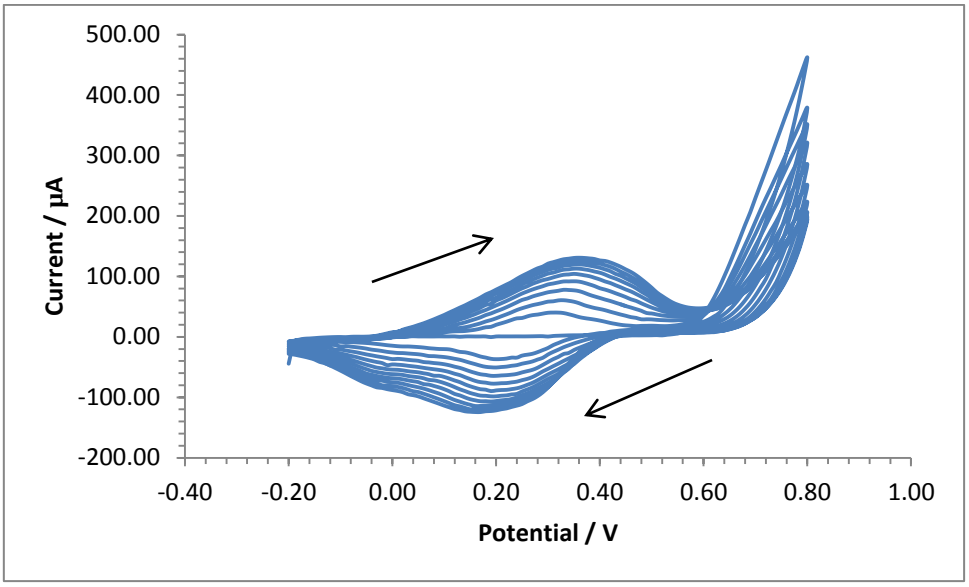

Figure 11.3 - The electropolymerisation of 0.2 M pH 7.0 aniline to form a thin film on an unmodified cobalt phthalocyanine screen-printed sensor (for 10 cycles at a scan rate of 50 mVs^{-1} vs. Ag/AgCl)

The resulting voltammetric profiles can be seen to be in essence remarkably similar, indicating that the electrodeposition stage of producing the polymer protrusions from the cavity microelectrodes should not be significantly affected by the change in pH. It is worth noting that at this stage, the biological species have been omitted. The electrodeposition of a pH 7.0 aniline solution onto a microelectrode array, fabricated as described earlier, can be observed in Figure 11.4. This electropolymerisation also did not include the enzyme and cofactor – the electrodeposition profile being the point of interest at this stage.

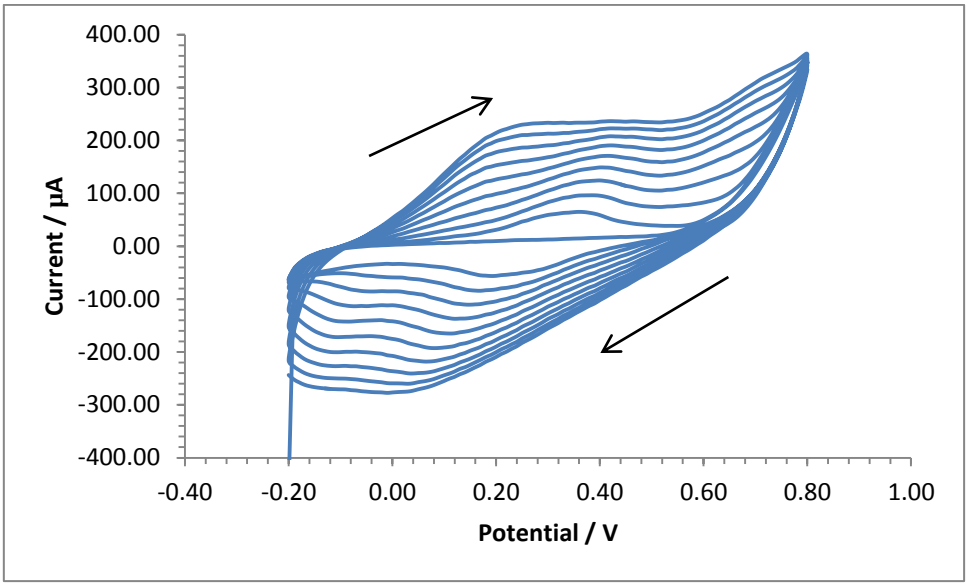

Figure 11.4 - The electropolymerisation of 0.2 M pH 7.0 aniline to form a thin film on a microelectrode array fabricated in-house (for 10 cycles at a scan rate of 50 mVs^{-1} vs. Ag/AgCl)

When the potential is scanned to +0.6 V on the initial sweep the oxidation process of aniline can be seen to initiate and a high oxidation current is attained – prior to this potential, on all three polymerisation examples presented above, there is very little current response. The electropolymerisation of aniline is said to occur in two stages, the first stage involves the polymerisation of aniline on a bare or partially coated surface and the second stage involves the subsequent polymerisation onto the polyaniline surface (Wang et al., 1987). Inevitably once the sensor has been entirely coated with polyaniline the polymerisation becomes more difficult and the rate decreases – this corresponds to the decreasing change in magnitude current response with increasing cycles; this can be demonstrated better in Figure 11.5 where the current response profile of cycles 1, 2, 5 and 10 are shown. The maximum oxidative peak current for each of these scans can be seen in Table 11.1.

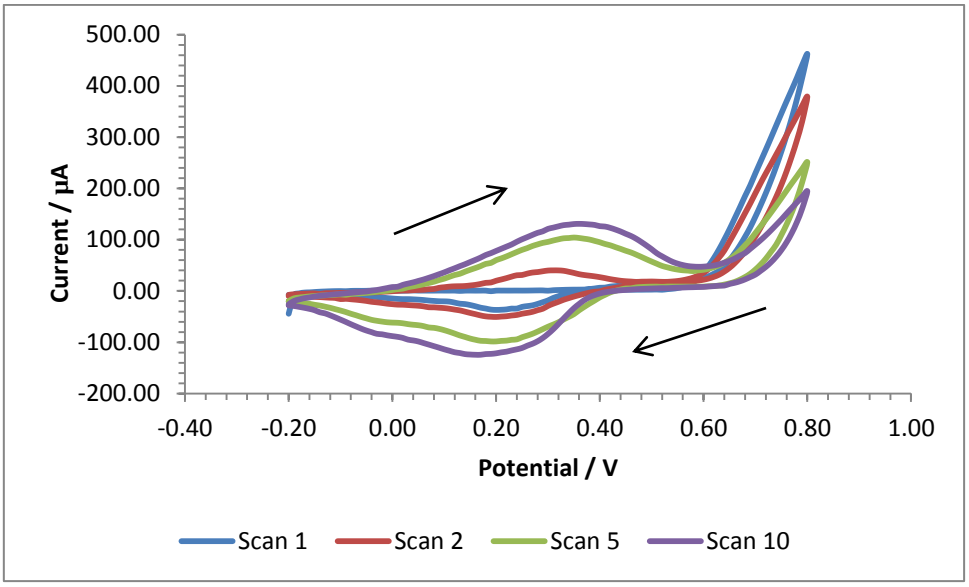

Figure 11.5 - Voltammetric profiles of scan 1, 2, 5 and 10 taken from the electropolymerisation of 0.2 M pH 7.0 aniline on an unmodified CoPc sensor (phosphate buffer supporting electrolyte, at a scan rate of 50 mVs^{-1} vs. Ag/AgCl)

	Scan 1	Scan 2	Scan 5	Scan 10
Peak current value (µA)	1.49	40.19	91.97	130.91

Table 11.1 - Maximum peak current taken from the oxidative peak at approximately +0.36 V, data from Figure 11.5 (vs. Ag/AgCl)

It can be observed that the magnitude of the current response has increased significantly when compared to the response gained with the unmodified CoPc sensors (Figure 11.2 and Figure 11.3). The increasing oxidation peak visible in the voltammetric profiles of the unmodified CoPc sensors can be observed to be remarkably similar; the peak position and magnitude were found to be +0.4 V / 122.4 µA and -0.36 V / 130.9 µA for pH 4.0 and pH 7.0, respectively (vs. Ag/AgCl). This peak, although initiating at the same potential as those gained with the unmodified sensors, can be observed to increase with increasing cycles more significantly when the aniline is polymerised upon the microelectrode array, this may be due to the increased electroactivity associated with an array of microelectrodes.

It should be noted, however, that the voltammetric profiles demonstrated here do not present the characteristic redox peaks associated with the electropolymerisation of polyaniline carried out with a sensor system comprising a more electroactive working electrode, such as platinum or gold. In the instance of platinum, three redox peaks are

apparent in the voltammetric profile the position of which depends on several factors, including the pH of the aniline solution, the type of anion in the supporting electrolyte and the presence of salts in the aqueous media (Wang et al., 1987; Wang et al., 1986; Duić and Mandić, 1992).

11.3. Characterisation of polyaniline film

11.3.1. Characterisation of response with the protrusion microelectrode array with ferrocenemonocarboxylic acid

To establish any similarities or differences between the polyaniline electrodeposited at different pH values a cyclic voltammogram was performed (between -0.2 and +0.65 vs. Ag/AgCl at a scan rate of 20 mVs^{-1}) in a 5 mM solution of ferrocenemonocarboxylic acid. These interrogations were performed without the addition of the enzyme and cofactor either to the aniline solution at the deposition stage or the FeCA solution interrogated here. This allows examination of the polyaniline polymer film without interference from the enzyme. The resulting voltammetric profiles can be observed in Figure 11.6.

It can be seen that, as discussed previously, the sensors with a pH 4.0 PANI electrodeposited film have produced a greater current response when used in the interrogation of ferrocenemonocarboxylic acid. Both the sensors with PANI deposition on an unmodified CoPc sensor and on a microelectrode array present significantly larger current profiles than those performed with a pH 7.0 PANI solution due to the conductivity of the polyaniline decreasing as the pH moves away from the optimal acidic values.

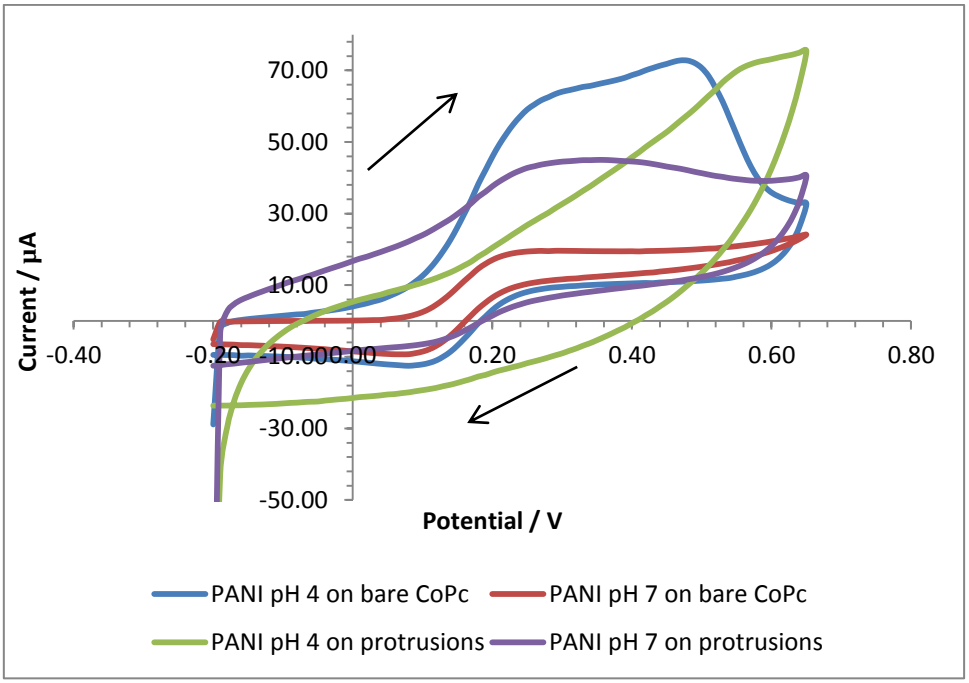

Figure 11.6 - Voltammetric profiles of sensors coated with PANI at different pH values (vs. Ag/AgCl at a scan rate of 20 mVs^{-1})

There is, however, a significant increase on the magnitude of the current response between an unmodified CoPc sensor coated with PANI and the microelectrode coated with PANI (both at pH7). This is likely to be the influence of the underlying microarray structure. It is promising that the improved response associated with the development of the microelectrode array has not been rescinded by the subsequent electrodeposition of a partially conducting polymer coating. As such, using a pH 7.0 PANI coating to develop an array of protruding polymer structures from the cavity array already fabricated and the co-immobilisation of the enzyme has been demonstrated to be possible at the neutral pH, which enables the activity of the enzyme to be retained.

11.3.2. Surface topographical examination

To better observe any changes the electrodeposition of polyaniline may have made to the surface of the sensor, already fabricated into a microelectrode array previously, scanning electron microscopy was performed. The resulting micrograph can be seen in Figure 11.7.

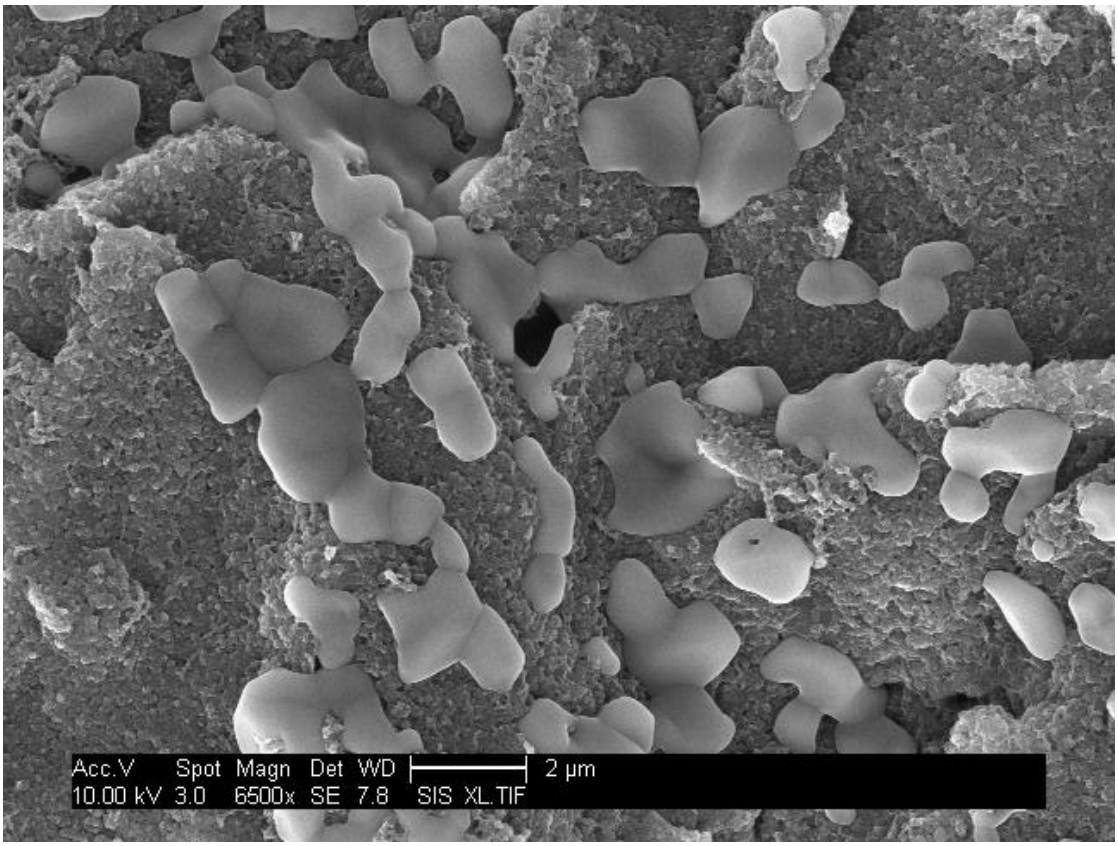

Figure 11.7 - An SFEG scanning electron micrograph of a polyaniline coated microelectrode array produced after 10 cycles (-0.2 to +0.8 V vs. Ag/AgCl) in a solution of 0.2 M pH 7.0 aniline (at 6500x magnification after sputter coating with gold palladium)

It can be observed that where cavities in the insulating polymer coated CoPc surface could be observed previously (see Figure 10.15), these cavities do not seem to be apparent. There is, however, a network of globular protrusions apparent, seen best at this magnification, which have formed on the surface of the insulated PoPDA and then sonicated sensor. As these protrusions were not apparent in any of the previous scanning electron micrographs (Figure 5.2, Figure 8.2, Figure 10.9, and Figure 10.10) it

is fair to assume that they can be associated with the polyaniline electrodeposition alone.

The size of the protrusions varies (the smallest of which was ≤0.2 μm) – this may be in correlation to the variety of sizes of the underlying cavities from which these protrusions have developed, as mentioned previously. It is interesting to note that while most of the cavities appear to have been filled with the polyaniline, there is one area in the centre of the micrograph that appears to have not been affected by the electrodeposition step. It may be the case that this cavity was not been sufficiently deep enough to have exposed the underlying conductive carbon surface to the aniline monomer solution. Without this exposure, it is unlikely that a polymer protrusion would have formed in this position.

The micrograph demonstrates that the PANI electropolymerisation stage has produced a network of protruding structures visible under SEM which have not been apparent in any other micrographs taken of the surface of a CoPc sensor at any stage of its modification. It is, therefore, postulated that these structures can be attributed to the electrodeposition of the polymer, polyaniline.

11.4. Trinitrotoluene detection with nitroreductase immobilised microelectrode arrays

The electrochemical interrogation of TNT with the cavity microelectrode arrays provided a significant increase in the magnitude of current response, but when a study was undertaken with a succession of concentrations of TNT it became apparent that the signal differentiation between these different concentrations of the analyte had diminished when compared to those observed with both plain carbon and a CoPc-doped carbon screen-printed sensor. This lack of differentiation was more evident still at lower concentrations of TNT, and in these interrogations there was a considerable depreciation in the peaks of the voltammetric profile such that they became indistinguishable.

To attempt to address these concerns, the microelectrode array was treated with the electropolymerisation of aniline including the co-entrapment of the enzyme, nitroreductase, and the cofactor, NADPH. It is hoped that this immobilisation of the enzyme near the conductive surface of the sensor may provide an increase in response and, perhaps more importantly in this context, an improvement in the differentiation between concentrations of the nitroaromatic compound, especially at the lower concentrations.

Following the investigation into the electrodeposition of aniline at different pH values (section 11.2) and the previous investigations into the optimal conditions to retain the activity of the enzyme during this stage (section 6.2.2) it was necessary to perform the electrodepositions with a pH 7.0 solution of aniline. A 0.1 mM solution of NADPH was made up in the 0.2 M pH 7.0 aniline solution and within this 20 units of the enzyme nitroreductase were included. This solution was utilised for the electropolymerisation of PANI on the microelectrode arrays, between -0.2 and +0.8 V at 20 mVs^{-1}.

A set of voltammetric interrogations were then performed to assess whether this enzyme immobilisation stage did indeed, improve the current response and therefore the signal differentiation between different concentrations of TNT when performed

using protrusion-covered microarrays. The resulting voltammetric plots for TNT at higher concentrations can be seen below in Figure 11.8.

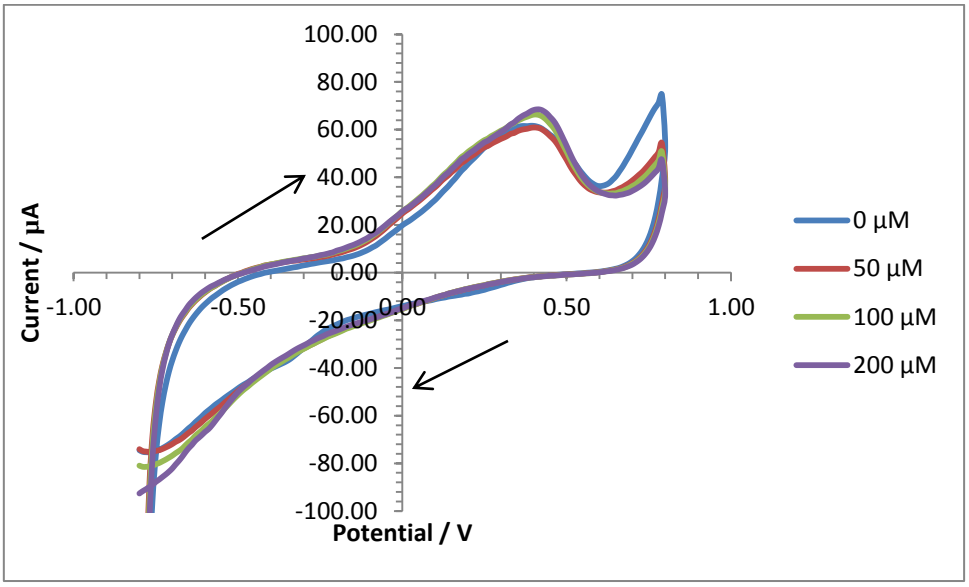

Figure 11.8 - Voltammograms gained from the interrogation of various concentrations of TNT with the protrusion covered microelectrode arrays in a phosphate buffer solution (scan rate 20 mVs^{-1} vs. Ag/AgCl)

It is apparent that the voltammograms gained of TNT in a phosphate buffer solution display very little differentiation between increasing TNT concentrations and when compared to a baseline solution of pH 7.0 phosphate buffer. While this was also the case with the microelectrode array of cavity electrodes, it is worth noting here that the peaks within the cathodic region representing the reduction of TNT are not observable in this case as they were with the bare/CoPc cavity electrodes. This may be attributed to the neutral pH that the PANI was electrodeposited upon the surface – it may be the case that, due to the polymer being deposited at a pH more associated with the production of its insulating form, any features that may be present with a more electroactive sensor are being suppressed somewhat by this insulating effect.

The immobilisation of the enzyme and cofactor may also have an influence on the voltammograms produced with the protrusion covered microelectrode array. The entrapment of enzymes within the polymer is not, in this manner, a controlled process; due to this, it may be that all of the available enzyme is entrapped within the polymer or equally that none of the enzyme was immobilised. As such, increasing the available enzyme within the aniline monomer solution might be an option to improve the

probability of immobilisation density. This option, however, highlights the issue of cost – one of the primary objectives of this project was to produce a sensor that is of low-cost to manufacture and maintain; increasing the enzyme available will, inevitably, increase the cost per sensor.

It should be noted, however, that while the features and the differentiation have not been improved with the introduction of the protrusion stage in the fabrication of these sensors, the magnitude of current response has increase once more. To better clarify this, Figure 11.9 contains the voltammograms from the interrogation of 200 µM TNT with an unmodified CoPc sensor, a microelectrode cavity array and a microelectrode array with the additional protrusions.

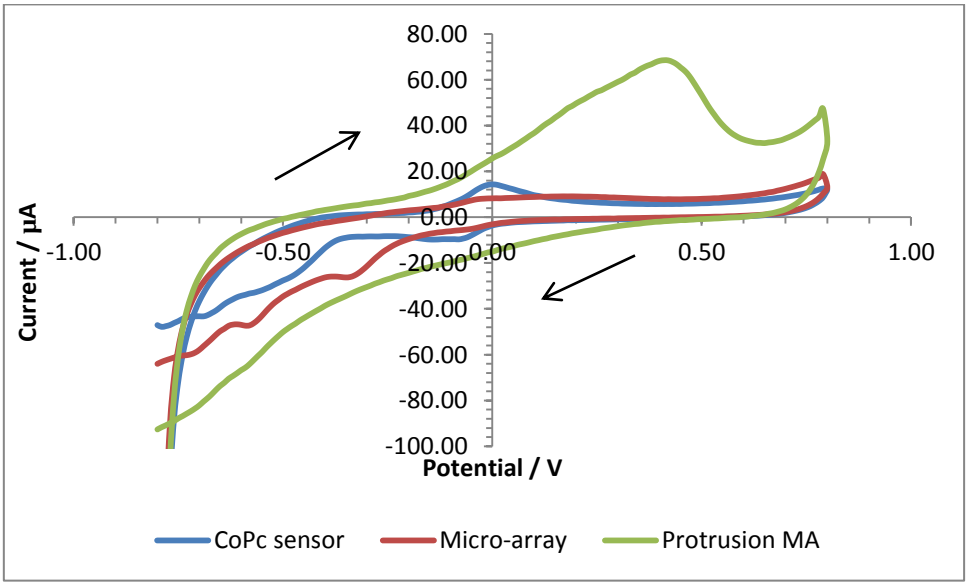

Figure 11.9 - Comparison of the voltammograms gained from the interrogation of 200 µM TNT with an unmodified CoPc sensor (blue line), a cavity microelectrode array (red line) and a protrusion cover microelectrode array (green line) all at 20 mVs^{-1} vs. Ag/AgCl

The most obvious difference between those voltammograms gained at bare / cavity-based surfaces and those produced with the protrusion covered microarray is the large oxidation peak apparent in the anodic region at +0.4 V; this peak could, therefore, be attributed to the polyaniline film on the sensor surface since it is present even when interrogating a solution of phosphate buffer (see Figure 11.9). An oxidative peak at or near to this location is apparent in all voltammograms gained from the electrodeposition of aniline (see section 11.2).

Due to the relatively poor differentiation between the concentrations of TNT it seems that, once again, the sensor in its present form is unsuitable for the detection of low concentrations of TNT. Further work is necessary to improve the differentiation to improve the detection of TNT species at lower concentrations.

11.5. Preliminary assessment of factors that may improve fabrication of PANI protrusions

11.5.1. Introduction

The fabrication of microelectrode arrays with electropolymerised depositions of PANI and the co-entrapment of NTR and NADPH has been demonstrated and the magnitude of current responses with reference to both TNT and the redox couple ferrocenemonocarboxylic acid have been shown to increase significantly. Despite these changes in the sensor design, the differentiation between different concentrations of TNT was found to be relatively poor. This factor was unexpected as the use of arrays of microelectrodes has been known to improve the sensitivity of sensing systems, particularly at low concentrations (Bond, 1994).

To attempt to improve the conditions by which the aniline is deposited on the microelectrode array so that it may retain some conductivity whilst not having a detrimental effect on the optimal conditions of the enzyme, a preliminary study was performed into alternative deposition techniques.

11.5.2. Increased ionic conductivity during deposition

While it is known that polyaniline is at its most electroactive at a low pH (Duić and Mandić, 1992) it has also been established that the inclusion of additional sodium chloride to the monomer solution of polyaniline can increase the conductivity of the deposited polymer film (Mu and Kan, 1998). As such, a proof of principle investigation was carried out with the inclusion of a 1 M quantity of NaCl in the aniline monomer solution. The voltammograms from the electrodeposition stage can be seen below where Figure 11.10 is gained from a solution of aniline with the enzyme and co-factor and with the additional NaCl.

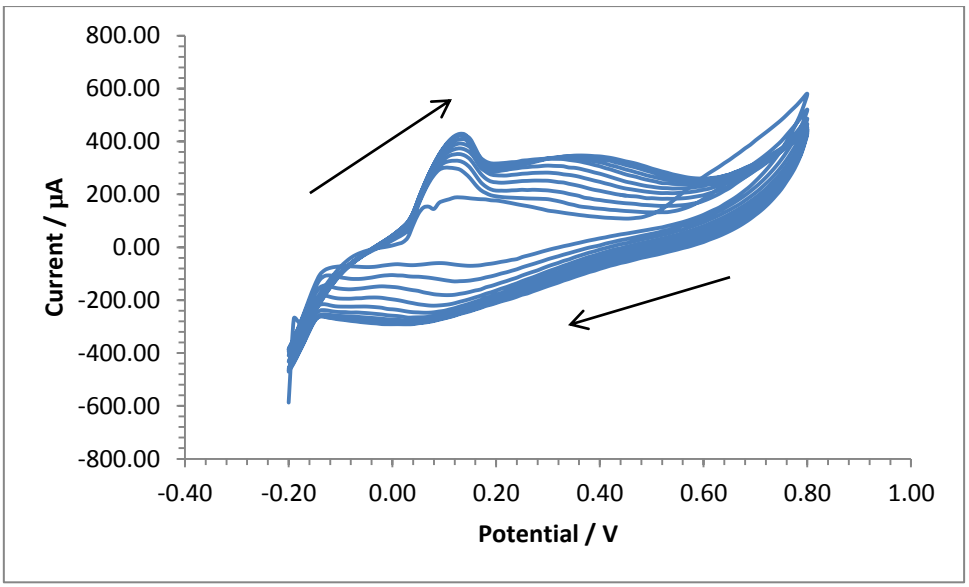

Figure 11.10 - Voltammetric profile gained from the electrodeposition of polyaniline in a pH 7.0 aniline solution with 20 units NTR, 0.1 mM NADPH and 1 M NaCl (50 mVs^{-1} scan rate vs. Ag/AgCl

Perhaps the most obvious factor to note is the additional peak present in the voltammetric profile representing the electrodeposition of aniline with additional NaCl (Figure 11.10). The position of this peak corresponds to the first of the three oxidation peaks reported in the literature to be associated with the electropolymerisation of aniline (Wang et al., 1987; Wang et al., 1986; Mu and Kan, 1998). It seems likely that the inclusion of salt in this manner has improved the conductivity of the PANI during deposition, thus enabling these conductive peaks to be present in the resulting voltammetric profile (Duić and Mandić, 1992).

To investigate whether this equates to any improvement in the current magnitude or peak clarity in the interrogation of TNT, this sensor was subsequently used in a solution of 200 µM TNT in phosphate buffer solution, this can be observed in Figure 11.11.

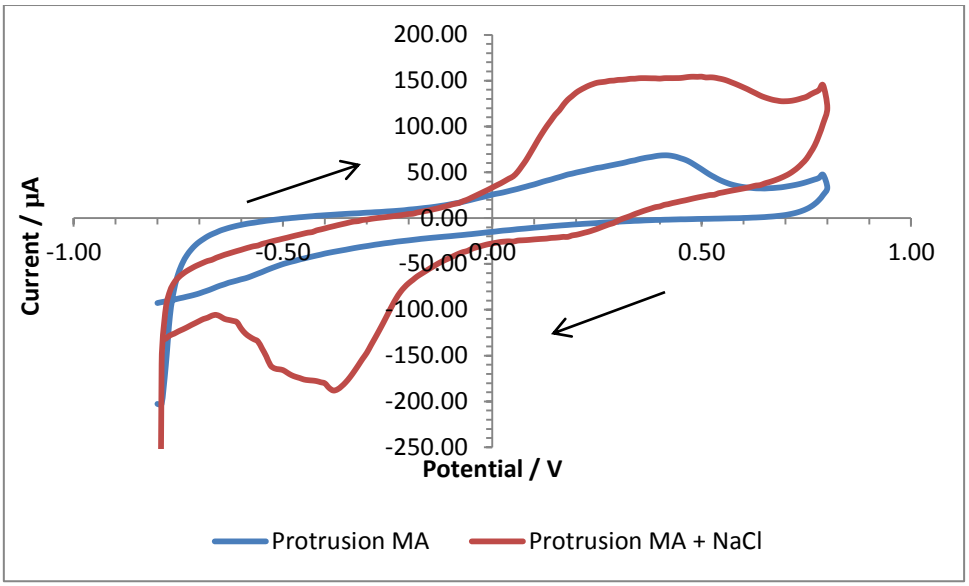

Figure 11.11 - Comparison of a voltammetric profile of 200 µM TNT interrogated by either the microelectrode protrusion array (blue line) or the microelectrode protrusion array with additional NaCl (red line)

The increase in current response here is considerable, as is the reductive peak present in the cathodic region of the voltammogram. This peak appears to be in a similar position to those gained with an unmodified CoPc sensor and an unmodified carbon sensor. It may be the case that the inclusion of salt in this manner does, indeed, improve the conductivity of the resulting PANI film. It would be necessary to conduct further investigations in this area with different concentrations of NaCl present and test the resulting sensors in lower concentrations of TNT.

11.5.3. Decrease in pH of the deposition electrolyte

As the activity of the enzyme has been demonstrated previously to depend on the pH of the solution within which the electropolymerisation takes place (Chapter 6) the pH of the aniline solution for this project was established as pH 7.0. To investigate whether the enzyme may be immobilised at a lower, and therefore more acidic, pH and retain some of its activity a study was proposed to conduct the electropolymerisation and co-entrapment stage at pH 6.2 as the enzyme was shown to demonstrate some activity at this level. The electropolymerisation step was carried out as before with 20 units of NTR and a 0.1 mM solution of NADPH with the aniline monomer, all at pH 6.2. The resulting voltammetric profile can be observed in Figure 11.12.

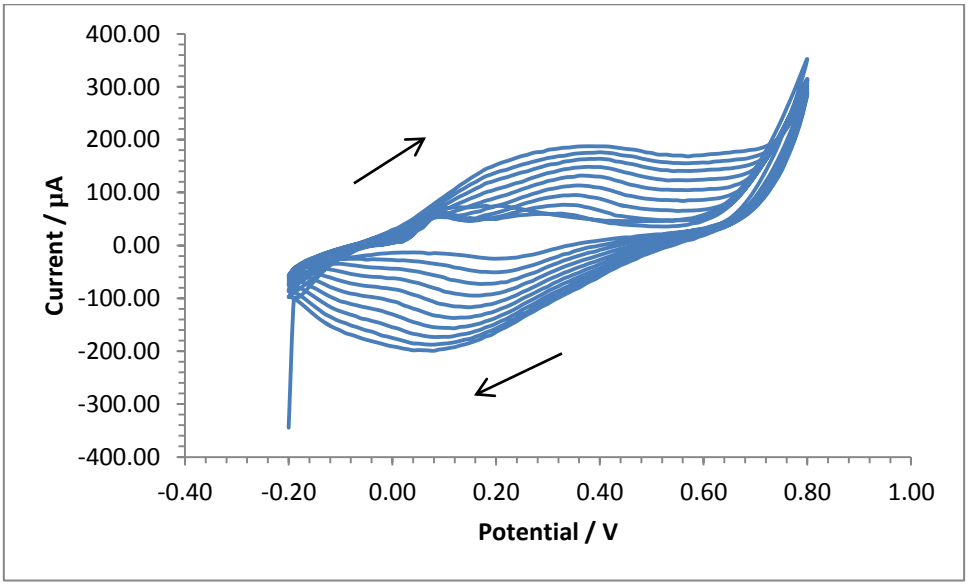

Figure 11.12 -Voltammetric profile gained from the electrodeposition of polyaniline in a pH 6.2 aniline solution with 20 units NTR and 0.1 mM NADPH (50 mVs^{-1} scan rate vs. Ag/AgCl)

Once more, a peak can be observed at +0.1 V (vs. Ag/AgCl) which corresponds to the first of three redox peaks present in a more electroactive, acidic deposition of PANI. The actual magnitude of the voltammetric profile is less than that obtained with the inclusion of the increased concentration of NaCl and, aside from the appearance of the additional oxidative peak, corresponds to that obtained with the electropolymerisation previously observed at pH 7.0.

A comparison set of voltammetric profiles can be seen below demonstrating the interrogation of TNT in a phosphate solution with the protrusion covered microelectrode arrays polymerised at pH 7.0 and pH 6.2 (Figure 11.13).

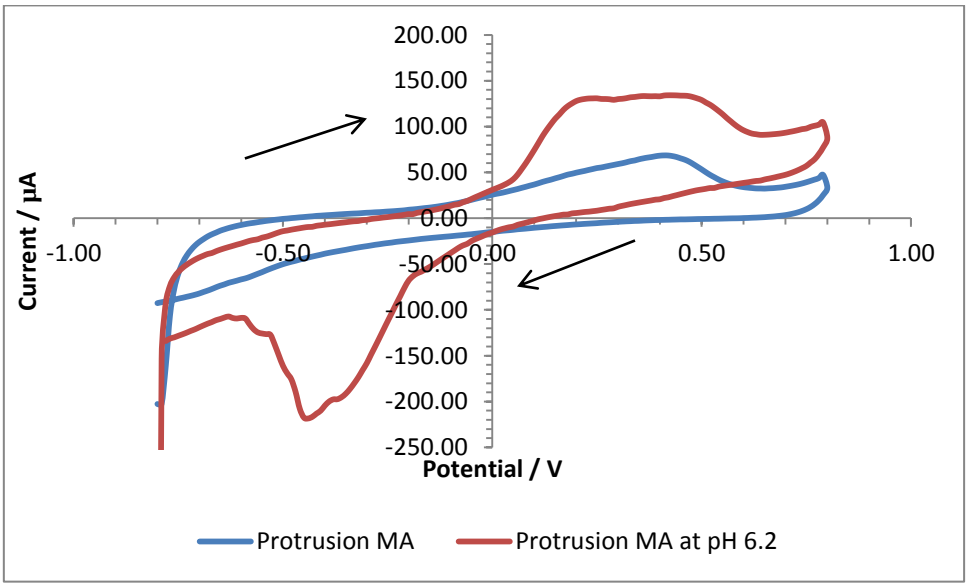

Figure 11.13 - Comparison of a voltammetric profile of 200 µM TNT interrogated by either the microelectrode protrusion array at pH 7.0 (blue line) or the protrusion array developed at pH 6.2 (red line) both including the enzyme and cofactor in the solution

A significant increase in the reductive peak in the cathodic region can be observed here as was demonstrated with the inclusion of increased NaCl in the solution (Figure 11.11). The magnitude of the peak is greater in this case, perhaps an indication of the improved conductivity with even a slight increase in the acidity of the solution. It is difficult, however, to establish the activity of the enzyme or to verify whether the enzyme has been degraded here from these voltammograms – as TNT shows electroactivity even without the presence of the enzyme system, it could very much be the case that it is this increased electroactivity which is being detected. Further work would need to be undertaken to determine for certain whether the enzyme activity when immobilised within a pH 6.2 PANI matrix is still adequate for this sensor system.

11.5.4. Increase in the enzyme available for immobilisation

One further area that was highlighted earlier as a means to improve the magnitude and clarity of the peaks gained from the electrochemical interrogation of TNT was to increase the amount of enzyme present in the monomer solution, it is postulated that this would increase the amount of enzyme subsequently immobilised within the protrusions on the surface of the microelectrode array, thus leading to an enhanced response for TNT measurement. While this would not provide an optimal solution due to the inherent increase in cost of the sensor, it is necessary to investigate the effect this may have when interrogating TNT to facilitate detection at lower concentrations. As such, the polymerisation of aniline was performed in the same manner as described above with the inclusion of 100 units of NTR instead of 20 units. The resulting voltammetric profile representing this electrodeposition stage can be seen in Figure 11.14.

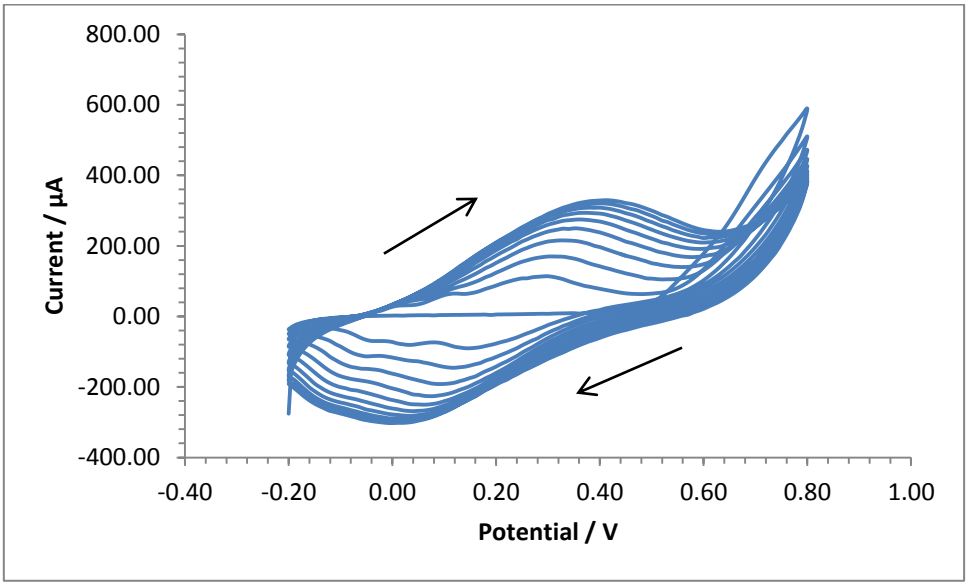

Figure 11.14 - Voltammetric profile gained from the electrodeposition of polyaniline in a pH 7.0 aniline solution with 100 units NTR and 0.1 mM NADPH (50 mVs^{-1} scan rate vs. Ag/AgCl)

The resulting voltammetric profile does not have as great a current magnitude as those gained with the other modifications conducted in this section or the presence of the oxidative peak observed when the pH was decreased and when NaCl was included in the system – this is, however, expected as the inclusion of the extra enzyme would not

be expected to improve the electroactivity of the PANI per se. It does, however look consistent to the response obtained with a pH 7.0 aniline solution containing 20 units of NTR and 0.1 mM NADPH.

The comparison between a microelectrode array with protrusions fabricated with 20 units of NTR and with 100 units NTR can be seen below in Figure 11.15.

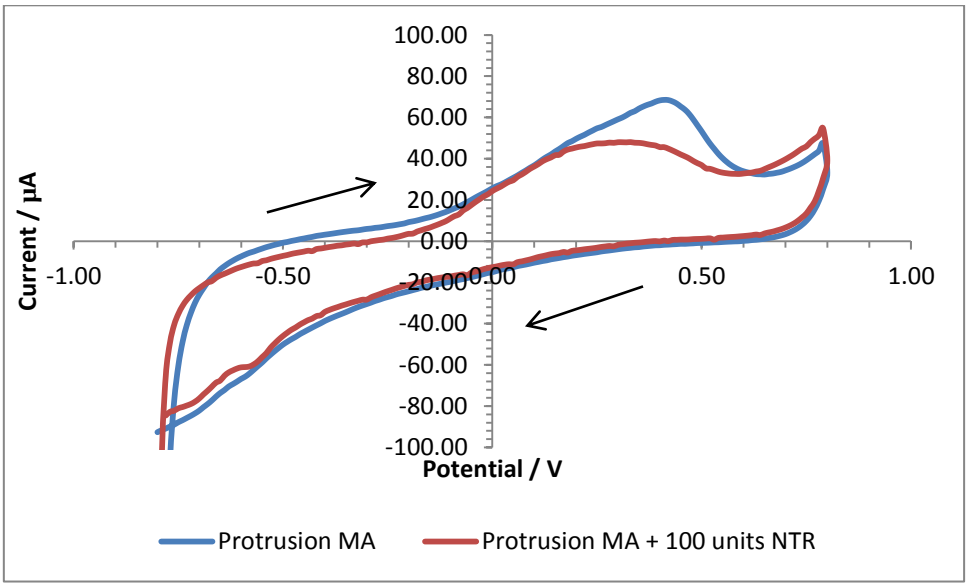

Figure 11.15 - Comparison of a voltammetric profile of 200 µM TNT interrogated by either the microelectrode protrusion array at pH 7.0 with 20 units of NTR (blue line) or with 100 units of NTR (red line) including the cofactor in the solution

Although there is no 'real' improvement in current response, it should be noted that the appearance of the peaks in the cathodic region have begun to become apparent once more, although not with the clarity demonstrated without the protrusions (Figure 10.21). Whilst this lack of signal response can be attributed to the pH of the deposition solution it is encouraging to note that the signal differentiation is enhanced with the increase in enzyme deposited. This is, therefore, an important aspect to be considered for any future work undertaken on this system.

11.6. Conclusions

The electrodeposition of polyaniline on the surface of both an unmodified and a microelectrode array based carbon sensor was demonstrated at a pH value of 4.0 and 7.0 to establish the difference in the electroactivity of the resulting polymer film at these different pH values. The sensor fabricated in PANI solutions at pH 4.0 demonstrated an enhanced conductivity, using ferrocenemonocarboxylic acid as a means to characterise this difference. The pH 7.0 PANI coated microelectrode array did, however, provide a greatly increased voltammetric profile, in terms of signal differentiation, when compared to the unmodified CoPc sensor coated with PANI pH 7.0.

The surface of the PANI coated microelectrode array was visualised using scanning electron microscopy and a network of globular protrusions, relating to PANI deposition, was demonstrated to be present. These protrusions have not been observed at any other stage of the development of a CoPc sensor and can, therefore be attributed to the PANI deposition on the surface on the microelectrode array.

The detection of various concentrations of TNT was evaluated using the protrusion covered sensors and the voltammetric profiles were presented. It was apparent that the addition of the PANI/NTR/NADPH stage did not improve the clarity of the peaks in the resulting profile or the differentiation between increasing concentrations of TNT. The current magnitude was, however, demonstrated to have increased once more when compared to sensors without the PANI stage, improving on the increase already demonstrated for the microelectrode arrays without the protrusion stage.

To attempt to redress the lack of clarity and differentiation in the voltammetric profiles gained when interrogating TNT, a preliminary study was carried out to assess the difference in response gained when modifying the various stages of the PANI deposition process. The first stage involved increasing the amount of sodium chloride available in the system to assess whether this increases the protonation and, therefore, the conductivity of the PANI film. An extra peak was observed in the resulting voltammogram of the electrodeposition step which corresponds to the first

oxidative peak present when electropolymerising aniline at lower pH values (i.e. more acidic). The increase in salt content did also increase the electroactivity of the sensor significantly when interrogating TNT but did not improve the clarity of the peaks in terms of differentiation. An increase in the acidity of the aniline solution also had this effect – increasing the magnitude of the response in TNT but not affecting the peak clarity. An additional peak was also present in the voltammogram of the electrodeposition of aniline corresponding to the first of three redox peaks associated with the deposition of PANI in its more conducting form.

The final alteration to the electropolymerisation step was to include a much greater amount of the enzyme available during deposition with the anticipation that this would, therefore, increase the amount of enzyme immobilised within the polymer matrix. Whilst this stage did not improve the current response itself, it did provide an increase in the clarity of the peaks in the cathodic region indicating that with an increased quantity of available and active enzyme, there will be an increase in the signal measurement in terms of differentiation.

12. Integration of microelectrode array with cyclone collection system

12.1. Introduction

One of the objectives defined within the remit of this project was the collection and detection of *airborne* particles of explosive compounds. The proposal to achieve this initially was based around a particle collection system to be supplied by ANTnano, the original sponsors of this project. Due to the unfortunate closure of this company, apparatus was sort elsewhere to enable the remit of this work to be satisfied.

Leeds University have kindly loaned an air cyclone collection system, the Coriolis®μ portable air sampler, and a proof of principle study was carried out to determine the feasibility of using a cyclone collection air sampler to collect airborne particles prior to analysis. The Coriolis®μ works essentially in an analogous manner as a cyclone vacuum cleaner; the air is taken in through an air inlet (in this instance at a flow rate of up to 300 litres per minute) and any airborne particles are collected and concentrated within an attached vessel. Air is aspirated into this vessel (the collection cone), which is pre-filled to an ideal level with a collection liquid, in a centrifugal motion which forms a vortex. Particles are pulled against the walls due to centrifugal force and separated from the air to be concentrated in the liquid. This liquid sample can then be analysed electrochemically and compared to a known value of the analyte of interest, in the form of a calibration plot. The calculated value can then be related back to the airborne concentration.

There are advantages associated with a system such as this such as, for example, the portability associated with its size and weight – this satisfies an aspect of the rationale behind this project. The fact that this apparatus is commercially available obviates the necessity to develop a system in-house which would extend the time period necessary to complete this project.

12.2. Characterisation of the cyclone collection system with ferrocenemonocarboxylic acid

Prior to the collection of an explosive substance the system was analysed for suitability using a well-defined sample species, namely ferrocenemonocarboxylic acid (FeCA), and to assess the comparative concentrations of the analyte collected from the cyclone to that introduced into the system initially (i.e. the airborne concentration. The Coriolis®μ collection system requires a collection solution to be present in the collection cone prior to sampling – this is to create the vortex into which any airborne particles will be collected through the centrifugal force exerted when the system is in activation. It was, therefore, necessary to add a 10 ml phosphate buffer solution into the collection cone prior to collection as this electrolyte has been used consistently throughout this study for FeCA interrogations.

To assess the baseline of the system a 10 ml phosphate buffer solution was added to the cone and the air sampling system was activated and allowed to complete a full 2 minute cycle without the injection of the FeCA. The voltammogram taken from the subsequent analysis of the collection fluid can be seen in Figure 12.1. This was done to assess the influence any airborne particles not intentionally introduced into the system had on the resulting voltammetric profiles prior to sample introduction.

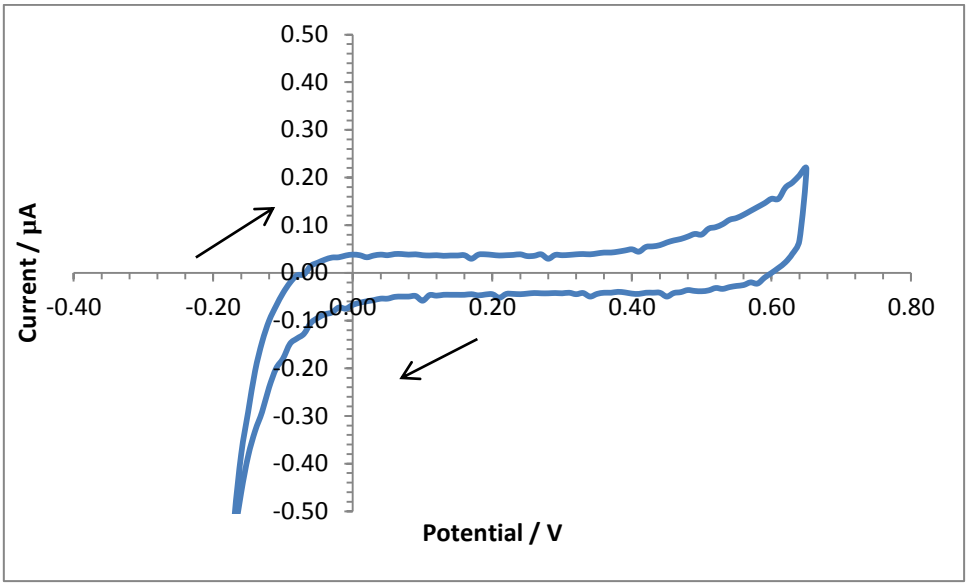

Figure 12.1 - Voltammogram obtained from the electrochemical interrogation of a phosphate buffer solution, with a CoPc sensor, taken from the collection chamber after the cyclone collection system was allowed to run for one cycle (scan rate 20 mVs^{-1} vs. Ag/AgCl)

It can be observed that there is a slight amount of noise present in the resulting voltammogram; this can be attributed to the interrogation of a non-clean system as the solution was used to form a vortex for two minutes while air was drawn in at a speed of 300 litres per minute. There is, however, no observable peak in the area of interest for either the collection of ferrocenemonocarboxylic acid or TNT that may cause ambiguity in subsequent analyses.

A solution of 5 mM ferrocenemonocarboxylic acid was subsequently introduced into the cyclone collection system using a spray bottle allowing liquid to be drawn from the bottle and dispensed in a mist. The air sampler was set to run for two minutes and the sample was aspirated in front of the collection valve once every 10 seconds for the entire collection period. The resulting sample was accumulated within the collection solution in the collection tube and interrogated electrochemically with an unmodified CoPc sensor, see Figure 12.2.

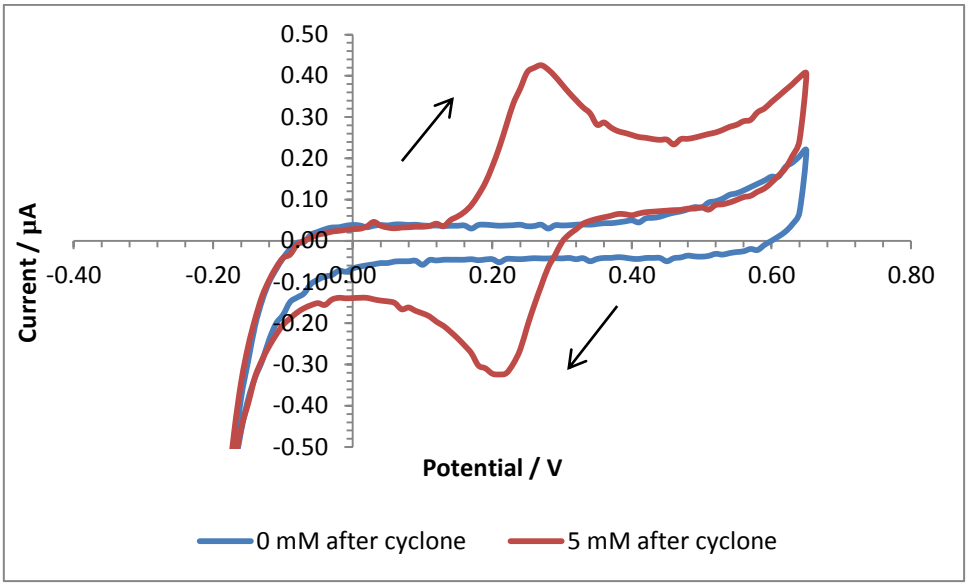

Figure 12.2 - Voltammograms obtained from the electrochemical interrogation of a phosphate buffer solution and a 5 mM ferrocenemonocarboxylic acid solution, with a CoPc sensor, taken from the collection chamber after the cyclone collection system was allowed to run for one cycle of 2 minutes/300 litres per minute (scan rate 20 mVs^{-1} vs. Ag/AgCl)

Despite the markedly low magnitude of current response, the voltammetric profile obtained is unmistakably due to ferrocenemonocarboxylic acid, as previously observed in section 5.2. It is obvious here that the current response obtained for a 5 mM FeCA solution via the cyclone system is lower than for a FeCA sample tested from a stock solution (0.028 mM corresponds to 5 mM). To assess the difference in the current response of the collected sample from that of an ideal sample (i.e. unaspirated) study was performed using serial dilutions from a solution of 5 mM ferrocenemonocarboxylic acid and interrogating them voltammetrically between -0.2 and +0.65 V (vs. Ag/AgCl). For clarity, the resulting voltammograms showing the peak values of interest can be seen in Figure 12.3.

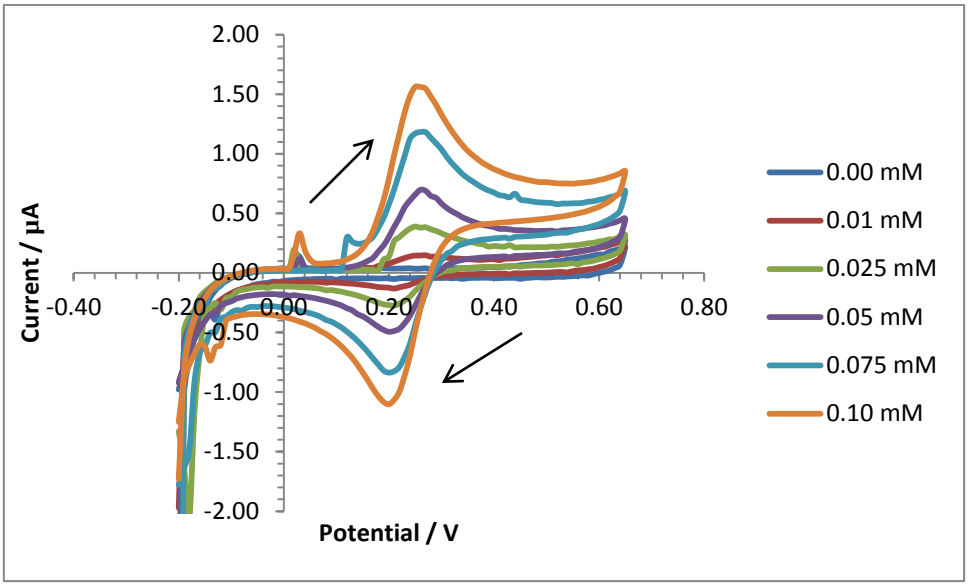

Figure 12.3 - Voltammograms obtained from the electrochemical interrogation of a variety of concentrations of ferrocenemonocarboxylic acid in a phosphate buffer solution, with a CoPc sensor (scan rate 20 mVs^{-1} vs. Ag/AgCl)

Leading on from this, a calibration curve was produced from which the concentration of the collected sample can be inferred from the maximum peak current obtained from voltammetric interrogation. This calibration curve can be seen below in Figure 12.4 where a linear profile was obtained that enables the estimation of the concentration of the collected samples of ferrocenemonocarboxylic acid, from a 5 mM stock solution.

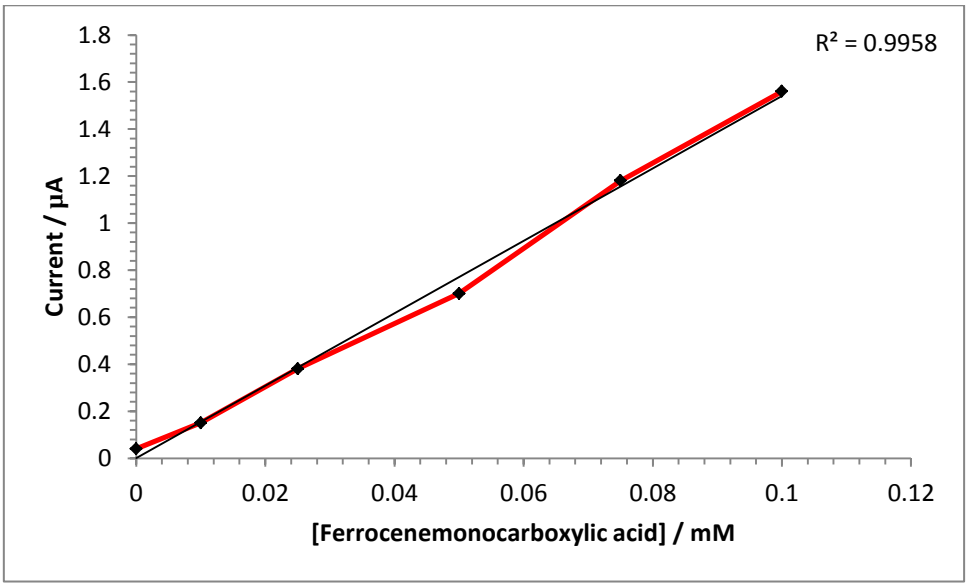

Figure 12.4 – Calibration plot taken from the maximum anodic peak current of a variety of concentrations of pure ferrocenemonocarboxylic acid in a phosphate buffer solution (scan rate 20 mVs^{-1} vs. Ag/AgCl)

Several collections were conducted, introducing different concentrations of the ferrocenemonocarboxylic acid into the air sampling device using the spray bottle, and the collected sample solutions were subsequently interrogated electrochemically as described previously. The resulting voltammetric profiles can be seen in Figure 12.5 and demonstrate that when different concentrations of the sample are sprayed into the atmosphere in front of the air intake valve a different concentration of the sample is collected once analysed.

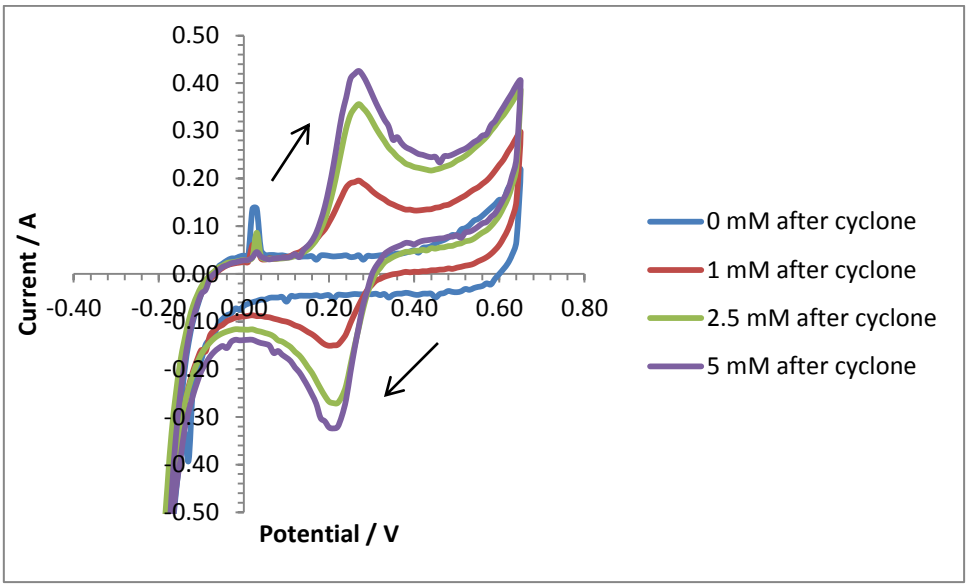

Figure 12.5 - Voltammograms obtained from the electrochemical interrogation of a variety of concentrations of ferrocenemonocarboxylic acid in a phosphate buffer solution after aspiration and collection using the air sampling system, with a CoPc sensor (scan rate 20 mVs^{-1} vs. Ag/AgCl)

The value from the maximum peak current for each concentration was taken and the percentage change calculated; this data is presented in Table 12.1.

Original concentration µM	**1.00**	**2.50**	**5.00**
Measured current µA	0.20	0.36	0.43
Collected concentration µM	0.013	0.024	0.028
% Change	98.70	99.04	99.44

Table 12.1 – Data taken from the maximum current at the anodic peak in Figure 12.5 demonstrating the percentage decrease in concentration between the initial concentration and that collected in the cyclone system

From this information it is possible to calculate an estimated concentration of stock TNT necessary to be aspirated in front of the air sampling system to enable detection using the system as described above.

12.3. Collection of TNT with the cyclone collection system and the subsequent electrochemical analysis

The introduction of TNT into the air sampling system was performed as described previously for FeCA (section 12.2). Using the data collated relating the difference between the concentration of sample collected from the concentration of the sample initially introduced to the system, in the case of FeCA, it is reasonable to make the assumption that this system dilutes the analyte by ~99% in each case (see Table 12.1). As such, as the concentration reliably detected by both the cavity microelectrode array and the protrusion covered microelectrode array was 200 μM it was assumed that the introduction of a sample of 20 mM (200 μM x 100 times = 20000 μM) of TNT would enable the electrochemical detection of the collected sample after aspiration. Unfortunately, since the commercially available TNT solution is purchased at a maximum concentration of 4.4 mM it is not possible to use 20 mM as the initial sample concentration.

As the figures calculated above depend on various assumptions, a study was undertaken regardless to assess the value of using this air sampling system coupled with the aspiration step, as described above, to detect TNT in the collected solution using the maximum concentration of TNT available, 4.4 mM. The resulting voltammograms can be seen below when interrogated electrochemically with an unmodified CoPc sensor both with and without the enzyme and cofactor included in the collected sample (the enzyme and cofactor were added to the collected sample after aspiration and cyclone collection), see Figure 12.6.

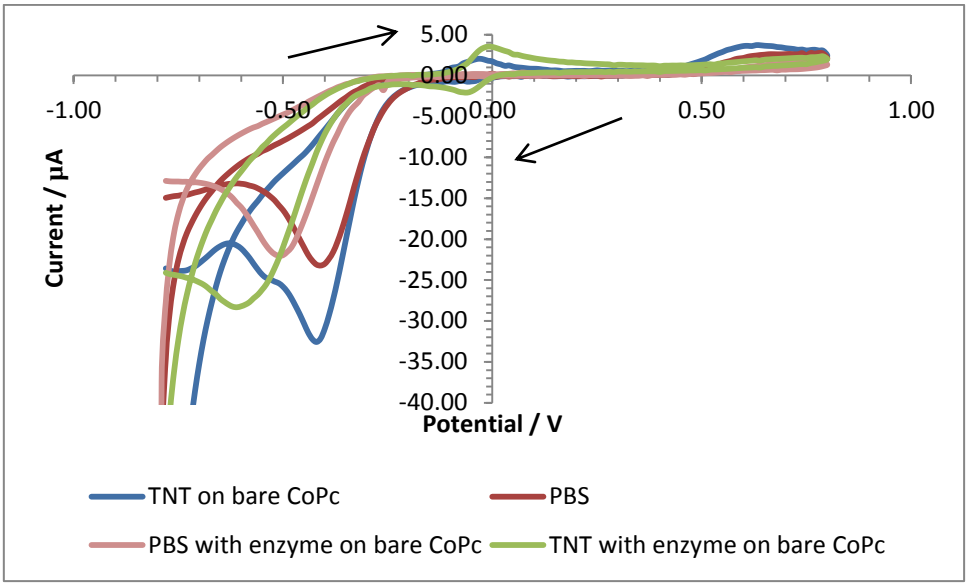

Figure 12.6 - Voltammograms obtained from the electrochemical interrogation of 4.4 mM TNT or baseline solutions after aspiration and collection using the air sampling system, with a CoPc sensor with 20 units NTR and 0.1 mM NADPH (scan rate 20 mVs^{-1} vs. Ag/AgCl)

It can be observed that when TNT is collected with the air sampling system in the manner described previously and interrogated electrochemically that a distinct set of peaks are again visible. The redox couple, known as R2 and O1, are clearly present around the 0.0 V potential in the voltammograms containing the TNT both with and without the enzyme system. The CoPc sensors were demonstrated previously to produce a peak in the cathodic region associated with the electrochemical reduction of cobalt and these peaks are again observed; however, there is a clear increase in the magnitude of the current response with the inclusion of the TNT sample from the cyclone system (green plot). Using the calibration curves in Chapters 8 and 9 (and assuming that the peaks present in the voltammograms above correspond to the -0.5 V peak present on the profiles of a voltammetric interrogation of a stock solution) it is possible to calculate the collected concentration of TNT to 389.8 µM for the TNT solution and 172.3 µM for the TNT solution above with additional enzyme and cofactor, which constitutes a percentage concentration decrease of 91.2 and 96.1 % for just TNT and TNT with NTR, respectively.

Following the same technique the collected sample was interrogated with both a cavity microelectrode array and the protrusion covered microelectrode array, the voltammograms can be seen below in Figure 12.7 and Figure 12.8, respectively.

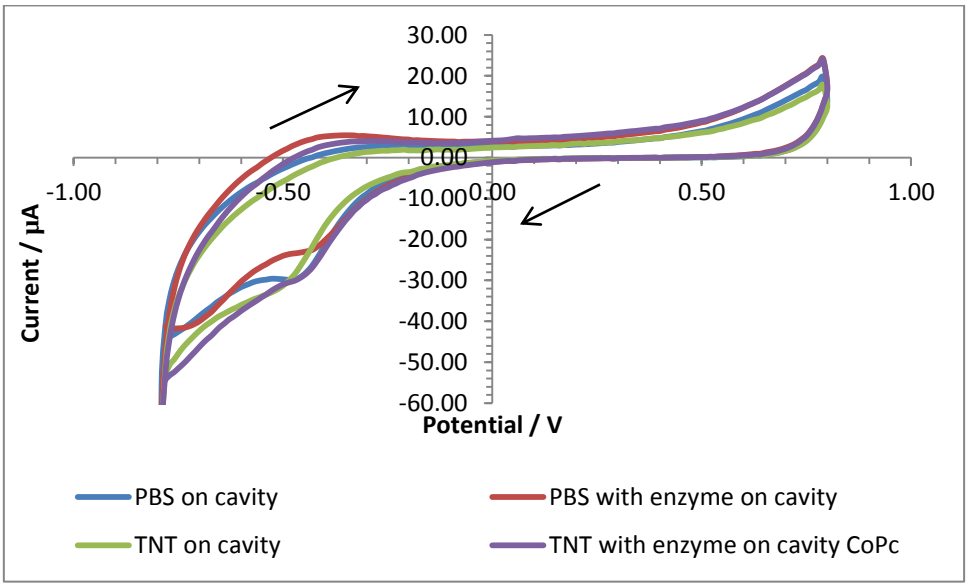

Figure 12.7 - Voltammograms obtained from the electrochemical interrogation of 4.4 mM TNT or baseline solutions after aspiration and collection using the air sampling system, with a cavity microelectrode array sensor both with 20 units NTR and 0.1 mM NADPH and without the enzyme and cofactor (scan rate 20 mVs^{-1} vs. Ag/AgCl)

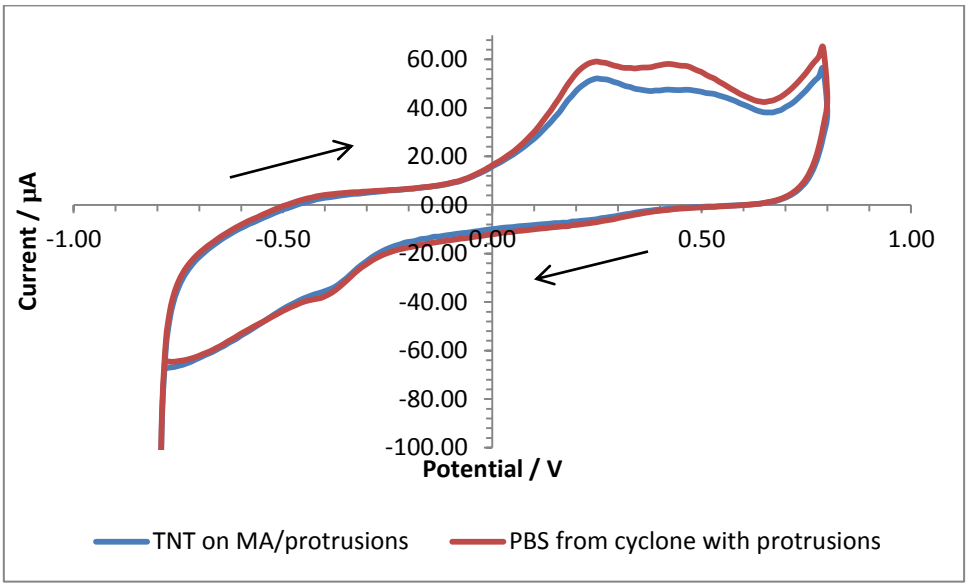

Figure 12.8 - Voltammograms obtained from the electrochemical interrogation of 4.4 mM TNT or baseline solutions after aspiration and collection using the air sampling system, with a cavity microelectrode array sensor both with 20 units NTR and 0.1 mM NADPH and without the enzyme and cofactor (scan rate 20 mVs^{-1} vs. Ag/AgCl)

While there was an obvious difference between the blank samples and the samples containing TNT for the cavity microelectrodes (Figure 12.7), again there was very little

difference when a protrusion covered microelectrode array was used for the electrochemical interrogation of the samples (Figure 12.8). This is likely to be due to the low concentration of TNT available for interrogation. As it is impossible to accurately establish what the available concentration of TNT is using the protrusion array to analyse the collected, aspirated sample without prior work to improve the sensitivity of the sensor, this will not be attempted here.

There is a slight difference between the blank samples and the TNT samples when interrogated with the cavity array and there does seem to be a shoulder in the cathodic region that could correspond to the reductive peak at -0.45 V (vs. Ag/AgCl) when an ideal sample of TNT is interrogated with these sensors (Figure 12.7). As such, making the assumption that these peaks are representative of one another, the calculated concentration of the sample of TNT collected from the cyclone and interrogated with the enzyme and cofactor is 342.2 μM which constitutes a 92.2% change in concentration. This change in concentration corresponds to those gained earlier with the unmodified CoPc sensor (Figure 12.6) and so it is likely that this concentration change is an accurate representation of the concentration calculation.

It has been demonstrated that the collection of TNT with the Coriolis®μ collection system is possible, with the change in concentration from the stock solution of 4.4 mM to the collected concentration corresponding to a 92-96% decrease. This is in close agreement to the results of the ferrocenemonocarboxylic acid study where the decrease in concentration of the initial sample was found to be around 99%. This decrease in concentration is not ideal for this type of system – the vapour pressure for an explosive like TNT is low and so it may not be possible for an air sampling system to collect an airborne aspirated sample of TNT concealed and well contained. However, explosives with a greater vapour pressure, such as peroxide based TATP, may be collected more easily. In the case of TNT, it would be necessary to improve the sensitivity of the detection system significantly to be able to detect airborne particles of a lower concentration than those demonstrated in this proof of principle piece.

12.4. Conclusions

As a pilot examination into the integration of an air sampling device with the electrochemical detection system developed over the course of this project, this study has proved successful. An experimental protocol was developed involving the introduction of the sample analyte into the collection solution using a spray bottle from which an aspiration was exuded every 10 seconds over a 2 minute period, the air sampling system was set to draw in the air at its maximum rate, 300 litres per minute.

Initially, a pilot study was carried out with the redox couple ferrocenemonocarboxylic acid and, following the development of a calibration curve of unaspirated FeCA, a value could be assigned as to the concentration of the collected (i.e. aspirated) sample. From this the percentage change from the initial stock sample could be calculated, which was a 99% decrease from the sample concentration originally aspirated in front of the air inlet valve.

This technique was then applied to a TNT solution at the maximum available concentration (using the stock solution as purchased at 4.4 mM) and the resulting sample was tested with an unmodified CoPc sensor, a cavity microelectrode array and a protrusion covered microelectrode array. The protrusion covered microelectrode array produced an indistinguishable response when the TNT was present in the sample when compared to a baseline sample from the cyclone consisting of just phosphate buffer solution due to the lack of sensitivity previously shown with this sensor platform. The unmodified CoPc sensor and the cavity microelectrode array did, however, produce voltammetric profiles that could be apportioned to the presence of TNT in the samples collected from the cyclone. The decrease in the concentration between that aspirated before the air inlet valve and that interrogated from the collection chamber was found to be between 92 and 96 %, a slight improvement when compared to the ferrocenemonocarboxylic acid collection study.

Whilst this collection technique coupled to the detection system developed over the course of this project is by no means a refined system, the proof of principle has been established here. Further work would be necessary to develop an optimised system.

13. General conclusions

This thesis has presented a body of work focussed towards the development of a detection system for a range of explosives, based upon the initial collection of airborne solution and their subsequent detection and analysis using electrochemical techniques.

This work involved the fabrication of microelectrode arrays, previously described within this group, with investigations into the optimal conditions for this fabrication when applied to a cobalt phthalocyanine-doped screen-printed electrode.

The intermediate aims of the research were to utilise screen-printed sensors to maintain simplicity in the design, to improve on the initial responses gained with planar sensors with the fabrication and optimisation of microelectrode arrays, to utilise commercially available products where appropriate and to attempt the incorporation of the developed sensing system with a cyclonic collection system.

The electrochemistry of the explosive compound utilised within this project was first studied using a carbon screen-printed electrode (SPCE) system in Chapter 5. This SPCE underwent an initial validation as an appropriate base sensor via electrochemical interrogation with a common redox couple, ferrocenemonocarboxylic acid. Here, the resulting redox peak couple, although showing the reversible reaction under examination, failed to display the 59mV peak separation as expected for a truly diffusion-controlled electrochemically reversible system. This was attributed to the non-homogenous nature of a carbon ink electrode, suggesting that a carbon ink electrode system is unlikely to produce the same optimal response as a more electroactive material such as gold or platinum. The advantage of using a screen-printed carbon-ink sensor above these other systems is the inherent low cost and disposability associated with carbon, whilst retaining the reproducibility of a mass fabricated screen-printed device.

When these screen-printed carbon electrodes were used to interrogate solutions containing the explosive compound 2,4,6-trinitrotoluene (TNT), the electroactivity of

the TNT was demonstrated with three electroactive peaks appearing in the voltammogram; one oxidative and two reductive, representing the reduction of the nitro groups firstly to a hydroxylamine and then reversibly into an amine moiety. These peaks were shown to increase with increasing concentrations of TNT and produced linear current response plots both at higher and lower concentrations, with r^2=0.99. A lower limit of detection of 400 nM was observed at a reductive peak at -0.79V, and due to trace quantities of explosive being postulated to exist at much lower levels in practical environments, it was deemed necessary to attempt to improve on this.

The inclusion of a biological entity was examined in Chapter 6 as a means to improve the detection limits of TNT when interrogated electrochemically with a SPCE. The suitability of a nitroreductase enzyme and its cofactor, NADPH, was first assessed using the absorbance peak at 340 nm, associated with NADPH, when interrogated in a UV visible spectrometer. When NADPH solution containing TNT was interrogated with a time scan in the spectrometer, a baseline was first reached depending on the concentration of the NADPH present. When the enzyme was then injected into the cuvette a reaction was initiated where the NADPH reduced the enzyme so that it in turn subsequently reduced the TNT; this occurs in a ping-pong Bi-Bi catalysis fashion. In the resulting UV enzyme-assay spectrum, the absorbance peak for NADPH was observed to decrease.

The demonstration of the activity of the enzyme system for the reduction of TNT enabled the inclusion of this system for use within the electrochemical reduction of TNT. The enzyme and cofactor were subsequently added to the TNT solution prior to electrochemical interrogations and this was found to increase the magnitude of the current response (Chapter 7). The limits of detection, however, were not improved with this inclusion of the enzyme system – the reductive peak in the far cathodic region was demonstrated to have a similar LOD at 500 nM.

To retain the screen-printed sensors so that the advantages already highlighted associated with them may be maintained, the use of a more electroactive base material was sort. Cobalt phthalocyanine-doped (CoPc) screen-printed sensors offer

the advantages of low cost, reproducibility and inherent disposability related to the plain carbon sensors but with the additional advantage of increased electroactivity when compared to plain carbon ink. When used in the interrogation of a TNT solution, CoPc-doped carbon ink sensors, with their intrinsic increased electroactivity had the effect of increasing the clarity (in terms of signal differentiation) of the reductive peak in the far cathodic region such that the single broad peak observed on bare carbon ink was now split into two distinct peaks. Detection limits were 2700 and 9000 nM for the two reductive peaks, R1a and R1b, respectively; and were 1000 nM for the oxidative peak O1 and 300 nM for the peak R2.

However, when the enzyme system described in chapter 6 was then added to this CoPc-doped screen-printed sensor interrogation of TNT, there was found to be no real increase in the magnitude of the current response. It is postulated here that this is due to the increased electroactivity associated with the CoPc-doped sensors being such that the reductive activity of the enzyme on the TNT is dominated by this improved electrochemical reduction of the TNT by the new sensor system. There was, however, a slight improvement in the differential clarity of the peaks when the enzyme and cofactor were included and this factor was demonstrated further when an increased amount of enzyme was incorporated in the solution prior to further interrogations.

An attempt was made to further improve the limit of detection by the fabrication and optimisation of a network of cavity microelectrodes (interlinked via the underlying carbon ink to form a microelectrode array) upon the surface of the screen-printed carbon surface (Chapter 10). Prior optimisation studies had already been completed utilising plain carbon / gold screen-printed electrodes within this research group; however the fabrication needed to be optimised with reference to a CoPc-doped screen-printed electrode system.

A pre-treatment through exposure of the sensor to ultrasound had been demonstrated previously to improve the electrodeposition of the insulating polymer, poly(phenylenediamine), due to the hydrophobicity of carbon causing the adherence of gas bubbles on the sensor surface. This ultrasonic treatment expelled these bubbles enabling a better deposition of the polymer. This was found not to be the case the

CoPc-doped sensors; it is postulated that the application of ultrasound in this manner may dislodge some of the CoPc particles exposing a less conductive surface and that it is possible that the CoPc sensors offer a more hydrophilic surface where there is less tendency for the adherence of bubbles to the surface.

Studies were made into the optimal number of scans applied to produce adequate insulation of the electroactive surface and 50 scans was demonstrated to provide a good level of insulation – increasing this to 60 scans produced little difference in the insulated effect. Analogous to previous studies observed on bare carbon surfaces.

The influence of the scan rate on the insulating polymer film was also investigated where the slowest scan rate investigated, 5 mVs^{-1}, was demonstrated to provide the greatest insulation of the sensor. This insulation was not, however, significantly greater than that gained with a 10 mVs^{-1} scan rate and so to benefit from this shortened time period for the electropolymerisation stage, the faster scan rate was selected for subsequent sensor fabrications.

Ultrasonic ablation was performed on these polymer insulated sensors in an ultrasonic bath at 25 KHz to produce cavities through the insulating polymer down to the conductive surface – these cavities form the basis of the microelectrode array. The optimal sonication period was elucidated so that the sensor exhibited microelectrode characteristics, such as stir-independence and enhanced signal response. A sonication time of 10 seconds was found to demonstrate these microelectrode features which were seen to diminish as the density of cavities increases beyond a critical value. These characteristics were assessed again using the redox couple ferrocenemonocarboxylic acid, and it was found that the characteristic sigmoidal shape associated with microelectrode behaviour was present following a 10 seconds sonication period, but gradually the voltammetric profile reverted to that obtained with a bare, planar CoPc sensor as the period of sonication exposure increased. A study to assess whether the microelectrode array displayed the characteristic stir-independent properties associated with microelectrodes was performed. The application of convection in a system where the potential is held and the current response measured as a function of time was demonstrated to have a significantly

greater effect when interrogated with an unmodified electrode as compared to the cavity microelectrode array.

The interrogation of TNT with the microelectrode arrays was found to further improve the clarity of the peaks – the two peaks observed in the far cathodic region were seen to become three distinct peaks, with the broad peak at -0.5 V splitting to become two separate peaks. These three peaks were postulated to be indicative of the reduction of the three nitro groups on the aromatic central structure of TNT. The magnitude of the current response also increased significantly when interrogating a solution containing TNT with both the enzyme and cofactor present. The differentiation between different concentrations of TNT was found to diminish, however, with the limit of detection of TNT in opposition to what one might expect when using a microelectrode array, (i.e. greater than that observed for a planar electrode). It was proposed that the cavity array may 'fill-up' with the analyte solution when submerged causing hindrance in the flux of reactants and products to and from the conductive surface. It may also be the case that the enzyme within the solution is not able to situate itself near the conductive surface adequately – this may require an increase in the available enzyme in solution or the immobilisation of it near to the conductive area.

To address this enzyme immobilisation a second electropolymerisation step was undertaken to incorporate the co-entrapment of the enzyme and cofactor in close proximity to the sensor surface with the development of a microelectrode array of protrusions of polyaniline grown from the exposed conductive surface at the base of the cavities (Chapter 11). Polyaniline has been used previously by our group to immobilise biological species in this manner, however, prior examination of the activity of the nitroreductase enzyme at various pH levels (Chapter 6) demonstrated that the enzyme barely retains any activity at pH levels lower than pH 7.0 (i.e. more acidic). As polyaniline is essentially non-conducting at neutral pH levels it was impossible to retain the electroactivity of the polymer and the activity of the enzyme. As such, this step was undertaken as an immobilisation stage rather than an improvement to the electroactivity with the incorporation of a conducting polymer. The resulting

interrogations of a TNT solution were found to have increased the magnitude of the current response once more but did little to alleviate the differentiation issues at low concentrations. This lack of improvement in the sensitivity of the device was attributed to the insulating effect of the polyaniline deposition at more alkaline pH values. An investigative study was performed to assess how modifications to the electropolymerisation of the polyaniline may affect the conductivity of the polymer coating. The addition of excess salt (i.e. an increase in monomer solution conductivity) was demonstrated to improve the deposited polymeric conductivity considerably, as was a slight decrease in the pH of the solution from which the aniline monomer is polymerised from. These aspects would require further investigation to determine the optimum deposition of PANI with the immobilisation of nitroreductase.

Finally, a proof of principle study was carried out using an air sampling device to incorporate the sensors developed throughout this project with a system that enables the collection of airborne particles (Chapter 13). Preliminary studies were undertaken on ferrocenemonocarboxylic acid and although the collected concentration of an aspirated sample of ferrocenemonocarboxylic acid was demonstrated to be 99% less than the stock sample concentration, a measurement of the collected sample was achievable via electrochemical interrogation. This concept was then applied to the collection of a sample of TNT and this too was successfully detected electrochemically although, once more, at a level much lower than the concentration of the initial aspirated sample. This study provided a proof of concept that enables the completion of one of the most important aims of this research project, namely to produce a sensing system that is able to take measurements of airborne explosive traces.

14. Suggestions for further work

The objective of this project has been the development of a screen-printed, disposable sensor system for the detection and subsequent electrochemical measurement of airborne explosive particulate matter. Each stage of the development process has been aimed towards the improvement of the LOD for the interrogation of TNT, from the first principles of detection through to airborne capture and measurement. Attempts have also been made to facilitate an enhancement of signal differentiation at each stage. Whilst successfully answering the question posed by the objective in terms of demonstrating a preliminary methodology for airborne TNT measurement, the work has led to further areas of research, which must in turn be fulfilled to fully demonstrate the potential of the proposed technique. This chapter therefore provides a number of suggestions for future research.

Whilst developmental studies within this thesis have improved on the signal response in terms of current levels afforded via the sensor detection technique, it would be advantageous to:-

- Further develop the polyaniline deposition process to improve the sensitivity of the resulting microelectrode array in terms of polymer film conductivity.
- Optimise the electrodeposition of PANI at lower pH to balance the polymeric conductivity and enzyme stability.
- Investigate different enzymes that may retain their activity at lower pH, whilst facilitating an enhanced response for TNT (and similar compounds) via an electrochemical interrogation regime.
- Assess differing conducting polymers in place of polyaniline, such as polypyrrole and polythiophene.

- Investigate the effects of interferrents on signal response in terms of voltammetric potential peaks.
- Facilitate an enhanced response at lower levels of TNT to mimic levels postulated to occur in 'real-life' environments.

The coupling of the cyclone collection to the sensor design was demonstrated successfully as a 'proof-of-principle'. However, further work is required to:-

- Optimise the process for introducing the sample into the collection chamber - to better mimic real-world collection environments.
- Assess any effects interferrents may have on the uptake of TNT (and its derivatives) via the cyclone technique.
- Improve the concentration of the collected analyte – increasing the draw of the air sampling system.
- Investigate the use of different sample media (such as differing solvents).

Finally, the detection technique has been developed with a view to allow for mass production of the sensor as described in this work. Therefore for this to be undertaken any further work should:-

- Investigate the longevity of the finalised sensor.
- Optimise the ideal storage conditions of the sensor.
- Investigate the effects of scaling up the production of a sonochemically fabricated sensor design with the application of industrial sized sonication tanks on the reliability and reproducibility of the sensors.

Finally, to achieve the commercialisation of such a device, the development of a hand-held instrument would be desirable where the sensor system can be easily placed inside and removed from the hand-set to provide the disposability; and the sample analyte for the optimised air sampling system can be either manually applied to the surface of the active sensor or, if possible, this step may be prepared through an automated integrated system between the cyclone collection system and the electrochemical device.

15. References

Real Life Economics : Understanding Wealth Creation, (1992), Routledge.

Abadie, A. and Gardeazabal, J. (2008), "Terrorism and the world economy", *European Economic Review,* vol. 52, no. 1, pp. 1-27.

Agüí, L., Vega-Montenegro, D., Yáñez-Sedeño, P. and Pingarrón, J. M. (2005), "Rapid voltammetric determination of nitroaromatic explosives at electrochemically activated carbon-fibre electrodes", *Anal.Bioanal.Chem.,* vol. 382, no. 2, pp. 381-387.

Alberici, R. M., Simas, R. C., Sanvido, G. B., Romão, W., Lalli, P. M., Benassi, M., Cunha, I. B. S. and Eberlin, M. N. (2010), "Ambient mass spectrometry: Bringing MS into the "real world"", *Analytical and Bioanalytical Chemistry,* vol. 398, no. 1, pp. 265-294.

Algarra, M., Campos, B. B., Miranda, M. S. and da Silva, J. C. G. E. "CdSe quantum dots capped PAMAM dendrimer nanocomposites for sensing nitroaromatic compounds", *Talanta,* .

Ali, E. M. A., Edwards, H. G. M., Hargreaves, M. D. and Scowen, I. J. (2009a), "Detection of explosives on human nail using confocal Raman microscopy", *Journal of Raman Spectroscopy,* vol. 40, no. 2, pp. 144-149.

Ali, E. M. A., Edwards, H. G. M. and Scowen, I. J. (2009b), "In-situ detection of single particles of explosive on clothing with confocal Raman microscopy", *Talanta,* vol. 78, no. 3, pp. 1201-1203.

Ali, E. M. A., Edwards, H. G. M. and Scowen, I. J. (2009c), "Raman spectroscopy and security applications: The detection of explosives and precursors on clothing", *Journal of Raman Spectroscopy,* vol. 40, no. 12, pp. 2009-2014.

Alizadeh, T., Zare, M., Ganjali, M. R., Norouzi, P. and Tavana, B. (2010), "A new molecularly imprinted polymer (MIP)-based electrochemical sensor for monitoring 2,4,6-trinitrotoluene (TNT) in natural waters and soil samples", *Biosensors and Bioelectronics,* vol. 25, no. 5, pp. 1166-1172.

Anderson, G. P., Moore, M., Charles, P. T. and Goldman, E. R. (2010), "Bead-based fluid array detection of pentaerythritol tetranitrate: Comparison of monoclonal vs. llama polyclonal antibodies", *Analytical Letters,* vol. 43, no. 18, pp. 2913-2922.

Anderson, G. P., Moreira, S. C., Charles, P. T., Medintz, I. L., Goldman, E. R., Zeinali, M. and Taitt, C. R. (2006), "TNT detection using multiplexed liquid array displacement immunoassays", *Analytical Chemistry,* vol. 78, no. 7, pp. 2279-2285.

Arduini, F., Amine, A., Moscone, D., Ricci, F. and Palleschi, G. (2007), "Fast, sensitive and cost-effective detection of nerve agents in the gas phase using a portable instrument and an electrochemical biosensor", *Analytical and Bioanalytical Chemistry,* vol. 388, no. 5-6, pp. 1049-1057.

Arin, K. P., Ciferri, D. and Spagnolo, N. (2008), "The price of terror: The effects of terrorism on stock market returns and volatility", *Economics Letters,* vol. 101, no. 3, pp. 164-167.

Armstrong, S., Miao, Z. -., Rowell, F. J. and Ali, Z. (2001), "Simple dip strip ELISA for airborne estrogenic steroids", *Analytica Chimica Acta,* vol. 444, no. 1, pp. 79-86.

Ates, M. and Sarac, A. S. (2009), "Conducting polymer coated carbon surfaces and biosensor applications", *Progress in Organic Coatings,* vol. 66, no. 4, pp. 337-358.

Babis, J. S., Sperline, R. P., Knight, A. K., Jones, D. A., Gresham, C. A. and Denton, M. B. (2009), "Performance evaluation of a miniature ion mobility spectrometer drift cell for application in hand-held explosives detection ion mobility spectrometers", *Analytical and Bioanalytical Chemistry,* vol. 395, no. 2, pp. 411-419.

Banerjee, S., Mohapatra, S. K., Misra, M. and Mishra, I. B. (2009), "The detection of improvised nonmilitary peroxide based explosives using a titania nanotube array sensor", *Nanotechnology,* vol. 20, no. 7.

Bard, A. J. (2001), *Electrochemical methods : fundamentals and applications,* 2nd ed, John Wiley, New York ; Chichester.

Bartlett, P. N. and Birkin, P. R. (1993), "The application of conducting polymers in biosensors", *Synthetic Metals,* vol. 61, no. 1-2, pp. 15-21.

Bartlett, P. N., Gardner, J. W. and Whitaker, R. G. (1990), "Electrochemical deposition of conducting polymers onto electronic substrates for sensor applications", *Sensors and Actuators A: Physical,* vol. 23, no. 1-3, pp. 911-914.

Bartlett, P. N. and Whitaker, R. G. (1988), "Strategies for the development of amperometric enzyme electrodes", *Biosensors,* vol. 3, no. 6, pp. 359-379.

Barton, A. C., Collyer, S. D., Davis, F., Gornall, D. D., Law, K. A., Lawrence, E. C. D., Mills, D. W., Myler, S., Pritchard, J. A., Thompson, M. and Higson, S. P. J. (2004), "Sonochemically fabricated microelectrode arrays for biosensors offering widespread applicability: Part I", *Biosens.Bioelectron.,* vol. 20, no. 2, pp. 328-337.

Beck, F. (1988), "Electrodeposition of polymer coatings", *Electrochimica Acta,* vol. 33, no. 7, pp. 839-850.

Berden, G., Peeters, R. and Meijer, G. (2000), "Cavity ring-down spectroscopy: Experimental schemes and applications", *International Reviews in Physical Chemistry,* vol. 19, no. 4, pp. 565-607.

Bhalla, V., Zhao, X. and Zazubovich, V. (2011), "Detection of explosive compounds using Photosystem II-based biosensor", *Journal of Electroanalytical Chemistry,* vol. 657, no. 1-2, pp. 84-90.

Blain, M. G., Riter, L. S., Cruz, D., Austin, D. E., Wu, G., Plass, W. R. and Cooks, R. G. (2004), "Towards the hand-held mass spectrometer: Design considerations, simulation, and fabrication of micrometer-scaled cylindrical ion traps", *International Journal of Mass Spectrometry,* vol. 236, no. 1-3, pp. 91-104.

Blomberg, S. B., Hess, G. D. and Orphanides, A. (2004a), "The macroeconomic consequences of terrorism", *Journal of Monetary Economics,* vol. 51, no. 5, pp. 1007-1032.

Blomberg, S. B., Hess, G. D. and Weerapana, A. (2004b), "Economic conditions and terrorism", *European Journal of Political Economy,* vol. 20, no. 2, pp. 463-478.

Bohling, C., Hohmann, K., Scheel, D., Bauer, C., Schippers, W., Burgmeier, J., Willer, U., Holl, G. and Schade, W. (2007), "All-fiber-coupled laser-induced breakdown spectroscopy sensor for hazardous materials analysis", *Spectrochimica Acta - Part B Atomic Spectroscopy,* vol. 62, no. 12, pp. 1519-1527.

Bond, A. M. (1994), "Past, present and future contributions of microelectrodes to analytical studies employing voltammetric detection. A review", *The Analyst,* vol. 119, no. 11, pp. R1-R21.

Bratin, K., Kissinger, P. T., Briner, R. C. and Bruntlett, C. S. (1981), "Determination of nitro aromatic, nitramine, and nitrate ester explosive compounds in explosive mixtures and gunshot residue by liquid chromatography and reductive electrochemical detection", *Anal.Chim.Acta,* vol. 130, no. 2, pp. 295-311.

Bryant, C. and DeLuca, M. (1991), "Purification and characterization of an oxygen-insensitive NAD(P)H nitroreductase from Enterobacter cloacae", *Journal of Biological Chemistry,* vol. 266, no. 7, pp. 4119-4125.

Bunte, G., Heil, M., Rüseling, D., Hürttlen, J., Pontius, H. and Krause, H. (2009), "Trace detection of explosives vapours by molecularly imprinted polymers for security measures", *Propellants, Explosives, Pyrotechnics,* vol. 34, no. 3, pp. 245-251.

Bunte, G., Hürttlen, J., Pontius, H., Hartlieb, K. and Krause, H. (2007), "Gas phase detection of explosives such as 2,4,6-trinitrotoluene by molecularly imprinted polymers", *Analytica Chimica Acta,* vol. 591, no. 1 SPEC. ISS., pp. 49-56.

Capitán-Vallvey, L. F. and Palma, A. J. (2011), "Recent developments in handheld and portable optosensing—A review", *Analytica Chimica Acta,* vol. 696, no. 1-2, pp. 27-46.

Caro, C. A., Bedioui, F. and Zagal, J. H. (2002), "Electrocatalytic oxidation of nitrite on a vitreous carbon electrode modified with cobalt phthalocyanine", *Electrochimica Acta,* vol. 47, no. 9, pp. 1489-1494.

Caron, T., Clavaguera, S., Huron, M., Montméat, P., Pasquinet, E., Lère-Porte, J. -., Serein-Spirau, F., Perraut, F. and Prené, P. (2010a), "Detection of explosive vapors: Development and performances of a fluorescence sensor", *International Conference on Environmental Odour Monitoring and Control, NOSE2010,* Vol. 23, 22 September 2010 through 24 September 2010, Florence, pp. 25.

Caron, T., Guillemot, M., Montméat, P., Veignal, F., Perraut, F., Prené, P. and Serein-Spirau, F. (2010b), "Ultra trace detection of explosives in air: Development of a portable fluorescent detector", *Talanta,* vol. 81, no. 1-2, pp. 543-548.

Cass, A. E. G., Davis, G., Francis, G. D., Allen O Hill, H., Aston, W. J., John Higgins, I., Plotkin, E. V., Scott, L. D. L. and Turner, A. P. F. (1984), "Ferrocene-mediated enzyme electrode for amperometric determination of glucose", *Analytical Chemistry®,* vol. 56, no. 4, pp. 667-671.

Caygill, J. S., Davis, F. and Higson, S. P. J. "Current trends in explosive detection techniques", *Talanta,* .

Cerruti, M., Jaworski, J., Raorane, D., Zueger, C., Varadarajan, J., Carraro, C., Lee, S. -., Maboudian, R. and Majumdar, A. (2009), "Polymer-oligopeptide composite

coating for selective detection of explosives in water", *Analytical Chemistry,* vol. 81, no. 11, pp. 4192-4199.

Chang, S., Ko, H., Singamaneni, S., Gunawidjaja, R. and Tsukruk, V. V. (2009), "Nanoporous membranes with mixed nanoclusters for Raman-based label-free monitoring of peroxide compounds", *Analytical Chemistry,* vol. 81, no. 14, pp. 5740-5748.

Chen, A. H. and Siems, T. F. (2004), "The effects of terrorism on global capital markets", *European Journal of Political Economy,* vol. 20, no. 2, pp. 349-366.

Chen, J., Chen, Y., Zhao, H., Bastiaans, G. J. and Zhang, X. -. (2007), "Absorption coefficients of selected explosives and related compounds in the range of 0.1-2.8 THz", *Optics Express,* vol. 15, no. 19, pp. 12060-12067.

Chen, J. -., Shih, J. -., Liu, C. -., Kuo, M. -. and Zen, J. -. (2006), "Disposable electrochemical sensor for determination of nitroaromatic compounds by a single-run approach", *Analytical Chemistry,* vol. 78, no. 11, pp. 3752-3757.

Chen, P. -., Sukcharoenchoke, S., Ryu, K., De Arco, L. G., Badmaev, A., Wang, C. and Zhou, C. (2010a), "2,4,6-Trinitrotoluene (TNT) chemical sensing based on aligned single-walled carbon nanotubes and ZnO nanowires", *Advanced Materials,* vol. 22, no. 17, pp. 1900-1904.

Chen, W., Zuckerman, N. B., Konopelski, J. P. and Chen, S. (2010b), "Pyrene-functionalized ruthenium nanoparticles as effective chemosensors for nitroaromatic derivatives", *Analytical Chemistry,* vol. 82, no. 2, pp. 461-465.

Chen, Y., Zhao, Y., Chu, J., Liu, S., Li, W., Liu, G., Tian, Y., Xiong, Y. and Yu, H. (2010c), "Fabrication and characterization of an innovative integrated solid-state microelectrode", *Electrochimica Acta,* vol. 55, no. 20, pp. 5984-5989.

Chianella, I., Piletsky, S. A., Karim, K., Piletska, E. V., Guerreiro, A., Romero Guerra, M. and and Turner, A. P. F. (2004), "Molecularly imprinted polymers as materials for crime prevention and detection", *MIP2004 – Third International Workshop on Molecularly Imprinted Polymers,* September 12–15th (2004), Cardiff, Wales, UK, .

Chuang, M. -., Windmiller, J. R., Santhosh, P., Ramírez, G. V., Galik, M., Chou, T. -. and Wang, J. (2010), "Textile-based Electrochemical Sensing: Effect of Fabric Substrate and Detection of Nitroaromatic Explosives", *Electroanalysis,* vol. 22, no. 21, pp. 2511-2518.

Cizek, K., Prior, C., Thammakhet, C., Galik, M., Linker, K., Tsui, R., Cagan, A., Wake, J., Belle, J. L. and Wang, J. (2010), "Integrated explosive preconcentrator and electrochemical detection system for 2,4,6-trinitrotoluene (TNT) vapor", *Analytica Chimica Acta,* vol. 661, no. 1, pp. 117-121.

Clark, L. C. and Lyons, C. (1962), "Electrode systems for continuous monitoring in cardiovascular surgery", *Ann. NY Acad. Sci.,* vol. 102, pp. 29-45.

Cody, R. B., Laramée, J. A. and Durst, H. D. (2005), "Versatile new ion source for the analysis of materials in open air under ambient conditions", *Analytical Chemistry,* vol. 77, no. 8, pp. 2297-2302.

Collyer, S. D., Davis, F. and Higson, S. P. J. (2010), "Sonochemically fabricated microelectrode arrays for use as sensing platforms", *Sensors,* vol. 10, no. 5, pp. 5090-5132.

Contakes, S. M. (2000), "π-Complexes of phthalocyanines and metallophthalocyanines", *Organometallics,* vol. 19, no. 23, pp. 4767-4774.

Cooks, R. G., Ouyang, Z., Takats, Z. and Wiseman, J. M. (2006), "Ambient mass spectrometry", *Science,* vol. 311, no. 5767, pp. 1566-1570.

Corcelli, A., Lobasso, S., Lopalco, P., Dibattista, M., Araneda, R., Peterlin, Z. and Firestein, S. (2010), "Detection of explosives by olfactory sensory neurons", *Journal of hazardous materials,* vol. 175, no. 1-3, pp. 1096-1100.

Cotte-Rodríguez, I., Hernández-Soto, H., Chen, H. and Cooks, R. G. (2008), "In situ trace detection of peroxide explosives by desorption electrospray ionization and desorption atmospheric pressure chemical ionization", *Analytical Chemistry,* vol. 80, no. 5, pp. 1512-1519.

Crouch, E., Cowell, D. C., Hoskins, S., Pittson, R. W. and Hart, J. P. (2005), "A novel, disposable, screen-printed amperometric biosensor for glucose in serum fabricated using a water-based carbon ink", *Biosensors and Bioelectronics,* vol. 21, no. 5, pp. 712-718.

Dasary, S. S. R., Singh, A. K., Senapati, D., Yu, H. and Ray, P. C. (2009), "Gold nanoparticle based label-free SERS probe for ultrasensitive and selective detection of trinitrotoluene", *Journal of the American Chemical Society,* vol. 131, no. 38, pp. 13806-13812.

De Lucia Jr., F. C., Gottfried, J. L., Munson, C. A. and Miziolek, A. W. (2007), "Double pulse laser-induced breakdown spectroscopy of explosives: Initial study towards improved discrimination", *Spectrochimica Acta - Part B Atomic Spectroscopy,* vol. 62, no. 12, pp. 1399-1404.

Degani, Y. and Heller, A. (1987), "Direct Electrical Communication between Chemically Modified Enzymes and Metal Electrodes. 1. Electron Transfer from Glucose Oxidase to Metal Electrodes via Electron Relays, Bound Covalently to the Enzyme", *Journal of Physical Chemistry,* vol. 91, no. 6, pp. 1285.

Deng, H. and Van Berkel, G. J. (1999), "Electrochemical polymerization of aniline investigated using on-line electrochemistry/electrospray mass spectrometry", *Analytical Chemistry,* vol. 71, no. 19, pp. 4284-4293.

Deshpande, M. V. and Amalnerkar, D. P. (1993), "Biosensors prepared from electrochemically-synthesized conducting polymers", *Progress in Polymer Science,* vol. 18, no. 4, pp. 623-649.

Didenko, Y. T., McNamara, W. B. and Suslick, K. S. (1999), "Temperature of multibubble sonoluminescence in water", *Journal of Physical Chemistry A,* vol. 103, no. 50, pp. 10783-10788.

Dikmelik, Y., McEnnis, C. and Spicer, J. B. (2008), "Femtosecond and nanosecond laser-induced breakdown spectroscopy of trinitrotoluene", *Optics Express,* vol. 16, no. 8, pp. 5332-5337.

Dixon, M. (1979), *Enzymes,* 3rd ed, Longman, London.

Dowling, J. P. and Chin-Fang, Y. (2007), *Modern developments in behavioual economics,* World Scientific Publishing Co., Singapore.

Drakos, K. and Müller, C. (2011), "Terrorism risk concern in Europe", *Economics Letters,* vol. 112, no. 2, pp. 195-197.

Drakos, K. (2004), "Terrorism-induced structural shifts in financial risk: airline stocks in the aftermath of the September 11th terror attacks", *European Journal of Political Economy,* vol. 20, no. 2, pp. 435-446.

Driscoll, L. (2011), *Airports: security blanket*, available at: http://www.flightglobal.com/news/articles/airports-security-blanket-357103/ (accessed 2/6).

Du, D., Wang, J., Smith, J. N., Timchalk, C. and Lin, Y. (2009), "Biomonitoring of organophosphorus agent exposure by reactivation of cholinesterase enzyme based on carbon nanotube-enhanced flow-injection amperometric detection", *Analytical Chemistry,* vol. 81, no. 22, pp. 9314-9320.

Du, H., He, G., Liu, T., Ding, L. and Fang, Y. (2011), "Preparation of pyrene-functionalized fluorescent film with a benzene ring in spacer and sensitive detection to picric acid in aqueous phase", *Journal of Photochemistry and Photobiology A: Chemistry,* vol. 217, no. 2-3, pp. 356-362.

Duić, L. and Mandić, Z. (1992), "Counter-ion and pH effect on the electrochemical synthesis of polyaniline", *Journal of Electroanalytical Chemistry,* vol. 335, no. 1-2, pp. 207-221.

Eckstein, Z. and Tsiddon, D. (2004), "Macroeconomic consequences of terror: Theory and the case of Israel", *Journal of Monetary Economics,* vol. 51, no. 5, pp. 971-1002.

Eggins, B. R. (2002), *Chemical Sensors and Biosensors,* 1st ed, John Wiley & Sons, Ltd, Chichester.

Esteve-Núñez, A., Caballero, A. and Ramos, J. L. (2001), "Biological degradation of 2,4,6-trinitrotoluene", *Microbiology and Molecular Biology Reviews,* vol. 65, no. 3, pp. 335-352.

Ewing, R. G., Atkinson, D. A., Eiceman, G. A. and Ewing, G. J. (2001), "A critical review of ion mobility spectrometry for the detection of explosives and explosive related compounds", *Talanta,* vol. 54, no. 3, pp. 515-529.

Ewing, R. G. and Waltman, M. J. (2009), "Mechanisms for negative reactant ion formation in an atmospheric pressure corona discharge", *International Journal for Ion Mobility Spectrometry,* vol. 12, no. 2, pp. 65-72.

Fang, X. and Ahmad, S. R. (2009), "Detection of explosive vapour using surface-enhanced Raman spectroscopy", *Applied Physics B: Lasers and Optics,* vol. 97, no. 3, pp. 723-726.

Fanjul-Bolado, P., Hernández-Santos, D., Lamas-Ardisana, P. J., Martín-Pernía, A. and Costa-García, A. (2008), "Electrochemical characterization of screen-printed and conventional carbon paste electrodes", *Electrochimica Acta,* vol. 53, no. 10, pp. 3635-3642.

Federici, J. F., Schulkin, B., Huang, F., Gary, D., Barat, R., Oliveira, F. and Zimdars, D. (2005), "THz imaging and sensing for security applications - Explosives, weapons and drugs", *Semiconductor Science and Technology,* vol. 20, no. 7.

Fleger, Y., Nagli, L., Gaft, M. and Rosenbluh, M. (2009), "Narrow gated Raman and luminescence of explosives", *Journal of Luminescence,* vol. 129, no. 9, pp. 979-983.

Flint, E. B. and Suslick, K. S. (1991), "The temperature of cavitation", *Science,* vol. 253, no. 5026, pp. 1397-1399.

Fortier, G., Brassard, E. and Bélanger, D. (1990), "Optimization of a polypyrrole glucose oxidase biosensor", *Biosensors and Bioelectronics,* vol. 5, no. 6, pp. 473-490.

Foulds, N. C. and Lowe, C. R. (1986), "Enzyme entrapment in electrically conducting polymers. Immobilisation of glucose oxidase in polypyrrole and its application in amperometric glucose sensors", *Journal of the Chemical Society, Faraday Transactions 1: Physical Chemistry in Condensed Phases,* vol. 82, no. 4, pp. 1259-1264.

Frey, B. S. (2009), "How can business cope with terrorism?", *Journal of Policy Modeling,* vol. 31, no. 5, pp. 779-787.

Fu, X. -., Chen, X., Wang, J., Liu, J. -. and Huang, X. -. (2010), "Amino functionalized mesoporous silica microspheres with perpendicularly aligned mesopore channels for electrochemical detection of trace 2,4,6-trinitrotoluene", *Electrochimica Acta,* vol. 56, no. 1, pp. 102-107.

Furton, K. G. and Myers, L. J. (2001), "The scientific foundation and efficacy of the use of canines as chemical detectors for explosives", *Talanta,* vol. 54, no. 3, pp. 487-500.

Gazit, I., Goldblatt, A. and Terkel, J. (2005), "Formation of an olfactory search image for explosives odours in sniffer dogs", *Ethology,* vol. 111, no. 7, pp. 669-680.

Gazit, I. and Terkel, J. (2003), "Explosives detection by sniffer dogs following strenuous physical activity", *Applied Animal Behaviour Science,* vol. 81, no. 2, pp. 149-161.

Genies, E. M. and Tsintavis, C. (1985), "Redox mechanism and electrochemical behaviour or polyaniline deposits", *Journal of Electroanalytical Chemistry and Interfacial Electrochemistry,* vol. 195, no. 1, pp. 109-128.

Gerard, M., Chaubey, A. and Malhotra, B. D. (2002), "Application of conducting polymers to biosensors", *Biosensors and Bioelectronics,* vol. 17, no. 5, pp. 345-359.

Glatz, R. and Bailey-Hill, K. (2011), "Mimicking nature's noses: From receptor deorphaning to olfactory biosensing", *Progress in neurobiology,* vol. 93, no. 2, pp. 270-296.

Gornall, D. D., Collyer, S. D. and Higson, S. P. J. (2009), "Investigations into the use of screen-printed carbon electrodes as templates for electrochemical sensors and sonochemically fabricated microelectrode arrays", *Sensors and Actuators B: Chemical,* vol. 141, no. 2, pp. 581-591.

Gottfried, J. L., De Lucia Jr., F. C., Munson, C. A. and Miziolek, A. W. (2009), "Laser-induced breakdown spectroscopy for detection of explosives residues: A review of recent advances, challenges, and future prospects", *Analytical and Bioanalytical Chemistry,* vol. 395, no. 2, pp. 283-300.

Gould, E. D. and Stecklov, G. (2009), "Terror and the costs of crime", *Journal of Public Economics,* vol. 93, no. 11-12, pp. 1175-1188.

Government, H. , *Best of British*, available at: http://www.bis.gov.uk/assets/biscore/corporate/docs/b/10-845-best-of-british.pdf.

Green, F. M., Salter, T. L., Stokes, P., Gilmore, I. S. and O'Connorb G. (2010), "Ambientmass spectrometry: Advances and applications in forensics", *Surface and Interface Analysis,* vol. 42, no. 5, pp. 347-357.

Grennan, K., Killard, A. J., Hanson, C. J., Cafolla, A. A. and Smyth, M. R. (2006), "Optimisation and characterisation of biosensors based on polyaniline", *Talanta,* vol. 68, no. 5, pp. 1591-1600.

Guilbault, G. G. and Lubrano, G. J. (1973), "An Enzyme Electrode for the Amperometric Determination of Glucose", *Analytica Chimica Acta,* vol. 64, no. 3, pp. 439-455.

Guimard, N. K., Gomez, N. and Schmidt, C. E. (2007), "Conducting polymers in biomedical engineering", *Progress in Polymer Science,* vol. 32, no. 8-9, pp. 876-921.

Guo, S., Wen, D., Zhai, Y., Dong, S. and Wang, E. (2011), "Ionic liquid–graphene hybrid nanosheets as an enhanced material for electrochemical determination of trinitrotoluene", *Biosensors and Bioelectronics,* vol. 26, no. 8, pp. 3475-3481.

Gwenin, C. D., Kalaji, M., Williams, P. A. and Jones, R. M. (2007), "The orientationally controlled assembly of genetically modified enzymes in an amperometric biosensor", *Biosensors and Bioelectronics,* vol. 22, no. 12, pp. 2869-2875.

Haccoun, J., Piro, B., Tran, L. D., Dang, L. A. and Pham, M. C. (2004), "Reagentless amperometric detection of l-lactate on an enzyme-modified conducting copolymer poly(5-hydroxy-1,4-naphthoquinone-co-5-hydroxy-3-thioacetic acid-1,4-naphthoquinone)", *Biosensors and Bioelectronics,* vol. 19, no. 10, pp. 1325-1329.

Hall, B. H. and Khan, B. (2003), *Adoption of new technology,* 9730, National Bureau of Economic Research, California, USA.

Hart, J. P. and Hartley, I. C. (1994), "Voltammetric and amperometric studies of thiocholine at a screen-printed carbon electrode chemically modified with cobalt phthalocyanine: studies towards a pesticide sensor", *Analyst,* vol. 119, pp. 259-263.

Hart, J. P., Crew, A., Crouch, E., Honeychurch, K. C. and Pemberton, R. M. (2004), "Some Recent Designs and Developments of Screen-Printed Carbon Electrochemical Sensors/Biosensors for Biomedical, Environmental, and Industrial Analyses", *Analytical Letters,* vol. 37, no. 5, pp. 789-830.

Hart, J. P. and Wring, S. A. (1997), "Recent developments in the design and application of screen-printed electrochemical sensors for biomedical, environmental and industrial analyses", *TrAC - Trends in Analytical Chemistry,* vol. 16, no. 2, pp. 89-103.

Haupt, S. G., Rowshan, S. and Sauntry, W. C. (2004), *Applicability of Portable Explosive Detection Devices in Transit Environments,* , Transportation Research Board, Washington D.C., USA.

Haynes, C. A., Koder, R. L., Miller, A. -. and Rodgers, D. W. (2002), "Structures of nitroreductase in three states. Effects of inhibitor binding and reduction", *Journal of Biological Chemistry,* vol. 277, no. 13, pp. 11513-11520.

Honeychurch, K. C., Hart, J. P., Pritchard, P. R. J., Hawkins, S. J. and Ratcliffe, N. M. (2003), "Development of an electrochemical assay for 2,6-dinitrotoluene, based on a screen-printed carbon electrode, and its potential application in bioanalysis, occupational and public health", *Biosensors and Bioelectronics,* vol. 19, no. 4, pp. 305-312.

Hrapovic, S., Majid, E., Liu, Y., Male, K. and Luong, J. H. T. (2006), "Metallic nanoparticle-carbon nanotube composites for electrochemical determination of explosive nitroaromatic compounds", *Analytical Chemistry,* vol. 78, no. 15, pp. 5504-5512.

Izake, E. L. (2010), "Forensic and homeland security applications of modern portable Raman spectroscopy", *Forensic science international,* vol. 202, no. 1-3, pp. 1-8.

Jaffari, S. A. and Turner, A. P. F. (1995), "Recent advances in amperometric glucose biosensors for in vivo monitoring", *Physiological Measurement,* vol. 16, no. 1, pp. 1-15.

Jiang, Y., Zhao, H., Zhu, N., Lin, Y., Yu, P. and Mao, L. (2008), "A simple assay for direct colorimetric visualization of trinitrotoluene at picomolar levels using gold nanoparticles", *Angewandte Chemie - International Edition,* vol. 47, no. 45, pp. 8601-8604.

Justes, D. R., Talaty, N., Cotte-Rodriguez, I. and Cooks, R. G. (2007), "Detection of explosives on skin using ambient ionization mass spectrometry.", *Chemical communications (Cambridge, England),* , no. 21, pp. 2142-2144.

Kanu, A. B., Wu, C. and Hill Jr., H. H. (2008), "Rapid preseparation of interferences for ion mobility spectrometry", *Analytica Chimica Acta,* vol. 610, no. 1, pp. 125-134.

Kawaguchi, T., Shankaran, D. R., Kim, S. J., Matsumoto, K., Toko, K. and Miura, N. (2008), "Surface plasmon resonance immunosensor using Au nanoparticle for detection of TNT", *Sensors and Actuators, B: Chemical,* vol. 133, no. 2, pp. 467-472.

Khayamian, T., Tabrizchi, M. and Jafari, M. T. (2003), "Analysis of 2,4,6-trinitrotoluene, pentaerythritol tetranitrate and cyclo-1,3,5-trimethylene-2,4,6-trinitramine using negative corona discharge ion mobility spectrometry", *Talanta,* vol. 59, no. 2, pp. 327-333.

Kim, H. -., Bennett, G. N. and Song, H. -. (2002), "Degradation of 2,4,6-trinitrotoluene by Klebsiella sp. isolated from activated sludge", *Biotechnology Letters,* vol. 24, no. 23, pp. 2023-2028.

Kim, H. -. and Song, H. -. (2005), "Purification and characterization of NAD(P)H-dependent nitroreductase I from Klebsiella sp. C1 and enzymatic transformation of 2,4,6-trinitrotoluene", *Applied Microbiology and Biotechnology,* vol. 68, no. 6, pp. 766-773.

Klausmeier, R. E., Appleton, J. A., Dupre, E. S. and Tenbarge, K. (2001), "The enzymology of trinitrotoluene reduction", *International Biodeterioration and Biodegradation,* vol. 48, no. 1-4, pp. 67-73.

Kollias, C., Papadamou, S. and Stagiannis, A. (2011), "Terrorism and capital markets: The effects of the Madrid and London bomb attacks", *International Review of Economics and Finance,* vol. 20, no. 4, pp. 532-541.

Kollias, C., Manou, E., Papadamou, S. and Stagiannis, A. "Stock markets and terrorist attacks: Comparative evidence from a large and a small capitalization market", *European Journal of Political Economy,* vol. In Press, Corrected Proof.

Kong, Y., Boopathi, M. and Shim, Y. (2003), "Direct electrochemistry of horseradish peroxidase bonded on a conducting polymer modified glassy carbon electrode", *Biosensors and Bioelectronics,* vol. 19, no. 3, pp. 227-232.

Krebs, F. C. (2009), "Fabrication and processing of polymer solar cells: A review of printing and coating techniques", *Solar Energy Materials and Solar Cells,* vol. 93, no. 4, pp. 394-412.

Larsson, A., Angbrant, J., Ekeroth, J., Månsson, P. and Liedberg, B. (2006a), "A novel biochip technology for detection of explosives - TNT: Synthesis, characterisation and application", *Sensors and Actuators, B: Chemical,* vol. 113, no. 2, pp. 730-748.

Larsson, A., Angbrant, J., Ekeroth, J., Månsson, P. and Liedberg, B. (2006b), "A novel biochip technology for detection of explosives - TNT: Synthesis, characterisation and application", *Sensors and Actuators, B: Chemical,* vol. 113, no. 2, pp. 730-748.

Leahy-Hoppa, M. R., Fitch, M. J. and Osiander, R. (2009), "Terahertz spectroscopy techniques for explosives detection", *Analytical and Bioanalytical Chemistry,* vol. 395, no. 2, pp. 247-257.

Leahy-Hoppa, M. R., Fitch, M. J., Zheng, X., Hayden, L. M. and Osiander, R. (2007), "Wideband terahertz spectroscopy of explosives", *Chemical Physics Letters,* vol. 434, no. 4-6, pp. 227-230.

Leighton, T. G. (1994), "Acoustic bubble detection - I: The detection of stable gas bodies", *Environmental Engineering,* vol. 7, no. 3, pp. 9-16.

Lesniak, A., Walczak, M., Jezierski, T., Sacharczuk, M., Gawkowski, M. and Jaszczak, K. (2008), "Canine olfactory receptor gene polymorphism and its relation to odor detection performance by sniffer dogs", *Journal of Heredity,* vol. 99, no. 5, pp. 518-527.

Liao, J. C., Mastali, M., Li, Y., Gau, V., Suchard, M. A., Babbitt, J., Gornbein, J., Landaw, E. M., McCabe, E. R. B., Churchill, B. M. and Haake, D. A. (2007), "Development of an advanced electrochemical DNA biosensor for bacterial pathogen detection", *Journal of Molecular Diagnostics,* vol. 9, no. 2, pp. 158-168.

Liu, H. -., Chen, Y., Bastiaans, G. J. and Zhang, X. -. (2006), "Detection and identification of explosive RDX by THz diffuse reflection spectroscopy", *Optics Express,* vol. 14, no. 1, pp. 415-423.

Liu, H. -., Zhong, H., Karpowicz, N., Chen, Y. and Zhang, X. -. (2007), "Terahertz spectroscopy and imaging for defense and security applications", *Proceedings of the IEEE,* vol. 95, no. 8, pp. 1514-1527.

Liu, J., Agarwal, M. and Varahramyan, K. (2008), "Glucose sensor based on organic thin film transistor using glucose oxidase and conducting polymer", *Sensors and Actuators B: Chemical,* vol. 135, no. 1, pp. 195-199.

Liu, X., Zhao, L., Shen, H., Xu, H. and Lu, L. (2011), "Ordered gold nanoparticle arrays as surface-enhanced Raman spectroscopy substrates for label-free detection of nitroexplosives", *Talanta,* vol. 83, no. 3, pp. 1023-1029.

Llussá, F. and Tavares, J. (2011), "Which terror at which cost? On the economic consequences of terrorist attacks", *Economics Letters,* vol. 110, no. 1, pp. 52-55.

Lo, T., Gregory, I. S., Baker, C., Taday, P. F., Tribe, W. R. and Kemp, M. C. (2006), "The very far-infrared spectra of energetic materials and possible confusion materials using terahertz pulsed spectroscopy", *Vibrational Spectroscopy,* vol. 42, no. 2, pp. 243-248.

Lock, J. P., Geraghty, E., Kagumba, L. C. and Mahmud, K. K. (2009), "Trace detection of peroxides using a microcantilever detector", *Thin Solid Films,* vol. 517, no. 12, pp. 3584-3587.

Long, Y., Chen, H., Yang, Y., Wang, H., Yang, Y., Li, N., Li, K., Pei, J. and Liu, F. (2009), "Electrospun nanofibrous film doped with a conjugated polymer for DNT fluorescence sensor", *Macromolecules,* vol. 42, no. 17, pp. 6501-6509.

Lu, D., Cagan, A., Munoz, R. A. A., Tangkuaram, T. and Wang, J. (2006), "Highly sensitive electrochemical detection of trace liquid peroxide explosives at a Prussian-blue 'artificial-peroxidase' modified electrode", *Analyst,* vol. 131, no. 12, pp. 1279-1281.

Lubczyk, D., Siering, C., Lörgen, J., Shifrina, Z. B., Müllen, K. and Waldvogel, S. R. "Simple and sensitive online detection of triacetone triperoxide explosive", *Sensors and Actuators B: Chemical,* vol. In Press, Corrected Proof.

Lucena, P., Doña, A., Tobaria, L. M. and Laserna, J. J. "New challenges and insights in the detection and spectral identification of organic explosives by laser induced breakdown spectroscopy", *Spectrochimica Acta - Part B Atomic Spectroscopy,* .

Macdiarmid, A. G., Chiang, J. C., Richter, A. F. and Epstein, A. J. (1987), "Polyaniline: a new concept in conducting polymers", *Synthetic Metals,* vol. 18, no. 1-3, pp. 285-290.

Mădăraş, M. B. and Buck, R. P. (1996), "Biosensors Employing Electropolymerized Permselective Films and Their Use for Creatinine Assays in Human Serum", *Analytical Chemistry,* vol. 68, no. 21, pp. 3832-3839.

Maree, S. and Nyokong, T. (2000), "Electrocatalytic behavior of substituted cobalt phthalocyanines towards the oxidation of cysteine", *Journal of Electroanalytical Chemistry,* vol. 492, no. 2, pp. 120-127.

Marshall, B., Warr, C. G. and de Bruyne, M. (2010), "Detection of volatile indicators of illicit substances by the olfactory receptors of Drosophila melanogaster", *Chemical senses,* vol. 35, no. 7, pp. 613-625.

Martin, M., Crain, M., Walsh, K., McGill, R. A., Houser, E., Stepnowski, J., Stepnowski, S., Wu, H. -. and Ross, S. (2007), "Microfabricated vapor preconcentrator for portable ion mobility spectroscopy", *Sensors and Actuators, B: Chemical,* vol. 126, no. 2, pp. 447-454.

Marx, K. A. (2003), "Quartz crystal microbalance: A useful tool for studying thin polymer films and complex biomolecular systems at the solution - Surface interface", *Biomacromolecules,* vol. 4, no. 5, pp. 1099-1120.

Mathew, F. P. and Alocilja, E. C. (2005), "Porous silicon-based biosensor for pathogen detection", *Biosensors and Bioelectronics,* vol. 20, no. 8 SPEC. ISS., pp. 1656-1661.

McCluskey, A., Holdsworth, C. I. and Bowyer, M. C. (2007), "Molecularly imprinted polymers (MIPs): Sensing, an explosive new opportunity?", *Organic and Biomolecular Chemistry,* vol. 5, no. 20, pp. 3233-3244.

McNeilly, C. (2011), *Belfact International Airport spends £10m a year on security*, available at: http://www.belfasttelegraph.co.uk/news/local-national/northern-ireland/belfast-international-airport-spends-10m-a-year-on-security-16052852.html.

Meaney, M. S. and McGuffin, V. L. (2008), "Luminescence-based methods for sensing and detection of explosives", *Analytical and Bioanalytical Chemistry,* vol. 391, no. 7, pp. 2557-2576.

Milmo, D. (2011), *After 9/11: airports 'wasting billions' on needless security checks for passengers*, available at: http://www.guardian.co.uk/world/2011/sep/07/airports-wasting-billions-needless-security (accessed 2/6).

Monterola, M. P. P., Smith, B. W., Omenetto, N. and Winefordner, J. D. (2008), "Photofragmentation of nitro-based explosives with chemiluminescence detection", *Analytical and Bioanalytical Chemistry,* vol. 391, no. 7, pp. 2617-2626.

Moore, D. S. (2004), "Instrumentation for trace detection of high explosives", *Review of Scientific Instruments,* vol. 75, no. 8, pp. 2499-2512.

Moore, D. S. and Scharff, R. J. (2009), "Portable Raman explosives detection", *Analytical and Bioanalytical Chemistry,* vol. 393, no. 6-7, pp. 1571-1578.

Mou, Y. and Rabalais, J. W. (2009), "Detection and Identification of Explosive Particles in Fingerprints Using Attenuated Total Reflection-Fourier Transform Infrared Spectromicroscopy", *Journal of forensic sciences,* vol. 54, no. 4, pp. 846-850.

Mu, S. and Kan, J. (1998), "The effect of salts on the electrochemical polymerization of aniline", *Synthetic Metals,* vol. 92, no. 2, pp. 149-155.

Mulchandani, A. and Rogers, K. R. (eds.) (1998), *Enzyme and Microbial Biosensors,* Humana Press Inc., New Jersey.

Mullen, C., Irwin, A., Pond, B. V., Huestis, D. L., Coggiola, M. J. and Oser, H. (2006), "Detection of explosives and explosives-related compounds by single photon laser ionization time-of-flight mass spectrometry", *Analytical Chemistry,* vol. 78, no. 11, pp. 3807-3814.

Mulligan, C. C., Talaty, N. and Cooks, R. G. (2006), "Desorption electrospray ionization with a portable mass spectrometer: In situ analysis of ambient surfaces", *Chemical Communications,* , no. 16, pp. 1709-1711.

Myler, S., Eaton, S. and Higson, S. J. (1997), "Poly(o-phenylenediamine) ultra-thin polymer-film composite membranes for enzyme electrodes", *Analytica Chimica Acta,* vol. 357, no. 1-2, pp. 55-61.

Naal, Z., Park, J. -., Bernhard, S., Shapleigh, J. P., Batt, C. A. and Abruña, H. D. (2002), "Amperometric TNT biosensor based on the oriented immobilization of a nitroreductase maltose binding protein fusion", *Analytical Chemistry,* vol. 74, no. 1, pp. 140-148.

Nagatomo, K., Kawaguchi, T., Miura, N., Toko, K. and Matsumoto, K. (2009), "Development of a sensitive surface plasmon resonance immunosensor for detection of 2,4-dinitrotoluene with a novel oligo (ethylene glycol)-based sensor surface", *Talanta,* vol. 79, no. 4, pp. 1142-1148.

Nellis, J. G. (2004), *Principles of macroeconomics,* Financial Times Prentice Hall, Harlow.

Nicholson, J. W. (2006), *The Chemistry of Polymers,* 3rd ed, Royal Society of Chemistry, Cambridge.

Nie, D., Jiang, D., Zhang, D., Liang, Y., Xue, Y., Zhou, T., Jin, L. and Shi, G. (2011), "Two-dimensional molecular imprinting approach for the electrochemical detection of trinitrotoluene", *Sensors and Actuators B: Chemical,* vol. 156, no. 1, pp. 43-49.

Nilles, J. M., Connell, T. R., Stokes, S. T. and Dupont Durst, H. (2010), "Explosives detection using direct analysis in real time (DART) mass spectrometry", *Propellants, Explosives, Pyrotechnics,* vol. 35, no. 5, pp. 446-451.

Nyokong, T. and Vilakazi, S. (2003), "Phthalocyanines and related complexes as electrocatalysts for the detection of nitric oxide", *Talanta,* vol. 61, no. 1, pp. 27-35.

Osaka, T. (1997), "Electrochemical formation and microstructure in thin films for high functional devices", *Electrochimica Acta,* vol. 42, no. 20-22, pp. 3015-3022.

Otto, J., Brown, M. F. and Long III, W. (2002), "Training rats to search and alert on contraband odors", *Applied Animal Behaviour Science,* vol. 77, no. 3, pp. 217-232.

Pacheco-Londoño, L. C., Ortiz-Rivera, W., Primera-Pedrozo, O. M. and Hernández-Rivera, S. P. (2009), "Vibrational spectroscopy standoff detection of explosives", *Analytical and Bioanalytical Chemistry,* vol. 395, no. 2, pp. 323-335.

Paldus, B. A. and Kachanov, A. A. (2005), "An historical overview of cavity-enhanced methods", *Canadian Journal of Physics,* vol. 83, no. 10, pp. 975-999.

Pandey, P. C., Pandey, V. and Mehta, S. (1994), "An amperometric enzyme electrode for lactate based on graphite paste modified with tetracyanoquinodimethane", *Biosensors and Bioelectronics,* vol. 9, no. 4-5, pp. 365-372.

Parajuli, S. and Miao, W. (2009), "Sensitive determination of hexamethylene triperoxide diamine explosives, using electrogenerated chemiluminescence enhanced by silver nitrate", *Analytical Chemistry,* vol. 81, no. 13, pp. 5267-5272.

Park, M., Cella, L. N., Chen, W., Myung, N. V. and Mulchandani, A. "Carbon nanotubes-based chemiresistive immunosensor for small molecules: Detection of nitroaromatic explosives", *Biosensors and Bioelectronics,* .

Pchelintsev, N. A. and Millner, P. A. (2008), "A novel procedure for rapid surface functionalisation and mediator loading of screen-printed carbon electrodes", *Analytica Chimica Acta,* vol. 612, no. 2, pp. 190-197.

Pettersson, A., Johansson, I., Wallin, S., Nordberg, M. and Östmark, H. (2009), "Near real-time standoff detection of explosives in a realistic outdoor environment at 55 m distance", *Propellants, Explosives, Pyrotechnics,* vol. 34, no. 4, pp. 297-306.

Pividori, M. I., Lermo, A., Hemández, S., Barbé, J., Alegret, S. and Campoy, S. (2006), "Rapid electrochemical DNA biosensing strategy for the detection of food pathogens based on enzyme-DNA-magnetic bead conjugate", *Afinidad,* vol. 63, no. 521, pp. 13-18.

Pohanka, M., Dobes, P., Drtinova, L. and Kuča, K. (2009), "Nerve agents assay using cholinesterase based biosensor", *Electroanalysis,* vol. 21, no. 10, pp. 1177-1182.

Ponnu, A. and Anslyn, E. V. (2010), "A fluorescence-based cyclodextrin sensor to detect nitroaromatic explosives", *Supramolecular Chemistry,* vol. 22, no. 1, pp. 65-71.

Portnov, A., Bar, I. and Rosenwaks, S. (2010), "Highly sensitive standoff detection of explosives via backward coherent anti-Stokes Raman scattering", *Applied Physics B: Lasers and Optics,* vol. 98, no. 2-3, pp. 529-535.

Primera-Pedrozo, O. M., Soto-Feliciano, Y. M., Pacheco-Londoño, L. C. and Hernández-Rivera, S. P. (2009), "Detection of high explosives using reflection absorption infrared spectroscopy with fiber coupled grazing angle probe/FTIR", *Sensing and Imaging,* vol. 10, no. 1-2, pp. 1-13.

Pritchard, J., Law, K., Vakurov, A., Millner, P. and Higson, S. P. J. (2004), "Sonochemically fabricated enzyme microelectrode arrays for the environmental monitoring of pesticides", *Biosensors and Bioelectronics,* vol. 20, no. 4, pp. 765-772.

Qasim, M., Gorb, L., Magers, D., Honea, P., Leszczynski, J., Moore, B., Taylor, L. and Middleton, M. (2009), "Structure and reactivity of TNT and related species: Application of spectroscopic approaches and quantum–chemical approximations toward understanding transformation mechanisms", *Journal of hazardous materials,* vol. 167, no. 1-3, pp. 154-163.

Rabenecker, P. and Pinkwart, K. (2009), "A look behind electrochemical detection of explosives", *Propellants, Explosives, Pyrotechnics,* vol. 34, no. 3, pp. 274-279.

Rahman, M. A., Park, D. and Shim, Y. (2004), "A performance comparison of choline biosensors: anodic or cathodic detections of H2O2 generated by enzyme immobilized on a conducting polymer", *Biosensors and Bioelectronics,* vol. 19, no. 12, pp. 1565-1571.

Ramanavičius, A., Kaušaitė, A. and Ramanavičienė, A. (2005), "Polypyrrole-coated glucose oxidase nanoparticles for biosensor design", *Sensors and Actuators B: Chemical,* vol. 111-112, pp. 532-539.

Ramos, C. and Dagdigian, P. J. (2007a), "Detection of vapours of explosives and explosive-related compounds by ultraviolet cavity ringdown spectroscopy", *Applied Optics,* vol. 46, no. 26, pp. 620-627.

Ramos, C. and Dagdigian, P. J. (2007b), "Effect of photochemistry on molecular detection by cavity ringdown spectroscopy: Case study of an explosive-related compound", *Applied Optics,* vol. 46, no. 26, pp. 6526-6532.

Rezaei, B. and Damiri, S. (2010), "Using of multi-walled carbon nanotubes electrode for adsorptive stripping voltammetric determination of ultratrace levels of RDX

explosive in the environmental samples", *Journal of hazardous materials,* vol. 183, no. 1-3, pp. 138-144.

Riskin, M., Tel-Vered, R. and Willner, I. (2010), "Imprinted au-nanoparticle composites for the ultrasensitive surface plasmon resonance detection of hexahydro-1,3,5-trinitro-1,3,5-triazine (RDX)", *Advanced Materials,* vol. 22, no. 12, pp. 1387-1391.

Roeseling, D., Tuercke, T., Krause, H. and Loebbecke, S. (2009), "Microreactor-based synthesis of molecularly imprinted polymer beads used for explosive detection", *Organic Process Research and Development,* vol. 13, no. 5, pp. 1007-1013.

Ross, B., Cammann, K., Mokwa, W. and Rospert, M. (1992), "Ultramicroelectrode arrays as transducers for new amperometric oxygen sensors", *Sensors and Actuators B: Chemical,* vol. 7, no. 1-3, pp. 758-762.

Saito, R. (1998), *Physical properties of carbon nanotubes,* Imperial College Press, London.

Sanchez, J. C., DiPasquale, A. G., Rheingold, A. L. and Trogler, W. C. (2007a), "Synthesis, luminescence properties, and explosives sensing with 1,1-tetraphenylsilole- and 1,1-silafluorene-vinylene polymers", *Chemistry of Materials,* vol. 19, no. 26, pp. 6459-6470.

Sanchez, J. C., Toal, S. J., Wang, Z., Dugan, R. E. and Trogler, W. C. (2007b), "Selective detection of trace nitroaromatic, nitramine, and nitrate ester explosive residues using a three-step fluorimetric sensing process: A tandem turn-off, turn-on sensor", *Journal of forensic sciences,* vol. 52, no. 6, pp. 1308-1313.

Sanchez, J. C. and Trogler, W. C. (2008), "Efficient blue-emitting silafluorene-fluorene-conjugated copolymers: Selective turn-off/turn-on detection of explosives", *Journal of Materials Chemistry,* vol. 18, no. 26, pp. 3143-3156.

Sanders, N. L., Kothari, S., Huang, G., Salazar, G. and Cooks, R. G. (2010), "Detection of explosives as negative ions directly from surfaces using a miniature mass spectrometer", *Analytical Chemistry,* vol. 82, no. 12, pp. 5313-5316.

Sandler, T. and Enders, W. (2004), "An economic perspective on transnational terrorism", *European Journal of Political Economy,* vol. 20, no. 2, pp. 301-316.

Saum, A. G. E., Cumming, R. H. and Rowell, F. J. (1998), "Use of substrate coated electrodes and AC impedance spectroscopy for the detection of enzyme activity", *Biosensors and Bioelectronics,* vol. 13, no. 5, pp. 511-518.

Schramm, E., Hölzer, J., Pütz, M., Schulte-Ladbeck, R., Schultze, R., Sklorz, M., Ulrich, A., Wieser, J. and Zimmermann, R. (2009), "Real-time trace detection of security-relevant compounds in complex sample matrices by thermal desorption-single photon ionization-ion trap mass spectrometry (TD-SPI-ITMS) Spectrometry (TD-SPI-ITMS)", *Analytical and Bioanalytical Chemistry,* vol. 395, no. 6, pp. 1795-1807.

Schulte-Ladbeck, R., Vogel, M. and Karst, U. (2006), "Recent methods for the determination of peroxide-based explosives", *Analytical and Bioanalytical Chemistry,* vol. 386, no. 3, pp. 559-565.

P. D. Schwartz, G. M. Murray, O. M. Uy, et al. *Apparatus and methods for detecting explosives and other substances.* Anonymous Patent no. WO/2001/086263.

Settles, G. S. (2005), "Sniffers: Fluid-dynamic sampling for olfactory trace detection in nature and homeland security - The 2004 freeman scholar lecture", *Journal of Fluids Engineering, Transactions of the ASME,* vol. 127, no. 2, pp. 189-218.

Shaidarova, L. G., Ziganshina, S. A., Medyantseva, E. P. and Budnikov, G. K. (2003), "Ampermetric cholinesterase biosensors with carbon paste electrodes modified with cobalt phthalocyanine", *Applied Electrochemistry and Corrosion Protection of Metals,* vol. 77, no. 2, pp. 241-248.

Shi, G., Qu, Y., Zhai, Y., Liu, Y., Sun, Z., Yang, J. and Jin, L. (2007), "{MSU/PDDA}$_n$ LBL assembled modified sensor for electrochemical detection of ultratrace explosive nitroaromatic compounds", *Electrochemistry Communications,* vol. 9, no. 7, pp. 1719-1724.

Shi, G. H., Shang, Z. B., Wang, Y., Jin, W. J. and Zhang, T. C. (2008), "Fluorescence quenching of CdSe quantum dots by nitroaromatic explosives and their relative compounds", *Spectrochimica Acta - Part A: Molecular and Biomolecular Spectroscopy,* vol. 70, no. 2, pp. 247-252.

Singh, P., Onodera, T., Mizuta, Y., Matsumoto, K., Miura, N. and Toko, K. (2009), "Dendrimer modified biochip for detection of 2,4,6 trinitrotoluene on SPR immunosensor: Fabrication and advantages", *Sensors and Actuators, B: Chemical,* vol. 137, no. 2, pp. 403-409.

Singh, S. (2007), "Sensors—An effective approach for the detection of explosives", *Journal of Hazardous Materials,* vol. 144, no. 1-2, pp. 15-28.

Sittampalam, G. and Wilson, G. S. (1983), "Surface-modified electrochemical detector for liquid chromatography", *Analytical Chemistry,* vol. 55, pp. 1608-1609-1610.

Sivakumar, R. and Saraswathi, R. (2002), "Characterization of poly(N-methylaniline) as a cathode active material in aqueous rechargeable batteries", *Journal of Power Sources,* vol. 104, no. 2, pp. 226-233.

Skládal, P. (1991), "Determination of organophosphate and carbamate pesticides using a cobalt phthalocyanine-modified carbon paste electrode and a cholinesterase enzyme membrane", *Analytica Chimica Acta,* vol. 252, no. 1-2, pp. 11-15.

Smets, B. F., Yin, H. and Esteve-Nuñez, A. (2007), "TNT biotransformation: When chemistry confronts mineralization", *Appl.Microbiol.Biotechnol.,* vol. 76, no. 2, pp. 267-277.

Smith, R. G., D'Souza, N. and Nicklin, S. (2008), "A review of biosensors and biologically-inspired systems for explosives detection", *Analyst,* vol. 133, no. 5, pp. 571-584.

Snels, M., Venezia, T. and Belfiore, L. (2010), "Detection and identification of TNT, 2,4-DNT and 2,6-DNT by near-infrared cavity ringdown spectroscopy", *Chemical Physics Letters,* vol. 489, no. 1-3, pp. 134-140.

Somerset, V. S., Klink, M. J., Baker, P. G. L. and Iwuoha, E. I. (2007), "Acetylcholinesterase-polyaniline biosensor investigation of organophosphate pesticides in selected organic solvents", *Journal of Environmental Science and Health - Part B Pesticides, Food Contaminants, and Agricultural Wastes,* vol. 42, no. 3, pp. 297-304.

Song, Y. and Cooks, R. G. (2006), "Atmospheric pressure ion/molecule reactions for the selective detection of nitroaromatic explosives using acetonitrile and air as reagents", *Rapid Communications in Mass Spectrometry,* vol. 20, no. 20, pp. 3130-3138.

Stringer, R. C., Gangopadhyay, S. and Grant, S. A. (2010), "Detection of nitroaromatic explosives using a fluorescent-labeled imprinted polymer", *Analytical Chemistry,* vol. 82, no. 10, pp. 4015-4019.

Štulík, K., Amatore, C., Holub, K., Mareček, V. and Kutner, W. (2000), "Microelectrodes. Definitions, characterization, and applications (Technical report)", *Pure and Applied Chemistry,* vol. 72, no. 8, pp. 1483-1492.

Suslick, K.S., (1986), *Organometallic Sonochemistry*.

Suslick, K. S. (1990), "Sonochemistry", *Science,* vol. 247, no. 4949, pp. 1439-1445.

Tabrizchi, M. and ILbeigi, V. (2010), "Detection of explosives by positive corona discharge ion mobility spectrometry", *Journal of hazardous materials,* vol. 176, no. 1-3, pp. 692-696.

Takada, Y., Nagano, H., Suga, M., Hashimoto, Y., Yamada, M., Sakairi, M., Kusumoto, K., Ota, T. and Nakamura, J. (2002), "Detection of military explosives by atmospheric pressure chemical ionization mass spectrometry with counter-flow introduction", *Propellants, Explosives, Pyrotechnics,* vol. 27, no. 4, pp. 224-228.

Takáts, Z., Wiseman, J. M., Gologan, B. and Cooks, R. G. (2004), "Mass spectrometry sampling under ambient conditions with desorption electrospray ionization", *Science,* vol. 306, no. 5695, pp. 471-473.

Tenhaeff, W. E., Mcintosh, L. D. and Gleason, K. K. (2010), "Synthesis of poly(4-vinylpyridine) thin films by initiated chemical vapor deposition (icvd) for selective nanotrench-based sensing of nitroaromatics", *Advanced Functional Materials,* vol. 20, no. 7, pp. 1144-1151.

Thiébaud, P., Beuret, C., de Rooij, N. F. and Koudelka-Hep, M. (2000), "Microfabrication of Pt-tip microelectrodes", *Sensors and Actuators B: Chemical,* vol. 70, no. 1-3, pp. 51-56.

Thomas III, S. W., Joly, G. D. and Swager, T. M. (2007), "Chemical sensors based on amplifying fluorescent conjugated polymers", *Chemical reviews,* vol. 107, no. 4, pp. 1339-1386.

Toal, S. J., Sanchez, J. C., Dugan, R. E. and Trogler, W. C. (2007), "Visual detection of trace nitroaromatic explosive residue using photoluminescent metallole-containing polymers", *Journal of forensic sciences,* vol. 52, no. 1, pp. 79-83.

Tolan, M., Vacca, G., Sinha, S. K., Li, Z., Rafailovich, M. H., Sokolov, J., Lorenz, H. and Kotthaus, J. P. (1996), "Si/Ge films on laterally structured surfaces: An x-ray study of conformal roughness", *Applied Physics Letters,* vol. 68, no. 2, pp. 191-193.

Turner, A. P. F., Karube, I. and Wilson, G. S. (1986), *Biosensors: Fundamentals and Applications,* Oxford University Press, Oxford, UK.

Turvey, C. G., Onyango, B., Cuite, C. and Hallman, W. K. (2010), "Risk, fear, bird flu and terrorists: A study of risk perceptions and economics", *Journal of Socio-economics,* vol. 39, no. 1, pp. 1-10.

Updike, S. J. and Hicks, G. P. (1967), "The Enzyme Electrode", *Nature,* vol. 214 (5092), pp. 986-988.

Vashist, S. K., Zheng, D., Al-Rubeaan, K., Luong, J. H. T. and Sheu, F. "Technology behind commercial devices for blood glucose monitoring in diabetes management: A review", *Analytica Chimica Acta,* vol. In Press, Corrected Proof.

Vowles, N., Thirkell, P. and Sinha, A. (2011), "Different determinants at different times: B2B adoption of a radical innovation", *Journal of Business Research,* vol. 64, no. 11, pp. 1162-1168.

Wackerbarth, H., Gundrum, L., Salb, C., Christou, K. and Viöl, W. (2010a), "Challenge of false alarms in nitroaromatic explosive detection-a detection device based on surface-enhanced Raman spectroscopy", *Applied Optics,* vol. 49, no. 23, pp. 4367-4371.

Wackerbarth, H., Salb, C., Gundrum, L., Niederkrüger, M., Christou, K., Beushausen, V. and Viöl, W. (2010b), "Detection of explosives based on surface-enhanced Raman spectroscopy", *Applied Optics,* vol. 49, no. 23, pp. 4362-4366.

Waltman, M. J., Dwivedi, P., Hill Jr., H. H., Blanchard, W. C. and Ewing, R. G. (2008), "Characterization of a distributed plasma ionization source (DPIS) for ion mobility spectrometry and mass spectrometry", *Talanta,* vol. 77, no. 1, pp. 249-255.

Wang, B., Tang, J. and Wang, F. (1986), "The effect of anions of supporting electrolyte on the electrochemical polymerization of aniline and the properties of polyaniline", *Synthetic Metals,* vol. 13, no. 4, pp. 329-334.

Wang, B., Tang, J. and Wang, F. (1987), "Electrochemical polymerization of aniline", *Synthetic Metals,* vol. 18, no. 1-3, pp. 323-328.

Wang, F., Wang, W., Liu, B., Wang, Z. and Zhang, Z. (2009), "Copolypeptide-doped polyaniline nanofibers for electrochemical detection of ultratrace trinitrotoluene", *Talanta,* vol. 79, no. 2, pp. 376-382.

Wang, H., Sun, W., Zhang, J., Yang, X., Lin, T. and Ding, L. (2010), "Desorption corona beam ionization source for mass spectrometry", *Analyst,* vol. 135, no. 4, pp. 688-695.

Wang, J. (2007a), "Electrochemical sensing of explosives", *Electroanalysis,* vol. 19, no. 4, pp. 415-423.

Wang, J. (2007b), "Electrochemical sensing of explosives", *Electroanalysis,* vol. 19, no. 4, pp. 415-423.

Wang, J. (2008), "Electrochemical glucose biosensors", *Chemical reviews,* vol. 108, no. 2, pp. 814-825.

Wang, J., Hocevar, S. B. and Ogorevc, B. (2004), "Carbon nanotube-modified glassy carbon electrode for adsorptive stripping voltammetric detection of ultratrace levels of 2,4,6-trinitrotoluene", *Electrochemistry Communications,* vol. 6, no. 2, pp. 176-179.

Wang, J., Liu, G., Wu, H. and Lin, Y. (2008), "Sensitive electrochemical immunoassay for 2,4,6-trinitrotoluene based on functionalized silica nanoparticle labels", *Analytica Chimica Acta,* vol. 610, no. 1, pp. 112-118.

Wang, J., Lu, F., MacDonald, D., Lu, J., Ozsoz, M. E. S. and Rogers, K. R. (1998), "Screen-printed voltammetric sensor for TNT", *Talanta,* vol. 46, no. 6, pp. 1405-1412.

Wang, J. (2001), "Glucose Biosensors: 40 Years of Advances and Challenges", *Electroanalysis,* vol. 13, no. 12, pp. 983-988.

Wang, J. (2006), *Analytical electrochemistry,* 3rd ed, Wiley; John Wiley distributor, Hoboken, N.J.; Chichester.

Wang, J. and Pumera, M. (2006), "Microchip flow-injection analysis of trace 2,4,6-trinitrotoluene (TNT) using mercury-amalgam electrochemical detector", *Talanta,* vol. 69, no. 4, pp. 984-987.

Wang, J., Tian, B., Nascimento, V. B. and Angnes, L. (1998), "Performance of screen-printed carbon electrodes fabricated from different carbon inks", *Electrochimica Acta,* vol. 43, no. 23, pp. 3459-3465.

Wang, J. and Zadeii, J. M. (1988), "Ensembles of carbon paste ultramicroelectrodes", *Journal of Electroanalytical Chemistry and Interfacial Electrochemistry,* vol. 249, no. 1-2, pp. 339-345.

Warriner, K., Higson, S. and Vadgama, P. (1997), "A lactate dehydrogenase amperometric pyruvate electrode exploiting direct detection of NAD+ at a poly(3-methylthiophene):poly(phenol red) modified platinum surface", *Materials Science and Engineering: C,* vol. 5, no. 2, pp. 91-99.

Wells, J. M., Roth, M. J., Keil, A. D., Grossenbacher, J. W., Justes, D. R., Patterson, G. E. and Barket Jr., D. J. (2008), "Implementation of DART and DESI Ionization on a Fieldable Mass Spectrometer", *Journal of the American Society for Mass Spectrometry,* vol. 19, no. 10, pp. 1419-1424.

White, P. (ed.) (2004), *Crime Scene to Court: the Essentials of Forensic Science,* 2nd ed, Royal Society of Chemistry, Cambridge.

Whiteway, J., Koziarz, P., Veall, J., Sandhu, N., Kumar, P., Hoecher, B. and Lambert, I. B. (1998), "Oxygen-insensitive nitroreductases: Analysis of the roles of nfsA and nfsB in development of resistance to 5-nitrofuran derivatives in Escherichia coli", *Journal of Bacteriology,* vol. 180, no. 21, pp. 5529-5539.

Wilson, R. and Turner, A. P. F. (1992), "Glucose oxidase: an ideal enzyme", *Biosensors and Bioelectronics,* vol. 7, no. 3, pp. 165-185.

Woodka, M. D., Schnee, V. P. and Polcha, M. P. (2010), "Fluorescent polymer sensor array for detection and discrimination of explosives in water", *Analytical Chemistry,* vol. 82, no. 23, pp. 9917-9924.

Woolard, D. L., Brown, E. R., Pepper, M. and Kemp, M. (2005), "Terahertz frequency sensing and imaging: A time of reckoning future applications?", *Proceedings of the IEEE,* vol. 93, no. 10, pp. 1722-1743.

Wu, J. T., Wu, L. H. and Knight, J. A. (1986), "Stability of NADPH: Effects of Various Factors on the Kinetics of Degradation", *Clinical Chemistry,* vol. 32, no. 2, pp. 314.

Wu, S., Lan, X., Zhao, W., Li, Y., Zhang, L., Wang, H., Han, M. and Tao, S. (2011), "Controlled immobilization of acetylcholinesterase on improved hydrophobic gold nanoparticle/Prussian blue modified surface for ultra-trace organophosphate pesticide detection", *Biosensors and Bioelectronics,* vol. 27, no. 1, pp. 82-87.

Yang, H., Shan, C., Li, F., Han, D., Zhang, Q. and Niu, L. (2009), "Covalent functionalization of polydisperse chemically-converted graphene sheets with amine-terminated ionic liquid", *Chemical Communications,* , no. 26, pp. 3880-3882.

Yang, L., Ma, L., Chen, G., Liu, J. and Tian, Z. -. (2010), "Ultrasensitive SERS detection of TNT by imprinting molecular recognition using a new type of stable substrate", *Chemistry - A European Journal,* vol. 16, no. 42, pp. 12683-12693.

Yano, J. (1995), "**Electrochemical and structural studies on soluble and conducting polymer from *o*-phenylenediamine**", *Journal of Polymer Science Part A: Polymer Chemistry,* vol. 33, no. 14, pp. 2435.

Yin, H., Wood, T. K. and Smets, B. F. (2005), "Reductive transformation of TNT by Escherichia coli: Pathway description", *Applied Microbiology and Biotechnology,* vol. 67, no. 3, pp. 397-404.

Yinon, J. (ed.) (2007), *Counterterrorist Detection Techniques of Explosives,* 1st ed, Elsevier, Oxford, UK.

Yinon, J. (2002), "Field detection and monitoring of explosives", *TrAC - Trends in Analytical Chemistry,* vol. 21, no. 4, pp. 292-301.

Yu, L., Huang, Y., Jin, X., Mason, A. J. and Zeng, X. (2009), "Ionic liquid thin layer EQCM explosives sensor", *Sensors and Actuators, B: Chemical,* vol. 140, no. 2, pp. 363-370.

Zang, J., Guo, C. X., Hu, F., Yu, L. and Li, C. M. (2011), "Electrochemical detection of ultratrace nitroaromatic explosives using ordered mesoporous carbon", *Analytica Chimica Acta,* vol. 683, no. 2, pp. 187-191.

Zenno, S., Koike, H., Kumar, A. N., Jayaraman, R., Tanokura, M. and Saigo, K. (1996), "Biochemical characterization of NfsA, the Escherichia coli major nitroreductase exhibiting a high amino acid sequence homology to Frp, a Vibrio harveyi flavin oxidoreductase", *Journal of Bacteriology,* vol. 178, no. 15, pp. 4508-4514.

Zhang, Z., Tong, J., Chen, D. -. and Lan, Y. -. (2008), "Electronic Nose with an Air Sensor Matrix for Detecting Beef Freshness", *J.Bionic Eng.,* vol. 5, no. 1, pp. 67-73.

Zhou, Z., Wu, Q. and Liu, C. (1994), "Microfabricated thin-film microelectrode for amperometric determination of CO2 in the gas phase", *Sensors and Actuators B: Chemical,* vol. 21, no. 2, pp. 101-108.

Zimmermann, S., Abel, N., Baether, W. and Barth, S. (2007), "An ion-focusing aspiration condenser as an ion mobility spectrometer", *Sensors and Actuators, B: Chemical,* vol. 125, no. 2, pp. 428-434.

Zoski, C. G. (2002), "Ultramicroelectrodes: Design, Fabrication, and Characterisation", *Electroanalysis,* vol. 14, pp. 1041.

16. Appendix 1

Review paper accepted for publication in Talanta on 11th November 2011

See: http://www.sciencedirect.com/science/article/pii/S0039914011010253

17. Appendix 2

Poster presented at the *Biosensing Conference 2011* in Amsterdam

Cranfield Health

Cranfield UNIVERSITY

Nitroreductase Micro-electrode Arrays linked to Air Cyclone Sampling for the Determination of Explosives for Homeland Security Applications

J. Sarah Caygill, Stuart Collyer and Séamus P. J. Higson

Introduction

There has in recent years been a heightened need for more simplified methods of determining airborne explosive traces, since current approaches typically suffer from one or more drawbacks, such as the size or cost of the instrumentation. This new approach utilises disposable screen-printed carbon sensors incorporating a sonochemically fabricated micro-electrode enzymatic array. The aim of this research is to provide a novel, simplified explosive detection device with low detection limits that works in real-time and is of low cost to both fabricate and use.

Methods/Materials

Cyclic voltammetry was carried out using a PG580 electrochemical workstation from Uniscan Instruments Ltd (Buxton, UK). Microarrays were produced (as shown in figure 1) on screen-printed sensors from Microarray Ltd. (Manchester, UK).

Carbon ink and cobalt phthalocyanine-doped carbon ink screen-printed sensors were both used as base substrate materials for microelectode array formation. The sensors were first coated with the insulating polymer phenylene diamine before ultrasonic ablation in an ultrasound bath (35KHz) for 10 seconds. The microelectrode arrays formed via this process were either interrogated in this form or subjected to a further electropolymerisation deposition step with the conducting polymer aniline, with the enzyme nitroreductase also being immobilised in this conducting polymer matrix. These sensors were used to electrochemically detect TNT in an electrolytic solution .

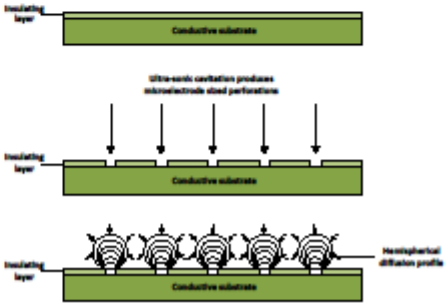

Figure 1. Schematic representing the production of a micro-electrode array through the insulating of a sensor before ultrasonic cavitation.

Results

Figure 2 displays the cathodic current response obtained from the interrogation of solutions containing increasing concentrations of TNT with firstly a screen-printed carbon sensor and then the improved response observed with a cobalt phthalocyanine doped carbon electrode sensor system. Figure 3 displays the voltammogram obtained when a TNT solution was interrogated with a microelectrode array and figure 4 illustrates the difference in signal enhancement between an array-based sensor and a plain cobalt phthalocyanine sensor. Figure 5 shows the cyclone collection device, which will enable collection of large volumes of air contaminated with explosive particles for subsequent concentration prior to electrochemical analysis.

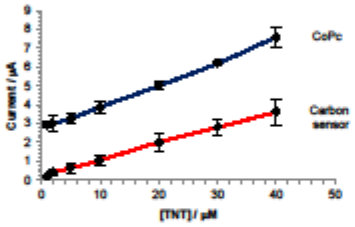

Figure 2. Calibration plots of the interrogation of 200 µM TNT by a carbon (red line) and CoPc (blue line) sensor (20 mVs-1 vs. Ag/AgCl)

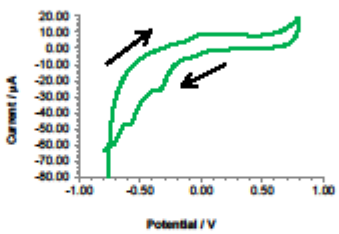

Figure 3. Cyclic voltammogram representing 200 µM TNT interrogated with a microelectrode array (20 mVs-1 vs. Ag/AgCl)

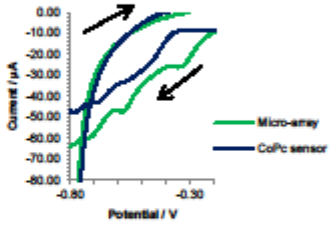

Figure 4. Cyclic voltammogram representing 200 µM TNT interrogated with a microelectrode array (purple line) or CoPc sensor (blue line) (20 mVs-1 vs. Ag/AgCl)

Figure 5. Coriolis µ biological air sampler

Conclusions

These studies have shown that TNT can be interrogated electrochemically using screen-printed carbon electrodes. Further investigations have shown enhancements over these initial results in a two-fold manner. Firstly the use of mediator-doped electrodes (cobalt phthalocyanine-doped carbon ink) show a significant increase in signal response, thus lowering the limits of detection from 400 nM to 200 nM. Secondly, the use of sonochemically fabricated microelectrode arrays have achieved significant enhancements in terms of signal derivation, that is not observed with planar carbon systems. These findings, coupled to the low costs associated with the fabrication regime/instrumentation offer significant promise in developing a viable measurement system.

j.a.caygill@cranfield.ac.uk

www.cranfield.ac.uk/health

18. Appendix 3

Price lists for carbon screen-printed electrode sensors from Dropsens and hand-held potentiostat PG581 form Uniscan

Metrohm U.K. ltd.

DropSens

Price List £

For further DropSens product & price information contact **Dr Andrew Osborne** on **07773 023 776**
alternatively contact Metrohm UK Office on **01928 579 600** or email **DropSens@metrohm.co.uk**

POTENTIOSTATS | NANOMATERIALS | REAGENTS | LAB PRACTICES

Part No.	Description	Quantity	Price £
STAT200	µStat 200 Bipotentiostat (Includes free: 1 x ref. DSC; 1 x ref. BICAST; 75 x ref. 110)	1	£2,375
STAT400	µStat 400 Bipotentiostat/Galvanostat (Includes free: 1 x ref. DSC; 1 x ref. BICAST; 75 x ref. 110)	1	£3,781
STAT8000	µStat 8000 Multi Potentiostat/Galvanostat (Includes free: 1 x ref. CABSTAT1;1 x ref. CAST; 1 x ref. CAST8X; 20 x ref. 8X110)	1	£15,686
FIAEC200	Complete FIA System for Electrochemical detection (Includes STAT200, VALVE, PPUMP, FLWCL, PVCTUBE ,FLOWFITTINGS, Tubes and containers)	1	£6,485
FIAEC400	Complete FIA System for Electrochemical detection (Includes STAT200, VALVE, PPUMP, FLWCL, PVCTUBE ,FLOWFITTINGS, Tubes and containers)	1	£7,892
CAST	µStat Cable connector for screen-printed electrodes	1	£70
BICAST	µStat Cable connector for Dual screen-printed electrodes	1	£81
CABSTAT1	µStat 8000 One Node Cable connector for electrodes	1	£81
CABSTATMULTI	µStat 8000 Multichannel Cable connector for electrodes	1	£200
CAST8X	µStat 8000 Cable connector for format 8X screen-printed electrodes	1	£297
CNFSOL1	Carbon Nanofibres Solution - 1.0 mL	1.0 mL	£216
CNFSOL5	Carbon Nanofibres Solution- 5.0 mL	5.0 mL	£649
CNTSOL05	COOH functionalized Multi-Walled Carbon Nanotubes Solution - 0.5 mL	0.5 mL	£189
CNTSOL1	COOH functionalized Multi-Walled Carbon Nanotubes Solution - 1.0 mL	1.0 mL	£346
GPHSOL1	Graphene Solution - 1.0 mL	1.0 mL	£162
GPHSOL5	Graphene Solution - 5.0 mL	5.0 mL	£487
GPHOXSOL1	Graphene Oxide Solution - 1.0 mL	1.0 mL	£87
GPHOXSOL5	Graphene Oxide Solution - 5.0 mL	5.0 mL	£270
GPHOXSOL-AQU1	Graphene Oxide Solution - Aqueous -1.0 mL	1.0 mL	£87
GPHOXSOL-AQU5	Graphene Oxide Solution - Aqueous - 5.0 mL	5.0 mL	£270
MWCNT	Multi-Walled Carbon Nanotubes	per gram	£97
MWCNTCOOH	-COOH functionalized Multi-Walled Carbon Nanotubes	per gram	£119
MWCNTNH2	-NH2 functionalized Multi-Walled Carbon Nanotubes	per gram	£141
SWCNT	Single-Walled Carbon Nanotubes	per gram	£622
SWCNTCOOH	-COOH functionalized Single-Walled Carbon Nanotubes	per gram	£676
GPHOX01	Graphene Oxide	0.1 g	£108
GPHOX10	Graphene Oxide	1 g	£649
PAPP250	p-AminoPhenyl Phosphate - 250 mg	250 mg	£325
PAPP500	p-AminoPhenyl Phosphate - 500 mg	500 mg	£541
PAPP750	p-AminoPhenyl Phosphate - 750 mg	750 mg	£682
PAPP1000	p-AminoPhenyl Phosphate - 1000 mg	1000 mg	£779
HQDP500	Hydroquinone Diphosphate - 500 mg	500 mg	£195
HQDP1	Hydroquinone Diphosphate - 1 g	1 g	£346
PPAR500	Phosphorilated Paracetamol - 500 mg	500 mg	£195
PPAR1	Phosphorilated Paracetamol - 1 g	1 g	£346
PL1	Laboratory Practice – Ascorbic Acid in juice	1	£92
PL2	Laboratory Practice – Uric Acid in urine	1	£227
PL3	Laboratory Practice – Paracetamol in drugs	1	£92
PL4	Laboratory Practice – Copper in tap water	1	£92

uniscan instruments

Uniscan Instruments Ltd.
Sigma House
Burlow Road
Buxton
Derbyshire
SK17 9JS
United Kingdom

Tel: +44 (0)1298 70981
Fax: +44 (0)1298 70886
Web: www.uniscan.com

PG581 UK and Ireland end user prices:

Effective 1st January 2012

Items	Description	End-user Price
PG581	Uniscan Model PG581 Electrochemical analyzer comes with: • UiEChem™ or UiECorr™ software suite (CD). • Mains power pack and battery re-charger. • Rechargeable NiMH battery. • Single WE flying leads (WE, CE, RE). • USB cable. • 1 GB miniSD card • Moulded Polypropylene carrying case. • Full operator's manual.	£ 2,775.00
UiECorr™	Corrosion software (for users who initially purchased with UiEChem™).	£ 402.00
UiEChem™	Electrochemistry software (for users who initially purchased UiECorr™).	£ 402.00
PG581-ISO	Factory fitted isolation option*.	£ 172.00
PG581-2	PG581 five working electrode flying lead (croc clip connectors) screened.	£ 187.00
PG581-3	Spare rechargeable battery.	£ 118.00
PG581-4	Replacement power supply (including adapters).	£ 119.00
PG581-5	Replacement USB cable.	£ 27.00
PG581-6	PG581 single working electrode flying lead (croc clip connectors) screened.	£ 102.00
PG581-7	Macro-programming (per hour).	£ 81.00
PG581-12	ActiveX control software for PG581.	£ 239.00
PG581-13	25 off blank electrodes (Defined composition Carbon WE, AE, Ag/AgCl RE.	£ 187.00
PG581-14	50 off blank electrodes.	£ 350.00